Title

Sequestration and release mechanisms of strontium and cesium in zeolite/feldspathoid systems and laboratory reacted Hanford sediments

Permalink

https://escholarship.org/uc/item/3dg161fc

Author

Rivera, Nelson Antonio, Jr.

Publication Date

2011-12-14

Peer reviewed|Thesis/dissertation

SEQUESTRATION AND RELEASE MECHANISMS OF STRONTIUM AND CESIUM IN ZEOLITE/FELDSPATHOID SYSTEMS AND LABORATORY REACTED HANFORD SEDIMENTS

by

Nelson Antonio Rivera, Jr.

B.S. (University of Notre Dame) 2001
M.S. (Arizona State University) 2004

A dissertation submitted in partial fulfillment

of the requirement for the degree of

Doctor of Philosophy

in

Environmental Systems

in the

GRADUATE DIVISION
of the
UNIVERSITY OF CALIFORNIA, MERCED

Committee in charge
Dr. Peggy A. O'Day, Chair
Dr. Samuel Traina
Dr. Thomas Harmon
Dr. Jon Chorover

2011

TABLE OF CONTENTS

Chapter 1: INTRODUCTION

During the Cold War, the U.S. Department of Energy Hanford Site (WA) was the primary location for plutonium (Pu) extraction within the Manhattan Project. The different chemical extraction and separation processes produced twenty-six chemically dissimilar waste streams that were combined in underground tanks, resulting in mixed wastes with elevated values of pH (8 to 14), ionic strength (2–16 M NaNO$_3$), temperature (60–110°C), and dissolved aluminum (Gee et al., 2007; McKinley et al., 2001; Zachara et al., 2007; Zachara et al., 2002a). For 60 years, Hanford housed the storage and disposal of this radioactive waste from nuclear reactor operations and the chemical extraction of plutonium for nuclear weapons production generating nearly 2 million cubic meters (525 million gallons) of high-level waste (Ahearne, 1997; Crowley, 1997; Gephart, 2003; Gephart and Lundgren, 1998; Heeb et al., 1996; Jackson, 1977; Routson et al., 1981). Up to 90% of this waste has been reduced through various means which include evaporation, treatment, intentional discharge to the subsurface (Gee et al., 2007), and tank leakage. Approximately 373,400 m^3 of high level radioactive waste have been stored in underground steel tanks at Department of Energy (DOE) sites across the United States(Ahearne, 1997). Of the 177 tanks onsite, 149 were single-shell carbon-steel tanks built from 1943 to 1964. It is believed that 67 of these tanks leaked up to 1 million gallons of contaminated fluids into the subsurface (Gephart, 2003; Gephart and Lundgren, 1998). More robust tanks (double-shelled carbon steel) were built in 1968 due to leaking of the single-shell tanks. No leaks have been detected from these tanks; however, the tanks were designed to last approximately 50 years.

Contaminated groundwater plumes covering 400 square kilometers (150 square miles) contain a variety of contaminants such as metals (e.g., chromium), chemicals (e.g., nitrates,

trichloroethene, carbon tetrachloride), and radionuclides (e.g., tritium, technetium-99, strontium-90). Numerous studies have looked at the health effects and geochemical processes associated with the release of these contaminants into the subsurface at Hanford (Bickmore et al., 2001; Bostick et al., 2002; Bowers et al., 2006; Choi et al., 2005a; Choi et al., 2005b; Choi et al., 2006; Chorover et al., 2003; Crosson et al., 2006; Flury et al., 2004; Fritz and Patton, 2006; Grossman et al., 1996; Hakem et al., 2000; Hansen et al., 2001; Hassan et al., 2003; Liu et al., 2003a; Liu et al., 2004; Liu et al., 2003b; Liu et al., 2005a; Liu et al., 2005b; Mashal et al., 2005a; Mashal et al., 2005b; Mashal et al., 2005c; Mashal et al., 2004; McKinley et al., 2004; McKinley et al., 2001; Mon et al., 2005; Moran et al., 1999; Samson et al., 2005; Serne et al., 1998; Um and Serne, 2005; Wan et al., 2004; Wendling et al., 2005; Zachara et al., 2002b; Zhao et al., 2004; Zhuang et al., 2003; Zhuang et al., 2004). The radioactivity at the Hanford site is predominantly from the release of strontium-90 and cesium-137 isotopes. Sr^{90} and Cs^{137} both have half-lives of approximately 30 years. Sr^{90} decays to Y^{90} (half-life = 64 hrs), which in turn decays to Zr^{90} (non-radioactive). Cs^{137} decays to meta-stable nuclear isomer Ba^{137m} (half-life =2.6 min) and the Ba^{137m} will then convert to a stable Ba^{137} through gamma-ray de-excitation (Wagner et al., 1997). It is important to track the mobility of these contaminants in the subsurface because their potential bio-availability. Strontium presents health problems since it substitutes for calcium in bone, preventing expulsion from the body. Cesium acts chemically like potassium in the body and enters muscle tissue.

In order to successfully predict waste plume migration and understand possible mechanisms of radionuclide sequestration at the Hanford Site, the impact of caustic waste leachate on the surrounding sediments and possible transport processes have to be elucidated. Previous studies have focused on mineral transformations caused by the caustic waste (Choi et

2

al., 2005a; Choi et al., 2005b; Choi et al., 2006; Chorover et al., 2003a; Mon et al., 2005; Zhuang et al., 2004). Previous laboratory experiments on specimen mineral systems showed that synthetic tank waste leachate (STWL) solutions dissolved primary silicates such as quartz and feldspars (Bickmore et al., 2001; Choi et al., 2005b; Choi et al., 2006; Um and Serne, 2005), and high surface area clay minerals (Choi et al., 2006; Chorover et al., 2003; Zhao et al., 2004), contributing to the release of Si. Because Si is dissolved into a hyperalkaline, Al-rich system, supersaturation is achieved with respect to feldspathoid and zeolite group minerals (Choi et al., 2005b; Choi et al., 2006; Crosson et al., 2006; Mashal et al., 2005c; Mashal et al., 2004). The feldspathoid and zeolite phases that form vary and may include sodalite, cancrinite, zeolite A, chabazite, and zeolite X (Choi et al., 2006; Crosson et al., 2006; Mashal et al., 2005b; Mashal et al., 2005c; Mon et al., 2005; Perdrial et al., 2011; Rivera et al., 2011; Zhao et al., 2004).

In prior studies of contaminant uptake by Hanford sediment, Cs^+ was shown to sorb selectively on frayed edges and interlamellae of native micaceous mineral phases (illite, biotite, muscovite, and vermiculite) (McKinley et al., 2004; Steefel et al., 2003; Thompson et al., 2010; Zachara et al., 2002a). Conversely, a large fraction of Sr^{2+} sorbed to labile ion exchange sites (Mg^{2+} exchangeable) early in the sediment reaction sequence, becoming increasingly recalcitrant to Mg^{2+} desorption with longer caustic waste reaction time. X-ray absorption spectroscopy data suggested that Sr is incorporated into multiple zeolite and feldspathoid neophases with bond distances consistent with zeolite-types phases (Chorover et al., 2008). While most studies have focused on contaminant uptake, less work has been done to examine contaminant release if subsurface conditions change.

Although previous studies have established that cesium and strontium can be strongly bound in sediments by the precipitation of neo-formed phases that sequester these contaminants,

3

key questions remain for remediation of the Hanford site. Recent studies (Chang et al., 2011; Thompson et al., 2010) have shown the ability to release Sr and Cs when reacted with an infiltrating groundwater solution. With multiple factors controlling sequestration and release of contaminant Sr and Cs, processes such as retention on or in neophases and aging effects on retention need to be further studied. The following work is broken into three sections:

(1) Sr and Cs incorporation into the feldspathoid and zeolite crystal structures that form from a synthesis solution;

(2) The release of Sr and Cs from these structures when reacted with a low ionic strength electrolyte solution in flow-through columns;

(3) A flow-through column study examining aging effects on Hanford sediments reacted with caustic waste and implications for Cs and Sr sequestration.

Through the combination of laboratory experimentation, micro- and macro-scale measurements, and reactive transport modeling, the studies presented in this dissertation help elucidate processes in order to gain a better understanding of the mechanisms needed to properly predict fate and mobility of Sr and Cs.

REFERENCES

Ahearne, J.F. (1997) Radioactive waste: The size of the problem. Physics Today, 50(6), 24-29.

Bickmore, B.R., Nagy, K.L., Young, J.S., and Drexler, J.W. (2001) Nitrate-Cancrinite Precipitation on Quartz Sand in Simulated Hanford tank Solutions. Environmental Science and Technology, 35, 4481-4486.

Bostick, B.C., Vairavamurthy, M.A., Karthikeyan, K.G., and Chorover, J. (2002) Cesium adsorption on clay minerals: An EXAFS spectroscopic investigation. Environmental Science & Technology, 36(12), 2670-2676.

Bowers, G.M., Ravella, R., Komarneni, S., and Mueller, K.T. (2006) NMR study of strontium binding by a micaceous mineral. Journal Of Physical Chemistry B, 110(14), 7159-7164.

Chang, H.-s., Um, W., Rod, K., Serne, R.J., Thompson, A., Perdrial, N., Steefel, C.I., and Chorover, J. (2011) Strontium and Cesium Release Mechanisms during Unsaturated Flow through Waste-Weathered Hanford Sediments. Environmental Science & Technology, 45(19), 8313-8320.

Choi, S., Amistadi, M.K., O'Day, P., and Chorover, J. (2005a) Desorption of contaminant Cs and Sr from clay systems after weathering in caustic waste solutions. Geochimica Et Cosmochimica Acta, 69(10), A812-A812.

Choi, S., Crosson, G., Mueller, K.T., Seraphin, S., and Chorover, J. (2005b) Clay mineral weathering and contaminant dynamics in a caustic aqueous system - II. Mineral transformation and microscale partitioning. Geochimica et Cosmochimica Acta, 69(18), 4437-4451.

Choi, S., O'Day, P.A., Rivera, N.A., Mueller, K.T., Vairavamurthy, M.A., Seraphin, S., and Chorover, J. (2006) Strontium speciation during reaction of kaolinite with simulated tank-waste leachate: Bulk and microfocused EXAFS analysis. Environmental Science & Technology, 40(8), 2608-2614.

Chorover, J., Choi, S., Amistadi, M.K., Karthikeyan, K.G., Crosson, G., and Mueller, K.T. (2003a) Linking Cesium and Strontium uptake to Kaolinite weathering in simulated tank waste leachate. Environmental Science and Technology, 37(10), 2200-2208.

Chorover, J., Choi, S., Rotenberg, P., Serne, R.J., Rivera, N., Strepka, C., Thompson, A., Mueller, K.T., and O'Day, P.A. (2008) Silicon control of strontium and cesium partitioning in hydroxide-weathered sediments. Geochimica Et Cosmochimica Acta, 72(8), 2024-2047.

Crosson, G.S., Choi, S., Chorover, J., Amistadi, M.K., O'Day, P.A., and Mueller, K.T. (2006) Solid-State NMR Identification and Quantification of Newly Formed Aluminosilicate Phases in Weathered Kaolinite Systems Journal of Physical Chemistry B, 110(2), 723-732.

Crowley, K.D. (1997) Nuclear waste disposal: The technical challenges. . Physics Today, 50, 32-39.

DOE. (1995) Closing the Circle on the Splitting of the Atom: The Environmental Legacy of Nuclear Weapons Production in the United States and What the Department of Energy is Doing About it. U.S. Department of Energy. Washington, D.C. (DOE/EM-0266) Department of Energy Officeof Environmental Management.

Flury, M., Czigany, S., Chen, G., and Harsh, J.B. (2004) Cesium migration in saturated silica sand and Hanford sediments as impacted by ionic strength. Journal Of Contaminant Hydrology, 71(1-4), 111-126.

Fritz, B.G., and Patton, G.W. (2006) Monitoring iodine-129 in air and milk samples collected near the Hanford Site: an investigation of historical iodine monitoring data. Journal Of Environmental Radioactivity, 86(1), 64-77.

Gee, G.W., Oostrom, M., Freshley, M.D., Rockhold, M.L., and Zachara, J.M. (2007) Hanford Site Vadose Zone Studies: An Overview. Vadose Zone Journal, 6(4), 899-905.

Gephart, R. (2003) A short history of Hanford waste generation storage and release., p. 1-39. Pacific Northwest National Laboratory.

Gephart, R., and Lundgren, R. (1998) Hanford tank clean up: A guide to understanding technical issues., p. 1-71, Columbus, Ohio.

Grossman, C.M., Morton, W.E., and Nussbaum, R.H. (1996) Hypothyroidism and spontaneous abortions among Hanford, Washington, Downwinders. Archives Of Environmental Health, 51(3), 175-176.

Hakem, N.L., Al Mahamid, I., Apps, J.A., and Moridis, G.J. (2000) Sorption of cesium and strontium on Hanford soil. Journal Of Radioanalytical And Nuclear Chemistry, 246(2), 275-278.

Hansen, B.O., Kwan, P., Benjamin, M.M., Li, C.W., and Korshin, G.V. (2001) Use of iron oxide-coated sand to remove strontium from simulated hanford tank wastes. Environmental Science & Technology, 35(24), 4905-4909.

Hassan, N.M., Nash, C.A., Hardy, B.J., and Marra, J.C. (2003) Evaluating the residence time for cesium removal from simulated Hanford tank wastes using SuperLig[(R)] 644 resin. Journal of Radioanalytical and Nuclear Chemistry, 258(3), 487-495.

Heeb, C.M., Gydesen, S.P., Simpson, J.C., and Bates, D.J. (1996) Reconstruction of radionuclide releases from the Hanford Site, 1944-1972. Health Physics, 71(4), 545-555.

Jackson, R.R. (1977) Hanford Waste Encapsulation - Strontium And Cesium. Nuclear Technology, 32(1), 10-15.

Liu, C., Zachara, J.M., Qafoku, O., and Smith, S.C. (2003a) Effect of temperature on Cs^+ sorption and desorption in subsurface sediments at the Hanford site, U.S.A. Environmental Science and Technology, 37, 2640-2645.

Liu, C.X., Zachara, J.M., and Smith, S.C. (2004) A cation exchange model to describe Cs+ sorption at high ionic strength in subsurface sediments at Hanford site, USA. Journal Of Contaminant Hydrology, 68(3-4), 217-238.

Liu, C.X., Zachara, J.M., Smith, S.C., McKinley, J.P., and Ainsworth, C.C. (2003b) Desorption kinetics of radiocesium from subsurface sediments at Hanford Site, USA. Geochimica Et Cosmochimica Acta, 67(16), 2893-2912.

Liu, J., Polak, A., Elsworth, D., and Grader, A. (2005a) Dissolution-induced preferential flow in a limestone fracture. Journal of Contaminant Hydrology, 78, 53-70.

Liu, Q.Y., Xu, H.W., and Navrotsky, A. (2005b) Nitrate cancrinite: Synthesis, characterization, and determination of the enthalpy of formation. Microporous And Mesoporous Materials, 87(2), 146-152.

Mashal, K., Cetiner, Z.S., Flury, M., and Harsh, J.B. (2005) Colloid formation and cesium mobility in Hanford sediment columns leached with simulated tank waste. Geochimica Et Cosmochimica Acta, 69(10), A816-A816.

Mashal, K., Harsh, J.B., and Flury, M. (2005b) Clay mineralogical transformations over time in hanford sediments reacted with simulated tank waste. Soil Science Society Of America Journal, 69(2), 531-538.

Mashal, K., Harsh, J.B., Flury, M., and Felmy, A.R. (2005c) Analysis of precipitates from reactions of hyperalkaline solutions with soluble silica. Applied Geochemistry, 20(7), 1357-1367.

Mashal, K., Harsh, J.B., Flury, M., Felmy, A.R., and Zhao, H.T. (2004a) Colloid formation in Hanford sediments reacted with simulated tank \waste. Environmental Science & Technology, 38(21), 5750-5756.

McKinley, J.P., Zachara, J.M., Heald, S.M., Dohnalkova, A., Newville, M.G., and Sutton, S.R. (2004) Microscale distribution of cesium sorbed to biotite and muscovite. Environmental Science & Technology, 38(4), 1017-1023.

McKinley, J.P., Zeissler, C.J., Zachara, J.M., Serne, R.J., Lindstrom, R.M., Schaef, H.T., and Orr, R.D. (2001) Distribution and Retention of ^{137}Cs in Sediments at the Hanford Site, Washington. Environmental Science & Technology, 35(17), 3433-3441.

Mon, J., Deng, Y.J., Flury, M., and Harsh, J.B. (2005) Cesium incorporation and diffusion in cancrinite, sodalite, zeolite, and allophane. Microporous And Mesoporous Materials, 86(1-3), 277-286.

Moran, J.E., Oktay, S., Santschi, P.H., and Schink, D.R. (1999) Atmospheric dispersal of (129)iodine from nuclear fuel reprocessing facilities. Environmental Science & Technology, 33(15), 2536-2542.

Perdrial, N., Rivera, N., Thompson, A., O'Day, P.A., and Chorover, J. (2011) Trace contaminant concentration affects mineral transformation and pollutant fate in hydroxide-weathered Hanford sediments. Journal of Hazardous materials, 197, 119-127.

Rivera, N., Choi, S., Strepka, C., Mueller, K., Perdrial, N., Chorover, J., and O'Day, P. (2011) Cesium and strontium incorporation into zeolite-type phases during homogeneous nucleation from caustic solutions. American Mineralogist, 96(11-12), 1809-1820.

Routson, R.C., Barney, G.S., and Smith., R.M. (1981) Hanford sites sorption studies for the control of radioactive wastes: A review. Nuclear Technology, 54, 100-106.

Samson, S.D., Nagy, K.L., and Cotton, W.B. (2005) Transient and quasi-steady state dissolution of biotite at 22-25° C in high pH, sodium, nitrate, and aluminate solutions. Geochimica et Cosmochimica Acta, 69(2), 399-413.

Serne, R.J., Zachara, J.M., and Burke, D.S. (1998) Chemical information on tank supernatants, Cs adsorption from tank liquids onto Hanford sediments, and field observations of Cs migration from past tank leaks. PNNL-11495 UC-510 Pacific Northwest National Laboratory, Richland, Washington 99352.

Steefel, C.I., Carroll, S., Zhao, P.H., and Roberts, S. (2003) Cesium migration in Hanford sediment: a multisite cation exchange model based on laboratory transport experiments. Journal Of Contaminant Hydrology, 67(1-4), 219-246.

Thompson, A., Steefel, C.I., Perdrial, N., and Chorover, J. (2010) Contaminant Desorption during long-term leaching of hydroxide-weathered Hanford sediments. Environmental Science and Technology, 44, 1992-1997.

Um, W., and Serne, R.J. (2005) Sorption and transport behavior of radionuclides in the proposed low-level radioactive waste disposal facility at the Hanford site, Washington. Radiochimica Acta, 93(1), 57-63.

Wagner, B.K., Garrett, P.E., Yeh, M., and Yates, S.W. (1997) On the first excited state of ^{137}Ba. Journal Of Radioanalytical And Nuclear Chemistry, 219(2), 217-220.

Wan, J., Tokunaga, T.K., Larsen, J.T., and Serne, R.J. (2004) Geochemical evolution of highly alkaline and saline tak waste plumes during seepage through vadose zone sediments. Geochimica et Cosmochimica Acta, 68(3), 491-502.

Wendling, L.A., Harsh, J.B., Ward, T.E., Palmer, C.D., Hamilton, M.A., Boyle, J.S., and Flury, M. (2005) Cesium desorption from lllite as affected by exudates from rhizosphere bacteria. Environmental Science & Technology, 39(12), 4505-4512.

Zachara, J.M., Serne, J., Freshley, M., Mann, F., Anderson, F., Wood, M., Jones, T., and Myers, D. (2007) Geochemical Processes Controlling Migration of Tank Wastes in Hanford's Vadose Zone. Vadose Zone Journal, 6(4), 985-1003.

Zachara, J.M., Smith, S.C., Liu, C., McKinley, J.P., Serne, R.J., and Gassman, P.L. (2002a) Sorption of Cs+ to micaceous subsurface sediments from the Hanford site, USA. Geochimica et Cosmochimica Acta, 66(2), 193-211.

Zachara, J.M., Smith, S.C., Serne, R.J., McKinley, J.P., and Gassman., P.L. (2002b) Sorption of Cs^+ to micaceous subsurface sediments from the Hanford site, USA. Geochimica et Cosmochimica Acta, 66, 193-211.

Zhao, H.T., Deng, Y.J., Harsh, J.B., Flury, M., and Boyle, J.S. (2004) Alteration of kaolinite to cancrinite and sodalite by simulated hanford tank waste and its impact on cesium retention. Clays And Clay Minerals, 52(1), 1-13.

Zhuang, J., Flury, M., and Jin, Y. (2003) Colloid-Facilitated Cs Transport through water-saturated Hanford sediment and Ottawa sand. Environmental Science and Technology, 37, 4905-4911.

Zhuang, J., Jin, Y., and Flury, M. (2004) Comparison of Hanford colloids and kaolinite transport in porous media. Vadose Zone Journal, 3(2), 395-402.

Chapter 2: Cesium and strontium incorporation into zeolite-type phases during homogeneous nucleation from caustic solutions

published in:

American Mineralogist, vol. 96 (11-12), p.1809-1820 (2011)

Authors: Nelson Rivera[1*], Sunkyung Choi[2], Caleb Strepka[3], Karl Mueller[3], Nicolas Perdrial[4], Jon Chorover[4], and Peggy A. O'Day[1]

[1]5200 N. Lake Rd, School of Natural Sciences, University of California, Merced, CA, 95343

[2]US EPA, Natl Risk Management Res Lab, Ada, OK 74820

[3]Department of Chemistry, Pennsylvania State University, University Park, Pennsylvania 16802

[4]Department of Soil, Water and Environmental Science, University of Arizona, Tucson, Arizona 85721

*corresponding author e-mail:nrivera@ucmerced.edu; phone:209-228-4393 fax: 209-228-4047

ABSTRACT

Formation of faujasite- and sodalite/cancrinite-type phases associated with caustic waste reactions in the environment may structurally incorporate contaminant species such as radioactive Sr^{2+} and Cs^+, and thus provide a mechanism of attenuation. In order to investigate mineral evolution and structural incorporation of cations in simplified experiments, aluminosilicate solids were precipitated homogeneously at room temperature from batch solutions containing a 1:1 molal ratio of Si to Al and 10^{-3} molal Sr and/or Cs, and aged for 30 or 548 d. Syntheses were done with solutions in equilibrium with atmospheric CO_2 and with gas-purged solutions. Experimental products were characterized by bulk chemical analyses, chemical extractions, XRD, SEM/TEM, TGA, solid-state ^{27}Al NMR, and Sr EXAFS. Chemical analysis showed that solids had a 1:1 Al:Si molar ratio, and that Sr was sequestered at higher amounts than Cs. After 30 d of aging in purged solutions, XRD showed that zeolite X (faujasite-type) was the only crystalline product. After aging 30 and 548 d in solutions equilibrated with atmospheric CO_2, a mixture of sodalite, cancrinite, and minor zeolite X were produced. Surface areas of solids at 30 d were much lower than published values for zeolite phases synthesized at high temperature, although particle aging produced more crystalline and less aggregated phases with higher bulk surface areas. Characterization of products by ^{27}Al NMR indicated only tetrahedrally coordinated Al. Measured isotropic shifts of primary resonances did not change substantially with precipitate aging although the primary mineral phase changed from zeolite X to sodalite/cancrinite, indicating local ordering of Al-Si tetrahedra. Analysis of reaction products by Sr EXAFS suggested Sr bonding in hexagonal prisms and six-membered rings of the supercages of zeolite X that may be more site-specific than those of monovalent cations. For samples aged for 548 d, interatomic distances from Sr-EXAFS are consistent with partial Sr

dehydration and bonding to framework oxygen atoms in sodalite cages or in large channels in cancrinite. Incorporation of Sr into both faujasite and sodalite/cancrinite phases is favored over Cs during room temperature synthesis, possibly because of increased cation site competition between Cs^+ and Na^+. Results of this study help to constrain cation incorporation into sodalite/cancrinite mineral assemblages that form at caustic waste-impacted field sites and may aid in the predictive modeling of contaminant release.

Keywords: Zeolite X, Sodalite, Cancrinite, Strontium, Cesium

1. INTRODUCTION

Zeolite and feldspathoid phases have been proposed to form in the environment at locations where caustic (pH > 13), high ionic strength, Al-rich waste solutions containing a variety of metal and radionuclide contaminants have reacted with subsurface sediments (Bickmore et al., 2001; Mashal et al., 2005a; Qafoku et al., 2003a; Zachara et al., 2002). Such solutions have been unintentionally released to the environment at locations such as the DOE Hanford site (WA, USA), a former nuclear weapons processing facility (Gephart, 2003; Gephart and Lundgren, 1998). Of particular interest are ^{90}Sr and ^{137}Cs, which account for the majority of radioactivity released at the Hanford site from leaking tanks (Behrens et al., 1998; Serne et al., 2002). Attenuation of these contaminants in the subsurface, either by adsorption by high surface area minerals such as clays or zeolites, or by mineralogical transformations associated with dissolution-precipitation processes, have been identified as critical mechanisms for the understanding and prediction of long-term contaminant behavior (Zachara et al., 2007).

Prior laboratory studies examining reaction of simulated tank wastes with model systems (quartz sand, biotite, reference clays) (Bickmore et al., 2001; Choi et al., 2005a; Choi et al.,

2005b; Choi et al., 2006; Chorover et al., 2003; Crosson et al., 2006; Um et al., 2005) and natural sediments (Ainsworth et al., 2005; Chorover et al., 2008; Mashal et al., 2005a; Mashal et al., 2005b; Perdrial et al., in review; Qafoku et al., 2003a; Qafoku et al., 2003b; Qafoku et al., 2004; Wan et al., 2004a; Wan et al., 2004b) have shown that a variety of aluminosilicate reaction products may form and potentially incorporate radioactive contaminants. Differences among product phases and cation uptake that have emerged from prior experimental investigations depend on (1) whether dissolved Si in the system is limited by release from weathering of primary Si-bearing phases (quartz, feldspar, or phyllosilicate), or is added to the experimental system at high concentration (similar to the concentration of dissolved Al); and (2) whether dissolved CO_2 is present at ambient levels or at higher concentrations from the dissolution of carbonate phases, or excluded from the aqueous and gas phases of the experimental system. These two factors, together with reaction time, appear to influence the kinetic pathways of product formation in addition to expected differences from thermodynamic considerations based on solution composition. The studies cited above have identified the feldspathoid phases cancrinite and sodalite, a number of zeolite phases, and other unidentified aluminosilicate phases as products of these base-neutralization reactions.

Feldspathoids and zeolites are large, diverse classes of minerals characterized by a crystalline framework of tetrahedral Al and Si with a three-dimensional pore system, multiple cation sites within cages and pores, and the ability to host different cations with various ion sizes and charges (Barrer, 1984; Bonaccorsi and Merlino, 2005; Depmeier, 2005; Frising and Leflaive, 2008). Because of the importance of zeolite-type phases as industrial catalysts and molecular sieves, their synthesis and stability under controlled laboratory conditions and often at hydrothermal temperatures (60-1000 °C) has been widely studied (Barrer, 1984; Davis and

Lobo, 1992; Navrotsky et al., 1995). Most investigations under controlled conditions, however, have been designed to optimize zeolite performance for industrial applications, and therefore do not specifically address the unique conditions of aluminosilicate formation and ion incorporation posed by caustic waste release in the environment.   Likewise, few studies have examined changes in zeolite-type product phases and cation sequestration on temporal scales relevant to the Earth's surface environment (e.g., Valtchev et al., 2005a; Valtchev et al., 2005b).

In this study, we characterized solids in a simplified experimental system, caustic Na-nitrate-hydroxide solutions at room temperature with 1:1 molal ratios of Al:Si, in order to examine the structural incorporation of dissolved Sr and Cs into product zeolite and feldspathoid phases in the presence or absence of dissolved CO_2 at relatively long aging time (1 month and 1.5 years). Prior work by Deng et al. (2006) examined solid phases produced from similar types of caustic Hanford solutions (up to 32 weeks), but their work focused on the structure-directing role of anions on products from Na-only solutions rather than on contaminant cation uptake. We focus in particular here on the structural incorporation of Sr^{2+} into neoformed aluminosilicate phases. As a divalent cation with a high hydration energy and affinity for complexation with carbonate (Chorover et al., 2008; Sahai et al., 2000), Sr^{2+} behaves differently from Na^+ and Cs^+ in caustic solutions. Identification of the mode(s) of incorporation of Sr and Cs into reaction products, in particular whether they are readily exchanged or irreversibly bound, is important for providing a mechanistic basis for the reactive transport modeling of contaminant release in complex systems.

8

2. EXPERIMENTAL METHODS

2.1 Synthesis

Nalgene[TM] polypropylene co-polymer (PPCO) vessels were used instead of glassware at all stages of the experiment to prevent Si contamination. Stock solutions were prepared using ultra-pure (MilliQ[TM]) water and reagent grade $NaNO_3$, $NaOH$, $CsCl$, $SrCl_2 \cdot 6H_2O$ (J.T. Baker) and $NaAlO_2 \cdot xH_2O$ powder (EM Science) as obtained from the manufacturer. Synthesis solutions similar to the synthetic tank waste leachate (STWL) described previously (Choi et al., 2006; Chorover et al., 2008; Crosson et al., 2006; Thompson et al., 2010) were prepared in batch on a mass basis (mol/kg solvent) with a total solvent weight (water) of 25 g. Solutions with atmospheric CO_2 (referred to as $+CO_2$) were not degassed at any step of the synthesis and consisted of 0.05 m Al^{3+}, 2.0 m Na^+, 1.0 m NO_3^-, and 1.0 m OH^- (pH ~13.7), and either 10^{-3} m Cs^+ or 10^{-3} m Sr^{2+}, both Cs^+ and Sr^{2+} (10^{-3} m each), or neither (Na only). For both sets of synthesis, chloride salts were used for Sr and Cs. This produced small differences in chloride concentration (0 mm for Na only to 3 mm for Sr+Cs). Each solution was then spiked with 0.05 m colloidal SiO_2 (from 40% w/w Ludox solution W.R. Grace and Co.), which resulted in immediate formation of a visible precipitate. Suspensions were shaken initially to ensure homogenization, but no other agitation of the solution was done during aging at ambient room temperature. Solutions and their precipitates were aged in individual batch experiments for 4 h, 3 d, 30 d, and 548 d. Typical solid yield was 0.2-0.3 g (8-12 g kg^{-1} STWL), which limited the extent of characterizations that could be performed.

Precipitates from batch, low CO_2 solutions (referred to as $-CO_2$) consisted of purging the initial water (400 g) for 24 hours with N_2 gas to remove carbon dioxide. The solution was further purged for 10 minutes after the addition of each reagent salt (same as above) to the water.

Solutions were prepared with either 10^{-3} m Cs^+ or 10^{-3} m Sr^{2+}, both Cs^+ and Sr^{2+} at 10^{-3} m each (duplicate samples denoted A and B), or neither (Na only). After the addition of the colloidal silica (stock solution not purged), the container was filled with a N_2 gas in the head space and aged for 30 d. No other measures were taken to exclude CO_2 from the system and dissolved CO_2 was not measured. Typical solid yield was 2.5-3.0 g (6.25-7.5 g kg^{-1} STWL). For all samples after the specified aging time, suspensions were centrifuged and supernatant solutions decanted. Solid precipitates were washed three times with 95% ethanol and then air dried.

2.2 Digestions and extractions

Complete dissolution of all product solids was done by concentrated hydrofluoric acid (HF) digestion at room temperature. Triplicate digestions were performed on 30 d $-CO_2$ (0.1 g) and on 548 d $+CO_2$ (0.02 g) precipitates for 2 h at a 1:50 solid-to-solution ratio. Selected samples with sufficient mass were also digested with hydrochloric acid (HCl) at high temperature to assess sample recalcitrance. Triplicate 30 d $-CO_2$ samples (0.1 g) and single 548 d $+CO_2$ Sr+Cs and Sr samples (0.02 g) were digested in 12 ml of 12 M trace-metal-grade HCl for 1 h at 200° C in an Anton Paar Multiwave 3000 digestion unit.

A two-step sequential extraction was performed on 30 d $-CO_2$ samples: (1) 1.0 M $MgCl_2$ (solution pH = 8) to target exchangeable sites; (2) 0.2 M ammonium oxalate/oxalic acid (AAO, solution pH = 3) to target poorly crystalline solids. Triplicate extractions (in the dark) were performed by reacting 0.03 g of solid with 10 ml of each extractant for 2 h, with a 30-min DI water wash between each step. Extractions of 548 d $+CO_2$ samples were not done because of limited sample mass. A 10^{-2} M H_3PO4, room-temperature extraction (2 h, pH 2, 1:100 solid to solution ratio) was performed on a separate split of a sample to remove carbonate solids that may have precipitated (Gilg et al., 2003; Weliky et al., 1983).

10

2.3 Chemical analysis

Element concentrations were measured by ICP-MS (Agilent 7500cs) for Sr, Cs, Al, and Si. The ICP-MS was run in a soft extraction mode with 1500 W RF power and a PFA introduction system. The system was optimized to keep oxide and doubly charged interferences below 2%. A H_2 collision cell was used to measure Si (detection limit 30 ppb) to limit N and O based interferences at mass 28. A He collision cell was used to measure the Sr, Cs, and Al. Low-level quantification of Sr and Cs resulted in a detection limit of 0.1 ppb for both elements and detection limits for Al of 25 ppb.

2.4 Solid phase characterizations

X-ray diffraction (XRD) data were collected on a PANalytical X'pert Pro diffractometer with an ultra-fast X'Celerator detector. Samples were mounted on zero-background Si holders and scanned from 4 to 75 degrees 2θ at 0.01-degree 2θ steps with a Co K-α source ($\lambda = 1.78$ Å). Quantitative XRD phase analysis was performed with the Rietveld module in the X'Pert HighScore Plus software using an internal library of structures taken from the literature. Analyses were based on the refinement of the structure of a Na-faujasite (Baur, 1964), two structures of sodalite (Ballirano and Maras, 2005; Buhl and Lons, 1996), and two structures of cancrinite (Buhl et al., 2000; Fechtelkord et al., 2001b). This method is accurate for phases that are > 0.5% of the total diffraction pattern (Hill et al., 1986; Wiles and Young, 1981). For Rietveld analyses, a loading of more than 20 mg/cm^2 was used for each sample to produce an "infinitely" thick sample (Stanjek and Häusler, 2004). Results were normalized to 100%.

Representative samples were examined by transmission electron microscopy (TEM). Ten μL of a 100 mg l^{-1} suspension of synthesis product in nanopure water was dropped on 200-

mesh Cu grids, air dried, and imaged using a Hitachi H8100 LaB6 TEM (University of Arizona) operating at 200 kV.

Surface area measurements by the BET method were performed using a Micrometrics 300 surface area analyzer. Samples were dried in a heating block at 110 °C to remove sorbed water. Ultra-high purity N_2 gas was used for all measurements. Five points were collected in the measurement and the isotherm was analyzed using the Tri-Star 3000 software from Micrometrics.

Thermogravimetric analyses were made with a dual beam SDT Q600 analyzer (TA instruments). Samples were placed in an alumina sample cup (10-20 mg) alongside an empty alumina cup as a reference. The samples were heated at a rate of 10°C/min in a temperature range of 30-1000° or 30-1500° C under ultra-high purity N_2 gas.

2.4.1 [27]Al nuclear magnetic resonance (NMR)

Magic-angle spinning (MAS) NMR experiments were preformed on a Varian/Chemagnetics Infinity-500 spectrometer with an 11.7 T magnet (^{1}H resonance frequency of 500 MHz). The low-frequency channel of a 3.2 mm HX double-resonance MAS probe was used at a frequency of 130.255 MHz for [27]Al measurements. Single-pulse [27]Al free induction decays (FID) were acquired after a radio frequency pulse of 0.6 μs (corresponding to an approximate tip angle of π/20). The spinning rate was approximately 15 kHz, and for each sample, 4800 transients were acquired using a recycle delay of 1 s, which allowed for good signal-to-noise ratios in the resulting frequency domain spectra. The FIDs were processed with Fourier transformation following the application of an exponential weighting in the time domain equivalent to 50 Hz of Lorentzian line broadening in the frequency spectra. The [27]Al shifts (in ppm) are reported with respect to the octahedral [27]Al resonance from a 1 M aqueous sample of

$AlCl_3$. Based on the shapes of the resonances and knowledge from previous data reduction (Crossen et al., 2006), the overlapping resonances in the tetrahedral region were modeled with four mixed Lorentzian/Gaussian lines allowing the overall shift position, linewidth, and percentage of Gaussian character to vary until a minimum in variance from the measured lineshape was achieved. Sufficient signal-to-noise could not be obtained for ^{29}Si NMR due to limited sample volume.

2.4.2 Strontium extended X-ray absorption fine structure (EXAFS) spectroscopy

Strontium K-edge X-ray absorption spectra were acquired at the Stanford Synchrotron Radiation Lightsource (SSRL) on beamline 11-2 under dedicated conditions (3 GeV, 80-100 mA) using a focused beam. Spectra were collected using Si(220) monochromator crystals (beam size = 1 mm vertical x 8 mm horizontal). A rhodium mirror (17 keV cutoff energy) was used for harmonic rejection, allowing for a fully tuned beam. Beam energy was calibrated on a $SrCO_3$(s) standard with the energy at the midpoint of the absorption edge set to 16,105 eV. Samples were held in a He cryostat at 3-5 K. Absorption spectra were collected using a 30-element solid-state Ge-array detector for fluorescence and a gas-filled ion chamber for transmission.

Averaged and unsmoothed EXAFS spectra were analyzed using the EXAFSPAK software packages (George and Pickering, 2000). Background was subtracted using a linear fit through the pre-edge region. Spectra were normalized to the average height of the post-edge absorbance oscillations and fit with a cubic spline above the absorption edge ($E_0 = 16115$ eV) to isolate the EXAFS. Normalized EXAFS spectra were fit by non-linear least-squares methods on individual atomic shells in k-space using the entire k-range in the fit (O'Day et al., 2000). Theoretical phase-shift and amplitude functions were calculated with the program FEFF v 8.4 (Ankudinov et al., 2003) using atomic clusters calculated with the program ATOMS (Ravel,

2001). The amplitude reduction factor (S_0^2) was fixed at 1.0. The difference in the

photoelectron threshold energy between the reference functions and data (ΔE_o) was an adjustable

component fit as a single parameter applied at the same value to all shells in a fit. Debye-waller

factors were fixed in all fits based on previous studies (Choi et al., 2006; Chorover et al., 2008;

O'Day et al., 2000), while the distance (R) and number of backscattering atoms (N) were varied

in the fits. Second-neighbor Al and Si cannot be distinguished by EXAFS analysis because of

their similar atomic mass and are indicated by Al/Si. Based on empirical fits to known reference

compounds, estimated errors were R ± 0.01 Å, N or σ^2 ± 15% for the first coordination shell, and

R ± 0.02Å, N or σ^2 ± 25% for atoms beyond the first shell (O'Day et al., 2000). Reported

reduced χ^2 values give a statistical goodness-of-fit between the model and data, but do not

indicate the accuracy of the fit.

3. RESULTS

3.1 Contaminant uptake and extractions

Incorporation of Sr and Cs into reaction products was determined by digestion and

analysis of solids (aqueous concentrations were not measured). Total digestions with HF showed

much higher uptake of Sr from solution (92-118 mmol/kg) than Cs (4.9-14 mmol/kg), which

corresponds to 32-84% Sr and 3.5-10% Cs uptake from solution (based on an initial

concentration of 10^{-3} m for each element) (Table 1 and Fig. 1). Overall, solids aged for 548 d

contained less Sr than those aged for 30 d, but the opposite trend was observed with Cs. At both

30 d and 548 d, samples synthesized from Sr+Cs solutions contained more Sr than those

synthesized with Sr-only solutions. Solid products from solutions with Cs only had less Cs

uptake than reaction products from Sr+Cs solutions at 30 d, but more uptake at 548 d. The Al/Si

molar ratios for solids were approximately 1:1 in all samples (within analytical error, Table 1). Concentrations of Sr and Cs measured in HCl digestions were uniformly lower than those determined in HF digestions (Fig. 1), indicating a recalcitrant solid fraction that sequestered ~10-30% of Sr and ~1-3% of Cs taken up from solution. A residual white solid was observed in the reaction vessel after the HCl digestions. The solid was not characterized, but was assumed to be Si-rich due to the low Si recovery from the digested solids compared to Al concentrations (Table 1).

Sequential extractions performed on 30 d $-CO_2$ samples showed that the $MgCl_2$ extraction step removed 7-20% more Sr than the AAO extraction step (46-52 mmol/kg vs. 30-38 mmol/kg). However, the summation of the two extractions did not achieve 100% recovery of Sr when compared to HF digestion. The opposite effect was seen for Cs. Less Cs was removed in the $MgCl_2$ extraction than in the AAO extraction (1-3 mmol/kg vs. 3-5 mmol/kg). Total Cs concentrations from sequential extractions ($MgCl_2$ + AAO steps) were within analytical error of total concentrations determined by HF digestion. Total Si (87%) and Al (83%) from sequential extractions were on average lower than concentrations measured in HF digestions, but extracted Si was systematically higher than extracted Al.

Extractions with H_3PO_4, which were intended to dissolve carbonate phases, removed the least amount of Sr and Cs compared to all of the methods. The amount of Sr extracted for all samples ranged from 0.03-1.2% of total Sr (determined from HF digestion), with the highest fraction from a 30 d $-CO_2$ Sr-only sample (1.4 mmol/kg). In all other samples, 20-30 times less Sr (0.023-0.075 mmol/kg) was extracted by H_3PO_4. Extracted Al was low for all solids, less than 0.6% of total Al. For 30 d samples, 0.6-6% of total Si was extracted, while up to 17% of total Si was extracted in 548 d samples (Table 1).

15

3.2 X-ray diffraction (XRD)

The synthesis products showed mineralogical differences between $+CO_2$ and $-CO_2$ preparations after 30 d of aging. All $-CO_2$ samples contained only faujasite-type phases (matched best to reference zeolite X), but the intensity of reflections was much lower for the Na-only sample than for samples containing Sr and/or Cs (Fig. 2), precluding Rietveld refinement. Whereas $+CO_2$ samples were composed mostly of cancrinite and sodalite with minor amounts of zeolite X (Fig. 2). Cancrinite was the most abundant phase in Sr+Cs (68%) and Na-endmember (61%) samples based on quantitative Rietveld simulations, whereas sodalite was more abundant (59%) in the Sr-only precipitate (Table 2). In the Na-endmember, no zeolite X was detected, and the cancrinite fraction was higher than the sodalite fraction (39% vs. 27%). In the Sr+Cs and Sr-only samples, the zeolite X fraction was 5-10%.

At 548 d in $+CO_2$ samples, the proportions of phases differed when Sr was present in the precipitate (Sr+Cs or Sr only) compared with no Sr (Cs or Na-endmember). Samples with Sr had cancrinite as the major phase (58-61%) and about 3% zeolite X, compared to Cs and Na-endmember samples with approximately equal proportions of sodalite and cancrinite, and no measurable zeolite X (Table 2). Diffractograms of 4-h and 3-d aged $+CO_2$ samples are not shown because the samples exhibited no diffraction peaks. No other crystalline phases, such as $SrCO_3(s)$, strontium hydrogarnet ($Sr_3Al_2(O_4H_4)_3(s)$), or strontium hydroxide ($Sr(OH)_2(s)$, see below), were detected in either $-CO_2$ or $+CO_2$ samples at any time step.

3.3 Particle Size and Morphology

Surface area analysis of precipitates by the BET method (Table 3) showed that 30 d $-CO_2$ samples had lower average surface areas than those reported in the literature for similar phases. Samples in which only zeolite X was identified by XRD had surface areas (1.7-6.1 m^2/g) two

orders-of-magnitude lower than values reported in the literature (300-850 m^2/g) (Linares et al., 2005; Maurin et al., 2005; Ocanto et al., 2008; Yagi et al., 1997). The surface area measured for the Cs-only solid at 30 d was three times higher than for the Sr-only solid. At 548 d, solids with sodalite and cancrinite had surface areas of 10.1-17.2 m^2/g, within range of reported literature values (10-60 m^2/g) (Linares et al., 2005; Maurin et al., 2005; Ocanto et al., 2008), and the Cs-only sample had the lowest surface area (Table 3).

Particle images from TEM exhibited morphologies consistent with formation of both zeolite X and sodalite/cancrinite minerals (Fig. 3) (Bickmore et al., 2001; Deng et al., 2006; Liu and Navrotsky, 2007; Liu et al., 2005; Ocanto et al., 2008; Shanbhag et al., 2009; Tanaka et al., 2002; Valtchev et al., 2007). At 30 d, precipitate morphology differed among samples as a function of solution composition (Fig. 3 a-c). Particles in the Sr-only sample had well-defined cubic crystals (Fig. 3b), whereas those in the Cs-only sample lacked cubic morphology and had some particles with needle-like habits which are possible precursors to a sodalite structure (Fig. 3c). Particles precipitated from Sr+Cs solutions showed both well-defined cubic crystals and needle-like forms. The Sr+Cs sample aged for 548 d (Fig. 3d) had a different morphology than those at 30 d, which showed spherical particles with columnar intergrowths. Particles synthesized at room temperature in this study exhibit less crystalline morphologies than particles synthesized at elevated temperature in published studies (Bickmore et al., 2001; Deng et al., 2006; Liu and Navrotsky, 2007).

3.4 Thermogravimetric Analysis (TGA)

Mass loss from solids aged for 30 and 548 d showed that $-CO_2$ samples had a larger mass loss (20-25%) over the first 650°C of temperature increase than did $+CO_2$ samples (6-10%) (Fig. 4a). Between 650 and 950° C, $+CO_2$ samples showed an increase in volatilization, with an

17

additional 9% mass loss over this range compared to 2% loss in the $-CO_2$ samples. Derivative

thermogravimetric data (mass % per °C) for 30 d Sr+Cs ($-CO_2$, $+CO_2$) and 548 d Sr+Cs ($+CO_2$)

samples (Fig. 4b) indicate two main regions of weight loss, 100°-350°C and 650°C-1000°C. The

first loss region is associated with water loss from the structure. Between 650°C -1000°C,

volatilization behavior differed among the three samples. The 30 d $-CO_2$ sample shows peaks at

~ 775° and ~ 975 °C. The first peak is assigned to the release of nitrate and the destruction of the

supercell of zeolite X, and the second peak is assigned to carbonate volatilization (Linares et al.,

2005; Ocanto et al., 2008). Analysis by XRD (not shown) showed a conversion from zeolite X

to nepheline ($NaAlSiO_4$) after heating this sample to 1000°C. The 30 d $+CO_2$ sample had three

volatilization events at 600°C, 775°C, and 950°C that were assigned to hydroxyl, nitrate, and

carbonate loss, respectively (Buhl, 1991a; Fechtelkord et al., 2001b; Hassan, 1996; Hassan et al.,

2006; Liu et al., 2005). Mass loss for 548 d $+CO_2$ samples showed shifts of those three peaks to

725°C, 800° C, and 900°C. The shifts in peak positions between the 30 d and 548 d samples are

attributed to longer aging and increased crystallinity of the samples. The sharp peak at 800°C in

these samples is interpreted as the release of nitrate after the conversion of cancrinite and

sodalite to a carnegieite/nepheline phase (Buhl, 1991b; Fechtelkord et al., 2001b; Hassan, 1996;

Linares et al., 2005; Liu et al., 2005; Sirbescu and Jenkins, 1999). For all the samples, heat flow

data (not shown) exhibited an exothermic peak between 800-900°C, corresponding to the

conversion to a carnegieite/nepheline phase.

3.5 [27]Aluminum NMR

Solid-state ^{27}Al NMR spectra of product phases showed differences between 30 d $-CO_2$

and 548 d $+CO_2$ samples (example spectra shown in Fig. 5). The resonance shifts exhibited by

the solids (58-66 ppm) indicate the presence of four-coordinated Al sites, with no evidence of

six-coordinated Al (Engelhardt and Michel, 1987). The 30 d samples displayed one broad resonance with an overall shift of approximately 60 ppm from Al^{3+}(aq). As shown in Figure 5(a), this resonance is asymmetric, but the presence of only one crystalline product in this sample, zeolite X, from XRD leads to the conclusion that this single site experiences a small quadrupolar interaction that is not removed by MAS NMR. The Sr-only sample at 30 d displayed a shoulder at 59 ppm, while the shoulder for the Cs-only sample shifted to 61 ppm. The shoulder position in Sr+Cs samples was at 60 ppm and between that of the single-cation samples. However, further assignment to particular cation siting in these structures is not possible with simple MAS spectra alone.

Spectra of samples aged for 548 d produced three resonances at 58, 60-62, and 66 ppm. In these samples, the main peak at 60-62 ppm demonstrated more asymmetry and was broader than the peak observed in 30 d samples. Deconvolution of the 60-62 ppm resonance for 548 d samples showed that it consists of two primary resonances centered at 60 and 62 ppm (Table 4). Two smaller resonances at 58 and 66 ppm each comprised 9-16% of the peak area. Based on previous results from similar experiments of kaolinite reacted with STWL (Crosson et al., 2006), the four resonances are assigned to: sodalite (60 ppm); cancrinite (62 ppm); a poorly crystalline aluminosilicate precursor phase (58 ppm); and an unknown Al-containing phase (66 ppm). Resonances from the minor quantities of zeolite X detected in XRD analyses at 548 d (3% or less) would most likely be undetectable in the NMR spectra based on the predominance of sodalite and cancrinite in these samples.

3.6 Strontium EXAFS

The dominant Sr EXAFS scattering in all samples was from the contribution of first-neighbor Sr-O backscattering atoms (Fig. 6). On average in all samples, Sr was coordinated by

8-10 oxygen atoms at a distance of 2.62-2.66 Å (Table 5), consistent with previous EXAFS

studies (Choi et al., 2006; Chorover et al., 2008; O'Day et al., 2000; Sahai et al., 2000).

Differences among the sample spectra arise from different interatomic distances from Sr to Al/Si

backscatterers. Two 30 d $-CO_2$ samples showed a contribution to the EXAFS from a $SrCO_3$-like

solid for both Sr+Cs and Sr-only samples (Fig. 6, Table 6). Although measures were taken to

remove CO_2 from the initial solution, a small amount of a phase with a $SrCO_3$-like local structure

was still able to form. In addition to the $SrCO_3$ component, Sr+Cs and Sr-only spectra were fit

with a shell of Al/Si backscatterers at a distance of 3.47 to 3.50 Å (±0.02 Å) (Table 5). The

number of Al/Si backscatterers from the least-squares best fit was higher for the Sr+Cs sample

(N=1.5 ±0.5) than for the Sr-only sample (N=0.7 ±0.2). Due to the overlying carbonate phase, it

was difficult to ascertain if any other Al/Si or Na backscatterers were present in the spectra. A

H_3PO_4 extraction was performed to remove the carbonate phase and EXAFS was collected on

the remaining solid. Analysis of phosphate-extracted spectra showed similar fits, with 7.4 and

7.7 (±1.5) O atoms at 2.63 Å and 1.6 (±0.5) Al/Si backscatterers at 3.46 and 3.47 Å. No $SrCO_3$

component was seen in the extracted samples. In samples with ambient CO_2 at 30 d, the EXAFS

spectrum showed only a $SrCO_3$ component that masked any backscattering from Al/Si atoms.

In samples aged for 548 d (+CO_2, Sr+Cs and Sr-only), neither unextracted sample

spectrum showed evidence for the $SrCO_3$ phase that was seen at 30 d. However, the Sr+Cs

sample spectrum had a large second-shell peak in the Fourier transform that was best fit with one

Sr-Sr distance at 3.99 Å and N = 7.0 (±2) (Table 5). This type of bonding environment is more

similar to a $Sr(OH)_2$ solid phase rather than a zeolite or feldspathoid (Table 6). In addition to the

contribution from Sr in a putative hydroxide phase, Al/Si backscatterers (at 3.41 Å) accounted

for the remaining EXAFS oscillations (Table 5). After phosphate extraction of this sample, the

EXAFS spectrum exhibited loss of the large second shell attributed to Sr backscattering, and was fit with 1.3 (±0.3) Al/Si at 3.41 Å (±0.02 Å). The Sr-only sample did not appear to have any non-aluminosilicate phases as seen in the other unextracted samples. Both unextracted and phosphate-extracted spectra were best fit with two shells, first-neighbor O atoms and second-neighbor Al/Si atoms, with similar distances and numbers of backscatters (Table 5).

4. DISCUSSION

4.1 Synthesis products

Room temperature precipitation and temporal evolution of zeolite and feldspathoid phases from caustic solutions, and Sr and Cs incorporation into solids, is influenced by the amount of CO_2 in the initial solution and by the presence or absence of Sr^{2+}. At both 30 and 548 d in all cases, aluminosilicate solids with ~1:1 Al to Si ratios formed. X-ray diffraction indicated no bulk mineralogical differences in solids at 30 d precipitated from $-CO_2$, solutions, with all solids identified as zeolite X (faujasite-type phase) regardless of the composition of the starting solution. However, the intensity of the diffraction peaks was markedly reduced in the Na-only sample. Although the presence of millimolar Sr or Cs (and equimolar Cl$^-$) did not affect the phase that formed in the absence of CO_2, particle crystallinity and growth was strongly influenced over the same time frame, similar to results reported by Deng et al. (2006). The 30 d $+CO_2$ samples contained mixtures of sodalite and cancrinite, and minor or no zeolite X. Prior studies of 1:1 zeolite synthesis under low-temperature hydrothermal conditions have shown that the presence of variable dissolved carbonate concentrations results in disordered and mixed sodalite/cancrinite phases (Buhl, 1991b; Hackbarth et al., 1999). Both total Cs and exchangeable Cs are lower in Cs-only samples compared to Sr+Cs samples at 30 d. However, the use of a $MgCl_2$ solution for measuring the exchangeable fraction could underestimate the amount of Cs in

exchangeable sites because the larger hydration shell of Mg^{2+} makes it less likely to displace the smaller hydrated Cs^+ ion (Colella, 1996). At 30 d, AAO solutions extracted a considerable fraction of near-equimolar Al and Si from solids, indicating that aluminosilicate phases at this time step are not strongly recalcitrant. Samples aged for 548 d $+CO_2$ showed a mixture of sodalite and cancrinite similar to that of 30 d $+CO_2$ samples, but precipitates with Sr present (Sr+Cs, Sr only) had a larger proportion of cancrinite (58-61%) than those without Sr (48-49%). Chloride was also present in solutions containing Sr and Cs, and has been shown to be a structure-directing ion as well as carbonate (Deng et al., 2006; Ocanto et al., 2008). For Na-only (0 mm Cl^-) samples aged for 548 d $+CO_2$, the absence of Cl^- did not influence the proportions of sodalite to cancrinite, which were similar to those determined for the Cs-only sample (Table 2). Overall, more uptake of Sr than Cs from initial solutions of equal concentrations shows preferential incorporation of Sr over Cs in both sodalite/cancrinite and zeolite X structures.

Measured surface areas of 30 d $-CO_2$ solids were found to be much lower than published values for zeolite X phases. This difference could be attributed to the room temperature synthesis method, which produced larger particles on average (750-1000 nm). Other factors could include the blockage of zeolite pores by amorphous coatings or salt precipitation or aggregation of the particles. Zeolite and feldspathoid synthesis reported from 25-700 °C showed faster crystallization rates and smaller particle sizes (13-250 nm) at higher temperature (Castagnola and Dutta, 1998; Cocks and Pope, 1995; Davis and Lobo, 1992; Freund, 1976). In general, particle aging produced more crystalline, less aggregated phases with higher bulk surface areas, but still lower than those produced from high-temperature synthesis.

Although steps were taken to remove CO_2 from solution in $-CO_2$ experiments, TGA showed that a small amount of CO_2 (0.4 wt % dry solid) evolved from the 30 d solids, and Sr

EXAFS indicated the formation of a minor $SrCO_3$-type phase. Strontium has a strong affinity to complex with carbonate (Busenberg et al., 1984; Fouillac and Criaud, 1984) and readily forms a $SrCO_3$-like surface precipitate (Sahai et al., 2000). It is possible that a small amount of carbonate entered the system from the salts used to make the caustic solutions, or was present in the colloidal silica solution. The EXAFS spectra before and after sample extraction by phosphoric acid demonstrated that the $SrCO_3$ component was removed by the extraction, but the amount of Sr measured in the extraction solution was very low (maximum of 1.2% of total Sr in the solids). This observation, in agreement with prior studies (Choi et al., 2006; Chorover et al., 2008), indicates that $SrCO_3$ is a small component of total Sr in the sample although it dominates the EXAFS. Precipitation of a $SrCO_3$ phase was detected by EXAFS in all 30 d unextracted samples synthesized from both $+CO_2$ and $-CO_2$ solutions, but not at 548 d from $+CO_2$ solutions, suggesting incorporation of dissolved carbonate into crystallizing aluminosilicate phases with time. Results from TGA are also consistent with the formation of more poorly crystalline precipitates at 30 d from $-CO_2$ solutions that show more rapid weight loss at lower temperatures compared to precipitates from $+CO_2$ solutions. One sample at 548 d ($+CO_2$, Sr+Cs) showed evidence from EXAFS for the formation of a putative Sr-hydroxide phase that was removed by phosphate extraction. The small amount of Sr measured in the extractant solution noted above indicates that this component was a very small fraction of Sr-bearing phases in the sample, similar to the $SrCO_3$ component.

4.2 Structural Observations

Analysis of XRD data showed a change in long-range crystal structure from zeolite X at 30 d and low CO_2 to sodalite/cancrinite mixtures at 30 and 548 d synthesized at ambient CO_2. However, analysis of ^{27}Al NMR indicated overlap in chemical shifts of the two primary

resonances in samples dominated by zeolite X or sodalite/cancrinite, suggesting that the local Al tetrahedral environments do not change significantly during changes in long-range crystal structure. Sample aging gave rise to two additional smaller Al resonances that are attributed to poorly crystalline aluminosilicate and Al-bearing phases (Crosson et al., 2006). Extraction of 548 d precipitates by phosphoric acid removed negligible Al (< 1% of total Al determined by HF digestion), but 15-25% of the Si was removed compared to HF digestion (Table 1). These results are consistent with the presence of minor amounts of amorphous or poorly crystalline aluminosilicate phases that remain after room temperature aging for 1.5 years, which is also suggested by TEM imaging, and possible reprecipitation of variscite ($AlPO_4.2H_2O$) or other hydrated Al-phosphate phase which would preferentially retain Al over Si in the solid phase. Although there is uncertainty in the thermodynamic solubility of variscite, this and related phases can form at low pH (Iuliano et al., 2008; Roncal-Herrero and Oelkers, 2011). In their study of precipitates from caustic waste solutions, Deng et al. (2006) also reported the persistence of poorly crystalline phases after room temperature aging. A previous study (Vaughan et al., 2009) suggested that peaks to the higher frequency side of the ^{27}Al NMR spectra of tetrahedrally-coordinated species in sodalite and cancrinite may arise from the influence of non-framework aluminum species on the tetrahedral species of the zeolites themselves. However, there was no indication of additional species with resonances above 80 ppm as described by Vaughan and coworkers.

After removal of excess Sr carbonate and hydroxide phases that masked Sr backscattering from aluminosilicate phases, interatomic distances from Sr EXAFS were similar in all 30 d –CO_2 samples. Second-neighbor framework Al/Si atoms were fit at 3.46-3.47 Å in samples identified by XRD as zeolite X. Zeolite X has a cubic structure and consists of four and six-membered

rings that link to form sodalite or β-cages with an internal diameter of approximately 6 Å. The sodalite cages are joined by double-sided six-membered rings (known as double-six rings, D6R) that create hexagonal prisms. Sodalite cages link to form larger cavities (supercages) in three dimensions through 12-ring windows (Fig. 7a) (Frising and Leflaive, 2008; Kim et al., 1999). Each unit cell has 8 sodalite (β) cages, 8 supercages, and 16 D6R sites. Cation-exchangeable sites are located in the hexagonal prism, β-cage, or supercage to balance the net negative charge of the aluminosilicate framework (Mon et al., 2005; Sherry, 1966; Yagi et al., 1997). Most commonly occupied are: Site I at the center of the hexagonal prism and surrounded by 12 Al/Si atoms; Site I' located in the face of the D6R on the β-cage with 6 Al/Si atoms; and Sites II and II' adjacent to six-membered rings that form the supercages and β-cages (Frising and Leflaive, 2008).

Interatomic distances between cations and framework Al or Si depend on the size of the cation and its extent of hydration. Comparison of published crystal structure determinations for Ca- and Sr-exchanged zeolite X (Table 6) with results from Sr-EXAFS fits suggest that Sr in precipitates dominated by zeolite X are probably located in several possible sites, with the average interatomic distance falling among those expected for Sites I, I', and II (Fig. 7a). The low N for Sr-Al/Si scattering (0.7-1.6) from EXAFS fits indicates substantial static disorder consistent with multiple site occupation. Monovalent cations such as Na^+ and Cs^+ tend to favor occupancy of Site I' under hydrated conditions, but Sites I and I' are typically not simultaneously occupied due to static repulsion (Frising and Leflaive, 2008). Since Na^+ was the dominant cation in all solutions and preferentially occupies Site I', it is likely that Sr occupies mostly a combination of Site I in the D6R prism, for which its cation size is better suited than Na+ or

Cs+, and Site II in the supercages (Frising and Leflaive, 2008; Kim et al., 1999). Occupation of Site II by Sr may be associated with the Sr-exchangeable fraction as measured by $MgCl_2$ extraction, which accounted for about 40-50% of total Sr in 30 d $-CO_2$ solids (Fig. 1). Low competition for cation sites between Sr^{2+} and either Na^+ or Cs^+ may explain the similar uptake behavior of Sr in the presence or absence of Cs. Uptake of Cs was generally much lower than Sr, and lower in the absence of Sr at 30 d ($-CO_2$), which may reflect competition between Na^+ and Cs^+ for similar cation sites in zeolite X. Stronger retention of Sr in highly coordinated sites of the D6R prism may be associated with the ~10-25% of total Sr in the residual recalcitrant fraction after AAO or HCl extractions.

In unextracted and phosphate-extracted samples aged for 548 d and dominated by sodalite and cancrinite, Al/Si atoms were fit at slightly shorter average distances from Sr (3.39-3.41 Å) than in 30 d samples. Sodalite, like zeolite X, has a cubic structure consisting of β or sodalite cages joined through four-membered rings (Buhl and Lons, 1996; Shanbhag et al., 2009) (Fig. 7b). Cancrinite is a polymorph of sodalite built from layers of six-membered rings of Al and Si tetrahedra, which gives rise to smaller cages (ε-cages) and larger 12-ring channels along the *c*-axis (Fechtelkord et al., 2001b; Linares et al., 2005; Sirbescu and Jenkins, 1999) (Fig. 7c). The 12-ring channels contain larger anions and cations while the ε-cages can house water molecules or cations (Fechtelkord et al., 2001b; Hackbarth et al., 1999). No direct spectroscopic Cs measurements were obtained in this study, but previous studies showed that Cs may occupy positions in the ε-cages of cancrinite in addition to sites in the sodalite cages (Fechtelkord et al., 2001a; Mon et al., 2005). Total Cs uptake from solution increased between 30 and 548 d, which may reflect more available sites for Cs uptake as precipitates evolve from dominantly zeolite X to sodalite/cancrinite.

Interatomic Sr-Al/Si distances from EXAFS are consistent with partial Sr dehydration and bonding to framework oxygen atoms in large open channels of sodalite or cancrinite rather than smaller ε-cages in cancrinite (Fig. 7b, c), and consistent with previous studies indicating occupation of the ε-cages mostly by monovalent cations and water (Bonaccorsi and Merlino, 2005). In the open channels of cancrinite and sodalite, cations are unrestricted and can occupy variable positions and hydration states, resulting in variable distances between cations and framework Al and Si atoms (Table 6). Total uptake of Sr from solution was lower at 548 d (32-46%) than at 30 d (59-84%), which could be related to more competition for non-specific cation sites in the large channels of cancrinite and sodalite.

The Sr distances from EXAFS analyses in this study are similar to those obtained from bulk and microfocused Sr EXAFS of specimen kaolinite reacted with a synthetic Si-free tank waste leachate in which sodalite/cancrinite reaction products were identified after one year of aging (Choi et al., 2006). Similar experiments with natural sediments from the Hanford site and synthetic Si-free caustic waste yielded more complex Sr EXAFS results, with a wider range of Sr-Al/Si distances and second-neighbor Sr backscattering than observed in this study (Chorover et al., 2008). The differences between model homogeneous and clay systems and natural sediments probably reflect a greater range of disordered and substituted phases, and perhaps smaller average neophase particle size, in experiments with natural sediments. However, similar bulk reaction products dominated by sodalite/cancrinite phases with low fractions of zeolite phases, and similar amounts of Sr uptake from caustic solutions, are observed in both the model and sediment systems after aging for more than a few months (Choi et al., 2005a; Choi et al., 2005b; Choi et al., 2006; Chorover et al., 2008; Chorover et al., 2003; Crosson et al., 2006). These observations suggest that the limitation in dissolved Si in the specimen clay and sediment

systems, in which Si is supplied only by the dissolution of reactant solid phases, is eventually eliminated and ~1:1 Al:Si neophases are produced, although the rate of neophase formation is dependent on the rate of Si dissolution. In the system examined here where dissolved Si is present in excess, rapid formation of zeolite X under low CO_2 conditions supplies a recalcitrant site for Sr uptake (Site I in D6R prisms), but short-range Al tetrahedral ordering indicated by NMR is retained even as long-range crystal structure changes to sodalite/cancrinite phases.

5. IMPLICATIONS

At the Hanford site, subsurface sediments were in contact with tank solutions that exceeded 60 °C with carbonate sources from both the atmosphere and sediments (Bickmore et al., 2001; Zachara et al., 2007). Under these conditions, there is an increased likelihood of a mixed, poorly crystalline, hydrated sodalite/cancrinite mineral assemblage in impacted sediments, and potential incorporation of Sr and Cs into cation sites in the neophases. In the hydrothermal synthesis of 1:1 Na-aluminosilicates, nitrite is well known to have a strong structure-directing role towards cancrinite formation, while the presence of carbonate is less specific and leads to the formation of mixed and disordered sodalite and cancrinite phases at low hydrothermal temperatures (Barnes et al., 1999; Barrer, 1984; Hackbarth et al., 1999). Therefore, a range of feldspathoid phases with different contaminant concentrations and recalcitrance may be expected at caustic waste-impacted field sites depending on the composition of the waste, the extent of reaction with sediments, the amount of carbonate, and the temperature. It may be possible for faujasite-type phases to form under low CO_2 conditions, but these neophases may be metastable during long-term aging. In general, results of this study show that the incorporation of Sr into both faujasite and sodalite/cancrinite phases is favored over Cs during room temperature synthesis. The distribution of Sr in faujasite-type phases such

28

as zeolite X may be more site-specific than those of other cations, with a preference for bonding in hexagonal prisms and six-membered rings of the supercages. Incorporation of Cs into faujasite- or sodalite/cancrinite-type phases is probably more strongly influenced by Na concentrations than by the presence of divalent cations. Although faujasite-type phases may not form abundantly in waste-impacted subsurface sediments such as those at Hanford, low temperature homogeneous precipitation of these types of phases might be useful for the preferential scavenging of radioactive Sr from caustic waste solutions.

ACKNOWLEDGEMENTS

REFERENCES

Ainsworth, C.C., Zachara, J.M., Wagnon, K., McKinley, S., Liu, C., Smith, S.C., Schaef, H.T., and Gassman, P.L. (2005) Impact of highly basic solutions on sorption of Cs$^+$ to subsurface sediments from the Hanford site, USA. Geochimica et Cosmochimica Acta, 69(20), 4787-4800.

Ankudinov, A.L., Nesvizhskii, A.I., and Rehr, J.J. (2003) Dynamic screening effects in x-ray absorption spectra. Physical Review B, 67(11), 115120.

Ballirano, P., and Maras, A. (2005) Crystal chemical and structural characterization of an unusual CO_3-bearing sodalite-group mineral. . European Journal of Mineralogy, 17(6), 805-812.

Barnes, M.C., Addai-Mensah, J., and Gerson, A.R. (1999) The mechanism of the sodalite-to-cancrinite phase transformation in synthetic spent Bayer liquor. Microporous And Mesoporous Materials, 31(3), 287-302.

Barrer, R.M. (1984) The Hydrothermal Chemistry of the Zeolites. Academic Press, London.

Baur, W.H. (1964) On cation + water positions in faujasite. American Mineralogist, 49(5-6), 697-&.

Behrens, E.A., Sylvester, P., and Clearfield, A. (1998) Assessment of a sodium nonatitanate and pharmacosiderite-type ion exchangers for strontium and cesium removal from DOE waste simulants. Environmental Science & Technology, 32(1), 101-107.

Bickmore, B.R., Nagy, K.L., Young, J.S., and Drexler, J.W. (2001) Nitrate-cancrinite precipitation on quartz sand in simulated Hanford tank solutions. Environmental Science & Technology, 35(22), 4481-4486.

Bonaccorsi, E., and Merlino, S. (2005) Modular microporous minerals: Cancrinite-Davyne group and C-S-H phases. In G. Ferraris, and S. Merlino, Eds. Micro- and Mesoporous Mineral Phases, 57, p. 241-290. Mineralogical Society of America, Washington DC.

Buhl, J.C. (1991a) The properties of salt-filled sodalite 2: Synthesis, decomposition reactions, and phase-transitions of nitrate sodalite $NA_8(AlSiO_4)_6(NO_3)_2$. Thermochimica Acta, 189(1), 75-82.

Buhl, J.C. (1991b) Synthesis and characterization of the basic and non-basic members of the cancrinite-natrodavyne family. Thermochimica Acta, 178, 19-31.

Buhl, J.C., and Lons, J. (1996) Synthesis and crystal structure of nitrate enclathrated sodalite $Na_8(AlSiO_4)_6(NO_3)_2$. Journal Of Alloys And Compounds, 235(1), 41-47.

Buhl, J.C., Stief, F., Fechtelkord, M., Gesing, T.M., Taphorn, U., and Taake, C. (2000) Synthesis, X-ray diffraction, and MAS NMR characteristics of nitrate cancrinite $Na_{7.6}(AlSiO4)_6(NO_3)_{1.6}(H_2O)_2$. Journal of Alloys and Compounds, 305(1-2), 93-102.

Busenberg, E., Plummer, L.N., and Parker, V.B. (1984) The solubility of strontianite ($SrCO_3$) in CO_2-H_2O solutions between 2 and 91°C, the association constants of $SrHCO_3^+$(aq) and $SrCO_3^o$(aq) between 5 and 80°C, and an evaluation of the thermodynamic properties of Sr^{2+}(aq) and $SrCO_3$(cr) at 25°C and 1 atm total pressure. Geochimica Et Cosmochimica Acta, 48(10), 2021-2035.

Castagnola, N.B., and Dutta, P.K. (1998) Nanometer-sized zeolite X crystals: Use as photochemical hosts. Journal of Physical Chemistry B, 102(10), 1696-1702.

Choi, S., Amistadi, M.K., and Chorover, J. (2005a) Clay mineral weathering and contaminant dynamics in a caustic aqueous system - I. Wet chemistry and aging effects. Geochimica et Cosmochimica Acta, 69(18), 4425-4436.

Choi, S., Crosson, G., Mueller, K.T., Seraphin, S., and Chorover, J. (2005b) Clay mineral weathering and contaminant dynamics in a caustic aqueous system - II. Mineral transformation and microscale partitioning. Geochimica et Cosmochimica Acta, 69(18), 4437-4451.

Choi, S., O'Day, P.A., Rivera, N.A., Mueller, K.T., Vairavamurthy, M.A., Seraphin, S., and Chorover, J. (2006) Strontium speciation during reaction of kaolinite with simulated

tank-waste leachate: Bulk and microfocused EXAFS analysis. Environmental Science & Technology, 40(8), 2608-2614.

Chorover, J., Choi, S., Rotenberg, P., Serne, R.J., Rivera, N., Strepka, C., Thompson, A., Mueller, K.T., and O'Day, P.A. (2008) Silicon control of strontium and cesium partitioning in hydroxide-weathered sediments. Geochimica Et Cosmochimica Acta, 72(8), 2024-2047.

Chorover, J., Choi, S.K., Amistadi, M.K., Karthikeyan, K.G., Crosson, G., and Mueller, K.T. (2003) Linking cesium and strontium uptake to kaolinite weathering in simulated tank waste leachate. Environmental Science & Technology, 37(10), 2200-2208.

Cocks, P.A., and Pope, C.G. (1995) Salt effects on the synthesis of some aluminous zeolites. Zeolites, 15(8), 701-707.

Colella, C. (1996) Ion exchange equilibria in zeolite minerals. Mineralium Deposita, 31(6), 554-562.

Crosson, G., Choi, S., Chorover, J., Amistadi, M., O'Day, P., and Mueller, K. (2006) Solid-State NMR identification and quantification of newly formed aluminosilicate phases in weathered kaolinite systems. Journal of Physical Chemistry B, 110, 723-732.

Davis, M.E., and Lobo, R.F. (1992) Zeolite and molecular-sieve synthesis. Chemistry of Materials, 4(4), 756-768.

De Villiers, J.P.R. (1971) Crystal structures of argaonite, strontianite, and witherite. American Mineralogist, 56(5-6), 758-767.

Deng, Y.J., Harsh, J.B., Flury, M., Young, J.S., and Boyle, J.S. (2006) Mineral formation during simulated leaks of Hanford waste tanks. Applied Geochemistry, 21(8), 1392-1409.

Depmeier, W. (2005) The sodalite family - A simple but versatile framework structure. In G. Ferraris, and S. Merlino, Eds. Micro- and Mesoporous Mineral Phases, 57, p. 203-240. Mineralogical Society of America, Washington, DC.

Engelhardt, G., and Michel, D. (1987) High-resolution solid-state NMR of silicates and zeolites. 499 p. John Wiley and Sons, New York, NY.

Fechtelkord, M., Posnatzki, B., Buhl, J.C., Fyfe, C.A., Groat, L.A., and Raudsepp, M. (2001a) Characterization of synthetic Cs-Li cancrinite grown in a butanediol-water system: An NMR spectroscopic and Rietveld refinement study. American Mineralogist, 86(7-8), 881-888.

Fechtelkord, M., Stief, F., and Buhl, J.C. (2001b) Sodium cation dynamics in nitrate cancrinite: A low and high temperature ^{23}Na and ^{1}H MAS NMR study and high temperature Rietveld structure refinement. American Mineralogist, 86(1-2), 165-175.

Fouillac, C., and Criaud, A. (1984) Carbonate and bicarbonate trace-metal complexes: critical reevaluation of stability-constants. Geochemical Journal, 18(6), 297-303.

Freund, E.F. (1976) Mechanism of crystallization of zeolite X. Journal of Crystal Growth, 34(1), 11-23.

Frising, T., and Leflaive, P. (2008a) Extraframework cation distributions in X and Y faujasite zeolites: A review. Microporous and Mesoporous Materials, 114(1-3), 27-63.

George, G.N., and Pickering, I.J. (2000) EXAFSPAK: A suite of computer programs for analysis of X-ray Absorption Spectra.

Gephart, R. (2003) A short history of Hanford waste generation storage and release., p. 1-39. Pacific Northwest National Laboratory.

Gephart, R., and Lundgren, R. (1998) Hanford tank clean up: A guide to understanding technical issues., p. 1-71, Columbus, Ohio.

Gilg, H.A., Struck, U., Vennemann, T., and Boni, M. (2003) Phosphoric acid fractionation factors for smithsonite and cerussite between 25 and 72 degrees C. Geochimica et Cosmochimica Acta, 67(21), 4049-4055.

Hackbarth, K., Gesing, T.M., Fechtelkord, M., Stief, F., and Buhl, J.C. (1999) Synthesis and crystal structure of carbonate cancrinite $Na_8(AlSiO_4)_6CO_3(H_2O)_{3.4}$, grown under low-temperature hydrothermal conditions. Microporous and Mesoporous Materials, 30(2-3), 347-358.

Hassan, I. (1996) The thermal behavior of cancrinite. Canadian Mineralogist, 34, 893-900.

Hassan, I., Antao, S.M., and Parise, J.B. (2004) Sodalite: High-temperature structures obtained from synchrotron radiation and Rietveld refinements. American Mineralogist, 89(2-3), 359-364.

Hassan, I., Antao, S.M., and Parise, J.B.. (2006) Cancrinite: Crystal structure, phase transitions, and dehydration behavior with temperature. American Mineralogist, 91(7), 1117-1124.

Hill, R.J., Howard, C.J., and Commission., A.A.E. (1986) A computer program for Rietveld analysis of fixed wavelength x-ray and neutron powder diffraction patterns. 15 p. ; p. Australian Atomic Energy Commission, Research Establishment, Lucas Heights Research Laboratories, Lucas Heights, N.S.W. :.

Kim, M.J., Jeong, M.S., Kim, Y., and Seff, K. (1999) Crystal structures of fully dehydrated fully Sr^{2+}-exchanged zeolite X and of its ammonia sorption complex. Microporous And Mesoporous Materials, 30(2-3), 233-241.

Linares, C.F., Sanchez, S., de Navarro, C.U., Rodriguez, K., and Goldwasser, M.R. (2005) Study of cancrinite-type zeolites as possible antacid agents. Microporous And Mesoporous Materials, 77(2-3), 215-221.

Liu, Q.Y., and Navrotsky, A. (2007) Synthesis of nitrate sodalite: An in situ scanning calorimetric study. Geochimica Et Cosmochimica Acta, 71(8), 2072-2078.

Liu, Q.Y., Xu, H.W., and Navrotsky, A. (2005) Nitrate cancrinite: Synthesis, characterization, and determination of the enthalpy of formation. Microporous And Mesoporous Materials, 87(2), 146-152.

Mashal, K., Harsh, J.B., and Flury, M. (2005a) Clay mineralogical transformations over time in Hanford sediments reacted with simulated tank waste. Soil Science Society of America Journal, 69(2), 531-538.

Mashal, K., Harsh, J.B., Flury, M., and Felmy, A.R. (2005b) Analysis of precipitates from reactions of hyperalkaline solutions with soluble silica. Applied Geochemistry, 20(7), 1357-1367.

Maurin, G., Llewellyn, P., Poyet, T., and Kuchta, B. (2005) Influence of extra-framework cations on the adsorption properties of X-faujasite systems: Microcalorimetry and molecular simulations. Journal of Physical Chemistry B, 109(1), 125-129.

Mon, J., Deng, Y.J., Flury, M., and Harsh, J.B. (2005) Cesium incorporation and diffusion in cancrinite, sodalite, zeolite, and allophane. Microporous And Mesoporous Materials, 86(1-3), 277-286.

Navrotsky, A., Petrovic, I., Hu, Y.T., Chen, C.Y., and Davis, M.E. (1995) Little energetic limitation to microporous and mesoporous materials. Microporous Materials, 4(1), 95-98.

O'Day, P.A., Newville, M., Neuhoff, P.S., Sahai, N., and Carroll, S.A. (2000) X-ray absorption spectroscopy of strontium(II) coordination - I. Static and thermal disorder in crystalline, hydrated, and precipitated solids and in aqueous solution. Journal Of Colloid And Interface Science, 222(2), 184-197.

Ocanto, F., Alvarez, R., de Navarro, C.U., Lieb, A., and Linares, C.F. (2008) Influence of the alkalinity and NO_3^-/Cl^- anionic composition on the synthesis of the cancrinite-sodalite system. Microporous And Mesoporous Materials, 116(1-3), 318-322.

Pannhorst, W., and Lohn, J. (1970) Crystal structure of strontianite, $SrCO_3$. Zeitschrift Fur Kristallograhie 131(6), 455.

Partin, D.E., and O'Keeffe, M. (1995) The crystal-structure of $Sr(OD)_2$. Journal of Solid State Chemistry, 119(1), 157-160.

Perdrial, N., Rivera, N., Thompson, A., O'Day, P.A., and Chorover, J. (2011) Trace contaminant concentration affects mineral transformation and pollutant fate in hydroxide-weathered Hanford sediments. Journal of Hazardous materials, 197, 119-127.

Qafoku, N.P., Ainsworth, C.C., Szecsody, J.E., and Qafoku, O.S. (2003a) Aluminum effect on dissolution and precipitation under hyperalkaline conditions: I. Liquid phase transformations. Journal of Environmental Quality, 32(6), 2354-2363.

Qafoku, N.P., Ainsworth, C.C., Szecsody, J.E., Bish, D.L., Young, J.S., McCready, D.E., and Qafoku, O.S. (2003b) Aluminum effect on dissolution and precipitation under hyperalkaline conditions: II. Solid phase transformations. Journal of Environmental Quality, 32(6), 2364-2372.

Qafoku, N.P., Ainsworth, C.C., Szecsody, J.E., and Qafoku, O.S. (2004) Transport-controlled kinetics of dissolution and precipitation in the sediments under alkaline and saline conditions. Geochimica et Cosmochimica Acta, 68(14), 2981-2995.

Ravel, B. (2001) ATOMS: crystallography for the X-ray absorption spectroscopist. Journal of Synchrotron Radiation, 8, 314-316.

Sahai, N., Carroll, S.A., Roberts, S., and O'Day, P.A. (2000) X-ray absorption spectroscopy of strontium(II) coordination - II. Sorption and precipitation at kaolinite, amorphous silica, and goethite surfaces. Journal Of Colloid And Interface Science, 222(2), 198-212.

Serne, R.J., Last, G.V., Schaef, H.T., Lanigan, D.C., Lindenmeir, C.W., Ainsworth, C.C., Clayton, R.E., LeGore, V.L., O'Hara, M.J., Brown, C.F., Orr, R.D., Kutnyakov, I.V., Wilson, T.C., Wagnon, K.B., Williams, B.A., and Burke, D. (2002) Characterization of Vadose Zone Sediment: Borehole 41-09-39 in the S-SX Waste Management Area, p. 162. Pacific Northwest National Laboratory, Richland, WA.

Shanbhag, G.V., Choi, M., Kim, J., and Ryoo, R. (2009) Mesoporous sodalite: A novel, stable solid catalyst for base-catalyzed organic transformations. Journal of Catalysis, 264(1), 88-92.

Sherry, H.S. (1966) Ion-exchange properties of zeolites I. Univalent ion exchange in synthetic faujasite. Journal Of Physical Chemistry, 70(4), 1158-1168.

Sirbescu, M., and Jenkins, D.M. (1999) Experiments on the stability of cancrinite in the system $Na_2O-CaO-Al_2O_3-SiO_2-CO_2-H_2O$. American Mineralogist, 84(11-12), 1850-1860.

Smolin, Y.I., Shepelev, Y.F., and Anderson, A.A. (1989) Atomic scale mechanism of CaX zeolite dehydration. Acta Crystallographica Section B: Structural Science, 45, 124-128.

Stanjek, H., and Häusler, W. (2004) Basics of X-ray Diffraction. Hyperfine Interactions, 54(1-4), 107- 119.

Tanaka, H., Sakai, Y., and Hino, R. (2002) Formation of Na-A and -X zeolites from waste solutions in conversion of coal fly ash to zeolites. Materials Research Bulletin, 37(11), 1873-1884.

Thompson, A., Steefel, C.I., Perdrial, N., and Chorover, J. (2010) Contaminant Desorption during long-term leaching of hydroxide-weathered Hanford sediments. Environmental Science and Technology, 44, 1992-1997.

Um, W., Serne, R.J., Yabusaki, S.B., and Owen, A.T. (2005) Enhanced radionuclide immobilization and flow path modifications by dissolution and secondary precipitates. Journal of Environmental Quality, 34(4), 1404-1414.

Valtchev, V., Rigolet, S., and Bozhilov, K.N. (2007) Gel evolution in a FAU-type zeolite yielding system at 90°C. Microporous and Mesoporous Materials, 101(1-2), 73-82.

Valtchev, V.P., Bozhilov, K.N., Smaihi, M., and Tosheva, L. (2005a) Room temperature synthesis: an efficient way for studying the zeolite formation. In J. Cejka, N. Zilkova, and P. Nachtigall, Eds. Molecular Sieves: From Basic Research to Industrial Applications, Pts A and B, 158, p. 73-80. Elsevier, Amsterdam.

Valtchev, V.P., Tosheva, L., and Bozhilov, K.N. (2005b) Synthesis of zeolite nanocrystals at room temperature. Langmuir, 21(23), 10724-10729.

Vaughan, D.E.W., Yennawar, H.P., Perrotta, A.J., and Benesi, A.J. (2009) Structure comparison of co-crystallized 6-and 12-sided large cancrinite crystals. Microporous and Mesoporous Materials, 123(1-3), 274-279.

Wan, J.M., Larsen, J.T., Tokunaga, T.K., and Zheng, Z.P. (2004a) pH neutralization and zonation in alkaline-saline tank waste plumes. Environmental Science & Technology, 38(5), 1321-1329.

Wan, J.M., Tokunaga, T.K., Larsen, J.T., and Serne, R.J. (2004b) Geochemical evolution of highly alkaline and saline tank waste plumes during seepage through vadose zone sediments. Geochimica et Cosmochimica Acta, 68(3), 491-502.

Weliky, K., Suess, E., Ungerer, C.A., Muller, P.J., and Fischer, K. (1983) Problems with accurate carbon measurements in marine-sediments and particulate matter in seawater - A new approach. Limnology and Oceanography, 28(6), 1252-1259.

Wiles, D.B., and Young, R.A. (1981) A new computer program for Rietveld analysis of X-ray powder diffraction patterns. Journal of Applied Crystallography, 14(APR), 149-151.

Yagi, F., Kanuka, N., Tsuji, H., Nakata, S., Kita, H., and Hattori, H. (1997) [133]Cs and ^{23}Na MAS NMR studies of Zeolite X containing cesium. Microporous Materials, 9(5-6), 229-235.

Zachara, J.M., Serne, J., Freshley, M., Mann, F., Anderson, F., Wood, M., Jones, T., and Myers, D. (2007) Geochemical processes controlling migration of tank wastes in Hanford's vadose zone. Vadose Zone Journal, 6(4), 985-1003.

Zachara, J.M., Smith, S.C., Liu, C.X., McKinley, J.P., Serne, R.J., and Gassman, P.L. (2002) Sorption of Cs+ to micaceous subsurface sediments from the Hanford site, USA. Geochimica et Cosmochimica Acta, 66(2), 193-211.

Tables

Table 1. Summary of solid phase extractions and digestions

Sample	MgCl$_2$	AAO	HCl	H$_3$PO$_4$	HF	Uptake[*] (%)
			Strontium (mmol/kg)			
30 d Sr+Cs −CO$_2$ A	52(2)[§]	30.(3)	69(1)	0.053	110.(2)	79
30 d Sr+Cs −CO$_2$ B	47(2)	38(2)	70.(5)	0.050	92(9)	66
30 d Sr −CO$_2$	46(2)	38(3)	78(0)	1.4	118(2)	84
30 d Sr+Cs +CO$_2$				0.15	83	59
548 d Sr+Cs +CO$_2$			30	0.075	45(4)	32
548 d Sr +CO$_2$			35	0.023	64(5)	46
			Cesium (mmol/kg)			(%)
30 d Sr+Cs −CO$_2$ A	3.2(2)	4.7(3)	4.8(1)	0.38	7.5(4)	5.4
30 d Sr+Cs −CO$_2$ B	3.4(1)	5.1(2)	5.3(7)	0.32	7.4(7)	5.3
30 d Cs −CO$_2$	1.0(1)	3.2(0)	2.8(0)	0.24	4.9(1)	3.5
30 d Sr+Cs +CO$_2$				0.073	6.9	4.9
548 d Sr+Cs +CO$_2$			7.4	0.79	12(1)	8.6
548 d Cs +CO$_2$				1.4	14(1)	10
			Aluminum (mol/kg)			
30 d Sr+Cs −CO$_2$ A	0.02(3)	4.7(2)	3.5(1)	0.0096	6.0(1)	
30 d Sr+Cs −CO$_2$ B	0.01(1)	4.6(1)	3.1(4)	0.0023	5.0(3)	
30 d Sr −CO$_2$	0.06(9)	4.4(1)	3.4(3)	0.036	5.8(1)	
30 d Cs −CO$_2$	0.02(9)	4.5(2)	3.0(1)	0.0075	5.5(2)	
30 d Na −CO$_2$[†]					4.0(1)	
30 d Sr+Cs +CO$_2$				0.021	7.1	
548 d Sr+Cs +CO$_2$			3.9	0.036	5.6(5)	
548 d Sr +CO$_2$			3.9	0.012	6.4(7)	
548 d Cs +CO$_2$				0.0049	6.1(4)	
548 d Na +CO$_2$[†]				0.035	5.8(1)	
			Silicon (mol/kg)			
30 d Sr+Cs −CO$_2$ A	0.04(3)	5.0(2)	0.074(8)	0.24	5.8(1)	
30 d Sr+Cs −CO$_2$ B	0.02(2)	5.0(1)	0.08(2)	0.041	5.2(3)	
30 d Sr −CO$_2$	0.1(1)	4.8(1)	0.059(4)	0.28	5.9(1)	
30 d Cs −CO$_2$	0.06(4)	5.0(2)	0.08(2)	0.22	5.8(1)	
30 d Na −CO$_2$[†]					4.9(1)	
30 d Sr+Cs +CO$_2$				0.45	6.8	
548 d Sr+Cs +CO$_2$			0.164	1.0	5.2(3)	
548 d Sr +CO$_2$			0.107	0.93	6.0(9)	
548 d Cs +CO$_2$				1.4	5.7(4)	
548 d Na +CO$_2$[†]				0.97	5.3(1)	

Notes: Sequential extraction of solids for MgCl$_2$ (1.0 M MgCl$_2$, pH = 8) followed by AAO (0.2 M ammonium oxalate/oxalic acid, pH = 3) on the same sample split; all others individual treatments. Numbers in () are standard deviations of three measurements. A and B indicate

replicate samples. [*]Calculated from HF digestion; $[Sr,Cs]_{solid}$=140 mmol/kg if 100% were removed from initial synthesis solution. [†] Na-endmember without Sr or Cs in synthesis solution.

Table 2. Quantitative results of XRD Rietveld simulations

	Zeolite X (%)	Sodalite (%)	Cancrinite (%)	Goodness of fit
30 d Sr+Cs –CO_2 A	100	-	-	5.17
30 d Sr+Cs –CO_2 B	100	-	-	9.31
30 d Sr –CO_2	100	-	-	7.38
30 d Cs –CO_2	100	-	-	6.64
30 d Sr+Cs +CO_2	5	27	68	3.46
30 d Sr +CO_2	10	59	31	4.84
30 d Na +CO_2	-	39	61	4.09
548 d Sr+Cs +CO_2	3	37	60	2.86
548 d Sr +CO_2	3	39	58	3.12
548 d Cs +CO_2	-	52	48	2.81
548 d Na +CO_2	-	51	49	3.66

Note: Detection limit ~0.5 wt. %. A and B indicate replicate samples.

Table 3. Surface area measurements by BET

Sample	Surface Area (m^2/g)
30 d Sr+Cs –CO_2 A	3.5(2)[*]
30 d Sr+Cs –CO_2 B	2.6(2)[*]
30 d Sr –CO_2	1.7(2)[*]
30 d Cs –CO_2	6.1(2)[*]
548 d Sr+Cs +CO_2	13.0(1)[†]
548 d Sr +CO_2	17.2(9)[†]
548 d Cs +CO_2	10.1(2)[†]

Note: A and B indicate replicate samples.
[*] Mean and standard deviation (in parentheses) of triplicate measurements.
[†] Mean and range (in parentheses) of duplicate measurements.

Table 4. Results of NMR peak decomposition for 548 d aged solids at 11.7 T magnetic field

Sample	ppm shift	Area (%)	ppm shift	Area (%)	ppm shift	Area (%)	ppm shift	Area (%)	Mineral Phases[*]
548 d Sr+Cs +CO_2	58	10	60	50	62	30	66	10	C/S/Z
548 d Sr +CO_2	58	15	60	43	62	33	66	9	C/S/Z
548 d Cs +CO_2	58	9	60	47	62	32	66	13	C/S
548 d Na +CO_2	58	11	60	42	62	31	66	16	C/S

[*] Determined by XRD (Table 2): C-cancrinite, S-sodalite, Z-zeolite X (<3% total abundance).

Table 5. Strontium K-edge EXAFS fits of untreated and H_3PO_4-extracted samples

Sample	Atom	N	R (Å)	σ^2 (Å^2)	ΔE_0 (eV)	χ^2
30 d $-CO_2$ Sr+Cs	O	9.8*	2.64*	0.010	-8.6*	0.46
	C	1.9*	3.05*	0.0023		
	Sr	2.6/	4.16*	0.0048		
	Sr	1.3/	4.31*	0.0046		
	Sr	2.6/	4.92*	0.0052		
	Al/Si	1.5*	3.47*	0.0060		
30 d $-CO_2$ Sr+Cs (ex)[†]	O	7.7*	2.63*	0.010	-9.6*	0.29
	Al/Si	1.6*	3.47*	0.0060		
30 d $-CO_2$ Sr	O	9.1*	2.64*	0.010	-9.9*	0.39
	C	1.3*	3.06*	0.0023		
	Sr	1.8/	4.17*	0.0048		
	Sr	0.9/	4.32*	0.0046		
	Sr	1.8/	4.93*	0.0052		
	Al/Si	0.7*	3.50*	0.0060		
30 d $-CO_2$ Sr (ex)[†]	O	7.4*	2.63*	0.010	-9.4*	0.21
	Al/Si	1.6*	3.46*	0.0060		
30 d $+CO_2$ Sr+Cs	O	8.8	2.66*	0.010	-13*	0.89
	C	3.0*	3.06*	0.0023		
	Sr	4.0/	4.19*	0.0048		
	Sr	2.0/	4.35*	0.0046		
	Sr	4.0/	4.91*	0.0052		
548 d $+CO_2$ Sr+Cs	O	8.6*	2.62*	0.010	-12*	0.73
	Al/Si	1.2*	3.41	0.0060		
	Sr	7.0*	3.99*	0.0090		
548 d $+CO_2$ Sr+Cs (ex)[†]	O	7.8*	2.63*	0.010	-9.5*	0.30
	Al/Si	1.3*	3.41*	0.0060		
548 d $+CO_2$ Sr	O	7.9*	2.63*	0.010	-9.4*	0.19
	Al/Si	1.3*	3.39*	0.0060		
548 d $+CO_2$ Sr (ex)[†]	O	8.1*	2.62*	0.010	-10*	0.27
	Al/Si	1.5*	3.39*	0.0060		

Notes: Atom is the backscattering atom contributing to the Sr EXAFS; N is the number of backscattering atoms at distance (R); σ^2, the Debye-Waller term, is the absorber-backscatterer mean-square relative displacement; ΔE_0 is the threshold energy difference; χ^2 is a reduced least-squares goodness-of-fit parameter (= (F-factor)/(# of points - # of variables). Shaded regions are the atomic contributions from a $SrCO_3$ phase.

* Parameter varied in least-squares fit using value from fits to reference compounds; / parameter linked in fit to the parameter directly above.

[†] Sample extracted by 10^{-2} M H_3PO_4.

Table 6. Crystallographic distances for reference compounds

Compound	Atom	N	R (Å)	Ref.	R (Å)	Ref.
Strontianite	O	9	2.547-2.730	1	2.552-2.725	2
($SrCO_3$)	C	3	3.026-3.064		3.026-3.037	
	Sr	4	4.097-4.116		4.085-4.117	
	Sr	2	4.253		4.236	
	Sr	4	4.902		4.893	
$Sr(OH)_2(s)$	O	7	2.522-2.737	3		
	Sr	2, 2	3.887, 3.095			
	Sr	4	4.032			
Zeolite X (Ca)				4		
I (D6R)	O	6	2.800			
	Al/Si	12	3.521-3.531			
I'	O	10	2.498-3.136			
	Al/Si	6	3.467-3.470			
II	O	9	2.755-3.255			
	Al/Si	6	3.593-3.615			
Zeolite X (Sr)				5		
I (D6R)	O	6	2.652			
	Si	6	3.530			
	Al	6	3.533			
I'	O	3, 3	2.655, 3.147			
	Al/Si	6	3.518			
II	O	3, 3	2.584, 2.900			
	Si	3	3.403			
	Al	3	3.458			
Sodalite (Na)	O	6	2.383-3.127	6		
	Al/Si	6	3.254-3.332			
Cancrinite (Na)				7		
ε-cage	O	8	2.205-2.947			
	Al	3	3.243			
	Si	3	3.334			
Channel	O	10	2.173-2.800			
	Al/Si	3	3.161-3.282			
	Al/Si	3	3.442-3.723			

Notes: Distances calculated from published crystallographic data; element in () was the central atom in the calculation for zeolites and feldspathoids. References: 1. (Pannhorst and Lohn, 1970); 2. (De Villiers, 1971); 3. (Partin and O'Keeffe, 1995); 4. Ca-exchanged zeolite X (Smolin et al., 1989); 5. Sr-exchanged zeolite X (Kim et al., 1999); 6. Synthetic nitrate sodalite ($Na_8[Al_6Si_6O_{24}](NO_3)_2$) (Buhl and Lons, 1996) and natural chloride sodalite ($Na_8[Al_6Si_6O_{24}]Cl_2$ (Hassan et al., 2004); 7. Natural carbonate cancrinite ($Na_{5.96}Ca_{1.52}[Al_6Si_6O_{24}](CO_3)_{1.57} \cdot 1.75H_2O$) (Hassan et al., 2006).

Figure Captions

Figure 1. Concentrations of a.) Sr and b.) Cs from digestions and extractions of solid products (per kg solid dry wt.). HF: Hydrofluoric acid total digestion; $MgCl_2$: 1.0 M ,pH = 8; AAO: 0.2 M ammonium oxalate/oxalic acid; HCl: 12 M, 200°C; H_3PO_4: 10^{-2} M, room temperature. All treatments on sample splits except for $MgCl_2$ and AAO, which were sequential.

Figure 2. X-ray diffractograms of solids from 30 d $-CO_2$ synthesis: a.) Sr+Cs A; b.) Sr+Cs B; c.) Sr only; and d.) Cs only; e.) Na-endmember; 30 d $+CO_2$: f.) Na-endmember; g.) Sr+Cs; and h.) Sr only; from 548 d $+CO_2$ synthesis: i.) Na-endmember; j.) Sr+Cs; k.) Sr only; l.) Cs only. Reference numbers from the ICDD PDF-2 2005 mineral database are: Z-zeolite X (PDF card: 01-088-0190), S-sodalite (PDF card: 00-050-0248), and C-cancrinite (PDF card: 01-086-1666).

Figure 3. Selected transmission electron microscopy microphotographs of solid products synthesized at: a.) 30 d $-CO_2$, Sr+Cs; b.) 30 d $-CO_2$, Sr only; c.) 30 d $-CO_2$, Cs only; and d.) 548 d $+CO_2$, Sr+Cs.

Figure 4. Thermogravimetric analysis of Sr+Cs solid products ($-CO_2$ and $+CO_2$). a.) Mass percent weight loss as a function of temperature from solids aged for 30 d and 548 d. b.) Derivative weight loss in mass percent (from graphs in a) of selected samples. Data for 30 d $-CO_2$ sample are plotted on the left axis; 30 and 548 d $+CO_2$ samples are

plotted on the right axis. Volatilization peaks are assigned to hydroxyl [OH$^-$], nitrate [NO$_3^-$], and carbonate [CO$_3^{2-}$] anion loss.

Figure 5. ^{27}Al NMR spectra for 30 d and 548 d samples at 11.7 T magnetic field. The two spectra shown are representative of samples from each time period. a.) 30 d Sr+Cs – CO$_2$; b.) 548 d Sr+Cs +CO$_2$. Spectra are plotted with ppm shifts relative to AlCl$_3$(aq).

Figure 6. Fits to Sr K-edge EXAFS data and Fourier transforms of solid products. Samples aged for 30 d –CO$_2$: a.) Sr+Cs; b.) Sr+Cs H$_3$PO$_4$ extracted; c.) Sr only; d.) Sr H$_3$PO$_4$ extracted; e.) 30 d +CO$_2$ Sr+Cs. Samples aged for 548 d +CO$_2$: f.) Sr+Cs; g.) Sr+Cs H$_3$PO$_4$ extracted; h.) Sr only; i.) Sr only H$_3$PO$_4$ extracted. The shaded regions of the Fourier transforms show the backscattering contribution to the spectra from a SrCO$_3$-like phase. Solid black lines are unsmoothed, normalized data; dotted lines are least-squares fits.

Figure 7. Example cation sites (yellow atoms) and typical distances between cations and framework Al (light blue) or Si (dark blue) atoms (see Table 6) for a.) Sr-exchanged zeolite-X; Site I (D6R hexagonal prism) is at the center of the bridging cavity; Site I' is at the openings of the D6R prism; Site II is outside the hexagonal window of the β-cage. b.) Na-sodalite; extraframework water molecules typically found in channels not shown. c.) Na-cancrinite; the smaller ε-cages (lower right) typically contain only monovalent cations and water; light blue atoms in the center of the large channels show typical anion

positions (e.g., NO_3^-, CO_3^{2-}). Note that not all cation positions would be fully occupied

due to repulsion.
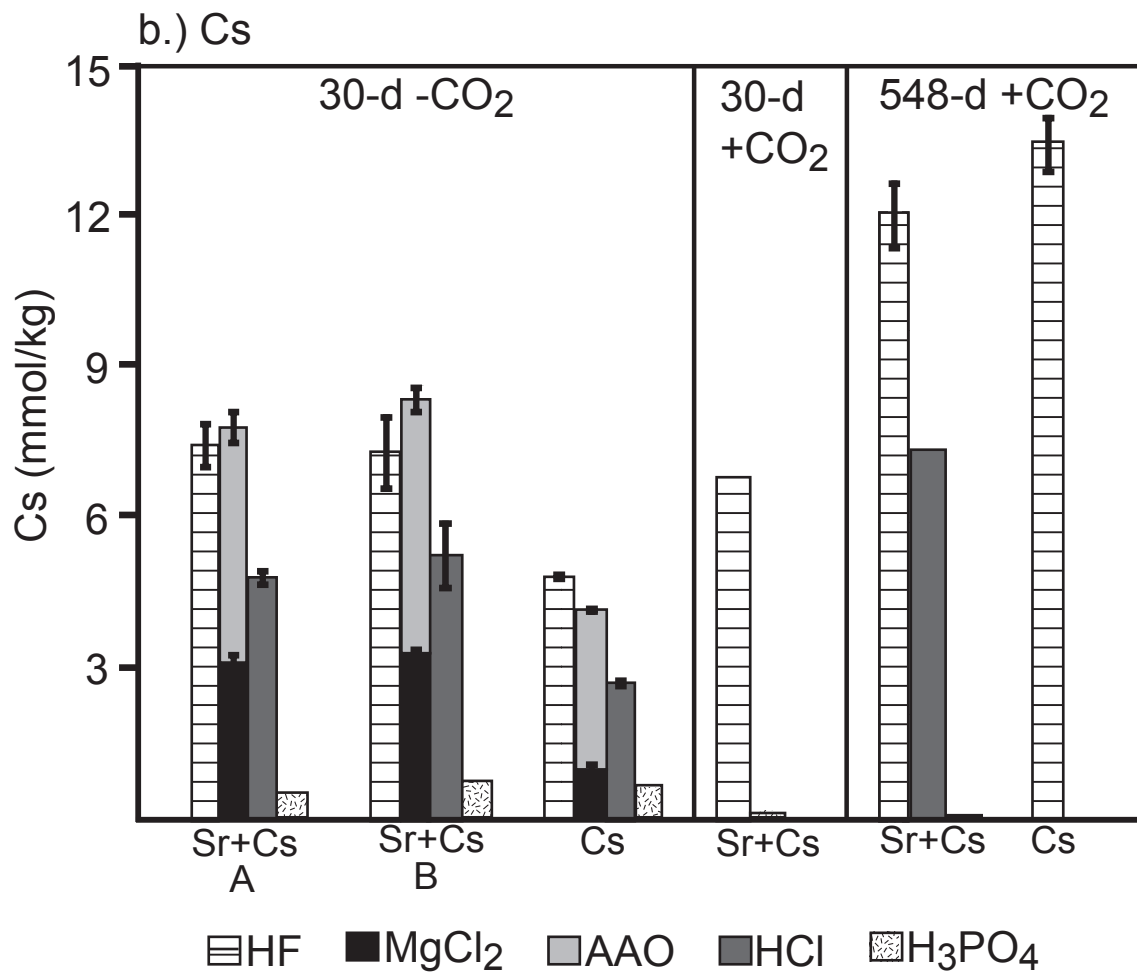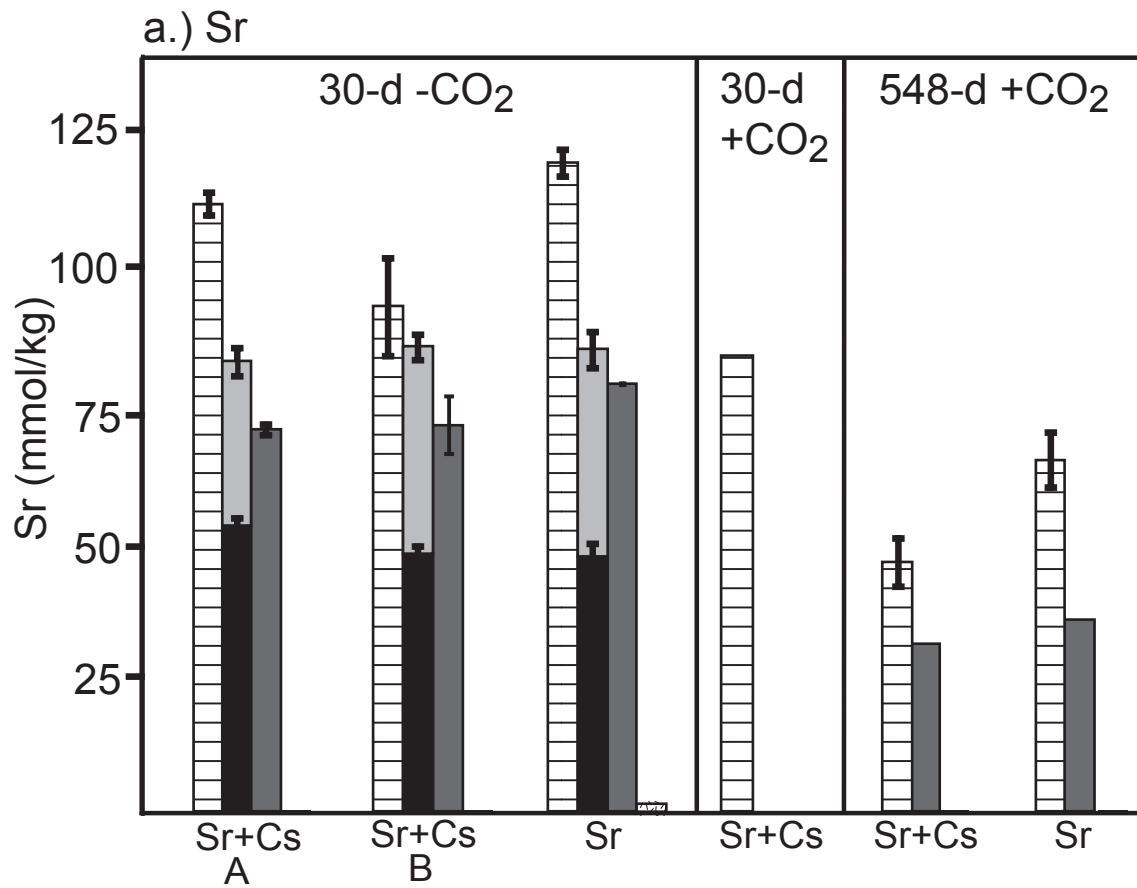
a.) Sr

b.) Cs

☐HF   ■MgCl$_2$ ☐AAO   ▨HCl   ▨H$_3$PO$_4$

Figure 1

Figure 2.

a.) 350 nm — Zeolite X

b.) 675 nm — Zeolite X

c.) 500 nm — Zeolite X, Zeolite X

d.) 1000 nm — sodalite /cancrinite

Figure 3

Figure 4

a.)

b.)

Frequency (ppm from AlCl$_3$)

Figure 5

30-d –CO_2

$k^3 \cdot \chi(k)$

k (Å^{-1})

FT magnitude

R+ΔR (Å)

a.

b.

c.

d.

e.

548-d +CO_2

$k^3 \cdot \chi(k)$

k (Å^{-1})

FT magnitude

R+ΔR (Å)

f.

g.

h.

i.

Figure 6

(a) Zeolite X

S-I'

S-I
3.53 Å

3.47-
3.52 Å   S-I'

S-II

3.40-
3.45 Å

(b) basic sodalite

Sr

3.25-3.33 Å
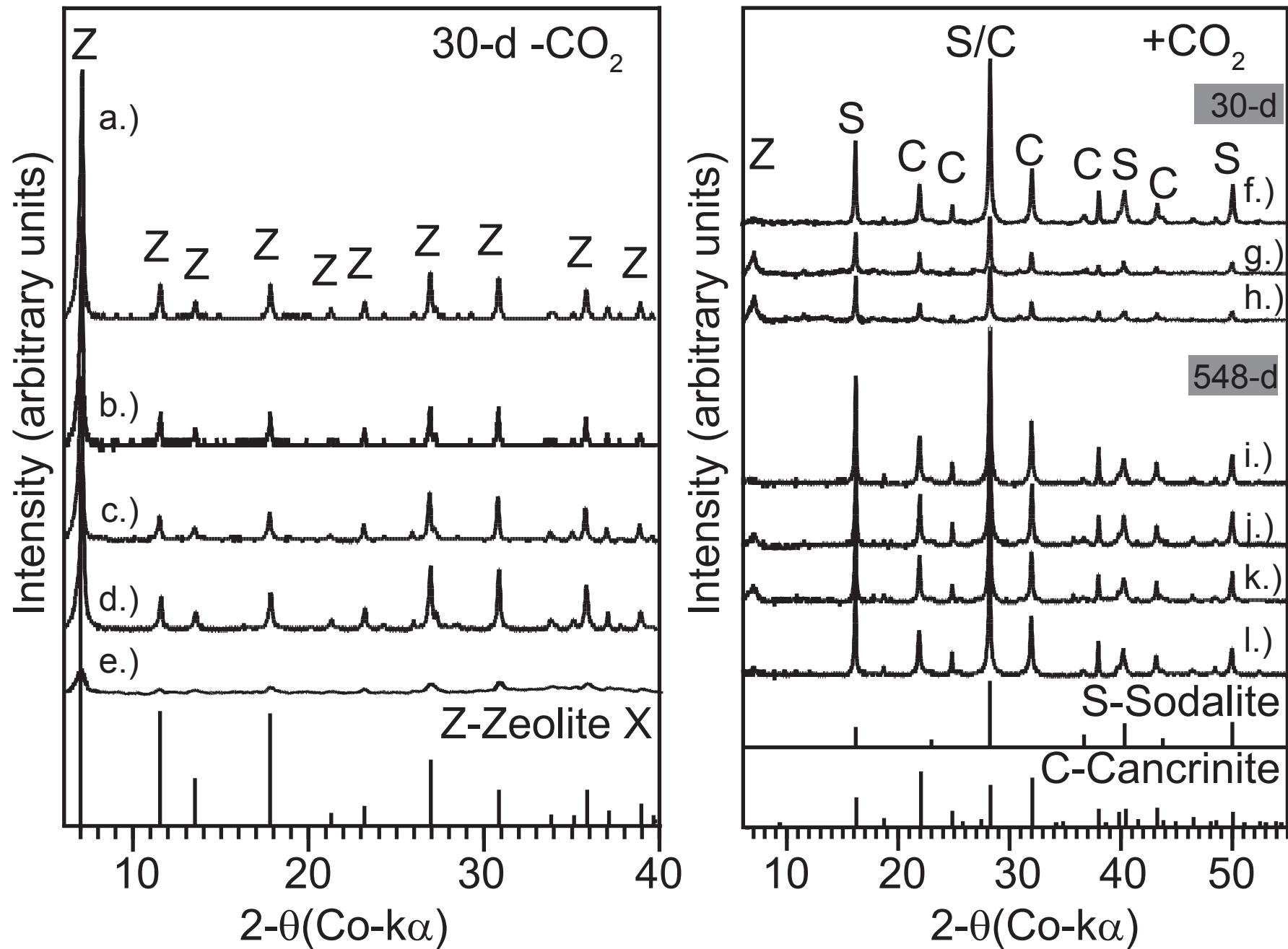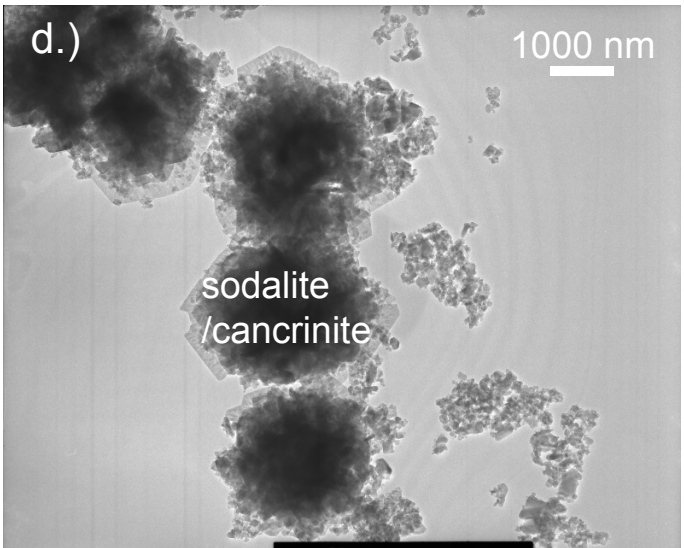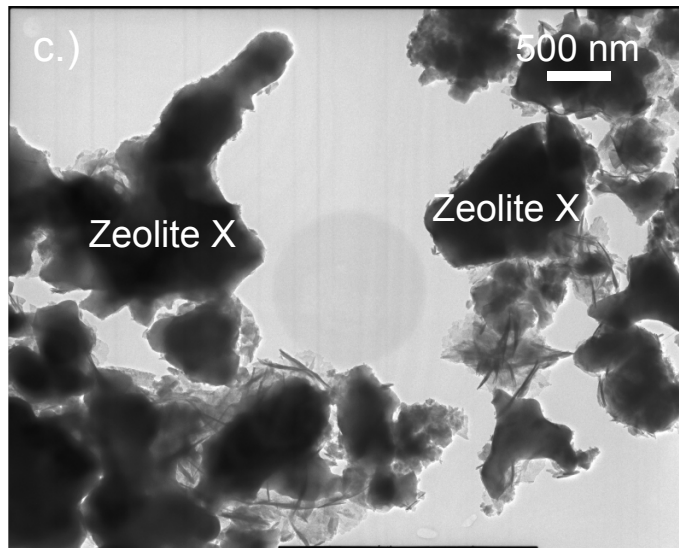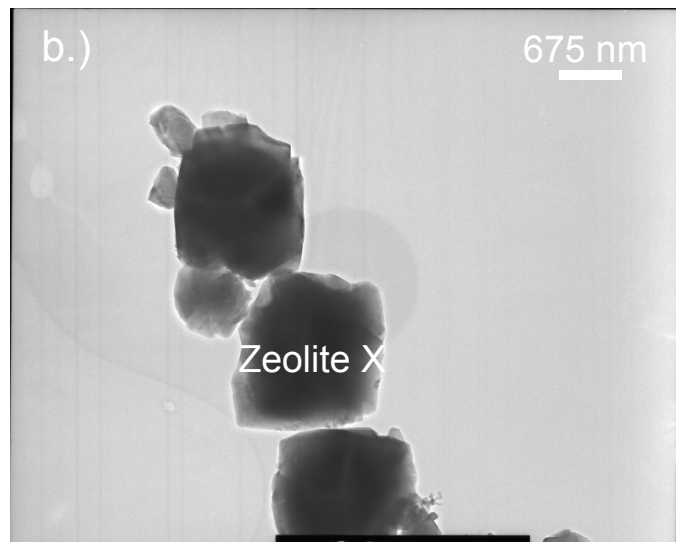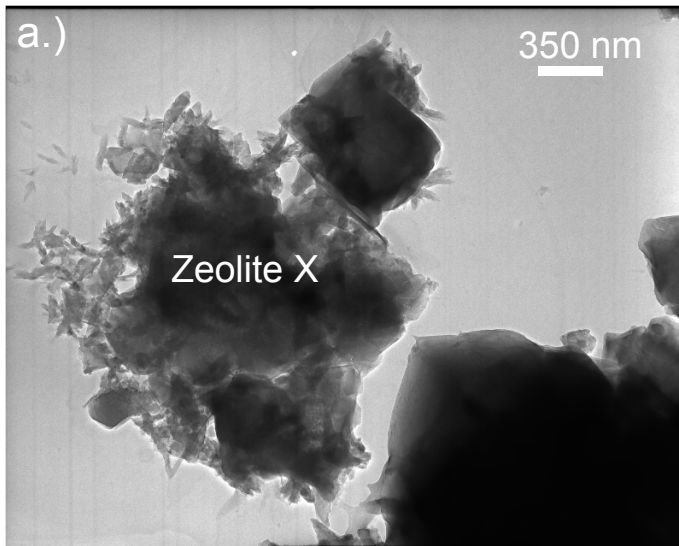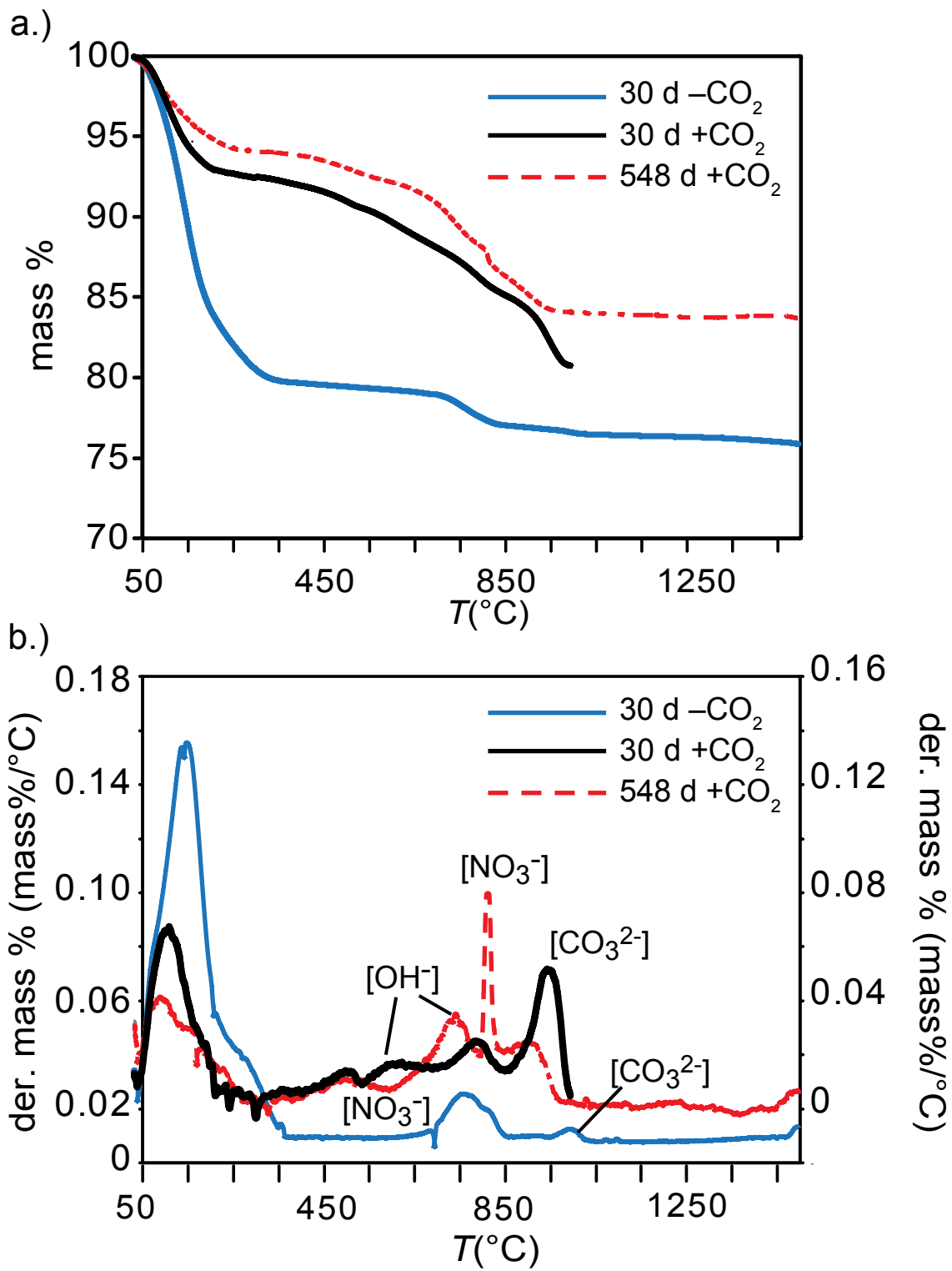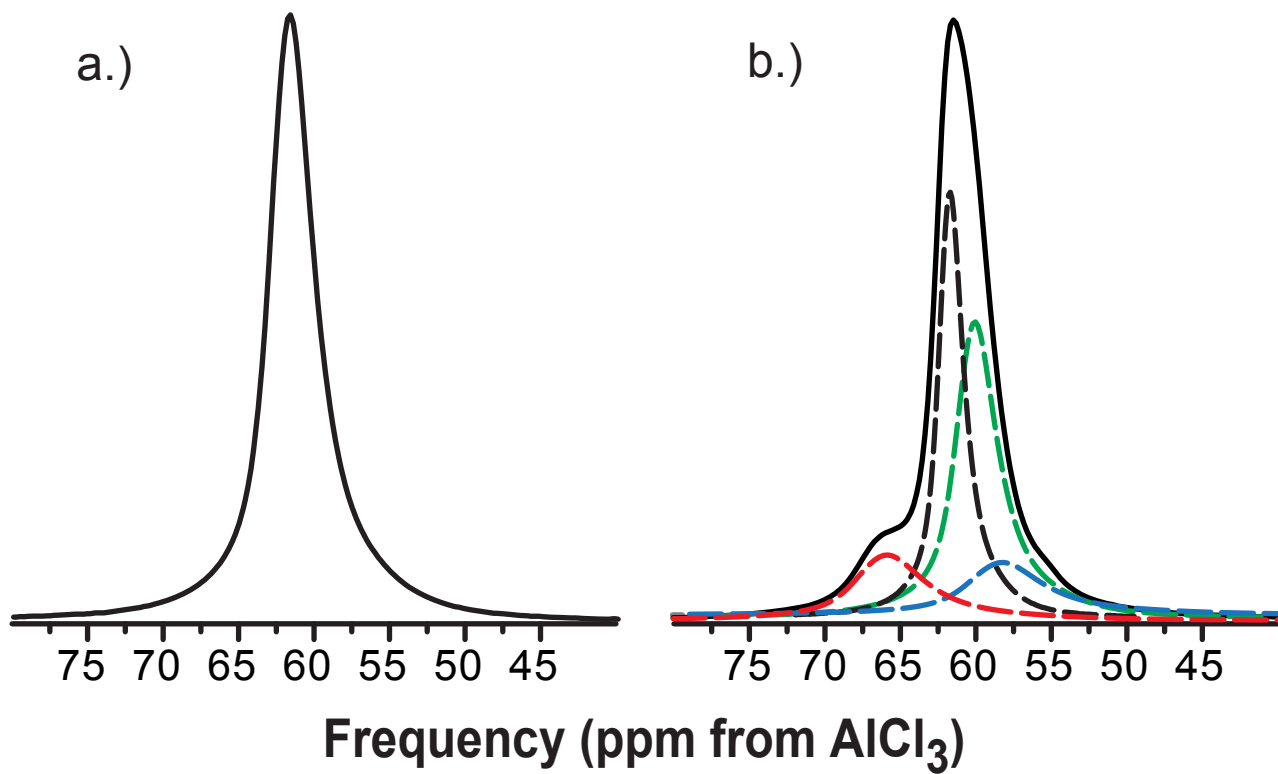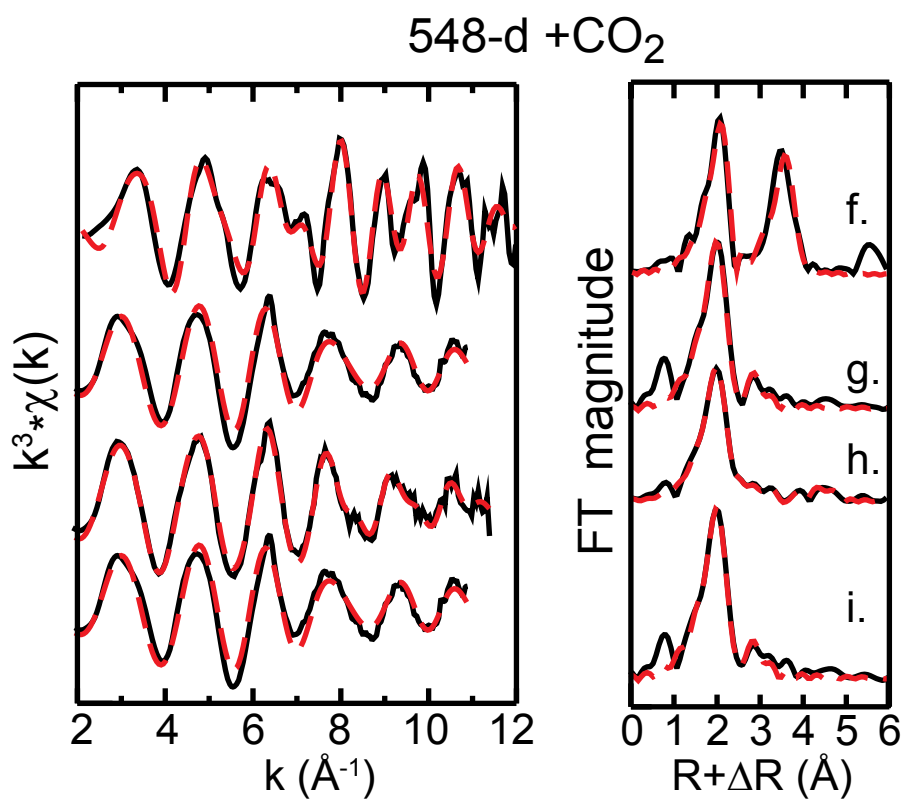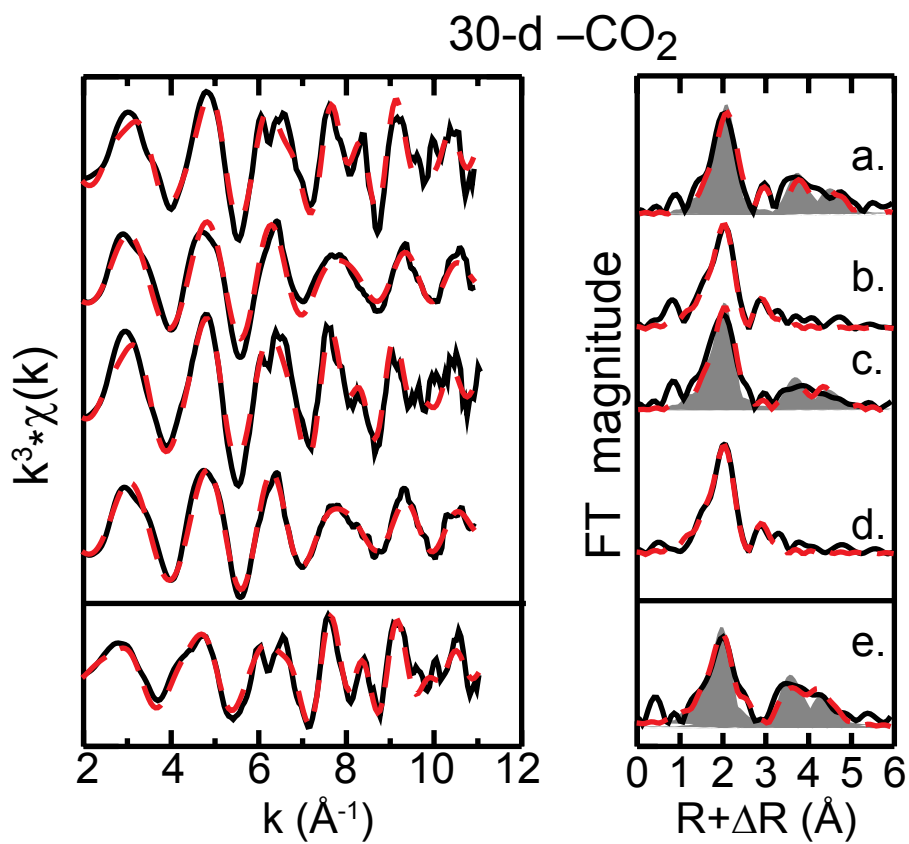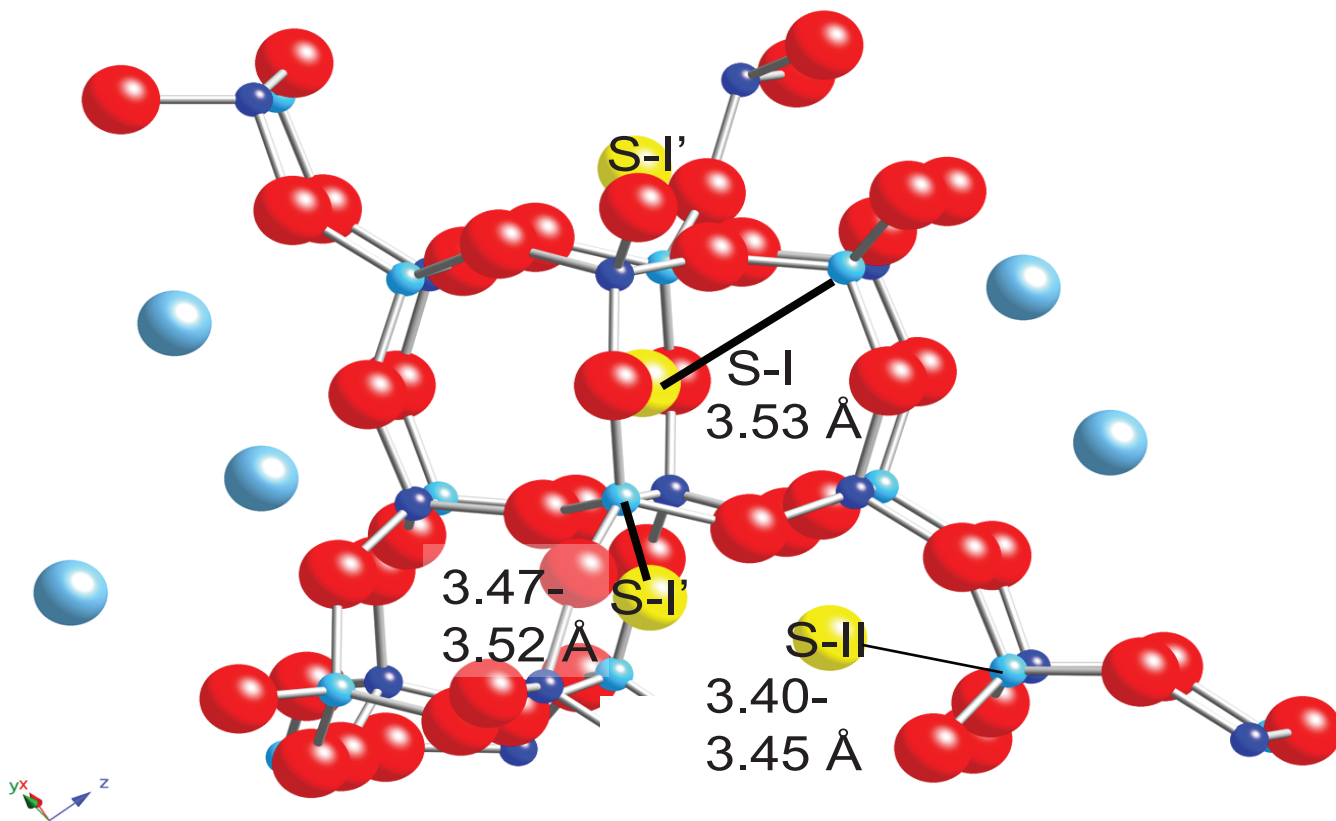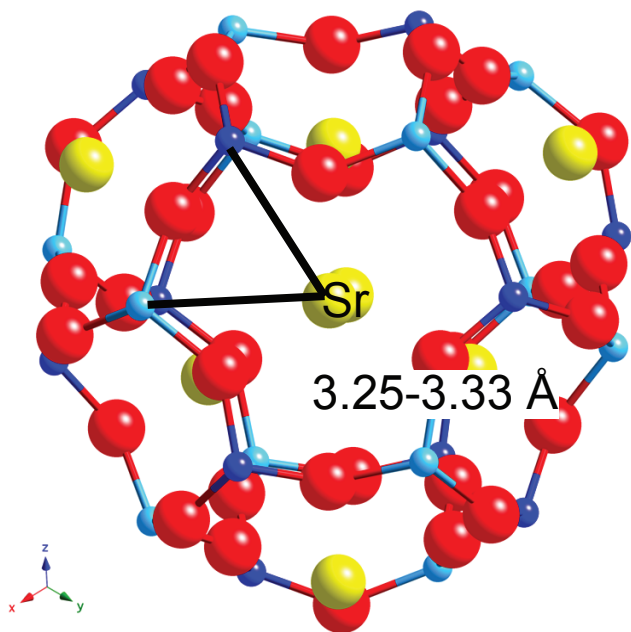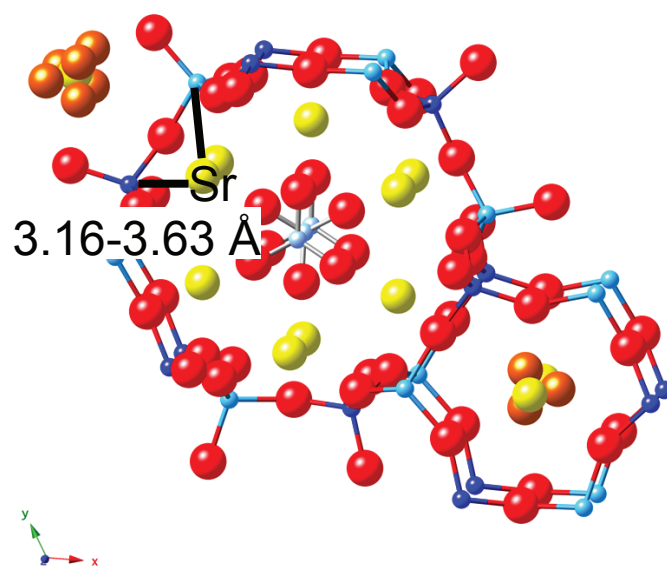
(c) nitrate cancrinite

Sr

3.16-3.63 Å

Figure 7.

Chapter 3: Cesium and strontium desorption from aluminosilicate phases

ABSTRACT

Release mechanisms of Sr and Cs co-precipitated in aluminosilicate phases were studied in column experiments with precipitates and simulated background pore water (BPW) for up to 500 pore volumes. Results were interpreted with a reactive transport model. For low CO_2 precipitates (identified as zeolite X) aged for 30 days, Cs was more readily desorbed from columns (up to 40% of total Cs in solids), while only 6% of the Sr was released to solution. Ion exchange, rather than dissolution of aluminosilicate neophases, appears to be the dominant release mechanism of Sr and Cs based on the total amount of Si and Al released ($\sim$ 1% of total in solids). For high-CO_2 precipitates (identified as cancrinite/sodalite) aged for 548 days, 6% and 14% of total Sr and Cs, respectively, were desorbed in column experiments with Sr or Cs present as a single contaminant. With Sr+Cs present as co-contaminants, up to 45% of total Sr was desorbed while only 8% of total Cs was removed. Differences in Sr and Cs release can be accounted for by the fraction of Sr strongly bound in inter-cage sites in zeolite X versus competition between Sr and Cs for exchangeable cage sites in sodalite and cancrinite.

1.0 INTRODUCTION

Sediment transformation and contaminant immobilization at the Hanford nuclear waste site has been a widely studied due to the possibility of contaminant transport from the area (Buck and McNamara, 2004; Chen et al., 2005; Choi et al., 2006; Chorover et al., 2008; Chorover et al., 2003; Deng et al., 2006b; Flury et al., 2004; Gephart, 2003; Gephart and Lundgren, 1998; Mashal et al., 2005; Mashal et al., 2004; Steefel et al., 2003; Thompson et al., 2010). Many contaminants exist at the site, particularly radioactive isotopes of Sr and Cs (Gephart, 2003). Some of the major phases believed to control the transport of these contaminants include clays, zeolites (Linde type A and X; chabazite) and feldspathoid phases (sodalite/cancrinite) (Deng et al., 2006a; Deng et al., 2006b; Flury et al., 2004; Perdrial et al., 2011; Steefel et al., 2003; Thompson et al., 2010; Zhao et al., 2004).

Although zeolite and feldspathoid phases are believed to incorporate Sr and Cs into their structures during sediment transformations, the role they play in the subsequent release of the contaminants is not clear. Both dissolution and ion exchange are possible mechanisms for Sr and Cs release. However, it is expected that ion exchange would be the dominant mechanism of release since zeolites and feldspathoid phases are silicates and, under normal groundwater conditions, would not be expected to dissolve rapidly. Recent reactive transport modeling studies of Sr and Cs release have included these phases as controls on the release of Sr and Cs (Chang et al., 2011; Thompson et al., 2010). However, these studies lacked controls on the ion exchange of the secondary phases and focused only on the rate of dissolution of the feldspathoid phases.

The studies of ion exchange on zeolites have been numerous and reviews have

summarized prior results (Colella, 1996; Townsend and Harjula, 2002; Townsend and Coker, 2001). Studies looked at pure sodium endmember zeolites with both monovalent and divalent exchangers. These studies have shown high exchange capacity for zeolites, with differences in uptake between monovalent and divalent cations but the ion exchange studies are optimized to zeolite performance for industrial applications, and therefore do not specifically address the unique conditions of incorporated ions posed by caustic waste release in the environment.

Zeolite X consists of multiple sites with the most commonly occupied as follows: Site I at the center of the hexagonal prism and surrounded by 12 Al/Si atoms; Site I' located in the face of the D6R on the β-cage with 6 Al/Si atoms; and Sites II and II' adjacent to six-membered rings that form the supercages and β-cages. Selectivity coefficients and standard free energies have been calculated for zeolite X (Barrer et al., 1969; Barros et al., 2003; Sherry, 1966). However, values derived in prior studies did not take into account multiple exchange sites in the crystal structure.   Sodalite, like zeolite X, has a cubic structure consisting of β or sodalite cages joined through four-membered rings (Buhl and Lons, 1996; Shanbhag et al., 2009). Cancrinite is a polymorph of sodalite built from layers of six-membered rings of Al and Si tetrahedra, which gives rise to smaller cages (ε-cages) and larger 12-ring channels along the *c*-axis (Fechtelkord et al., 2001; Sirbescu and Jenkins, 1999). The 12-ring channels contain larger anions and cations while the ε-cages can house water molecules or cations (Hackbarth et al., 1999).

In this study, we examined the release of Sr and Cs contaminants from precipitated zeolite and feldspathoid phases. The characterization of these solids has

been described in a previous publication (Rivera et al., 2011). The zeolite and feldspathoid phases had Sr and Cs incorporated into the structure during the synthesis process and therefore resided in sites not typically occupied at room temperature. Solids were reacted with simulated groundwater in flow-through columns to derive information on contaminant release over time and to characterize difference in contaminant retention between the two types of mineral phases. Reactive transport modeling was done in conjunction with parameter estimation tools to derive ion selectivity coefficients for a multi-site ion exchange model.

2.0 MATERIALS AND METHOD

2.1 Column experiments

The description of the synthesis of the homogeneously nucleated (HN) samples can be found in a previous publication (Rivera et al., 2011). The initial conditions of the columns and starting mineralogy of the precipitates are given in **Table 1**. A mixture of quartz and HN sample was dry-packed into Rezorian tubes[TM] (Sigma Aldrich part #57609-U) with a 1-ml volume. The polypropylene columns had a dimension of 0.8 cm I.D. x 2 cm length and were capped with PE frits with a 20 micrometer pore size. Standard quartz (from Unimin, Inc.) was used as the background filler. The certificate of analysis showed the quartz particle size was a mixture consisting of 33% at 240 μm, 49% at 149 μm, 17% at 105 μm, and 1% at 74 μm. The major trace impurity was aluminum at 15 mg/kg, but this contribution was negligible (0.8-1.0 total μmoles) compared to Al concentrations in the HN samples (**see Table 7**). Columns were run with continuous upward leaching of a background pore water solution (**Table 2**) using a Ismatec

54

peristaltic pump and pharmed 2-stop tubing (orange-blue, 0.25 mm ID) for a uniform flow rate of ~0.075 ml min^{-1}. Columns were leached for 500 – 600 pore volumes (PVs), depending on small differences in the flow rate and pore volumes (nominal 0. 50 cm^3) between columns. For the 30 d -CO_2 samples, triplicate columns were run. Because of limited sample quantities, single columns were run for the +CO_2 columns with varying amounts of HN samples per experiment. A total of ~1.75 g total solid (quartz plus precipitate) was used for all experiments. A control column filled with quartz was run to characterize any background silica and aluminum release.

2.2 Chemical analysis

Element concentrations were measured by ICP-MS (Agilent 7500cs) for Sr, Cs, Na, Al, Si. The ICP-MS was run in a soft extraction mode with 1500 W RF power and a PFA introduction system. The system was optimized to keep oxide and doubly charged interferences below 2%. A H_2 collision cell was used to measure Si (detection limit 30 ppb) to limit N and O based interferences at mass 28. A He collision cell was used to measure the Sr, Cs, Na and Al. Low-level quantification of Sr and Cs resulted in a detection limit of 0.1 ppb for both elements and detection limits for Na and Al of 25 ppb.

2.3 X-ray Absorption Spectroscopy (XAS)

Strontium K-edge X-ray absorption spectra were acquired at SSRL on beamline 11-2 under dedicated conditions (3 GeV, 80-100 mA) using a focused beam. Spectra were collected using a Si(220) monochromator crystal (beam size = 1 mm vertical x 8 mm horizontal). A rhodium mirror (17 keV cutoff energy) was used for harmonic rejection, allowing for a fully tuned beam. Beam energy was calibrated on a $SrCO_3$(s) standard with the energy at the midpoint of the absorption edge set to 16105 eV.

Samples were held in a He cryostat at 3-5 K. Absorption spectra were collected using a 30-element solid-state Ge-array detector for fluorescence and a gas-filled ion chamber for transmission.

Averaged and unsmoothed Extended X-ray Absorption Fine Structure (EXAFS) spectra were background subtracted and normalized using EXAFSPAK software packages (George and Pickering, 2000). Background was subtracted using a linear fit through the pre-edge region. Spectra were normalized to the average height of the post-edge absorbance oscillations, and fit with a cubic spline above the absorption edge ($E_0 =$ 16115 eV) to isolate the EXAFS. Normalized EXAFS spectra were fit by non-linear least-squares methods on individual atomic shells in k-space using the entire k-range in the fit (O'Day et al., 2000). Theoretical phase-shift and amplitude functions were calculated with the program FEFF v 8.4 (Ankudinov et al., 2003) using atomic clusters calculated with the program ATOMS (Ravel, 2001). The amplitude reduction factor (S_0^2) was fixed at 1.0. The difference in the photoelectron threshold energy between the reference functions and data (ΔE_o) was an adjustable component fit as a single parameter applied at the same value to all shells in a fit. Debye-waller factors were fixed in all fits based on previous studies (Choi et al., 2006; Chorover et al., 2008; O'Day et al., 2000) while the distance (R) and number of backscattering atoms (N) were varied in the fits. Second-neighbor Al and Si cannot be distinguished by EXAFS analysis because of their similar atomic mass and are indicated by Al/Si. Based on empirical fits to known reference compounds, estimated errors were R ± 0.01 Å, N or σ^2 ± 15% for the first coordination shell, and R ± 0.02Å, N or σ^2 ± 25% for atoms beyond the first shell (O'Day et al., 2000). For EXAFS non-linear least-squares fits, the reported reduced χ^2 values

give a statistical goodness-of-fit between the model and data but do not indicate the accuracy of the fit.

2.4 Modeling

Inverse modeling of the effluent data was performed using the CrunchFlow reactive transport program (Steefel and Lasaga, 1992; Steefel and Lasaga, 1994) in conjunction with the parameter estimation program, PEST (Doherty, 2002). The EQ3 database was used for the thermodynamic values in the model (**Table 3**). Prior characterization of the zeolite and feldspathoid phases (Rivera et al., 2011) informed the modeling approach. Due to the similarities of sodalite and cancrinite, the phase was treated in the model as one composite mineral. Both dissolution and ion exchange were considered as possible release mechanisms of Sr and Cs. To account for ion exchange, a three-site exchange model was used for experiments containing zeolite X and a two-site exchange model was employed for experiments with sodalite/cancrinite using the Gaines-Thomas ion exchange formulation (**Table 4**). Site concentrations were estimated crystallographic data and held fixed during model optimization. Conditional equilibrium constants for ion exchange were adjusted during the optimization process. Additionally the rates of dissolution for the feldspathoid and zeolite X phases as well gibbsite were adjusted in the optimization process. The program PEST was used to solve the non-linear regression problem by minimizing a weighted least-squares objective function with respect to the adjusted parameter values using the Gauss– Marquardt–Levenberg algorithm. The model was iteratively optimized to the end member contaminant phases (Sr-only and Cs-only) for each mineral type. The selectivity values found for the end members were then used for experiments with the co-contaminant minerals (Sr+Cs) to

57

test the transferability of the values.   Reactions whose adjusted parameters did not statistically contribute to the overall variance reduction of the optimization process were progressively eliminated from the final model.

3.0 RESULTS

3.1 Solid phase characterization

Strontium EXAFs analysis on both the reacted and unreacted HN precipitates were performed to determine Sr site occupation before and after reaction with BPW. The unreacted HN precipitates are discussed in more detail in a previous publication (Rivera et al., 2011). The dominant Sr EXAFS scattering in all samples was from the contribution of first-neighbor Sr-O backscattering atoms (**Figure 1**), with the differences among the sample spectra arising from different interatomic distances from Sr to Al/Si backscatterers. The unflushed spectra at 30 d $-CO_2$ showed a contribution to the EXAFS from a $SrCO_3$-like solid for both Sr+Cs and Sr-only samples (**Figure 1, Table 5**). In addition to the $SrCO_3$ component, Sr+Cs and Sr-only spectra were fit with a shell of Al/Si backscatterers at a distance of 3.47 to 3.50 Å (±0.02 Å) (**Table 5**). In samples aged for 548 d (+CO_2, Sr+Cs and Sr-only), neither unflushed sample spectrum showed evidence for the $SrCO_3$ phase that was seen at 30 d. However, the Sr+Cs sample spectrum had a large second-shell peak in the Fourier transform that was best fit with one Sr-Sr distance at 3.99 Å and N = 7.0 (±2) (**Table 5**). This type of bonding environment is more similar to a $Sr(OH)_2$ solid phase rather than a zeolite or feldspathoid (**Table 3**). In addition to the contribution from Sr in a putative hydroxide phase, Al/Si backscatterers (at 3.41 Å) accounted for the remaining EXAFS oscillations (**Table 5**). The Sr-only

sample did not appear to have any non-aluminosilicate phases as seen in the other unflushed samples.

The EXAFS results for the BPW flushed samples showed a difference from the unflushed counterparts (**Table 5**). At 30 d -CO_2, the Sr+Cs and Sr samples did not exhibit the $SrCO_3$ component seen previously. The Sr+Cs sample had a large second shell with Si/Al backscatterers (N=3.4) at 3.42 (±0.02) Å, which is slightly shorter than the unflushed distance (3.45 Å) but with more Si/Al backscatterers. The Sr-only sample did not show a large second shell and had a similar number of Si/Al backscatterers (N=0.8) as the unflushed sample (N= 0.7). However, the Si/Al distance decreased from 3.50 Åto 3.45 Å after flushing. At 548 d, the Sr+Cs spectrum no longer contained a $Sr(OH)_2$-type solid. The second shell was fit with a Si/Al distance of 3.45 Å with N=2.3 backscatterers. The number of backscatterers was slightly higher than that of the unflushed sample (N=1.3) at a longer distance (3.42Å). There was no data collected for the Sr-only endmember at 548 d. X-ray diffractograms collected on these samples (data not shown) showed no mineralogical change from the starting materials.

3.2 Contaminant release

3.2.1 -CO_2 columns

Over the first 50 pore volumes, the Sr+Cs and Sr columns exhibited an initial high Sr release followed by a sharp drop over the first 50 pore volumes. For the Sr-only column, Sr release recovered over the next 100 pore volumes and reached a steady state concentration of ~10 μM. For the Sr+Cs case, steady-state Sr release does not occur until 250 pore volumes and only reaches an effluent concentration of ~5 μM. Additionally, there is a more gradual increase in which the Sr reaches steady state in the range of 125-

250 pore volumes (**Figure 2a**). In total, Sr released an average of 2.4 μmoles from the Sr only columns which corresponds to a Sr retention of 93.4% for the triplicate columns. The Sr+Cs columns released an average of 1.7 μmoles with a Sr retention of 95.2%, slightly higher than the Sr only columns (**Table 6**). Inverse modeling of the data was able to mimic the effluent results for the Sr-only data. Strontium was allowed to exchange with the infiltrating BPW solution on two possible sites (out of 3). . The model showed slightly more retardation of the Sr and overestimated the steady state region (13 μM vs 10 μM) (**Figure 2a**). The Sr+Cs model mimicked the effluent Sr over the first 300 pore volumes. However, the steady-state release was twice the concentration in the model compared with the experimental data.

Similar to the Sr -CO_2 experiments, there is an initial flush of Cs over the first 50 pore volumes for the Sr+Cs and Cs columns (**Figure 2b**). The Sr+Cs columns showed an elevated release of Cs at 4 μM over the next 150 pore volumes, while the Cs-only experiment showed a gradual decrease of Cs release from 4 μM to 1.5 μM over the same time interval . At 200 pore volumes, the effluent data for the Cs-only columns reached a steady state of 1.5 μM, while the Sr+Cs columns gradually decreased to 2 μM at 400 pore volumes where it reached its steady state concentration. Overall, an average of 0.96 μmoles of Cs was eluted from the Sr+Cs columns with a total retention of 61.2%. The Cs-only columns eluted less Cs at 1.57 μmoles and have a total retention of 68.9% (**Table 6**). The model simulation for Sr+Cs and Cs (**Figure 2b**) underestimated the Cs release over the first 150 pore volumes although the profile of the release over this range displayed similar behavior. The release was two times lower for the Cs only and up to 4

time lower for the Sr+Cs data set. After the 150 pore volumes, the Cs-only model follows the steady-state release at 1.5 μM. The Cs-only model fit does not follow the effluent behavior seen in the experiments and the Cs effluent was underestimated by a factor of two.

3.2.2 +CO$_2$ columns

The +CO$_2$ columns behaved differently than the -CO$_2$ counterparts. In the Sr+Cs columns (30 d, 548 d A/B), a large initial Sr release was not observed compared with the -CO$_2$ case (**Figure 2b.**). Instead, there is an approximately 30 pore volume retardation of Sr release followed by a large pulse of Sr ranging from 11-16 μM. This pulse lasts up to 150 pore volumes before a gradual release occurs for the duration of the experiment. The Sr+Cs columns released 1.3-2.2 μmoles of total Sr. When normalized for starting amounts, this corresponds to 54-56% Sr retention (**Table 6**). Approximately 40% more Sr was released for +CO$_2$ columns compared to the Sr+Cs -CO$_2$ case. The Sr-only column released similar amounts of Sr as the -CO$_2$ columns (93.9% vs. 93.4%) and much less than the Sr+Cs +CO$_2$ columns. The Sr release edge is similar to the Sr+Cs cases where an increase of Sr occurred around 30 pore volumes. However, the effluent Sr only reached a maximum of 3 μM over the next 100 pore volumes gradually decreasing to 1.2 μM. Model simulations did not match the Sr data well at less than100 pore volumes. The large Sr flush was not captured for all three experiment types (**Figure 2c**). The Sr-only data matched the steady-state region of the data (>200 pore volumes), but the model simulations overestimated the Sr effluent for the 30 d and 548 d Sr+Cs experiments.

The +CO_2 Cs columns exhibited similar release for all column types (30 d Sr+Cs, 5480d Sr+Cs, Cs) (**Figure 2d**). All columns showed a decline in effluent Cs over the first 100 pore volumes. The initial effluent Cs was 1.3-1.8 µM with the Cs release reaching steady state after 100 pore volumes. The Cs remaining on the solids ranged from 86% (Cs only) to 95% (30 d Sr+Cs). This retention is about 20-30% higher than the -CO_2 columns. As with the -CO_2 model simulations, the first 100 pore volumes were not accurately described by the model. The steady state region showed better agreement between the model and effluent data. The 30 d experiments had less starting feldspathoid material than the 548 d columns, which could account for the lower effluent raw data.

3.2.3 Sr/Cs fraction retained

Due to the varying amounts of initial material (particularly between the -CO_2 and +CO_2 columns), the Sr and Cs fraction remaining on the solid material was plotted to compare release trends between the two types of material and contaminants (**Figure 3**). These graphs illustrate a clear delineation between the release of Sr and Cs on zeolite X (-CO_2 columns) and on sodalite/cancrinite (+CO_2 columns). With the exception of 548 d Sr only (**Figure 2a,b**), the +CO_2 columns retained less Sr on the mineral than the -CO_2 columns. The inset (**Figure 2b**) shows the differences for the Sr+Cs and Sr-only columns for the -CO_2 columns compared with the 548 d Sr-only column. The Cs retention was much higher overall on the solid for the +CO_2 columns than the -CO_2 columns. Comparing the single contaminant and co-contaminant minerals, the Cs retention for the -CO_2 data set did not change. However, the Cs-only +CO_2 column retained less Cs than the co-contaminant columns containing sodalite/cancrinite.

62

3.3 Ion release

3.3.1 -CO$_2$ columns

Effluent Al and Si for -CO$_2$ columns were very low, with only 0.1% of the initial

Si and Al released from the columns. The Si estimate does not include the quartz

background because the quartz-only column released 0.9 µmoles whereas the HN

columns released 11-34 µmoles. The Si/Al release ratio ranges from 1.1-1.6 for the –CO$_2$

columns (**Table 7**). The normalized effluent Al and Si showed a high initial release of

Al/Si then a steady state region around 100 pore volumes (**Figure 4**). There is little

variation for the –CO$_2$ data sets between the different contaminant types (Sr/Cs, Sr, Cs).

The divalent cations (Mg,Ca) showed different effluent behavior (**Figure 5a,b**).

Magnesium demonstrated a faster breakthrough than Ca and approached its influent

concentration of 0.85 mM. The model fit for the Sr-only column showed much faster

breakthrough than the data, with breakthrough occurring at 50 pore volumes while the

data breakthrough starts around 100 pore volumes. The Cs-only data and model had

better agreement, with breakthrough for both starting at 100 pore volumes. However, the

model showed a more rapid approach to the influent concentration, reaching complete

breakthrough at 150 pore volumes, while breakthrough did not occur for Mg until 300

pore volumes. The Sr+Cs model fit differed because it showed a retardation greater than

that of the effluent data (150 vs 250 pore volumes), but the model and data matched in

the steady state region of the graph.

Calcium release had a more gradual breakthrough than Mg. For all -CO$_2$

experiments, Ca never reached its influent concentration of 2.79 mM and Ca did not

reach a steady state release (**Figure 5b**). The Sr-only model matched the release edge of

the data between 75 and 150 pore volumes but achieved total breakthrough, whereas the data did not. The Sr+Cs and Cs-only models did not capture the data for any part of the curve and also showed complete breakthrough (2.79 mM). The Sr+Cs simulation overestimated the Ca concentration between 150 and 250 pore volumes before returning to the influent concentration of the feed solution.

Sodium release (**Figure 5c**) is a convolution of Na from the crystal structure and from the BPW solution. There was a steep release for the first 50 pore volumes followed by a 10 mM effluent from 50-150 pore volumes before showing a gradual release of Na over the remainder of the experiment. The Sr-only model captured the release between 50-150 pore volumes and reached a steady state below the observed concentrations. The Sr+Cs and Cs-only models display effluent behavior similar to the data over the first 100 pore volumes, but achieve a steady-state concentration faster than the data and underestimate total Na release from the column.

The K effluent data (**Figure 5d**) followed release patterns of the other cations. Potassium was retarded over the first 100 pore volumes before breakthrough and approached the influent concentration of 0.35 mM, although no column showed complete breakthrough. The Sr- and Cs- only models matched the breakthrough behavior exhibited by the columns, but overestimated the total K released from the columns. The model for the Sr+Cs did not match well with K and never reached an appreciable breakthrough.

3.3.2 +CO$_2$ columns

The +CO$_2$ columns showed elevated effluent concentrations compared to the –CO$_2$ data set. The column data was compared to a quartz-only column due to limited

sample quantity.   There was more variability in the Si/Al ratios for the $+CO_2$ columns, with Si/Al ratios ranging from 0.55-3.2. Depending on the initial starting mass (**Table 1**) of the solids, total Al released ranged from 8.06-57.3 micromoles while total Si release was between 5.11-50.5 micromoles. These values exceed the Al and Si released from the quartz-only column. Total Al from the quartz-only column was 0.059 micromoles and 0.891 micromoles were solubilized for Si. Although the quartz background filler constitutes the majority of mass in the column, it contributes negligible amounts of Al and Si to the effluent solutions (**Table 7**). The normalized effluent Al and Si for the $+CO_2$ columns followed similar effluent patterns as the $-CO_2$ columns with a high initial release of Al/Si then a steady state region around 100 pore volumes (**Figure 4**). There is little variation for the $+CO_2$ data sets between the different contaminant types (Sr/Cs, Sr, Cs).

The breakthrough for Ca and Mg demonstrated similar behavior. (**Figure 6 a,b**). Both divalent cations reached breakthrough after 20 pore volumes and maintained a steady-state effluent concentration at 50 pore volumes. Neither Mg nor Ca quite reached its concentration in the influent BPW solution, with Mg having a steady-state concentration of 0.8 mM and Ca of 2.5 mM, except for the 30 d experiments where effluent Ca reached the influent concentration.   The breakthrough behavior appears to be independent of precipitate age or contaminant type (30 d vs 548 d and Sr/Cs, Sr, or Cs). The single contaminant (Sr, Cs) models both showed a retardation of the Mg effluent of about 50 pore volumes, but matched the observed steady-state concentrations. The co-contaminant models (30 d and 548 d) did not show this retardation and matched the Mg breakthrough curves. For Ca, the model matched the Ca breakthrough but overestimated

the steady-state concentration. The quartz-only column had Mg and Ca breakthrough within the first 5 pore volumes of the experiment (resolution of the sample collection).

The Na data for all column types showed a large flush of Na over the first 75 pore volumes of the experiment (**Figure 6c**) followed by a steady-state concentration of 5 mM. The models showed similar behavior and matched the effluent data. The K breakthrough showed the most retardation of any of the cations ranging from 50-100 pore volumes (**Figure 6d**). The effluent data did not reach the influent BPW concentration of 0.35 mM but reached a steady state around 0.28 mM. The models showed greater retardation of K for the Sr+Cs and Sr-only cases. At 548 d, the Sr+Cs and Sr have a retardation of 125 pore volumes, but matched the steady state after 200 pore volumes. At 30 d, the Sr+Cs column model had less retardation (75 pore volumes) and reached steady state faster at 100 pore volumes. The Cs-only model exhibited breakthrough before the effluent data but it matched the effluent data in the steady-state region of the curve. As with Ca and Mg, the quartz column had immediate breakthrough of both Na and K.

3.3.3 Nitrate and pH

Nitrate release was similar for both the -CO_2 and +CO_2 columns. An initial flush of nitrate was observed until 100 pore volumes, then a steady-state release was achieved for the remainder of the experiment (**Figure 7 a,b**). For pH, the -CO_2 columns exhibited higher effluent pH compared to the +CO_2 columns (**Figure 7c**). The initial effluent pH was ~13, while the +CO_2 effluent columns had an initial pH of ~10. The pH in both sets of columns decreased over the first 50 pore volumes, with the +CO_2 columns maintaining an elevated pH. All columns reach a steady state pH ranging from 7.5-8 but none of them reach the influent pH of 6.8.

4.0 Discussion

EXAFS and XRD data indicated no loss of zeolite or feldspathoid phases after flushing the solids with BPW.   EXAFS analysis of the Sr+Cs BPW flushed sample showed an increase in the coordination number and shortening of the Sr-Si/Al distance after flushing. These results are consistent with Sr retention in D6R prisms relative to the Site II supercage site. The Sr-only spectrum did not show strong second shell backscattering as dis the Sr+Cs. The coordination for the second shell Al/Si backscatterers was reduced indicating less Sr residing in the D6R prisms and more occupnacy in the large pore stuctures (Site II).

For the sodalite/cancrinite system, interatomic Sr-Al/Si distances are consistent with partial Sr dehydration and bonding to framework oxygen atoms in large open channels of cancrinite or sodalite rather than smaller ε-cages in cancrinite. These results are also consistent with previous studies indicating occupation of the ε-cages mostly by monovalent cations and water (Bresciani Pahor et al., 1982). In the open channels of cancrinite and sodalite, cations are unrestricted and can occupy variable positions and hydration states, resulting in variable distances between cations and framework Al and Si atoms.

Measured effluent Si and Al accounted for only 0.1% of the total Si and Al available for release for the zeolite X phase and 0.2-0.8% for the sodalite/cancrinite system. The lack of evidence for Al or Si secondary precipitates in the columns from XRD and the 1:1 Al/Si effluent ratios indicated the zeolite and feldspathoid phases were dissolving congruently.   The amount of Sr or Cs in the effluent was 12-20 times higher

for Sr and 20-30 times higher for Cs than expected by congruent dissolution based on observed Si and Al effluent concentrations. The zeolites and feldspathoid structures are susceptible to dissolution at acidic pH due to Al leaching and destabilization of the structures (Dyer and Keir, 1989). However, in these experiments, the initial pH of the infiltrating solution was 6.8 and steady state effluent pH ranged from 7.5-8.5.

Based on the results of the EXAFS data and the effluent Si and Al concentrations, ion exchange was presumed to be the dominant mechanism in Sr and Cs release. Multiple ion exchange sites are possible in both the zeolite X and sodalite/cancrinite crystal structures. In the zeolite X structure, monovalent cations such as Na^+ and Cs^+ tend to favor occupancy of Site I' under hydrated conditions as well as Site II (Rivera et al., 2011). Since Na^+ was the dominant cation in all solutions and preferentially occupies Site I', it is likely that Sr occupies mostly a combination of Site I in the D6R prism, for which its cation size is better suited than Na^+ or Cs^+, and Site II in the supercages. Prior knowledge of the contaminant site preferences was used in the reactive transport model to constrain the sites where Sr and Cs were initially loaded and allowed to exchange. In addition to the spectroscopic data, the appearance of inflections in the curve shapes would indicate multiple site occupations for the cations (Colella, 1996). For the $-CO_2$ column sets, Sr was allowed to occupy sites I and II, Cs occupied sites I' and II, and Na, K, Ca, and Mg could occupy any of the sites (**Table 6**). Strontium showed a higher selectivity for site II over site I (log K=-4.4 vs. 0.41) . Site II would be expected to have higher loading than site I since Sr would need to lose its solvation shell to occupy the D6R site. Modeling did not account for a lower rate of exchange of Sr from the D6R site compared with other sites. For Cs, site II was more selective than site I' (log K = -2.3 vs.

-1.2), where Cs must partially dehydrate in order to occupy site I. In general, the model did not capture the behavior of the divalent cations well. Calcium exhibits a high affinity for the zeolite structure but the model overestimated effluent Ca concentrations. Monovalent effluent ions showed more agreement between the effluent data and model predictions, perhaps because Na was the most abundant cation in the system.

The $+CO_2$ data sets showed less selectivity than the $-CO_2$ experiments dominated by zeolite X. The structures of sodalite and cancrinite have smaller pore channels for ions than pores in zeolite X. For ions to exchange within sodalite, the pore size opening of the 6-membered faces (2.2 Å) and charge repulsion hinder exchange. Cancrinite behaves more like zeolite X due to the larger pore channel in its structure at (5.9 Å). Potassium was the only cation to show a retardation effect greater than 25 pore volumes and was estimated to have the greatest selectivity in the sodalite/cancrinite system. Potassium, like cesium, has a low heat of hydration, allowing for the dehydration of the ion to occur more easily (Smith, 1977). The model optimization for Ca and Mg exchange showed low selectivity (more positive number) for Ca and Mg. These ions have larger hydrated radii and larger heat of hydration, making it difficult to exchange with Na and Sr or Cs.

5.0 Implications

The results of this study demonstrate the difference in behavior between contaminants bound in a zeolite structure versus those bound in a feldspathoid structure. Both phases release contaminants when reacted with an infiltrating solution that simulates a near-neutral groundwater. Mineral phases released the most contaminant into solution when both Sr+Cs were present in the mineral. Zeolite X preferentially released

69

Cs over Sr and sodalite/cancrinite released Sr. Estimations of ion exchange selectivity coefficients matched the single contaminant effluent data for both Sr and Cs. Model fits were less robust for the co-contaminant data, indicating that other factors may be influencing the ion release not captured in the model.

Tables

Table 1. Summary of column parameters for HN packed columns.

	Flow Rate	Total Volume BPW[a]	Retention Time[b]	Pore Volumes	Mass HN solid	Mass Quartz[c]	Mineral[d]
	ml/min	L	min		grams	grams	
30 d Sr+Cs A -CO_2	0.0738	0.322	6.1	716	0.3400	1.4164	Z
30 d Sr+Cs B -CO_2	0.0750	0.315	6.0	700	0.3278	1.4120	Z
30 d Sr+Cs C -CO_2	0.0789	0.229	5.7	509	0.3160	1.4146	Z
30 d Sr A -CO_2	0.8040	0.232	5.6	516	0.3217	1.4246	Z
30 d Sr B -CO_2	0.0738	0.226	6.1	503	0.3022	1.4506	Z
30 d Sr C -CO_2	0.0714	0.224	6.3	497	0.3080	1.4303	Z
30 d Cs A -CO_2	0.0738	0.229	6.1	509	0.3146	1.4041	Z
30 d Cs B -CO_2	0.0738	0.225	6.1	500	0.3156	1.4058	Z
30 d Cs C -CO_2	0.0789	0.226	5.7	501	0.3389	1.4076	Z
30 d Sr+Cs +CO_2	0.0804	0.244	5.6	543	0.0601	1.6509	Z/S/C
548 d Sr+Cs +CO_2	0.0804	0.241	5.6	535	0.1034	1.6122	S/C
548 d Sr +CO_2	0.0763	0.227	5.9	505	0.1002	1.6061	S/C
548 d Cs +CO_2	0.0703	0.227	6.4	505	0.1060	1.7026	S/C
Quartz only	0.0804	0.240	5.6	533	--	1.8000	Q

[a]total volume of influent solution used in the experiment
[b]column dimensions-0.8 cm I.D. x 2 cm length, 0.5 cm^3 estimated volume when column packed
[c]Quartz was used as filler in column
[d]Z-Zeolite X, S-Sodalite, C-cancrinite, Q-quartz

Table 2: Initial background pore water concentrations.

	mmol/kg	SD	ppm	SD
Ca	2.79	0.07	112	2.8
K	0.35	0.02	14	0.8
Mg	0.83	0.02	20	0.5
Na*	4.25	0.18	98	4.1
SO$_4$-S	1.86	0.04	60	1.3

pH$_{initial}$=6.8 *Initial Na varied due to pH adjustment with NaOH.

Table 3. Equilibrium constants (K) and rates for mineral dissolution reactions used in reactive transport modeling.

Mineral phase[+]	Log K	Log Rate ($mol_{mineral}$ $m^{-2}_{mineral}$ s^{-1})
ZeoliteX: $Na_{96}Sr_xCs_yAl_{96}Si_{96}O_{384\,(s)}$ + 384 H^+ → 96-2x-y Na^+ + 96 Al^{+3} + 96 $SiO_{2(aq)}$ + 192 H_2O + x Sr^{+2} + y Cs^+	-50.0^	-12.0*
Sodalite/Cancrinite: $Na_8Sr_xCs_yAl_6Si_6O_{24}(NO_3)_{2(s)}$ + 24 H^+ → 8-2x-y Na^+ + 6 Al^{+3} + 6 $SiO_{2(aq)}$ + 12 H_2O + x Sr^{+2} + y Cs^+ + 2 NO_3^-	-36.9[#]	-7.79*
$Quartz_{(s)}$ → $SiO_{2(aq)}$	-4.00[$]	-14.3[$]
$Gibbsite_{(s)}$ + 3 H^+ → Al^{+3} + 3 H_2O	7.76[$]	
$Strontianite_{(s)}$ + H^+ → Sr^{+2} + HCO_3^-	1.06[$]	-6.19[$]

+dissolution reactions written in the form of basis species of the thermodynamic database

^Log K estimated from thermodynamic data from (Qiu et al., 2006)

Log K from (Thompson et al., 2010)

$Values from EQ3 database

*parameter optimized in model fits

Table 4. Log selectivity coefficients (K) for optimized model.

Mineralogical Fraction	Site type	Site Density[+] (moles g^{-1} mineral)	Reaction	Log K
Zeolite X	Site I	0.009	$0.5 \text{ Sr-Site I} \rightarrow 0.5 \text{ Sr}^{+2} + \text{Site I}^-$	0.41*
			$0.5 \text{ Ca-Site I} \rightarrow 0.5 \text{ Ca}^{+2} + \text{Site}$	2.0*
			$0.5 \text{ Mg-Site I} \rightarrow 0.5 \text{ Mg}^{+2} + \text{Site}$	2.3*
			$\text{K-Site I} \rightarrow \text{K}^+ + \text{Site I}^-$	-0.40*
			$\text{Na-Site I} \rightarrow \text{Na}^+ + \text{Site I}^-$	0.0
	Site II	0.0520	$0.5 \text{ Sr-Site II} \rightarrow 0.5 \text{ Sr}^{+2} + \text{Site}$	-4.4*
			$0.5 \text{ Ca-Site II} \rightarrow 0.5 \text{ Ca}^{+2} + \text{Site}$	-1.7*
			$0.5 \text{ Mg-Site II} \rightarrow 0.5 \text{ Mg}^{+2}$	1.0*
			$\text{Cs-Site II} \rightarrow \text{Cs}^+ + \text{Site II}^-$	-2.3*
			$\text{K-Site II} \rightarrow \text{K}^+ + \text{Site II}^-$	-1.1*
			$\text{Na-Site II} \rightarrow \text{Na}^+ + \text{Site II}^-$	0.0
	Site I'	0.008	$\text{Cs-Site I'} \rightarrow \text{Cs}^+ + \text{Site I'}^-$	-1.2*
			$0.5 \text{ Ca-Site I'} \rightarrow 0.5 \text{ Ca}^{+2} + \text{Site}$	0.71*
			$0.5 \text{ Mg-Site I'} \rightarrow 0.5 \text{ Mg}^{+2}$	0.50*
			$\text{K-Site I'} \rightarrow \text{K}^+ + \text{Site I'}^-$	-1.3*
			$\text{Na-Site I'} \rightarrow \text{Na}^+ + \text{Site I'}^-$	0.0
Sodalite/Cancrinite	Sod1	0.006	$0.5 \text{ Sr-Sod1} \rightarrow 0.5 \text{ Sr}^{+2} + \text{Site II}^-$	2.2*
			$0.5 \text{ Ca- Sod1} \rightarrow 0.5 \text{ Ca}^{+2} + \text{Site}$	5.5*
			$0.5 \text{ Mg-Sod1} \rightarrow 0.5 \text{ Mg}^{+2}$	3.4*
			$\text{Cs-Sod1} \rightarrow \text{Cs}^+ + \text{Sod1}^-$	3.7*
			$\text{K-Sod1} \rightarrow \text{K}^+ + \text{Sod1}^-$	3.1*
			$\text{Na-Sod1} \rightarrow \text{Na}^+ + \text{Sod1}^-$	0.0
	Can1	0.002	$0.5 \text{ Sr-Can1} \rightarrow 0.5 \text{ Sr}^{+2} + \text{Can1}^-$	1.3*
			$0.5 \text{ Ca-Can1} \rightarrow 0.5 \text{ Ca}^{+2}$	4.3*
			$0.5 \text{ Mg-Can1} \rightarrow 0.5 \text{ Mg}^{+2}$	4.6*
			$\text{Cs-Can1} \rightarrow \text{Cs}^+ + \text{Can1}^-$	2.7*
			$\text{K-Can1} \rightarrow \text{K}^+ + \text{Can1}^-$	1.5*
			$\text{Na-Can1} \rightarrow \text{Na}^+ + \text{Can1}^-$	0.0

+estimated from crystallographic data: Zeolite X (Olson, 1970); Sodalite (Buhl and Lons, 1996); Cancrinite (Hassan and Grundy, 1991)
*parameters optimized during model run

Table 5. EXAFS fits of leached samples.

Sample	Atom	N	R (Å)	σ^2 (Å^2)	ΔE_0 (eV)	χ^2
30-d $-CO_2$ Sr+Cs	O	9.8*	2.64*	0.010	-8.6*	0.46
	C	1.9*	3.05*	0.0023		
	Sr	2.6/	4.16*	0.0048		
	Sr	1.3/	4.31*	0.0046		
	Sr	2.6/	4.92*	0.0052		
	Al/Si	1.5*	3.47*	0.0060		
30-d $-CO_2$ Sr+Cs (BPW)[†]	O	5.0*	2.57*	0.010	-5.4*	0.21
	Al/Si	3.4*	3.42*	0.006		
30-d $-CO_2$ Sr	O	9.1*	2.64*	0.010	-9.9*	0.39
	C	1.3*	3.06*	0.0023		
	Sr	1.8/	4.17*	0.0048		
	Sr	0.9/	4.32*	0.0046		
	Sr	1.8/	4.93*	0.0052		
	Al/Si	0.7*	3.50*	0.0060		
30-d $-CO_2$ Sr (BPW)[†]	O	7.9*	2.59*	0.010	-5.1*	0.19
	Al	0.8*	3.45*	0.006		
548-d $+CO_2$ Sr+Cs	O	8.6*	2.62*	0.010	-12*	0.73
	Al/Si	1.2*	3.41	0.0060		
	Sr	7.0*	3.99*	0.0090		
548-d $+CO_2$ Sr+Cs (BPW)[†]	O	7.2*	2.59*	0.009	-5.1*	0.24
	Al	2.3*	3.45*	0.006		
548-d $+CO_2$ Sr	O	7.9*	2.63*	0.010	-9.4*	0.19
	Al/Si	1.3*	3.39*	0.0060		

Notes: Atom is the backscattering atom contributing to the Sr EXAFS; N is the number of backscattering atoms at distance (R); σ^2, the Debye-Waller term, is the absorber-backscatterer mean-square relative displacement; ΔE_0 is the threshold energy difference; χ^2 is a reduced least-squares goodness-of-fit parameter (= (F-factor)/(# of points - # of variables). Shaded regions are the atomic contributions from a $SrCO_3$ phase.
[*] Parameter varied in least-squares fit using value from fits to reference compounds; / parameter linked in fit to the parameter directly above.
[†] Sample flushed with background pore water (BPW).

Table 6. Summary of initial Sr,Cs and total Sr,Cs released in the columns.

	Initial Sr HN solid μmoles	Total effluent Sr μmoles	% Total Retained	Initial Cs HN solid μmoles	Total effluent Cs μmoles	% Total Retained
30-d Sr+Cs A -CO$_2$	37.4	1.70	95.4	2.55	1.04	59.2
30-d Sr+Cs B -CO$_2$	36.1	2.43	93.3	2.46	1.02	58.6
30-d Sr+Cs C -CO$_2$	34.8	1.11	96.8	2.37	0.807	65.9
30-d Sr A -CO$_2$	38.0	2.40	93.7	--	--	--
30-d Sr B -CO$_2$	35.7	2.53	92.9	--	--	--
30-d Sr C -CO$_2$	36.3	2.29	93.7	--	--	--
30-d Cs A -CO$_2$	--	--	--	1.54	0.488	68.1
30-d Cs B -CO$_2$	--	--	--	1.53	0.485	68.4
30-d Cs C -CO$_2$	--	--	--	1.65	0.490	70.2
30-d Sr+Cs +CO$_2$	5.00	2.18	56.1	0.413	0.0207	95.0
548-d Sr+Cs +CO$_2$	4.66	2.10	55.0	1.25	0.0922	92.6
548-d Sr+Cs B +CO$_2$	2.83	1.32	53.5	0.760	0.0574	92.4
548-d Sr +CO$_2$	6.40	0.388	93.9	--	--	--
548-d Cs +CO$_2$	--	--	--	1.43	0.198	86.2

Table 7. Summary of initial Al/Si and total Al /Si released in the columns.

	Initial Al HN solid μmoles	Total effluent Al μmoles	% Total Retained	Initial Si HN solid[a] μmoles	Total effluent Si[a] μmoles	% Total Retained	Si/Al ratio
30-d Sr+Cs A -CO_2	20264	8.06	99.96	19686	12.8	99.93	1.6
30-d Sr+Cs B -CO_2	19537	20.0	99.90	18980	24.9	99.87	1.2
30-d Sr+Cs C -CO_2	18834	9.95	99.95	18296	11.4	99.94	1.1
30-d Sr A -CO_2	18498	16.9	99.91	18884	22.7	99.88	1.3
30-d Sr B -CO_2	17377	14.8	99.91	17739	17.7	99.90	1.2
30-d Sr C -CO_2	17710	12.6	99.93	18080	15.9	99.91	1.3
30-d Cs A -CO_2	17146	26.7	99.84	18310	34.1	99.81	1.3
30-d Cs B -CO_2	17200	18.0	99.90	18368	22.6	99.88	1.3
30-d Cs C -CO_2	18470	18.5	99.90	19724	23.4	99.88	1.3
30-d Sr+Cs +CO_2	4243	2.69	99.94	4099	8.70	99.79	3.23
548-d Sr+Cs A +CO_2	5801	20.4	99.65	5408	11.2	99.79	0.55
548-d Sr +CO_2	6413	20.3	99.68	5992	15.1	99.75	0.74
548-d Cs +CO_2	6466	57.3	99.11	6010	50.5	99.16	0.88
Quartz only	1.0	0.059	94.10	29950	0.891	99.997	15

[a]Estimate does not include quartz background filler

Figure Captions

Figure 1. Fits to Sr K-edge EXAFS data and Fourier transforms of solid products. Samples aged for 30 d $-CO_2$: a.) Sr+Cs; b.) Sr+Cs A BPW flushed; c.) Sr only; d.) Sr A BPW flushed; Samples aged for 548 d $+CO_2$: e.) Sr+Cs; f.) Sr+Cs A BPW flushed; h.) Sr only; The shaded regions of the Fourier transforms show the backscattering contribution to the spectra from a $SrCO_3$-like phase. Solid black lines are unsmoothed, normalized data; dotted lines are least-squares fits.

Figure 2. a.) and b.) 30 d $-CO_2$ columns. a.) Effluent Sr (μM) for Sr+Cs columns (■) and the Sr only (▲) columns show the composite data for the triplicate columns. b.) Effluent Cs (μM) for Sr+Cs columns (■) and the Cs only (♦) columns show the composite data for the triplicate columns. c.) and d.) 30 d and 548 d $+CO_2$ columns. c.) Effluent Sr includes (μM) 30 d Sr+Cs (■),548 d Sr+Cs (▲), and 548 d Sr (▲) only column. d.) Effluent Cs includes (μM) 30 d Sr+Cs (■),548 d Sr+Cs (▲) A, and 548 d Cs (♦) only column. The solid lines show the model fits to the data.

Figure 3. Solid fraction of both Sr and Cs remaining during flush out with BPW. a.) Sr fraction remaining for both $+CO_2$ and $-CO_2$ experiments. 30 days Sr+Cs (♦) and Sr only (●) retain more Sr than the $+CO_2$ columns (▲ and ■). b.) Inset showing $-CO_2$ Sr fraction remaining. The 548 d Sr only $+CO_2$ (▲) shows similar retention as the $-CO_2$ columns. c.) Cs fraction remaining for

both $+CO_2$ and $-CO_2$ experiments. 30 days Sr+Cs (♦) and Cs only (●) retain less Cs than the

$+CO_2$ columns (▲ and ■).

Figure 4. Normalized effluent Al data for a) $-CO_2$ and b.) $+CO_2$ and normalized effluent Si for c.)

CO_2 and d.) $+CO_2$

Figure 5. $-CO_2$ effluent cation data (mM) for Sr+Cs (■), Sr only (▲), and Cs only (♦) with model

fits. a.) Mg (C_o=0.85 mm) b.) Ca (C_o=2.8 mm) c.) Na (C_o=4.25 mm) d.) K (C_o=0.35 mm).

Figure 6. $+CO_2$ effluent cation data (mM) for 30 d Sr+Cs (■), 548 d Sr+Cs (▲), 548 d Sr only

(▲), 548 d Cs only (♦) with model fits. a.) Mg (C_o=0.85 mm) b.) Ca (C_o=2.8 mm) c.) Na

(C_o=4.25 mm) d.) K (C_o=0.35 mm).

Figure 7. a.) and b.) Effluent Nitrate data. c.) Effluent pH data for $-CO_2$ and $+CO_2$ columns.

Figure 1.

Figure 2.

Figure 3.

a.)

b.)

c.)
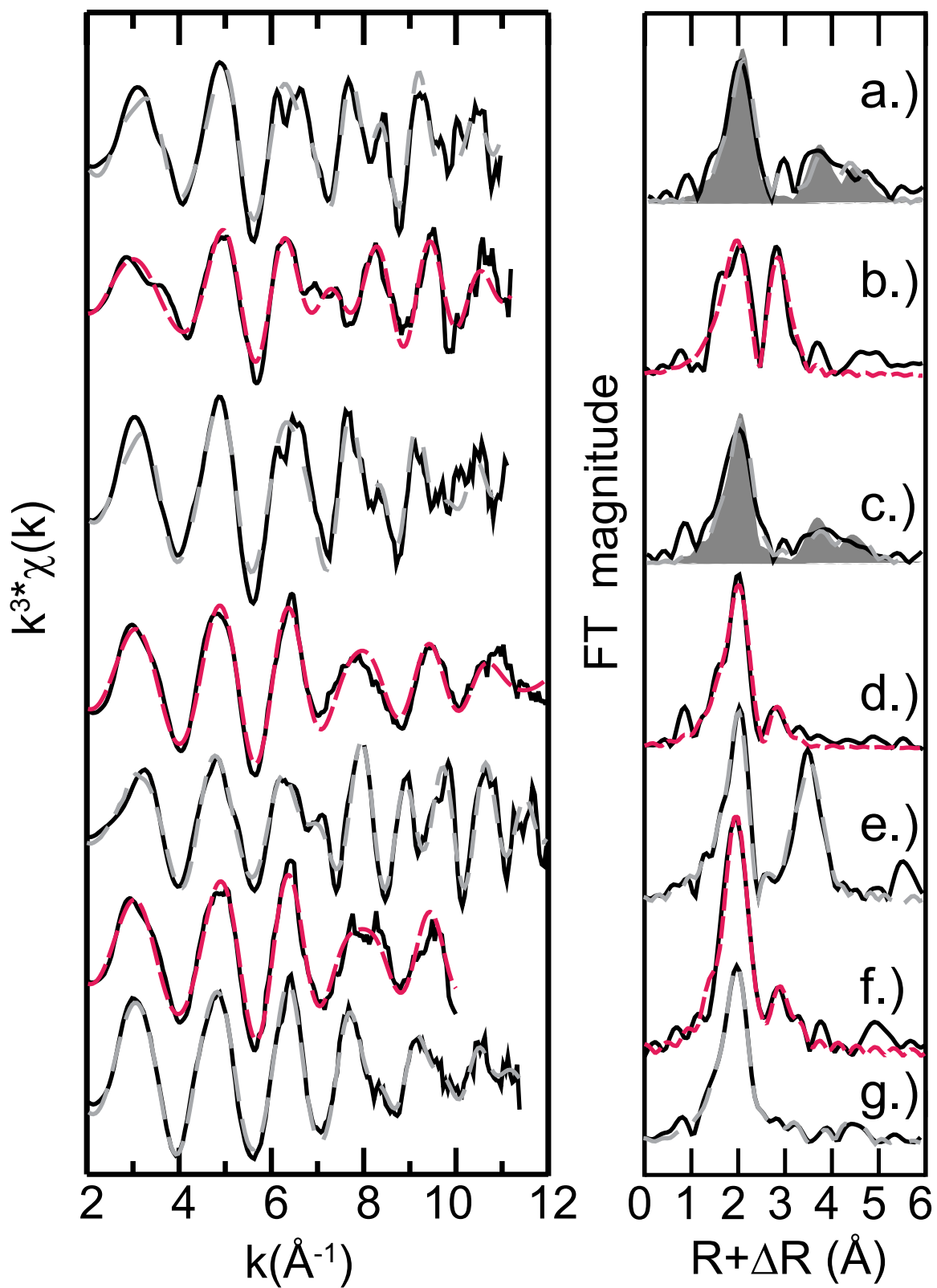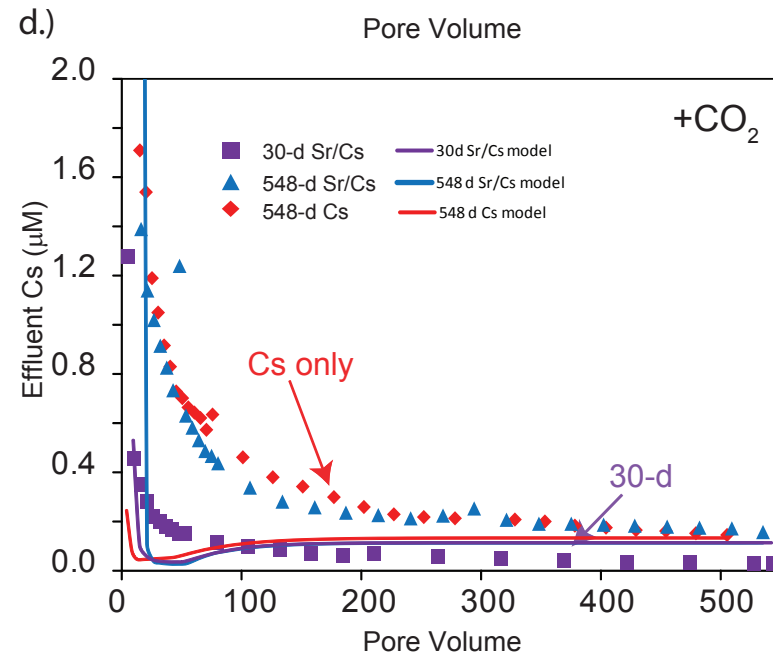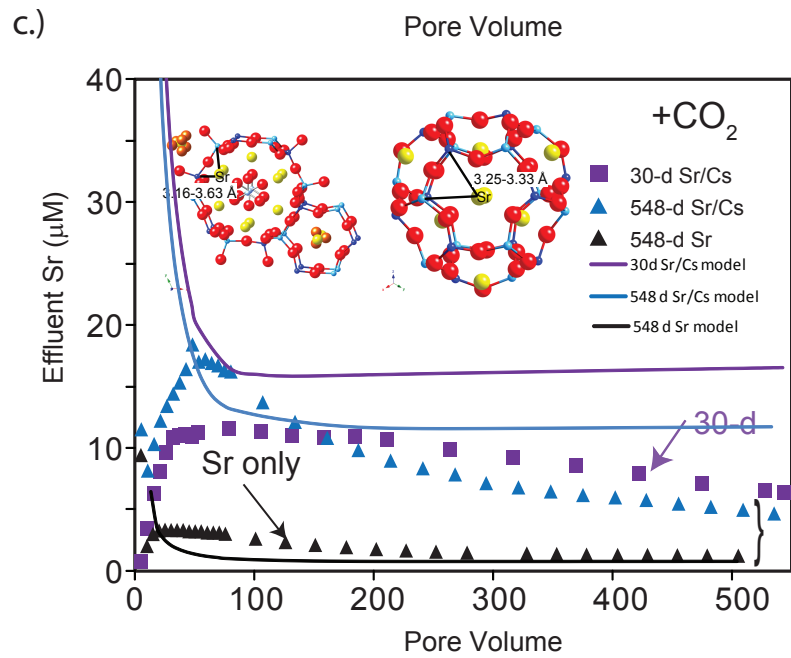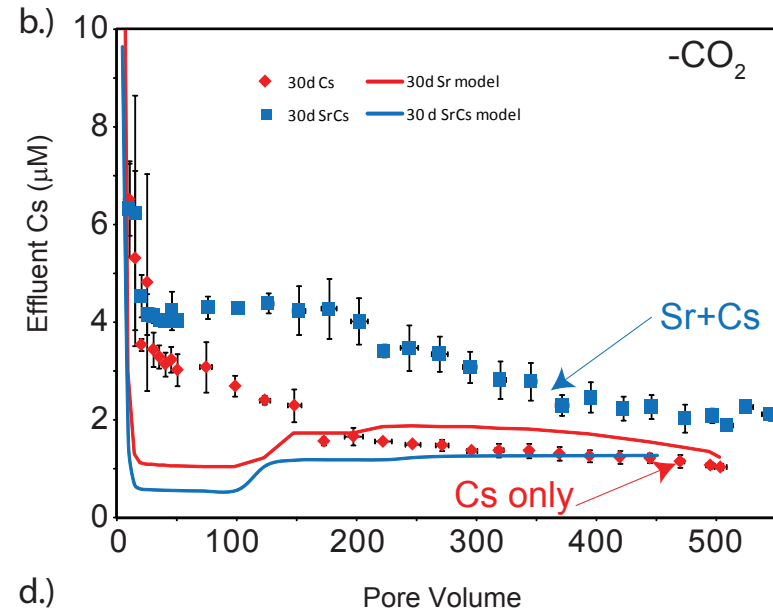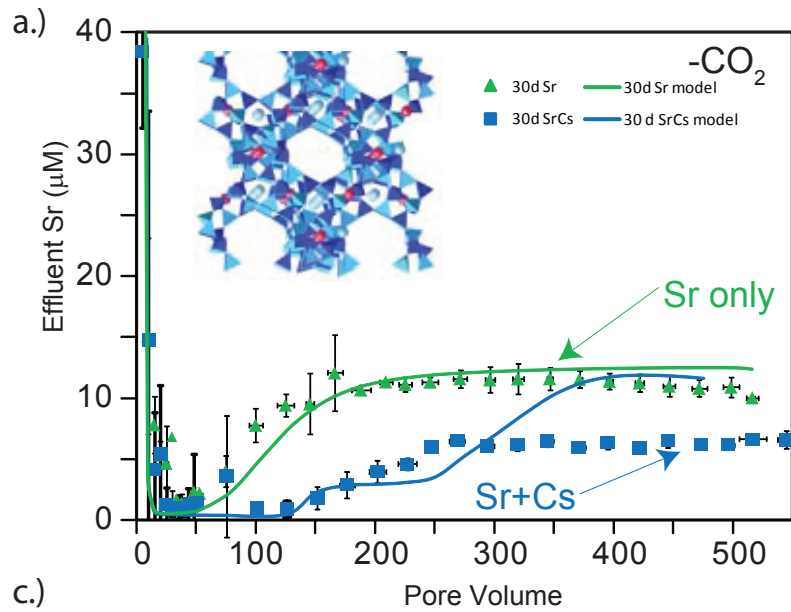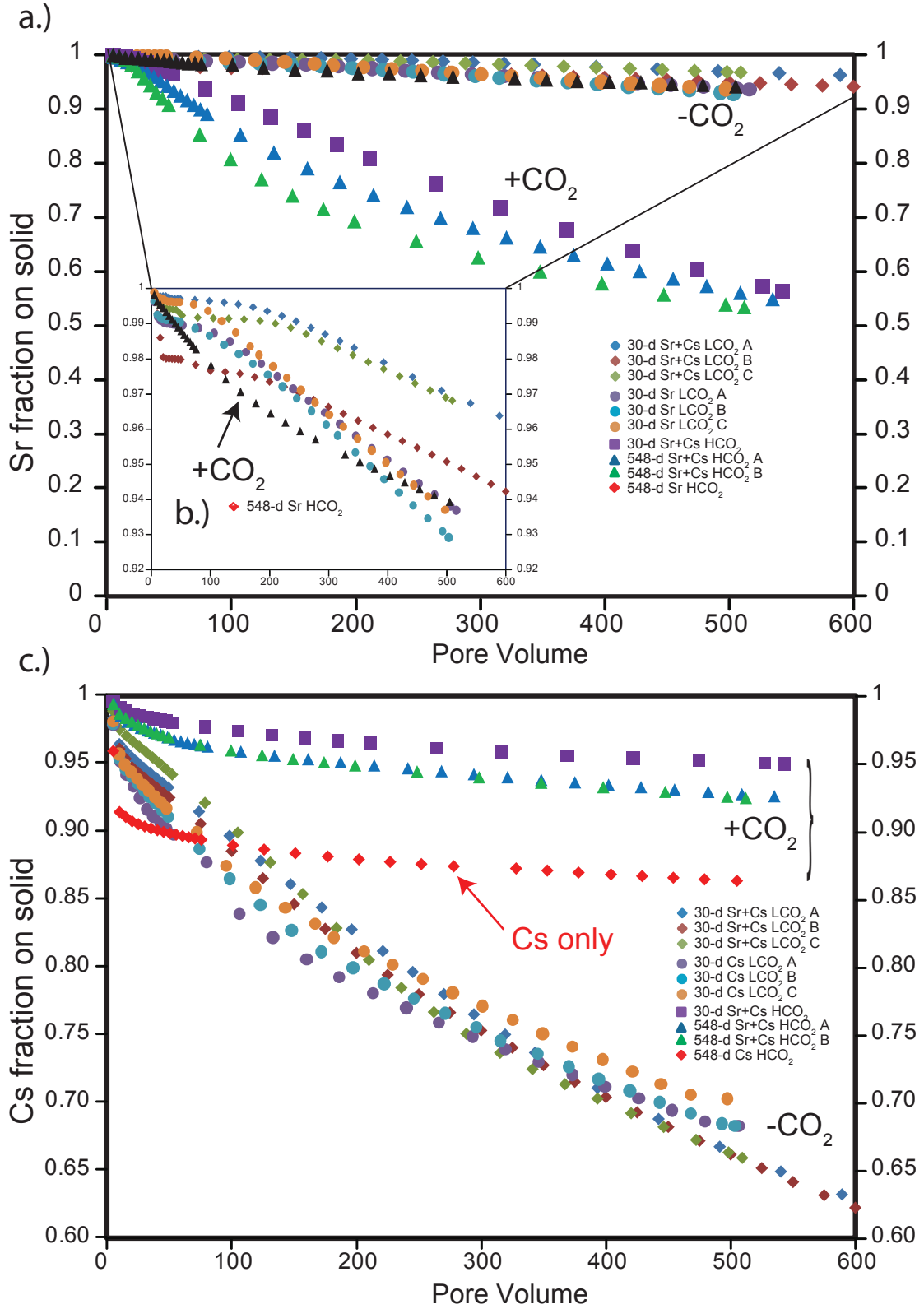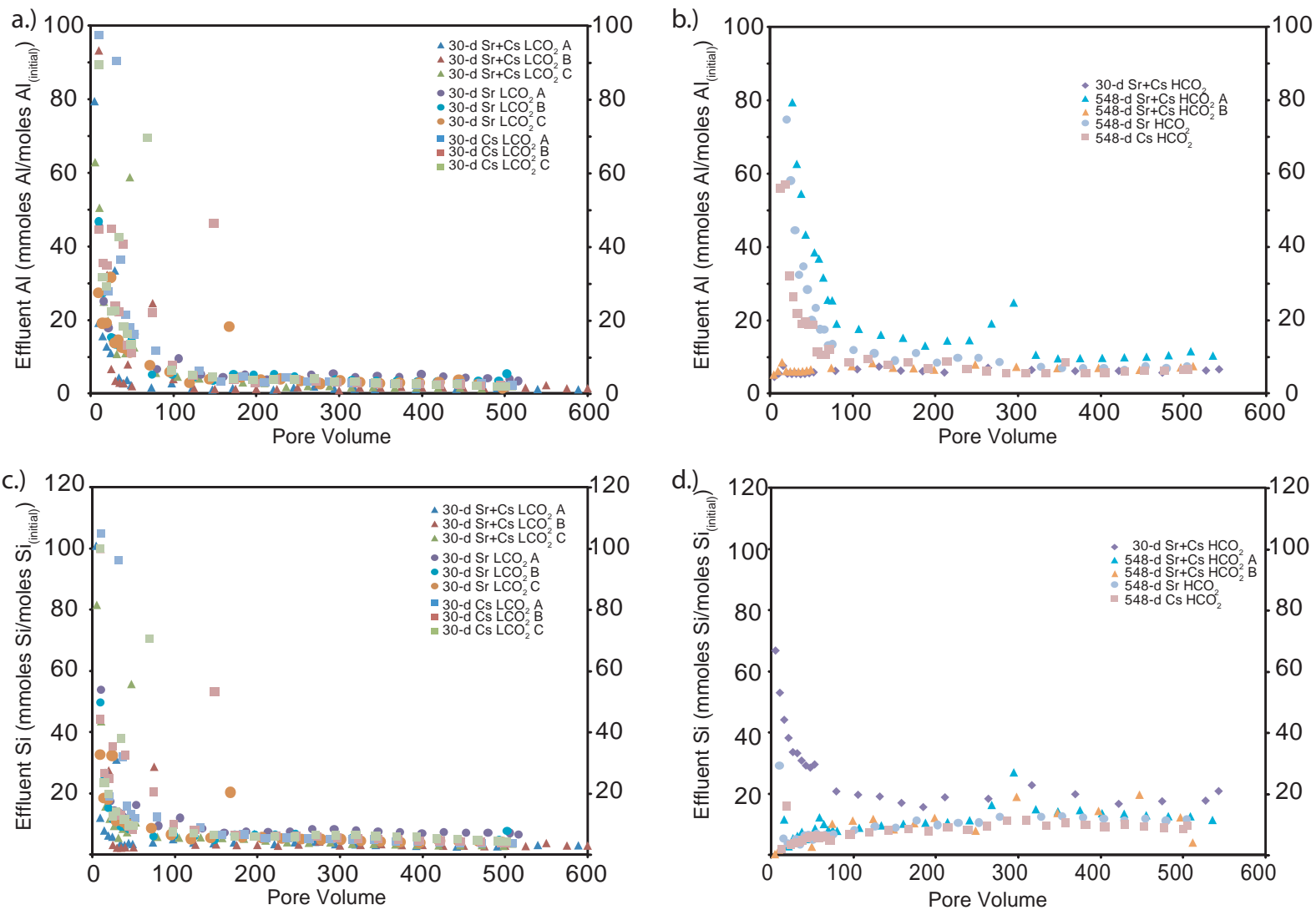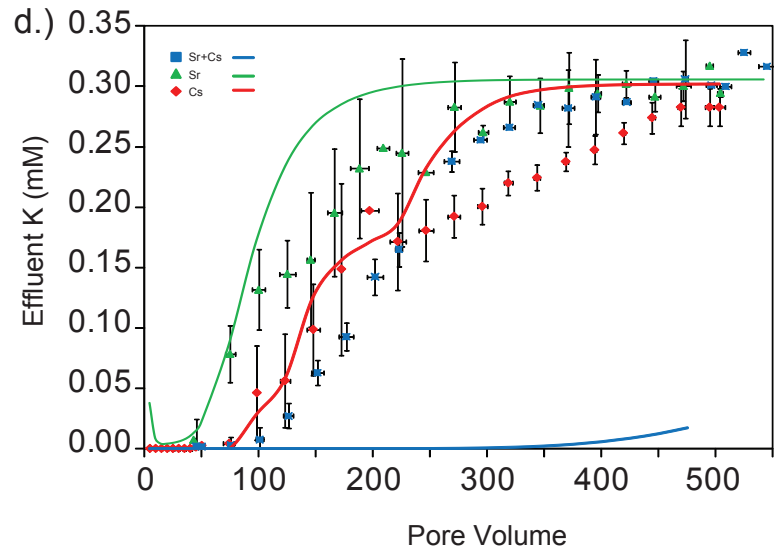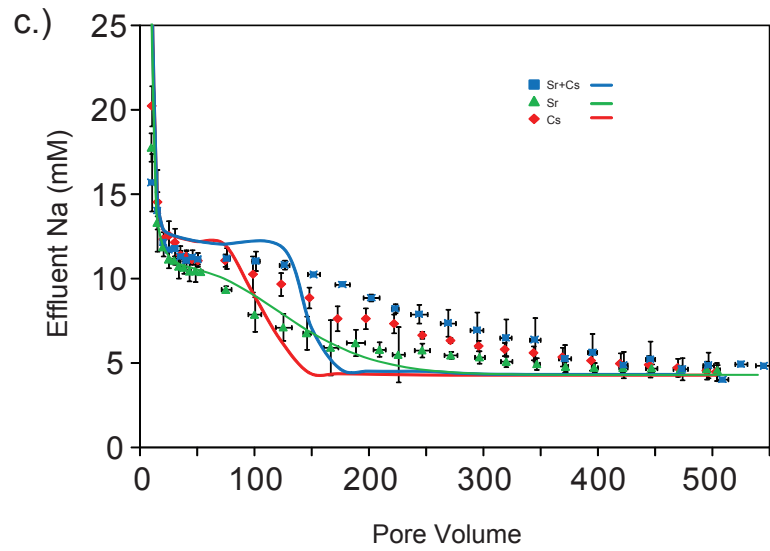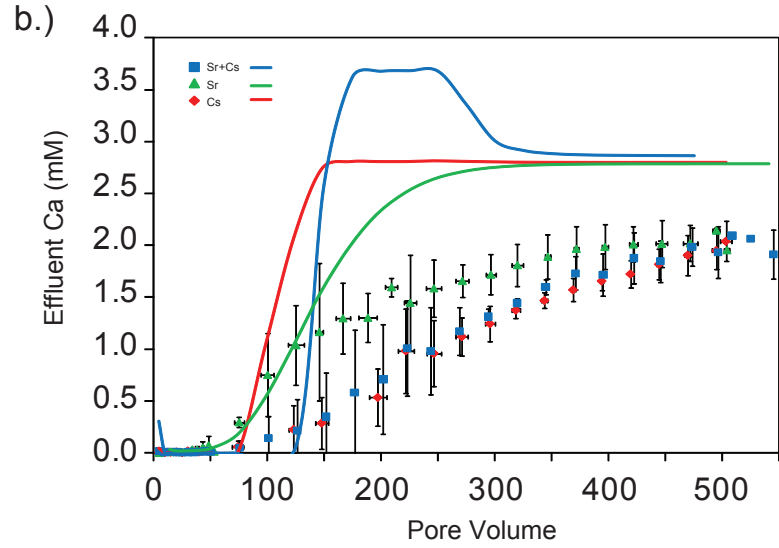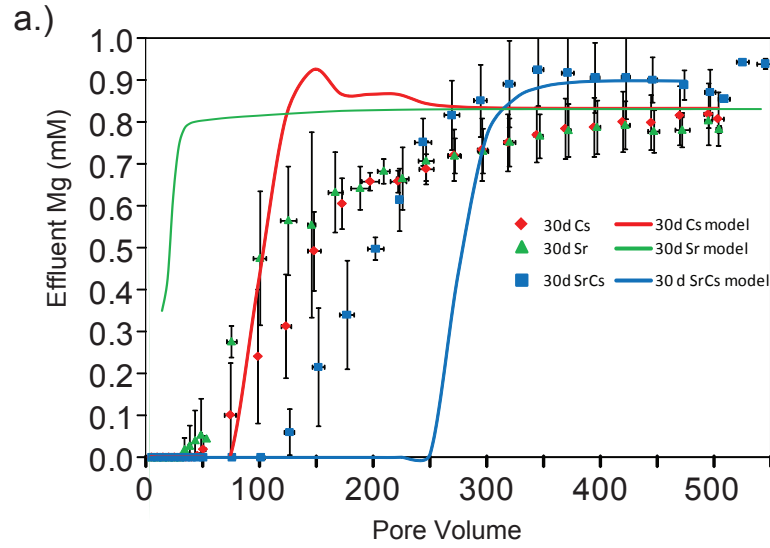
Figure 4.
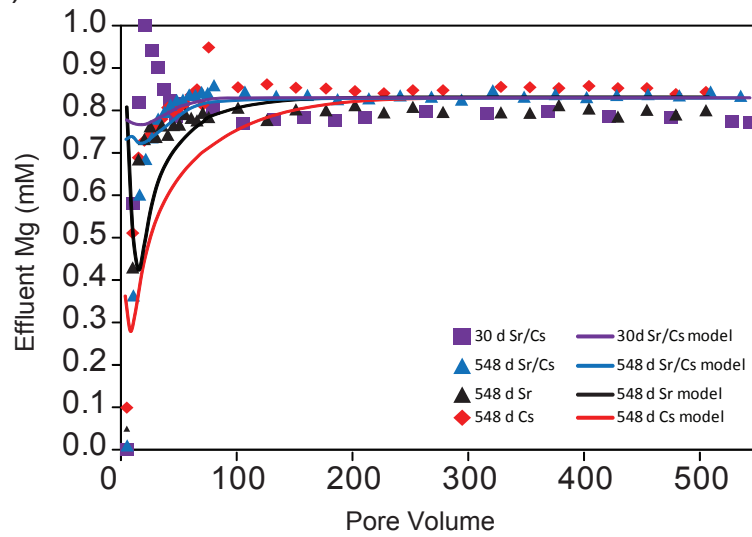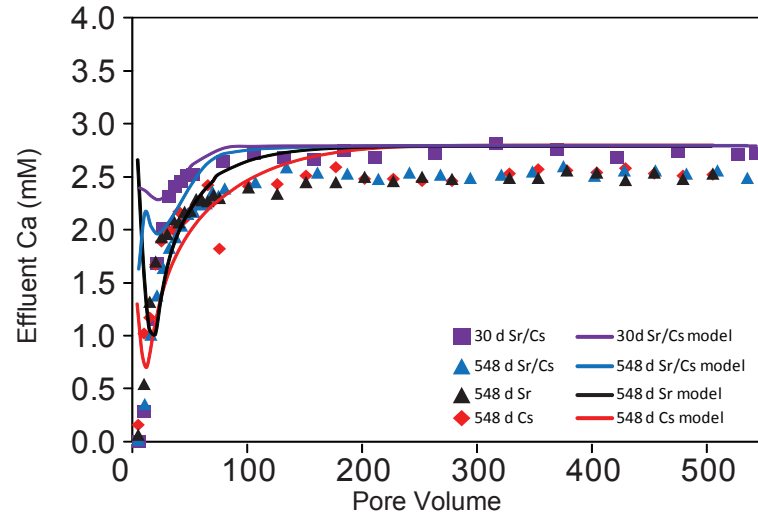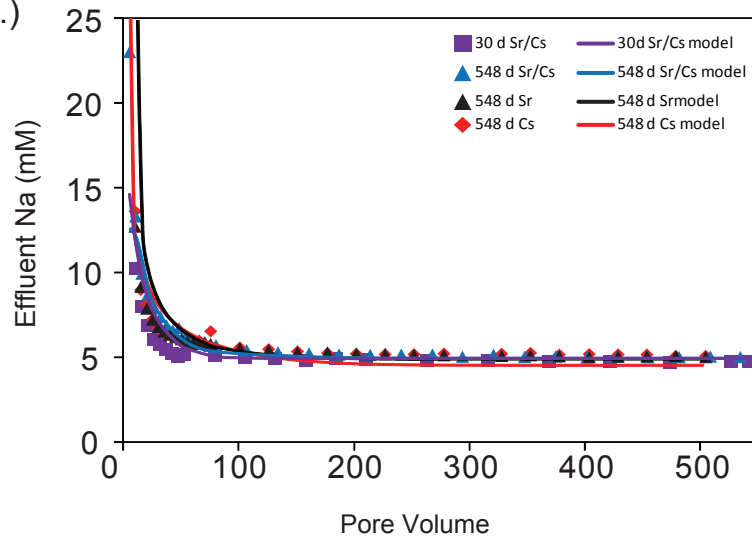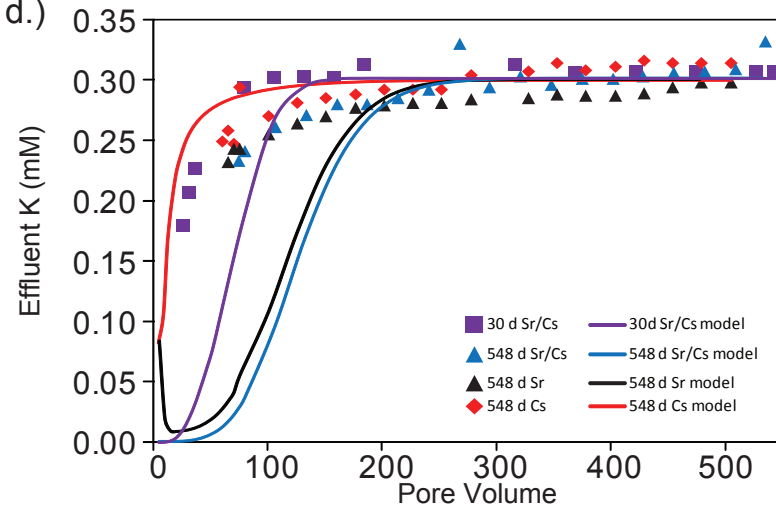
Figure 5.

Figure 6.

Figure 7.
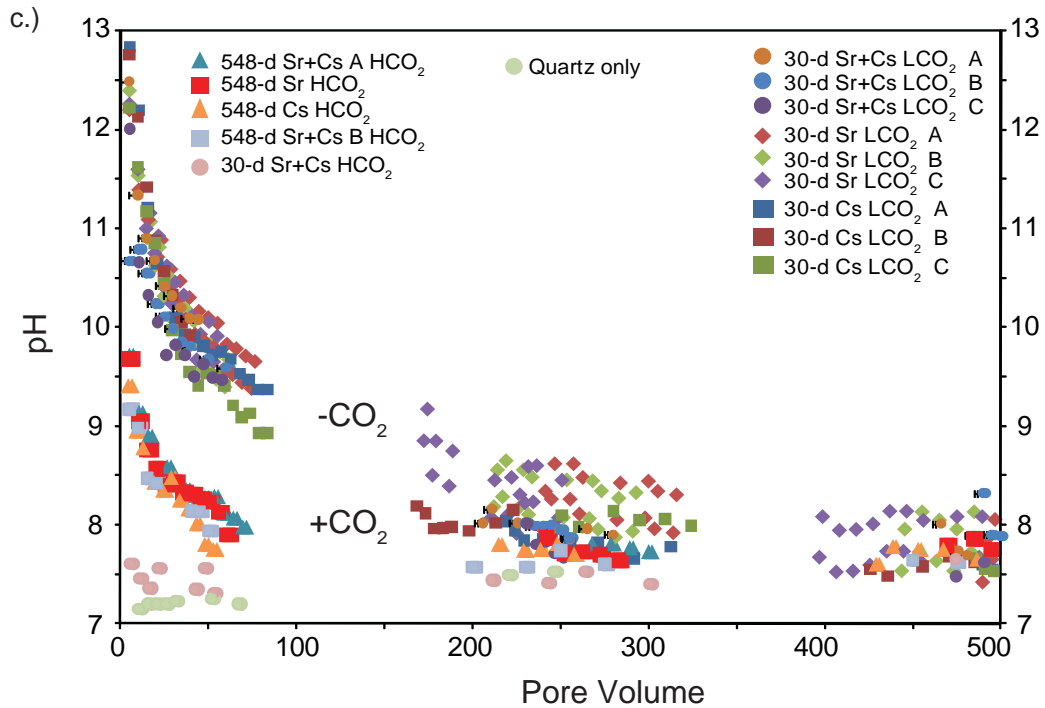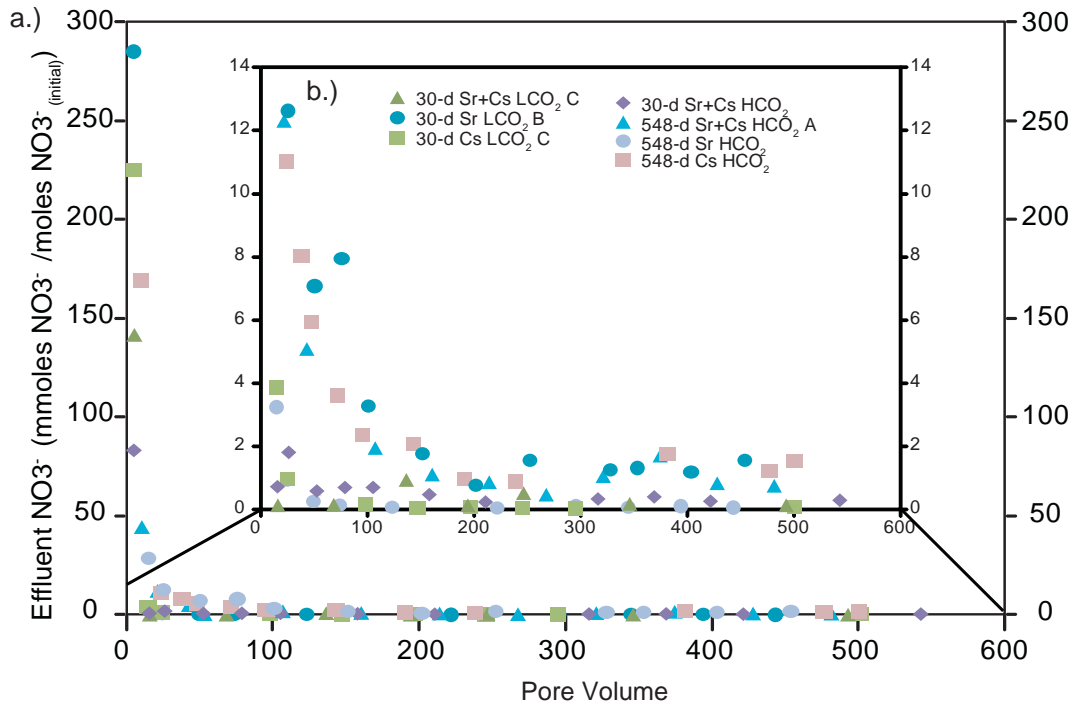
Supporting information:

SI I: Summary of initial Na and total Na released in the columns.

	Initial Na HN solid μmoles	Initial Na SGW μmoles	Total Na Solid + SGW μmoles	Total effluent Na μmoles	% Total Retained
30-d Sr+Cs A -CO$_2$	2013	1192	3205	2515	21.54
30-d Sr+Cs B -CO$_2$	1941	1166	3106	2447	21.23
30-d Sr+Cs C -CO$_2$	1871	847	2718	1778	34.60
30-d Sr A -CO$_2$	2047	834	2881	1841	36.12
30-d Sr B -CO$_2$	1940	859	2799	1751	37.43
30-d Sr C -CO$_2$	1822	837	2660	1684	36.70
30-d Cs A -CO$_2$	1857	828	2685	1509	43.79
30-d Cs B -CO$_2$	1900	847	2748	1850	32.67
30-d Cs C -CO$_2$	1906	833	2739	1868	31.80
30-d Sr+Cs +CO$_2$	485	904	1389	1252	9.84
548-d Sr+Cs +CO$_2$	718	891	1608	1344	16.46
548-d Sr+Cs B +CO$_2$	436	852	1288	1168	9.32
548-d Sr +CO$_2$	791	841	1631	1298	20.43
548-d Cs +CO$_2$	831	841	1672	1335	20.17

-Initial concentration of SGW: Na-3.7 m*m*

SI II: Summary of initial Ca/Mg/K and total Ca/Mg/K released in the columns.

	Initial Ca[a]	Total effluent Ca	% Total Retained	Initial Mg[a]	Total effluent Mg	% Total Retained	Initial K[a]	Total effluent K	% Total Retained
	μmoles	μmoles		μmoles	μmoles		μmoles	μmoles	
30 d Sr+Cs A -CO_2	870	425	51.2	322	211	34.6	96.7	68.2	29.4
30 d Sr+Cs B -CO_2	851	391	54.0	315	205	35.1	94.5	69.0	27.0
30 d Sr+Cs C -CO_2	618	218	64.7	229	132	42.6	68.7	39.0	43.2
30 d Sr A -CO_2	627	292	53.5	232	131	43.8	69.7	48.6	30.3
30 d Sr B -CO_2	611	290	52.5	226	132	41.7	67.9	45.8	32.5
30 d Sr C -CO_2	604	350	42.0	224	145	35.3	67.1	53.6	20.1
30 d Cs A -CO_2	618	255	58.7	229	126	44.9	68.7	34.0	50.5
30 d Cs B -CO_2	608	246	59.5	225	129	42.9	67.5	35.6	47.3
30 d Cs C -CO_2	609	257	57.9	225	125	44.6	67.6	38.5	43.1
30 d Sr+Cs +CO2	660	637	3.45	244	191	22.0	73.0	71.3	2.3
548 Sr+Cs +CO2	650	577	11.2	241	196	18.6	72.2	64.7	10.4
548 Sr+Cs B +CO2	622	420	32.4	230	163	29.2	69.1	64.7	6.4
548 Sr +CO2	614	538	12.4	227	177	22.1	68.2	58.7	13.9
548 Cs +CO2	614	543	11.5	227	189	16.7	68.2	63.4	7.0

[a]Initial concentration of SGW: Ca-2.7 mm, Mg-1.0 mm, K-0.3 mm

SI III. Crystallographic distances for reference compounds

Compound	Atom	N	R (Å)	Ref.	R (Å)	Ref.
Strontianite	O	9	2.547-2.730	1	2.552-2.725	2
(SrCO$_3$)	C	3	3.026-3.064		3.026-3.037	
	Sr	4	4.097-4.116		4.085-4.117	
	Sr	2	4.253		4.236	
	Sr	4	4.902		4.893	
Sr(OH)$_2$(s)	O	7	2.522-2.737	3		
	Sr	2, 2	3.887, 3.095			
	Sr	4	4.032			
Zeolite X (Ca)				4		
I (D6R)	O	6	2.800			
	Al/Si	12	3.521-3.531			
I'	O	10	2.498-3.136			
	Al/Si	6	3.467-3.470			
II	O	9	2.755-3.255			
	Al/Si	6	3.593-3.615			
Zeolite X (Sr)				5		
I (D6R)	O	6	2.652			
	Si	6	3.530			
	Al	6	3.533			
I'	O	3, 3	2.655, 3.147			
	Al/Si	6	3.518			
II	O	3, 3	2.584, 2.900			
	Si	3	3.403			
	Al	3	3.458			
Sodalite (Na)	O	6	2.383-3.127	6		
	Al/Si	6	3.254-3.332			
Cancrinite (Na)				7		
ε-cage	O	8	2.205-2.947			
	Al	3	3.243			
	Si	3	3.334			
Channel	O	10	2.173-2.800			
	Al/Si	3	3.161-3.282			
	Al/Si	3	3.442-3.723			

Notes: Distances calculated from published crystallographic data; element in () was the central atom in the calculation for zeolites and feldspathoids. References: 1. (Pannhorst and Lohn, 1970); 2. (De Villiers, 1971); 3. (Partin and O'Keeffe, 1995); 4. Ca-exchanged zeolite X (Smolin et al., 1989); 5. Sr-exchanged zeolite X (Kim et al., 1999); 6. Synthetic nitrate sodalite (Na$_8$[Al$_6$Si$_6$O$_{24}$](NO$_3$)$_2$) (Buhl and Lons, 1996) and natural chloride sodalite (Na$_8$[Al$_6$Si$_6$O$_{24}$]Cl$_2$ (Hassan et al., 2004); 7. Natural carbonate cancrinite (Na$_{5.96}$Ca$_{1.52}$[Al$_6$Si$_6$O$_{24}$](CO$_3$)$_{1.57}$·1.75H$_2$O) (Hassan et al., 2006).

REFERENCES

Ankudinov, A.L., Nesvizhskii, A.I., and Rehr, J.J. (2003) Dynamic screening effects in x-ray absorption spectra. Physical Review B, 67(11), 115120.

Barrer, R.M., Davies, J.A., and Rees, L.V.C. (1969) Comparison of ion exchange properties of zeolites X and Y. Journal of Inorganic and Nuclear Chemistry, 31(8), 2599-&.

Barros, M., Araujo, I.F., Arroyo, P.A., Sousa-Aguiar, E.F., and Tavares, C.R.G. (2003) Multicomponent ion exchange isotherms in NaX zeolite. Latin American Applied Research, 33(3), 339-344.

Bresciani Pahor, N., Calligaris, M., Nardin, G., and Randaccio, L. (1982) Structure of a basic cancrinite. Acta Crystallographica, Section B (Structural Crystallography and Crystal Chemistry), B38, pt.3, 893-5.

Buck, E., and McNamara, B. (2004) Precipitation of nitrate-cancrinite in Hanford tank sludge. Environmental Science and Technology, 38, 4432-4438.

Buhl, J.C., and Lons, J. (1996) Synthesis and crystal structure of nitrate enclathrated sodalite $Na_8(AlSiO_4)_6(NO_3)_2$. Journal Of Alloys And Compounds, 235(1), 41-47.

Chang, H.-s., Um, W., Rod, K., Serne, R.J., Thompson, A., Perdrial, N., Steefel, C.I., and Chorover, J. (2011) Strontium and Cesium Release Mechanisms during Unsaturated Flow through Waste-Weathered Hanford Sediments. Environmental Science & Technology, 45(19), 8313-8320.

Chen, G., Flury, M., Harsh, J.B., and Lichtner, P.C. (2005) Colloid-facilitated transport of cesium in variably saturated Hanford sediments. Environmental Science & Technology, 39(10), 3435-3442.

Choi, S., O'Day, P.A., Rivera, N.A., Mueller, K.T., Vairavamurthy, M.A., Seraphin, S., and Chorover, J. (2006) Strontium speciation during reaction of kaolinite with simulated tank-waste leachate: Bulk and microfocused EXAFS analysis. Environmental Science & Technology, 40(8), 2608-2614.

Chorover, J., Choi, S., Rotenberg, P., Serne, R.J., Rivera, N., Strepka, C., Thompson, A., Mueller, K.T., and O'Day, P.A. (2008) Silicon control of strontium and cesium partitioning in hydroxide-weathered sediments. Geochimica Et Cosmochimica Acta, 72(8), 2024-2047.

Chorover, J., Choi, S.K., Amistadi, M.K., Karthikeyan, K.G., Crosson, G., and Mueller, K.T. (2003) Linking cesium and strontium uptake to kaolinite weathering in simulated tank waste leachate. Environmental Science & Technology, 37(10), 2200-2208.

Colella, C. (1996) Ion exchange equilibria in zeolite minerals. Miner. Deposita, 31(Copyright (C) 2010 American Chemical Society (ACS). All Rights Reserved.), 554-562.

Deng, Y.J., Flury, M., Harsh, J.B., Felmy, A.R., and Qafoku, O. (2006a) Cancrinite and sodalite formation in the presence of cesium, potassium, magnesium, calcium and strontium in Hanford tank waste simulants. Applied Geochemistry, 21(12), 2049-2063.

Deng, Y.J., Harsh, J.B., Flury, M., Young, J.S., and Boyle, J.S. (2006b) Mineral formation during simulated leaks of Hanford waste tanks. Applied Geochemistry, 21(8), 1392-1409.

Doherty, J. (2002) PEST: Model-independent Parameter Estimation. Watermark Numerical Computing, Corinda, Australia.

Dyer, A., and Keir, D. (1989) Ion exchange and pH tolerance in molecular sieve zeolites. Journal of Radioanalytical and Nuclear Chemistry, 132(2), 423-441.

Fechtelkord, M., Stief, F., and Buhl, J.C. (2001) Sodium cation dynamics in nitrate cancrinite: A low and high temperature ^{23}Na and ^{1}H MAS NMR study and high temperature Rietveld structure refinement. American Mineralogist, 86(1-2), 165-175.

Flury, M., Czigany, S., Chen, G., and Harsh, J.B. (2004) Cesium migration in saturated silica sand and Hanford sediments as impacted by ionic strength. Journal Of Contaminant Hydrology, 71(1-4), 111-126.

Frising, T., and Leflaive, P. (2008) Extraframework cation distributions in X and Y faujasite zeolites: A review. Microporous and Mesoporous Materials, 114(1-3), 27-63.

George, G.N., and Pickering, I.J. (2000) EXAFSPAK: A suite of computer programs for analysis of X-ray Absorption Spectra.

Gephart, R. (2003) A short history of Hanford waste generation storage and release., p. 1-39. Pacific Northwest National Laboratory.

Gephart, R., and Lundgren, R. (1998) Hanford tank clean up: A guide to understanding technical issues., p. 1-71, Columbus, Ohio.

Hackbarth, K., Gesing, T.M., Fechtelkord, M., Stief, F., and Buhl, J.C. (1999) Synthesis and crystal structure of carbonate cancrinite $Na_8(AlSiO_4)_6CO_3(H_2O)_{3.4}$, grown under low-temperature hydrothermal conditions. Microporous and Mesoporous Materials, 30(2-3), 347-358.

Hassan, I., and Grundy, H.D. (1991) The crystal structure of basic cancrinite, ideally $Na_8Al_6Si_6O_{24}](OH)_2\cdot 3H_2O$. The Canadian Mineralogist, 29(2), 377-383.

Mashal, K., Cetiner, Z.S., Flury, M., and Harsh, J.B. (2005) Colloid formation and cesium mobility in Hanford sediment columns leached with simulated tank waste. Geochimica Et Cosmochimica Acta, 69(10), A816-A816.

Mashal, K., Harsh, J.B., Flury, M., Felmy, A.R., and Zhao, H.T. (2004) Colloid formation in Hanford sediments reacted with simulated tank waste. Environmental Science & Technology, 38(21), 5750-5756.

O'Day, P.A., Newville, M., Neuhoff, P.S., Sahai, N., and Carroll, S.A. (2000) X-ray absorption spectroscopy of strontium(II) coordination - I. Static and thermal disorder in crystalline, hydrated, and precipitated solids and in aqueous solution. Journal Of Colloid And Interface Science, 222(2), 184-197.

Olson, D.H. (1970) Reinvestigation of the crystal structure of the zeolite hydrated NaX. The Journal of Physical Chemistry, 74(14), 2758-2764.

Perdrial, N., Rivera, N., Thompson, A., O'Day, P.A., and Chorover, J. (2011) Trace contaminant concentration affects mineral transformation and pollutant fate in hydroxide-weathered Hanford sediments. Journal of Hazardous materials, 197, 119-127.

Qiu, L., Laws, P.A., Zhan, B.-Z., and White, M.A. (2006) Thermodynamic investigations of zeolites NaX and NaY. Canadian Journal of Chemistry, 84(2), 134-139.

Ravel, B. (2001) ATOMS: crystallography for the X-ray absorption spectroscopist. Journal of Synchrotron Radiation, 8, 314-316.

Rivera, N., Choi, S., Strepka, C., Mueller, K., Perdrial, N., Chorover, J., and O'Day, P. (2011) Cesium and strontium incorporation into zeolite-type phases during homogeneous nucleation from caustic solutions. American Mineralogist, 96(11-12), 1809-1820.

Shanbhag, G.V., Choi, M., Kim, J., and Ryoo, R. (2009) Mesoporous sodalite: A novel, stable solid catalyst for base-catalyzed organic transformations. Journal Of Catalysis, 264(1), 88-92.

Sherry, H.S. (1966) Ion-exchange properties of zeolites I. Univalent ion exchange in synthetic faujasite. Journal Of Physical Chemistry, 70(4), 1158-1168.

Sirbescu, M., and Jenkins, D.M. (1999) Experiments on the stability of cancrinite in the system Na_2O-CaO-Al_2O_3-SiO_2-CO_2-H_2O. American Mineralogist, 84(11-12), 1850-1860.

Smith, D.W. (1977) Ionic hydration enthalpies. Journal of Chemical Education, 54(9), 540.

Steefel, C.I., Carroll, S., Zhao, P.H., and Roberts, S. (2003) Cesium migration in Hanford sediment: a multisite cation exchange model based on laboratory transport experiments. Journal Of Contaminant Hydrology, 67(1-4), 219-246.

Steefel, C.I., and Lasaga, A.C. (1992) Putting transport into water-rock interaction models. Geology, 20(8), 680-684.

Steefel, C.I., and Lasaga, A.C. (1994) A coupled model for transport of multiple chemical species and kinetic precipitation/dissolution reactions with application to reactive flow in single phase hydrothermal systems. American Journal of Science, 294(5), 529-592.

Thompson, A., Steefel, C.I., Perdrial, N., and Chorover, J. (2010) Contaminant Desorption during long-term leaching of hydroxide-weathered Hanford sediments. Environmental Science and Technology, 44, 1992-1997.

Townsend, R., and Harjula, R. (2002) Ion exchange in molecular sieves. 41 p.

Townsend, R.P., and Coker, E.N. (2001) Ion exchange in zeolites. In E.M.F.P.A.J. H. van Bekkum, and J.C. Jansen, Eds. Studies in Surface Science and Catalysis, Volume 137, p. 467-524. Elsevier.

Zhao, H.T., Deng, Y.J., Harsh, J.B., Flury, M., and Boyle, J.S. (2004) Alteration of kaolinite to cancrinite and sodalite by simulated hanford tank waste and its impact on cesium retention. Clays And Clay Minerals, 52(1), 1-13.

Chapter 4: Aging effects on Hanford sediments reacted with caustic waste and implications for cesium and strontium sequestration.

ABSTRACT

Sediments from the Hanford nuclear waste site were reacted with a hyperalkaline and high ionic strength synthetic tank waste leachate (STWL) and Sr and Cs release from the alteration products was examined. Column experiments were performed with two types of STWL solutions (Na, Na+K) containing 10^{-3} *molal* Sr and Cs. Solutions were pumped into the column, flow was stopped, and sediments were reacted for 3 days to 4 months. After reaction, columns were flushed with a background pore water (BPW) solution and characterized, or compared with reacted but unflushed colums. There was preferential uptake of Sr over Cs by the sediments. In addition, Cs uptake was further hindered by the presence of K while Sr did not appear to be affected by the additional cation in the initial solution. Solid phase characterization by EXAFS and SEM/TEM showed the production of neophases. Sequential extractions performed on the sediments indicated as the sediment aged more Sr was being sequestered in a more recalcitrant phase but Cs demonstrated similar extraction behavior over time. In columns flushed with (BPW), 15-50% of total Sr and Cs sequestered by the sediment was released. Strontium release was less from aged sediments than short-term experiments, but Cs did not appear to have a time dependence on its release except at the shortest equilibration time (3 d). EXAFS characterization showed that neophases were present in the sediment after flushing with BPW. Sequential extractions performed on flushed sediments showed a migration of the contaminants from the front to the back of the columns. Additionally, the easily exchangeable fraction of the sediment decreased for both Sr and Cs with longer reaction time and a higher fraction was associated with more recalcitrant phases. Results from this study indicate that the aging of sediments in contact with STWL and the uptake

of Sr and Cs into different retention sites (clays for Cs and neophases for Sr) can limit the mobility of these contaminants in the environment.

1. INTRODUCTION

Radioactive leaks that occurred at the Hanford nuclear waste site are estimated to cover 400 square kilometers and have up to 2,000,000 curies of radioactivity, mostly in the form of ^{90}Sr and ^{137}Cs (Gephart, 2003; Gephart and Lundgren, 1998). Sediments located at the Hanford nuclear waste site contaminated with high-level radioactive, caustic wastes have been studied to provide insight into contaminant retention mechanisms (Buck and McNamara, 2004; Chen et al., 2005; Choi et al., 2006; Chorover et al., 2008; Chorover et al., 2003; Deng et al., 2006b; Flury et al., 2004; Gephart, 2003; Gephart and Lundgren, 1998; Mashal et al., 2005; Mashal et al., 2004; Perdrial et al., 2011; Steefel et al., 2003; Thompson et al., 2010). These studies have shown that sediments undergo transformations in the presence of high pH and ionic strength solutions and form secondary phases that can incorporate contaminants such as Sr and Cs. Another possible retention mechanism is sorption of dissolved contaminants by clay minerals and phyllosilicates (McKinley et al., 2007;Steefel et al., 2003). Studies of Hanford sediments reacted with caustic waste have been done mostly in batch conditions (Buck and McNamara, 2004; Choi et al., 2006; Chorover et al., 2008; Chorover et al., 2003; Deng et al., 2006b; Perdrial et al., in press); fewer studies have been performed introducing caustic waste to model systems or sediment systems in a flow-through experiments (Cai et al., 2009; Rod et al., 2010; Um et al., 2005; Wan et al., 2004). These studies showed retardation of Sr and to a lesser extent Cs. In both flow-through and batch experiments, secondary mineral formation and sorption onto clay sites were cited

as retention mechanisms. While many studies have been performed to assess contaminant uptake, fewer studies have examined the release of contaminants.

Although previous studies have established that Cs and Sr can be strongly bound in the soil by precipitation of neoformed phases that sequester these contaminants, key questions remain for remediation of the Hanford site. Recent studies (Chang et al., 2011; Thompson et al., 2010) have shown that Sr and Cs are released from sediments when reacted with an infiltrating groundwater solution. However, these studies aged sediments with simulated tank waste in a batch setting (1:50 sediment: solution ratio) before reaction with a synthetic groundwater. Additionally, the sediments were washed and freeze-dried before the experiment. The goal of this study was to examine Sr and Cs sequestration and release with Hanford sediments in a flow-through setting. This allows a sediment: solution ratio closer to what may be observed in the field as well as capturing the heterogeneity of reaction between the sediment column and the simulated tank waste. The observed neophases found in previous studies may change due to the availability of the soluble Si thus affecting Sr and Cs uptake. Finally, flushing the aged caustic-waste reacted sediments with a synthetic groundwater without alteration to the sediment (washing and drying) provides a more realistic view of the reactions occurring at the Hanford site.

2. MATERIALS AND METHOD

2.1 Column design

For the preparation of the STWL, Nalgene^{TM} polypropylene co-polymer (PPCO) vessels were used instead of glassware at all stages of the experiment to prevent Si contamination. Stock solutions were prepared using ultra-pure (MilliQ^{TM}) water and

reagent grade $NaNO_3$, $NaOH$, $CsCl$, $SrCl_2 \cdot 6H_2O$ (J.T. Baker) and $NaAlO_2 \cdot xH_2O$ powder (EM Science) as obtained from the manufacturer and described previously (Choi et al., 2006; Chorover et al., 2008; Crosson et al., 2006; Thompson et al., 2010). The STWL composition is summarized in **Table 1.** Two types of STWL were used: 2.05 molal Na and Na+K (1molal + 0.8 molal). To prevent the precipitation of Sr from solution, the $SrCl_2 \cdot 6H_2O$ was dissolved separately and then combined to a degassed STWL solution. The background pore water (BPW) solution used for leaching the STWL-reacted sediment is given in **Table 1**.

Columns were designed of PEEK due to its inert properties when in contact with high pH solutions. The column parameters are summarized in **Table 2**. The columns measured 1.91 cm inner diameter by 7.75 cm length for a total empty bed volume of 22.2 cm^3. The columns were packed with an average of 34.2 grams of uncontaminated sediment from the Hanford site, giving a pore volume of 13.8 cm^3. The sediment contains a native Sr concentration ranging from 3.7-4.3 mmol/kg sediment and a Cs concentration between 0.022-0.026 mmol/kg sediment. Further characterization of the sediment can be found in the following publications (Chorover et al., 2008; Perdrial et al., in press; Thompson et al., 2010). Column experiments (run in up-flow) consisted of the following:

1) STWL solutions were pumped into the columns using a Ismatec peritstaltic pump (IPC-4) and pharmed 2-stop tubing. The number of pore volumes (PVs) of STWL reacted with the sediment varied for each experiment (**see Table 2**). The caustic nature of the STWL limited the uptake portion of the experiment due to the back pressure produced by the dissolution of the sediment;

2) flow was stopped and the column closed off to allow for sediment reaction with the STWL for time periods between 1 day to 4 months (**Table 2**);

3) the aged columns were then flushed with BPW to characterize the release behavior for Sr and Cs. The experiments ran for approximately 500 PVs except for experiments 5 and 11, which were not flushed (Table 2).

2.2 Chemical analysis

Selected sediments from the front (0-13 mm) and back (52-76 mm) of the unflushed (7-d and 4-mo) and flushed (1-mo A and 3-mo A) as well as the unreacted Hanford fine sediments were subjected to a three-step sequential extraction. The sediments from the selected zones were homogenized and triplicate extractions were performed on each. The extraction sequence consisted of a 1.0 M $MgCl_2$ initial extraction step (pH=8) followed by a 0.2 M acidic ammonium oxalate (AAO, pH=3), with a final extraction by trace metal grade concentrated hydrofluoric acid (49% HF) at room temperature. Triplicate extractions were performed using 0.3 g and 10 mL of each extractant. All extraction steps had a 2 hour reaction followed by a 30 minute wash step with DI water.

Element concentrations were measured by ICP-MS (Agilent 7500cs) for Sr, Cs, Na, Al, Si. The ICP-MS was run in a soft extraction mode with 1500 W RF power and a PFA introduction system. The system was optimized to keep oxide and doubly charged interferences below 2%. A H_2 collision cell was used to measure Si (detection limit 30 ppb) to limit N and O based interferences at mass 28. A He collision cell was used to measure the Sr, Cs, Na and Al. Low-level quantification of Sr and Cs resulted in a

detection limit of 0.1 ppb for both elements and detection limits for Na and Al of 25 ppb.

2.4 Solid phase characterizations

Precipitates were mounted on Al-alloy stub mounts with double-stick carbon tape and gold-coated because the samples are nonconductive. Images were collected with a FEI Quanta 200 ESEM with a tungsten filament and EDAX Genesis energy-dispersive X-ray spectrometer housed at the Imaging and Microscopy Facility at the University of California, Merced. Images were collected at 15-25 kV at a working distance of 5-10 mm.

Representative samples were examined by transmission electron microscopy (TEM). Ten μL of a 100 mg l^{-1} suspension of synthesis product in nanopure water was dropped on 200-mesh Cu grids, air dried, and imaged using a Hitachi H8100 LaB6 TEM (University of Arizona) operating at 200 kV.

Strontium K-edge X-ray absorption spectra of the both the STWL-reacted and BPW-leached sediments were acquired at the Stanford Synchrotron Radiation Lightsource (SSRL) on beamlines 11-2 and 4-1 under dedicated conditions (3 GeV, 80-100 mA). Spectra were collected using a Si(220) monochromator crystals (vertical beam size = 1 mm) and a focused beam. A rhodium mirror was used for harmonic rejection (17 keV cutoff energy), allowing for a fully tuned beam. Beam energy was calibrated with a $SrCO_3(s)$ standard for which the energy at the midpoint of the edge jump was set to 16105 eV. Samples were held in a He cryostat at 3-5 K during data collection. Fluorescence absorption spectra were collected using a solid-state Ge-array detector and success scans (6-12) were averaged.

Data were analyzed using the programs Sixpack (Webb, 2010) and EXAFSPAK
(George and Pickering, 2000). Absorption background was subtracted using a linear fit
through the pre-edge region and normalized to the average height of the post-edge jump.
Normalization was extended into the EXAFS region (above threshold energy $E_0 = 16115$
eV) using a cubic spline, a Victoreen polynomial, and McMaster coefficients (Brown et
al., 1988). Sediment spectra were analyzed by least-squares linear combination fits using
reference compound spectra to determine the primary Sr-bearing phases. The four
reference spectra used in final fits (unreacted sediment with 275 ppm Sr and three
compounds) were selected based on XRD analysis from a previous study(Perdrial et al.,
in press) of the sediments and trial-and-error fitting using a larger reference compound
library. Reference compounds were a natural chabazite collected from Önundarfjördur,
Iceland with 1355 ppm Sr; natural strontianite, $SrCO_3(s)$ (O'Day et al., 2000) and an
experimentally precipitated and aged (Sr,Cs)-bearing aluminosilicate neophase identified
as a mixed sodalite/cancrinite (Rivera et al., 2011). Reference spectra were analyzed
with non-linear least-squares methods on individual atomic shells in k-space using the
entire k-range in the fit (O'Day et al., 2000). Theoretical phase-shift and amplitude
functions were calculated with the program FEFF9 (Rehr et al., 2010) using atomic
clusters calculated with the program ATOMS(Ravel, 2001). Amplitude reduction factor
(S_0^2) was fixed at 1.0 and photoelectron threshold energy difference (ΔE_o) was treated as
a single adjustable parameter. Reported errors are statistical estimated standard
deviations or least-squares goodness-of-fit parameters.

3. RESULTS

3.1 Initial contaminant uptake

Initial Sr uptake from the STWL reaction ranged from 6-18 mmol/kg sediment, (including 3 mmol/kg native Sr)(**Table 1**). This corresponds to 72-99% Sr uptake from the STWL solution. Experiment 1 was reacted for only 10 PV and had the lowest amount of Sr uptake. More Sr uptake was observed (12 mmol/kg to 17 mmol/kg) with more STWL reacted with the sediment (between 40 and 75 PVs). The columns did not attain complete breakthrough of Sr.

Cesium retention by column sediments (2.6-6.7 mmol/kg sediment; 25-84% uptake) was lower than Sr retention. As with Sr, experiment 1 showed the lowest Cs uptake. For 40 and 75 PV of STWL reacted with sediment, Cs uptake was similar (5.7 mmol/kg and 7.0 mmol/kg respectively). Experiments (2, 9-11) reacted with Na+K STWL exhibited different retention of Cs but not Sr compared to Na-STWL. Strontium uptake ranged from 9-17 mmol/kg (72-91% uptake), depending on the number of PVs introduced to the column (**Table 1**). This was similar to the uptake seen in the Na-STWL columns. For Cs, the sediment retained 1.9-3.2 mmol/kg (15-28% uptake), which was lower than the Na-STWL Cs uptake.

3.2 Background Pore Water (BPW) flush

3.2.1 Sediments reacted with Na-STWL

At all equilibration times, there was minimal release of Sr before 20-35 PVs (**Figure 1a**). The Sr effluent edge was time-dependent, with the 3 d column releasing Sr first followed by the 14 d column, 1 mo, and 3 mo column, respectively. The 3 d column exhibited the maximum effluent concentration of 2.7 mmoles Sr/moles $Sr_{initial}$. For the 3

mo column, the major flush of Sr was between 100-200 PVs, and the concentrations of Sr in the effluent was more sustained than in the other columns. The Sr fraction remaining on the solids (**Figure 2a**) showed that, for the first 100 PVs, the 3 mo column retained more Sr than 3 d and 1 mo columns. The 3 mo column released the most overall Sr (48% of the initial loading) with the majority of Sr loss occurring between 100-200 pore volumes. Cesium (**Figure 1c**) exhibited a large initial flush followed by a steady state release between 50-75 pore volumes. The 3 d column deviated from this behavior with a large Cs flush between 10-200 PVs and did not reach a steady state Cs effluent until after 300 pore volumes. The 3 d and 14 d columns showed elevated release of Cs (**Figure 2b**) and retained 50-60% of the initial Cs loaded, while the 1m and 3 mo A columns retained 70-85% of the initial Cs.

The effluent cation behavior showed differences between the divalent cations (Ca, Mg) and the monovalent cations (Na,K) (**Figure 3**). Calcium in the effluent had a retardation of 50-100 PVs. When Ca breakthrough occurred, the maximum concentration rose above the influent concentration of the BPW (2.8 mmolar) at 3.5-4.5 mM at 50 PVs, but reached the inlet concentration soon afterwards. There were slight differences in Ca release with column aging time. The 3 mo column showed a retardation of 50 PV compared to the less-aged columns, defined as 3 d-1 mo columns hereafter, with maximum breakthrough at 100 PVs. Effluent Mg was retarded to a larger extent than the Ca. The breakthrough for Mg occurred between 100-125 PVs. Unlike Ca, Mg did not exceed its influent BPW concentration. Column aging also played a role in Mg breakthrough, with the 3 mo column showing more retardation of Mg than the other columns. The less-aged columns reached complete breakthrough around 150 PVs, but

the 3 mo column took approximately 200 PVs to reach the inlet BPW concentration (0.85 mmolar). Sodium effluent showed a rapid decrease over the first 50 PVs from 20 mM to 4 mM for all columns. Column aging did not appear to influence effluent Na. Potassium showed retardation of up to 100 PVs before complete breakthrough (0.35 mM). There was no K data for the 1 mo A column due to contamination from pH measurements. The 3 mo A sediment column displayed behavior similar to that of the less-aged columns with no discernible K retardation due to aging.

Aluminum and Si showed high initial release over the first 100 PVs (**Figure 5**). The initial Al release was up to 1 mM in the effluent solution and Si initial release was up to 2.5 mM. After 100 PVs, effluent Al dropped below 20 mM (inset **Figure 5b**). After 100 PVs, Si showed a steady release between 75-125 mM, with the 3 mo A column exhibiting higher Si steady state release at 200 mM. At 3 d and 14 d, the total Si/Al ratio for the experiment was 0.63 and 1.1, respectively. As the columns aged, the Si/Al ratio increased with a range of 2.3-2.6 for the 1 mo columns and a Si/Al ratio of 9 for the 3 mo column.

The effluent pH for all experiments was near 13 at the beginning of flush out with BPW (**Figure 6**). As BPW was pumped into the system, there was a steady decline of pH, with three main regions emerging in the data. The initial flush was 50 PVs and pH dropped from 13 to 11.5. From 50-100 PVs, pH ranged from 10.5-11.5. Between 100-200 PVs, the 3 mo column and less-aged columns diverged, with the latter showing a steeper pH decrease to 8 and the 3 mo columns decreasing to a pH of 9. After 200 PVs, a steady state pH was reached with no experiments reaching the influent pH of 6.8.

3.2.2 Sediments reacted with Na+K-STWL

Experiments 9-11 (3 mo columns) demonstrated lower effluent Sr concentrations than experiments 3-6,8 but column effluent behavior was similar (**Figure 1b**). The total Sr retained ranged from 70-80% initial Sr (**Figure 2a**). Experiment 7 (1m C) had Sr retention at levels of the 3 mo columns deviating from behavior of the other 1 mo columns .

Although less Cs was removed from Na+K STWL solutions compared with Na-STWL columns, Cs in BPW effluent followed similar patterns. Cesium release (**Figure 1d**) exhibited a large initial flush followed by a steady state release between 50-75 pore volumes. Between 60-80% of total Cs loaded on the sediments was not desorbed (**Figure 2b**). Experiment 10 had a large initial Cs release of 10% of total Cs, whereas initial Cs release from the other columns was 5% or less. After this large release, experiment 10 exhibited similar desorption behavior as the other columns of the same reaction time.

Divalent cations in column effluent did not appear to be affected by the composition of the initial STWL solution. Effluent Ca had a retardation of 50-100 PVs and the maximum concentration (3.5-4.5 mM) rose above the influent concentration of the BPW (2.8 mmolar) (**Figure 4a**). The breakthrough for Mg occurred between 100-125 PVs and did not exceed its influent BPW concentration (**Figure 4b**). Sodium release was rapid for all columns and reached the influent BPW concentration after 50 PVs (**Figure 4c**). Potassium release was similar to that of Na but required 200 PVs of flushing to reach the influent BPW concentration (**Figure 4d**).

The release of Al and Si was similar to the Na-STWL columns where Si effluent

concentration was higher than Al. The Si/Al ratio ranged from 5.6-24 and was higher

than for 1 and 7 d columns (**Table 3**).

3.3 Solid phase characterization

3.3.1 Sequential extractions

The unreacted sediments showed negligible release of Sr and Cs for the $MgCl_2$

and AAO extraction steps. No Cs was detected from the two-step extraction and 0.1

mmol/kg sediment of Sr was extracted from the sediment. The HF extraction removed

measurable amounts of Sr and Cs (0.020 mmol Cs/kg sediment and 3.1 mmol Sr/kg

sediment) (**Figure 7, Table 4**). The amounts of Sr and Cs recovered from the extractions

were below the native concentrations measured in the sediment (3.7-4.3 mmol Sr/kg

sediment and 0.022-0.026 mmol Cs/kg sediment).

The two unflushed sediments (STWL reacted only) demonstrated Sr and Cs

uptake by the sediments. For both columns (7 d and 4 mo), the front 0-13 mm of

sediment in the column showed increased uptake of the contaminants when compared to

the back 52-76 mm of the sediment. After 7 days, the $MgCl_2$ extraction removed the

majority of the Sr from the front-end sediments, with the AAO and HF extractions only

accounting for 15% of the total 4.6 mmol Sr/kg sediment (**Figure 7a**). The back portion

of the 7 d column had a total Sr extraction of 1.0 mmol Sr/kg sediment, with 44%

extraction by the $MgCl_2$ extraction and 56% by the AAO and HF extractions. The 4 mo

front-end sediments showed only 23% Sr release in the $MgCl_2$ step.   The AAO

extraction recovered 21% of the Sr while the HF extraction step released 55% of the total

Sr. The back end of the column differed in Sr release, with 52% recovered in the $MgCl_2$

step, 10% extraction in the AAO step, and the HF extraction accounting for the remaining 38% of the Sr.

Cesium extractions for the 7 d front end showed different proportions of Cs release compared with Sr (**Figure 7b**). The $MgCl_2$ extraction accounted for 48% of the Cs, the AAO step for 45%, and the HF digestion for 7%. Although the back end of the column had lower Cs associated with the solid (1.8 vs. 1.2 mmol/kg), it showed similar extraction behavior as the front end ($MgCl_2$: 42%; AAO: 48%; HF: 10%). At 4 mo reaction time, the front and back ends of the column (1.0 and 0.6 mmol Cs/kg) exhibited less Cs uptake compared to the 7 d column; however, the proportions recovered in each extraction step were similar. For the three steps, the Cs proportion was 44%,48%, and 8% at the front end and 42%, 49%, and 9% at the back end.

In contrast to the unflushed sediments, the flushed sediments tended to show higher sediment Sr and Cs in the back 52-76 mm of the column compared to the front end (**Figure 7**). At 1 mo, there is an increase in Sr extracted by $MgCl_2$ (25% vs 35%) from the front to back end and decreases in the other two extraction steps (AAO 16% to 12% and HF 59% to 52%). The 3 mo column was similar, with t a larger proportion of Sr extracted in the $MgCl_2$ step (16% vs 24%) from front to back, AAO extraction remained the same at 10%, and the HF extraction decreased from 74 to 66%.

For Cs at 1 mo, the back end of the column has 2.4 times the amount of Cs than the front end. However, the extraction proportions were similar for the three steps: $MgCl_2$ (26% vs. 29%), AAO (66% vs 62%), and HF (8% vs 9%). At 3 mo, the back end of the column had ~2.7 times more Cs than the front end. The proportion of Cs associated with the $MgCl_2$ extraction increased from 19% to 41%, the AAO fraction

107

decreased from 67% to 42%, and the HF fraction remained approximately the same (15% to 17%).

3.3.2 Microscopy

Images were obtained by SEM and TEM on the unreacted sediment and unflushed samples from the 7-d and 4-month front of the columns (**Figures 8,9**). The unreacted sediment had particles with no precipitates associated with them (**Figure 8a,b**). The 7-d unflushed sample (**Figure 8c**) exhibited needle-like and spherical structures between 2.0-5.0 micrometers in length. **Figure 8d** shows a particle from the 4-month unflushed sediment with precipitate morphologies not seen in the unreacted sediment. The TEM images (**Figure 9**) further demonstrate precipitates forming on the 7-d (a,b) and 4-m sediments (c,d).

3.3.3 Strontium X-ray Absorption Spectroscopy

Linear combination fits indicated that Sr was associated with three phases: Sr in unreacted sediment, a feldspathoid phase (best fit by sodalite/cancrinite), and a zeolite phase (best fit by chabazite) (**Figure 10**, **Table 5**). For the unflushed samples (7 d and 4 mo), the front 0-13 mm of the column showed an unreacted sediment fraction and a sodalite/cancrinite phase. The unreacted fraction decreased and another secondary phase increased from 7 d to 4 mo. A sediment spectrum from the back 52-76 mm of the 7 d column was dominated by the unreacted sediment with a small fraction of a secondary phase.

Spectra for 1 mo and 3 mo reacted sediment likewise showed an unreacted component and a feldspathoid phase. An additional Sr-chabazite phase that was not present in the other spectra was detected in the 1 mo A and B spectra. The 3 mo A

108

spectra was fit with two phases, unreacted sediment and feldspathoid, of similar

abundance.XRD spectra (data not shown) do not show any secondary phases.

4. Discussion

4.1 Solid phase

Although XRD showed no secondary phase formation in sediments reacted with

STWL, SEM and TEM images of the unflushed sediment showed secondary phases on

sediment grains consistent with feldspathoid morphologies (Perdrial et al., 2011). In

addition, Sr EXAFS at 7 d and 4 mo indicated an increasing abundance of feldspathoid

phases over time. Structural analyses from EXAFS indicates that Sr in these phases is

consistent with partial Sr dehydration and bonding to framework oxygen atoms in

sodalite cages or in large channels in cancrinite (Rivera et al., 2011). It is likely that Cs

and Sr have different retention mechanisms in the sediment. Strontium could partition

into zeolite and feldspathoid neophases and Cs may be retained to a large extent by clay

minerals and phyllosilicates (Chorover et al., 2008; McKinley et al., 2007; Perdrial et al.,

2011; Thompson et al., 2010). High concentrations of Na in the STWL would most likely

keep Cs from incorporating into feldspathoid structures (Rivera et al., 2011). Sequential

extractions of unflushed sediments corroborate different retention mechanisms for the

two contaminants. At 7 d, Sr was predominantly associated with an easily exchangeable

fraction in the sediment. Studies have shown that secondary phases can take up to 30

days to form crystal structures at room temperature (Deng et al., 2006a; Deng et al.,

2006b; Rivera et al., 2011; Valtchev et al., 2005),. From 7 d to 4 mo, Sr was

incorporated into more recalcitrant phases based on AAO and HF extractions. Similar

results were found in prior studies of sediments reacted with STWL in batch experiments

(Choi et al., 2006; Chorover et al., 2008; Chorover et al., 2003; Thompson et al., 2010). The fraction of Sr extracted by HF may be a combination of the native Sr in plagioclase, the conversion of the native Sr phase into secondary phases, and uptake of contaminant Sr. The EXAFS data at 4 mo showed an increase in the fraction of secondary phases relative to the native Sr phase. Cesium uptake decreased from 7 d to 4 mo mainly because the 4 mo sediment was reacted with Na+K STWL rather than Na STWL. However, the proportions of Cs associated with each extraction step was similar, which suggests that the Cs retention mechanism does not change with aging time.

4.2 Contaminant uptake and release in column experiments

Results indicated an overall preference for Sr uptake over Cs by the Hanford sediment when reacted with STWL in stopped-flow column experiments. These results are consistent with similar batch and flow-through studies on Hanford sediments (Choi et al., 2006; Chorover et al., 2008; Chorover et al., 2003; Perdrial et al., in press; Thompson et al., 2010). Cesium achieved complete breakthrough of the STWL concentration but Sr did not over the length of the experiment. Cesium has been shown to readily pass through the Hanford sediment in prior column experiments (Steefel et al., 2003). When comparing overall removal from solution, Sr uptake is 2-4 times higher than Cs uptake with Na-STWL, and a factor of 5-6 times higher from Na+K STWL. Potassium inhibited Cs uptake, probably by competing with Cs for sorption sites on clay minerals (Perdrial et al., in press; Steefel et al., 2003; Thompson et al., 2010).

After the stopped-flow with STWL, the BPW flush showed that Sr and Cs was resolubilzed by an infiltrating solution. For Sr, there appeared to be a time dependence where the 3 mo aged sediments tended to retain more Sr than observed at shorter reaction

110

times, although this trend was not followed for 1 and 3 mo A sediment columns.. For these columns, the ratio of retained Sr:Cs after STWL reaction was the lowest for all columns at ~2:1. Higher Cs retention relative to Sr suggests that some competition occurs between the Sr and Cs. When comparing Cs release at 1 mo and 3 mo, Cs had the highest retention for all of the columns but Sr had the largest amount of desorption. In general, Sr release was gradual, with the majority of Sr removed between 100-300 PVs. The lack of an initial pulse of Sr suggests uptake from pore water during equilibration. Cesium desorption showed some dependence on aging of the sediments, with 3 d and 14 day columns releasing the most Cs after 100 PVs. The 3 mo C column showed a deviation from the time dependence of Cs retention. In the initial 20 PVs of BPW flush, 10% of the total Cs was desorbed. After this initial flush, only 30% of total Cs was desorbed and effluent concentrations followed the release behavior of the other 3 month columns. The other 3 mo columns (B and D), which were reacted with Na+K STWL solution, also showed a high initial flush but not to the extent of the 3 month C column. This large flush could be the result of competition between the K and Cs where K has a higher selectivity over Cs for similar sorption sites on clays (Steefel et al., 2003). During the 3 month equilibration period, Cs remained in the pore water at higher concentrations in the Na STWL than in columns with Na+K STWL, which would account for the observed Cs desorption behavior.

The behavior of other cations in the BPW further demonstrated changes in the sediment over time. For all columns regardless of STWL type, there was retardation of all cations in the BPW that increased with aging of the columns. This retardation could be attributed to the increased weathering of the sediment and the formation of more sites

111

for cation exchange. From 3 d to 3 mo, the ratio of effluent Si/Al increased, which suggests higher Si availability for neophase formation. Also, the pH at 3 mo was elevated compared to the lower equilibration times, indicating more weathering of the sediments during the stopped-flow interval. Sequential extractions showed movement of the Sr and Cs contaminants from the front of the column to the back. The proportion of Sr and Cs associated with more recalcitrant phases increased after flushing. However, most Sr was extracted by HF, indicating partitioning to recalcitrant silicate phases. Most Cs was extracted by AAO, which targets poorly crystalline phases. The easily exchangeable fraction was mostly removed from the sediment column by the BPW flush.. The EXAFS spectrum of flushed sediment at 1 mo indicated a chabazite-like structure which was not observed in the flushed sediment. With soluble Si present during flushing and the mobilization of the contaminants, it is possible that the chabazite phase formed after the stopped-flow equilibration time and not during the STWL interaction. The appearance of this phase shows the heterogeneity of the sediment system as well as the complex geochemical dynamics occurring in the system.

5. IMPLICATIONS

The results of this study provide a window into the complexity of the geochemical interactions occurring during reaction of Hanford sediments with caustic waste and the ability of contaminants to remain associated with solid phases. Results show that Sr and Cs appear to partition differently to the sediment during reaction with STWL. The Cs mostly partitions to the clay fraction and phyllosilicates of the sediment and Sr tends to associate with aluminosilicate neophases formed by reaction with the hyperalkaline solution. The two different retention mechanisms for Sr and Cs is important because Sr

and Cs release is affected when Sr and Cs are co-contaminants compared to when they are retained in separate phases. Strontium has a much higher retention on sodalite and cancrinite in the absence of Cs. The condition for Sr retention in the sediment is favorable since sodalite and cancrinite are the dominant neophases present. Although sediments in these experiments were aged for relatively short times when compared to the Hanford nuclear waste site, the results indicate that contaminants will be more difficult to solubilize when contacted with a near-neutral pore-water solution when aged for increasing time periods.

Tables

Table 1: Column influent solutions

STWL[a]		STWL		BPW[b]	
Na	*molal*	Na+K	*molal*		*millimolal*
Na^+	2.05	Na^+	1.05	Na^+	4.3
K^+	--	K^+	0.7	K^+	0.35
pH	13	pH	13	pH	6.8
Sr^{+2}	0.001	Sr^{+2}	0.001	Mg^{+2}	0.83
Cs^+	0.001	Cs^+	0.001	Ca^{+2}	2.8
Al^{+3}	0.05	Al^{+3}	0.05	SO_4^{2-}-S	1.9
NO_3^-	1.0	NO_3^-	1.0	CO_3^{2-}	1.5

[a]Simulated Tank Waste Leachate; [b]Background Pore Water

Table 2: Column parameters for uptake and desorption experiments.

Experiment Number	Sediment Loaded g	STWL type[a]	STWL flushed g	PVs[b]	Sr uptake[c]	Cs uptake[c]	Stopped Flow duration	BPW[d] interaction	Volume flushed L	PVs[b]	Sr retained[c]	Cs retained[c]
1	35.00	Na	82	10.3	6.23	2.60	7 d	No	--	--	--	--
2	33.53	Na+K	210	28.7	9.28	1.88	4 mo	No	--	--	--	--
3	33.99	Na	526	71.8	17.2	4.97	3 d	Yes	3.97	552	9.10	2.53
4	33.55	Na	552	75.2	18.4	6.11	14 d	Yes	3.84	521	12.3	3.81
5	32.80	Na	298	40.7	11.8	6.09	1 mo A	Yes	1.50	202	8.08	5.52
6	35.13	Na	552	75.4	15.9	4.04	1 mo B	Yes	3.67	491	9.68	2.87
7	33.93	Na	369	50.3	12.5	4.36	1 mo C	Yes	3.61	515	9.52	3.21
8	34.20	Na	303	41.4	11.6	6.70	3 mo A	Yes	4.03	548	6.03	5.70
9	34.61	Na+K	608	82.8	16.8	3.15	3 mo B	Yes	3.87	538	13.7	2.54
10	35.04	Na+K	320	43.6	11.2	2.02	3 mo C	Yes	3.69	498	8.10	1.48
11	34.50	Na+K	580	79.3	15.5	2.52	3 mo D	Yes	5.85	799	11.5	1.71

[a]Simulated Tank Waste Leachate; [b]Pore Volumes;;[c]mmol/kg sediment; [d]Background Pore Water

Table 3. Total moles Al and Si eluted after BPW flush

Experiment	Si eluted	Al eluted	Si/Al
	moles		ratio
3	0.52	0.82	0.63
4	0.62	0.56	1.1
5	0.67	0.275	2.5
6	0.91	0.39	2.3
7	0.91	0.35	2.6
8	2.4	0.27	9.1
9	1.1	0.20	5.6
10	1.1	0.046	24
11	1.2	0.22	5.4

Table 4: Sequential extractions of selected sediment columns.

Experiment			Sr MgCl$_2$[c]	Sr AAO[c]	Sr HF[c]	Cs MgCl$_2$[c]	Cs AAO[c]	Cs HF[c]
			mmol Sr/kg sediment			mmol Cs/kg sediment		
Front[a]	1	7 d	3.9(5)[d]	0.21(3)	0.47(6)	0.87(6)	0.81(3)	0.12(2)
	2	4 mo	1.0(0)	1.0(1)	2.5(4)	0.44(2)	0.48(5)	0.087(2)
	5	1 mo A	0.73(1)	0.46(2)	1.7(1)	0.25(3)	0.64(9)	0.080(1)
	8	3 mo A	0.42(1)	0.27(0)	2.0(2)	0.11(0)	0.41(3)	0.09(3)
Back[b]	1	7 d	0.44(1)	0.078(1)	0.5(2)	0.51(1)	0.58(5)	0.12(2)
	2	4 mo	2.0(1)	0.38(1)	1.5(3)	0.24(0)	0.28((1)	0.06(1)
	5	1 mo A	1.2(0)	0.44(7)	1.8(8)	0.69(2)	1.5(1)	0.21(4)
	8	3 mo A	0.77(5)	0.31(2)	2.1(3)	0.65(3)	0.66(2)	0.26(4)
unreacted sediment					3.1(2)			0.020(3)

[a]Front 0-13 mm of column; [b]Back 52-76 mm of column; [c]Sequential extraction consisted of 1.0 M MgCl$_2$ initial extraction step (pH=8) followed by a 0.2 M acidic ammonium oxalate (AAO, pH=3), with a final extraction by trace metal grade concentrated hydrofluoric acid (49% HF) at room temperature. [d]Numbers in () are standard deviations of triplicate measurements.

Table 5: Linear combination fits of Sr EXAFS spectra of reacted Hanford sediments.

Experiment		Front 0-13 mm			Back 52-76 mm		
		HF unreacted	Sodalite	Chabazite	HF Unreacted	Sodalite	Chabazite
1	7 d	51	49		88	12	
2	4 mo	38	62		--	--	--
5	1 mo A	32	29	39	36	16	48
6	1 mo B	58	29	13	43	30	27
8	3 mo A	52	48		50	50	--

REFERENCES

Buck, E., and McNamara, B. (2004) Precipitation of nitrate-cancrinite in Hanford tank sludge. Environmental Science and Technology, 38, 4432-4438.

Cai, R., Lindquist, W.B., Um, W., and Jones, K.W. (2009) Tomographic analysis of reactive flow induced pore structure changes in column experiments. Advances in Water Resources, 32(9), 1396-1403.

Chen, G., Flury, M., Harsh, J.B., and Lichtner, P.C. (2005) Colloid-facilitated transport of cesium in variably saturated Hanford sediments. Environmental Science & Technology, 39(10), 3435-3442.

Choi, S., O'Day, P.A., Rivera, N.A., Mueller, K.T., Vairavamurthy, M.A., Seraphin, S., and Chorover, J. (2006) Strontium speciation during reaction of kaolinite with simulated tank-waste leachate: Bulk and microfocused EXAFS analysis. Environmental Science & Technology, 40(8), 2608-2614.

Chorover, J., Choi, S., Rotenberg, P., Serne, R.J., Rivera, N., Strepka, C., Thompson, A., Mueller, K.T., and O'Day, P.A. (2008) Silicon control of strontium and cesium partitioning in hydroxide-weathered sediments. Geochimica Et Cosmochimica Acta, 72(8), 2024-2047.

Chorover, J., Choi, S.K., Amistadi, M.K., Karthikeyan, K.G., Crosson, G., and Mueller, K.T. (2003) Linking cesium and strontium uptake to kaolinite weathering in simulated tank waste leachate. Environmental Science & Technology, 37(10), 2200-2208.

Crosson, G., Choi, S., Chorover, J., Amistadi, M., O'Day, P., and Mueller, K. (2006) Solid-State NMR identification and quantification of newly formed aluminosilicate phases in weathered kaolinite systems. Journal of Physical Chemistry B, 110, 723-732.

Deng, Y.J., Flury, M., Harsh, J.B., Felmy, A.R., and Qafoku, O. (2006a) Cancrinite and sodalite formation in the presence of cesium, potassium, magnesium, calcium and strontium in Hanford tank waste simulants. Applied Geochemistry, 21(12), 2049-2063.

Deng, Y.J., Harsh, J.B., Flury, M., Young, J.S., and Boyle, J.S. (2006b) Mineral formation during simulated leaks of Hanford waste tanks. Applied Geochemistry, 21(8), 1392-1409.

Flury, M., Czigany, S., Chen, G., and Harsh, J.B. (2004) Cesium migration in saturated silica sand and Hanford sediments as impacted by ionic strength. Journal Of Contaminant Hydrology, 71(1-4), 111-126.

George, G.N., and Pickering, I.J. (2000) EXAFSPAK: A suite of computer programs for analysis of X-ray Absorption Spectra.

Gephart, R. (2003) A short history of Hanford waste generation storage and release., p. 1-39. Pacific Northwest National Laboratory.

Gephart, R., and Lundgren, R. (1998) Hanford tank clean up: A guide to understanding technical issues., p. 1-71, Columbus, Ohio.

Mashal, K., Cetiner, Z.S., Flury, M., and Harsh, J.B. (2005) Colloid formation and cesium mobility in Hanford sediment columns leached with simulated tank waste. Geochimica Et Cosmochimica Acta, 69(10), A816-A816.

Mashal, K., Harsh, J.B., Flury, M., Felmy, A.R., and Zhao, H.T. (2004) Colloid formation in Hanford sediments reacted with simulated tank waste. Environmental Science & Technology, 38(21), 5750-5756.

McKinley, J.P., Zeissler, C.J., Zachara, J.M., Serne, R.J., Lindstrom, R.M., Schaef, H.T., and Orr, R.D. (2001) Distribution and Retention of ^{137}Cs in Sediments at the Hanford Site, Washington. Environmental Science & Technology, 35(17), 3433-3441.

O'Day, P.A., Newville, M., Neuhoff, P.S., Sahai, N., and Carroll, S.A. (2000) X-ray absorption spectroscopy of strontium(II) coordination - I. Static and thermal disorder in crystalline, hydrated, and precipitated solids and in aqueous solution. Journal Of Colloid And Interface Science, 222(2), 184-197.

Perdrial, N., Rivera, N., Thompson, A., O'Day, P.A., and Chorover, J. (2011) Trace contaminant concentration affects mineral transformation and pollutant fate in hydroxide-weathered Hanford sediments. Journal of Hazardous materials, 197, 119-127.

Ravel, B. (2001) ATOMS: crystallography for the X-ray absorption spectroscopist. Journal of Synchrotron Radiation, 8, 314-316.

Rivera, N., Choi, S., Strepka, C., Mueller, K., Perdrial, N., Chorover, J., and O'Day, P. (2011) Cesium and strontium incorporation into zeolite-type phases during homogeneous nucleation from caustic solutions. American Mineralogist, 96(11-12), 1809-1820.

Rod, K.A., Um, W., and Flury, M. (2010) Transport of Strontium and Cesium in Simulated Hanford Tank Waste Leachate through Quartz Sand under Saturated and Unsaturated Flow. Environmental Science & Technology, 44(21), 8089-8094.

Steefel, C.I., Carroll, S., Zhao, P.H., and Roberts, S. (2003) Cesium migration in Hanford sediment: a multisite cation exchange model based on laboratory transport experiments. Journal Of Contaminant Hydrology, 67(1-4), 219-246.

Thompson, A., Steefel, C.I., Perdrial, N., and Chorover, J. (2010) Contaminant Desorption during long-term leaching of hydroxide-weathered Hanford sediments. Environmental Science and Technology, 44, 1992-1997.

Um, W., Serne, R.J., Yabusaki, S.B., and Owen, A.T. (2005) Enhanced Radionuclide Immobilization and Flow Path Modifications by Dissolution and Secondary Precipitates. Journal of Environment Quality, 34(4), 1404-1414.

Valtchev, V.P., Bozhilov, K.N., Smaihi, M., and Tosheva, L. (2005) Room temperature synthesis: an efficient way for studying the zeolite formation. In J. Cejka, N. Zilkova, and P. Nachtigall, Eds. Molecular Sieves: From Basic Research to Industrial Applications, Pts a and B, 158, p. 73-80.

Wan, J., Tokunaga, T.K., Larsen, J.T., and Serne, R.J. (2004) Geochemical evolution of highly alkaline and saline tank waste plumes during seepage through vadose zone sediments. Geochimica et Cosmochimica Acta, 68(3), 491-502.

Zhao, H.T., Deng, Y.J., Harsh, J.B., Flury, M., and Boyle, J.S. (2004) Alteration of kaolinite to cancrinite and sodalite by simulated hanford tank waste and its impact on cesium retention. Clays And Clay Minerals, 52(1), 1-13.

Figure Captions

Figure 1. Effluent Sr (micromoles) normalized to moles of initial Sr including native Sr. a.) for 3 d and 14 d columns ($\blacklozenge$), the 1 mo columns ($\blacktriangle$), and 3 mo A column ($\blacksquare$) and b.) 3 mo B,C,and D column. Plots c.) and d.) show effluent Cs (micromoles) normalized to moles of initial Cs with c.) 3 d and 14 d columns ($\blacklozenge$), the 1 mo columns ($\blacktriangle$), and 3 mo A column ($\blacksquare$) and d.) 3 mo B,C,and D column.

Figure 2. Solid fraction of both Sr and Cs remaining during flush out with BPW. a.) Sr fraction remaining for 3 d and 14 d columns ($\blacklozenge$), 1 mo columns ($\blacktriangle$) and 3 mo columns ($\blacksquare$). b.) Cs fraction remaining for 3 d and 14 d columns ($\blacklozenge$), 1 mo columns ($\blacktriangle$) and 3 m columns ($\blacksquare$).

Figure 3. Effluent data showing the cation releases for 3 d and 14 d columns ($\blacklozenge$), the 1 mo columns ($\blacktriangle$), and 3 m A column ($\blacksquare$) a.) Ca (C_o=2.8 mm) b.) Mg (C_o=0.85 mm) c.) Na (C_o=4.25 mm) d.) K (C_o=0.35 mm).

Figure 4. Effluent data showing the cation releases for 3 m B,C, and D columns ($\blacksquare$) a.) Ca (C_o=2.8 mm) b.) Mg (C_o=0.85 mm) c.) Na (C_o=4.25 mm) d.) K (C_o=0.35 mm).

Figure 5. a.) Al release for 3 d and 14 d columns ($\blacklozenge$), 1 mo columns ($\blacktriangle$) and 3 m columns ($\blacksquare$) with inset (b). c.) Si release for 3 d and 14 d columns ($\blacklozenge$), 1 mo columns ($\blacktriangle$) and 3 m columns ($\blacksquare$) with inset (d).

Figure 6. Effluent pH for 3 d and 14 d columns (♦), 1 mo columns (▲) and 3 m columns (■). The 3 m columns have a higher steady state pH than the shorter term columns. No column reaches the inlet solution pH of 7.

Figure 7. Sequential extractions performed on for the unreacted, 7 days, and 4 months STWL reacted sediments and the 1 mo A and 3 m A flushed sediments. The front (0-13 mm) and back (52-76 mm) of the sediment columns were reacted with $MgCl_2$ (⊠), AAO (☐), and HF (◼). Error bars are for triplicate extractions. a.) Sr concentrations (mmol/kg sediment) b.) Cs concentrations (mmol/kg sediment).

Figure 8. SEM images for the unreacted sediment (a. and b.), the 7 days unflushed sediment (c.), and the 4 months unflushed sediments (d.). Image c. shows needle like precipitates while image d. shows weathering on a mineral surface.

Figure 9. TEM images for 7 days unflushed sediment (a. and b.) and 4 months unflushed sediments (c. and d.). All images show precipitation on mineral surfaces resulting from the interaction with STWL.

Figure 10. Strontium K-edge EXAFS of a) reference compounds, b) Front 0-13 mm of sediment column and c) Back 52-76 mm of sediment column. Dashed lines in a) are non-linear least-squares fits of individual atomic shells using theoretical phase shift and amplitude functions; in b) and c), dashed lines are linear combination least-squares fits using the reference compounds shown in a).

Figure 1.
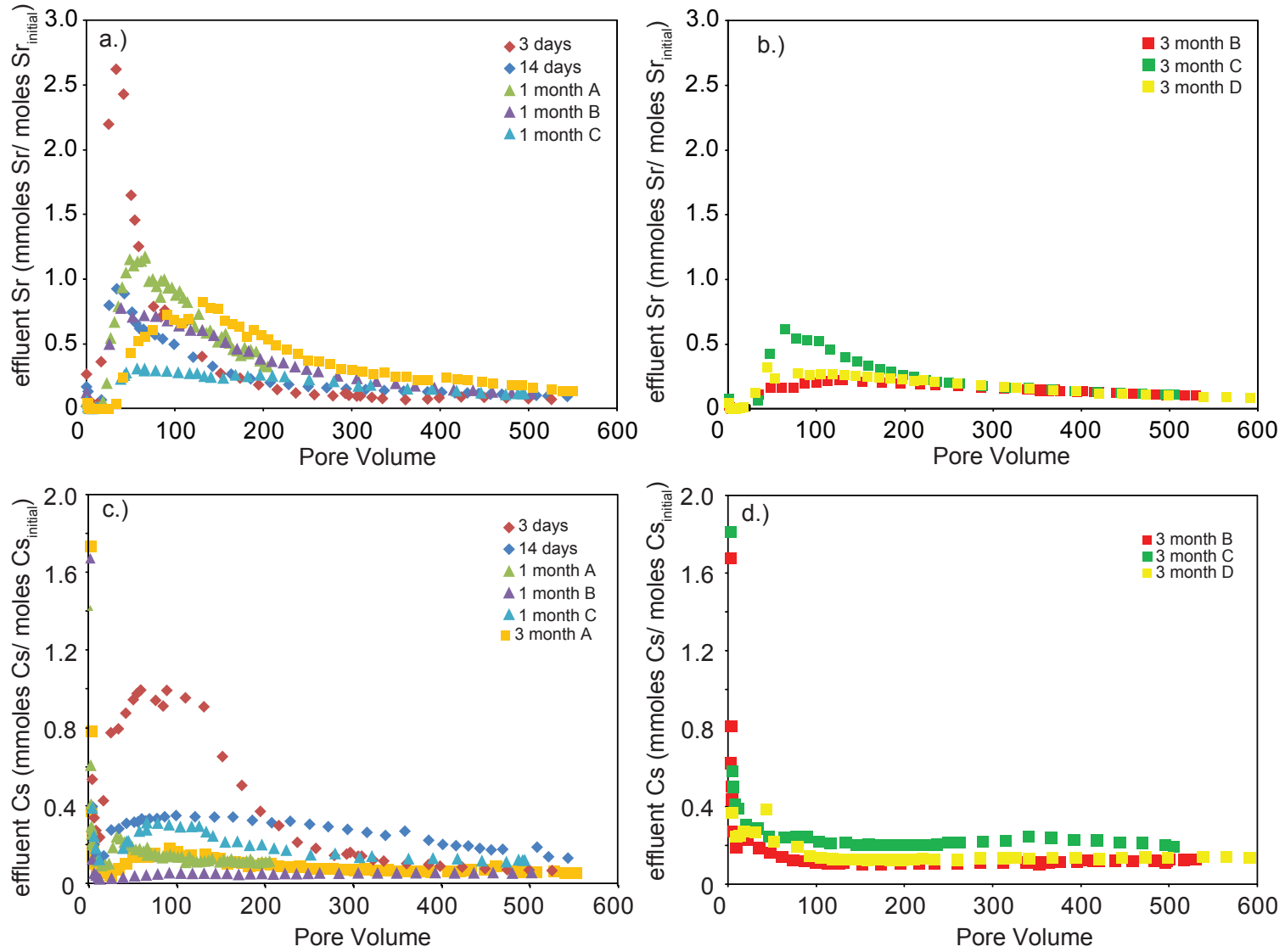
Figure 2.
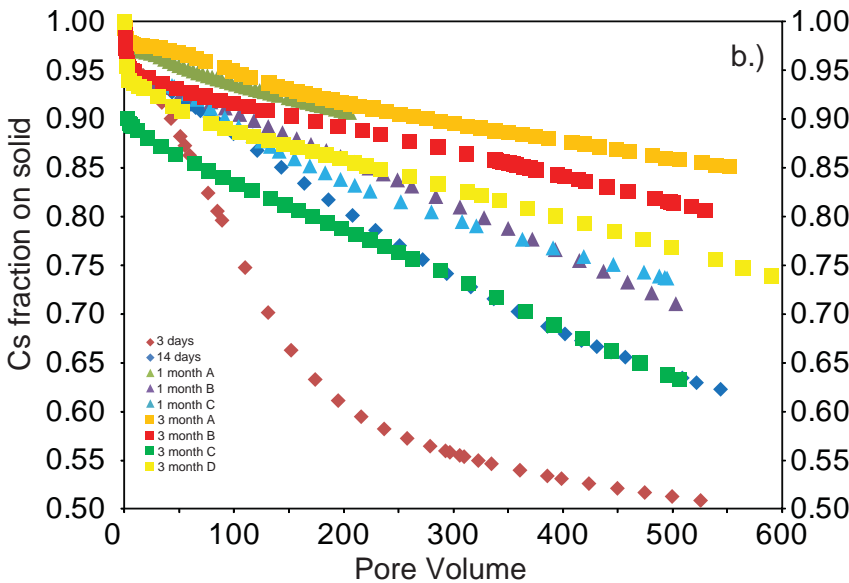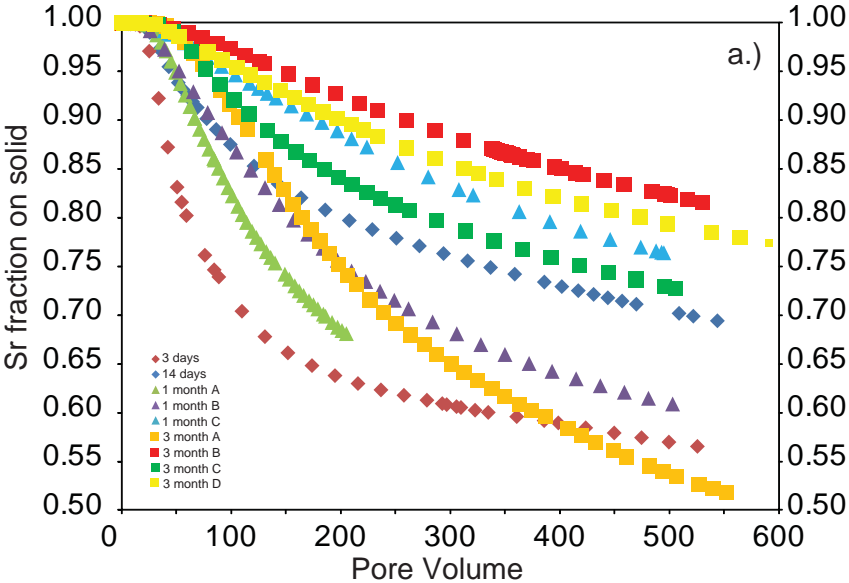
Figure 3.
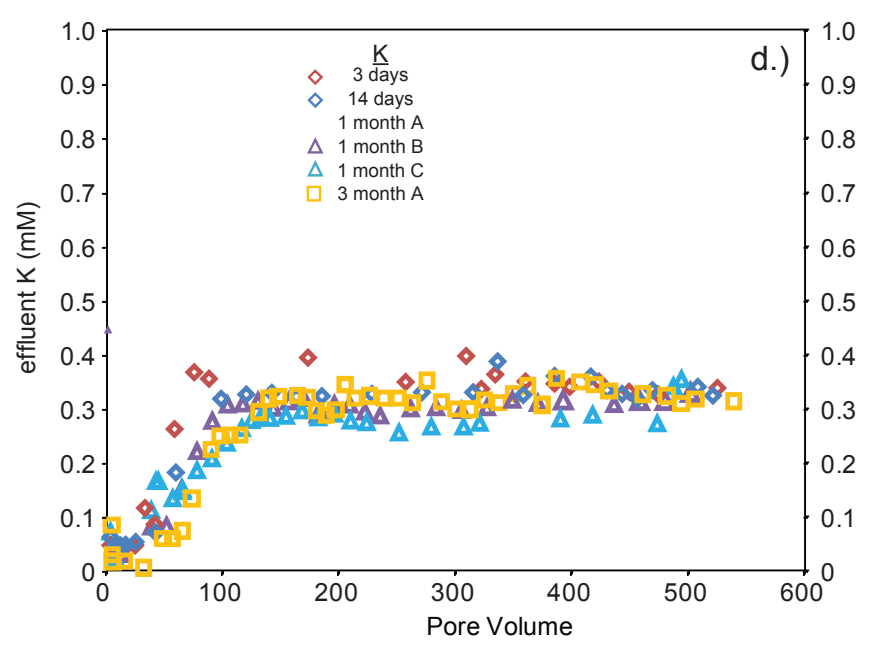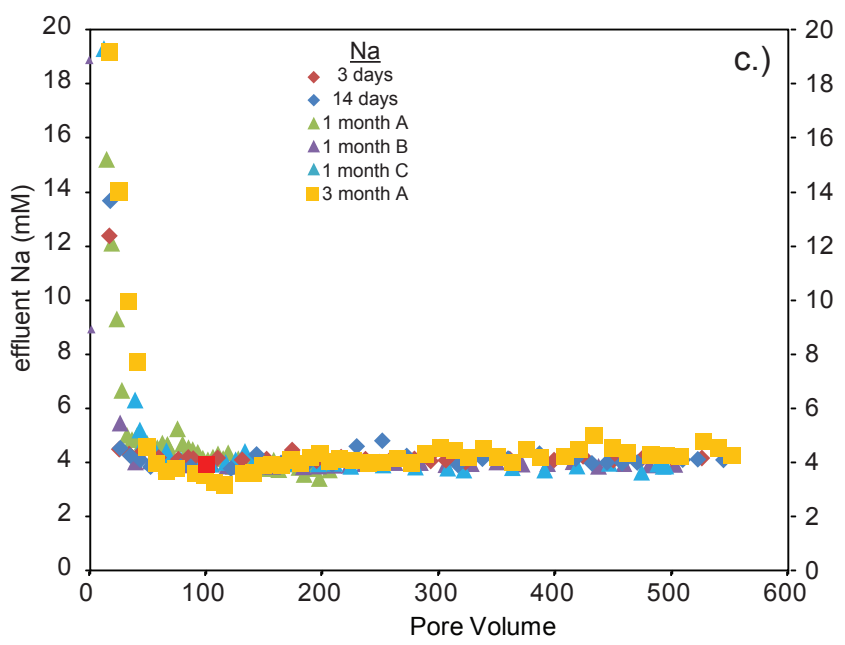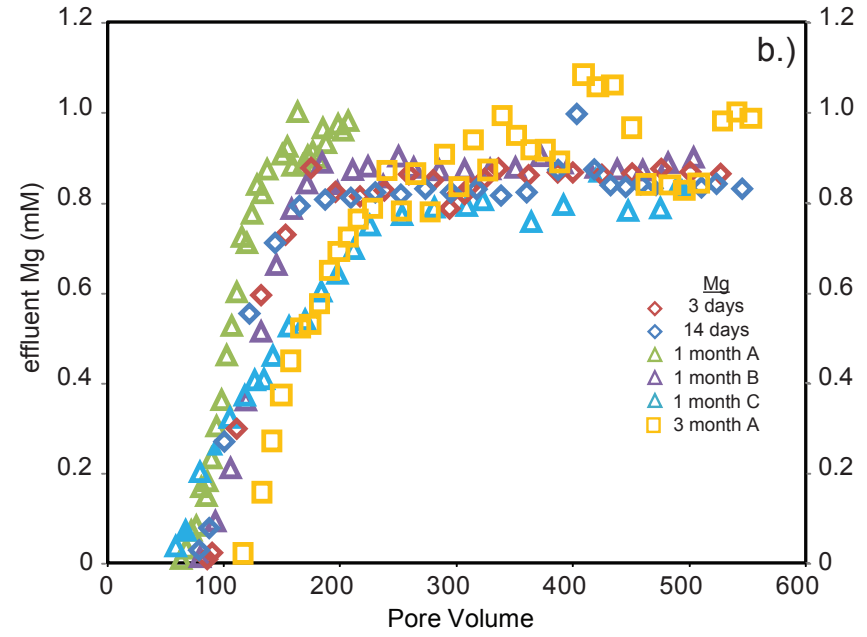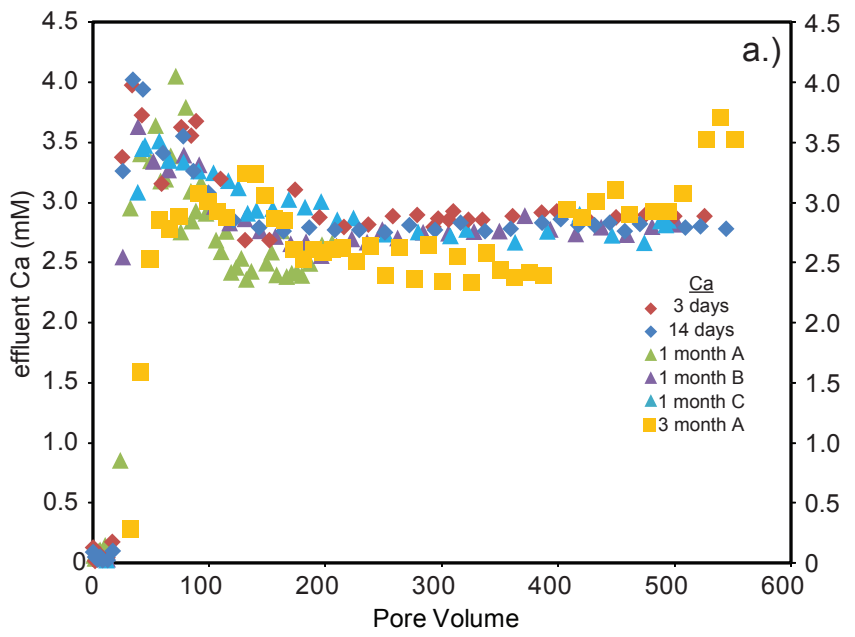
Figure 4.
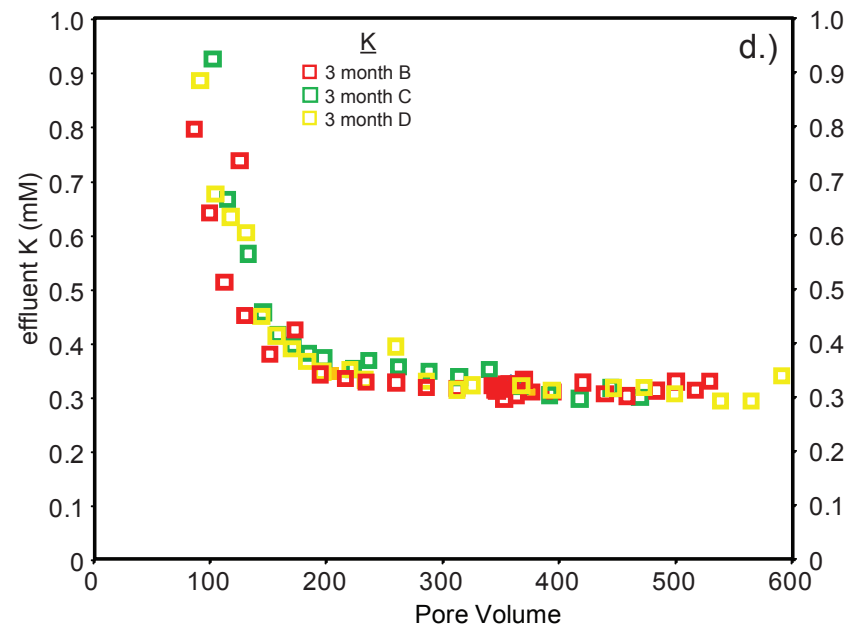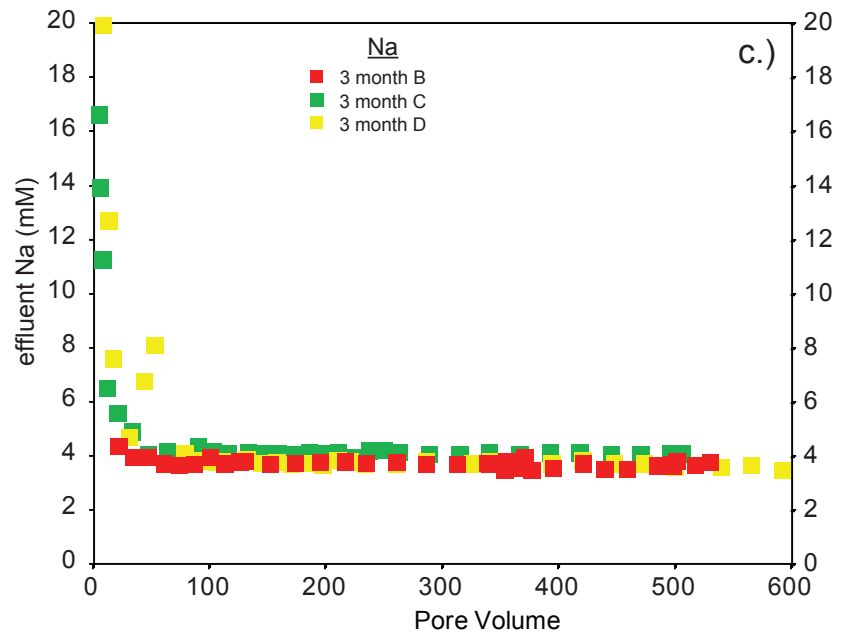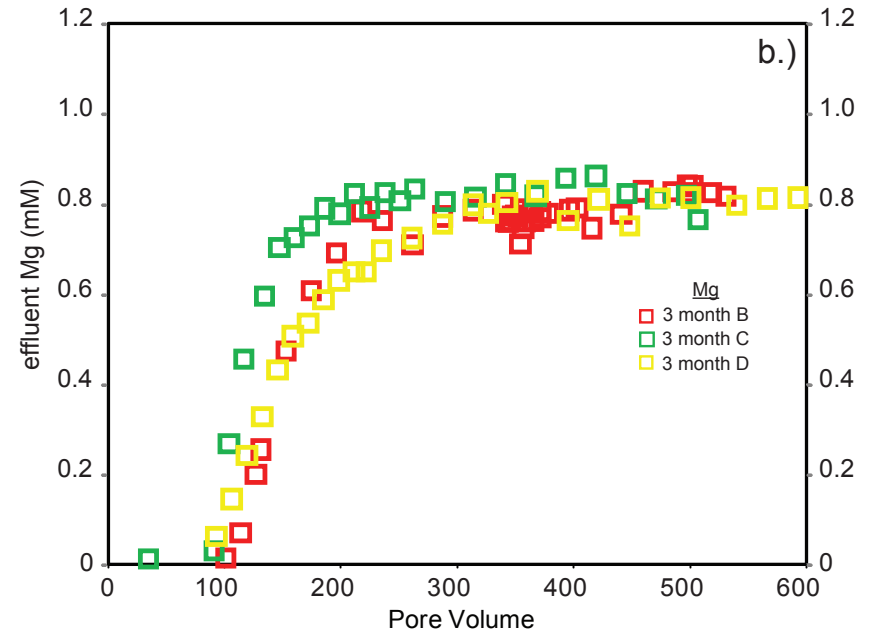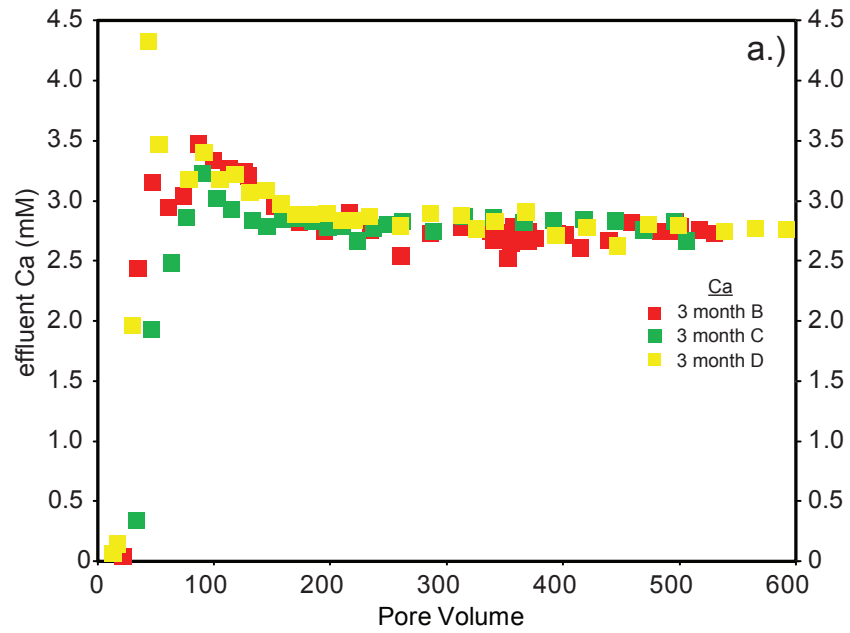
Figure 5.
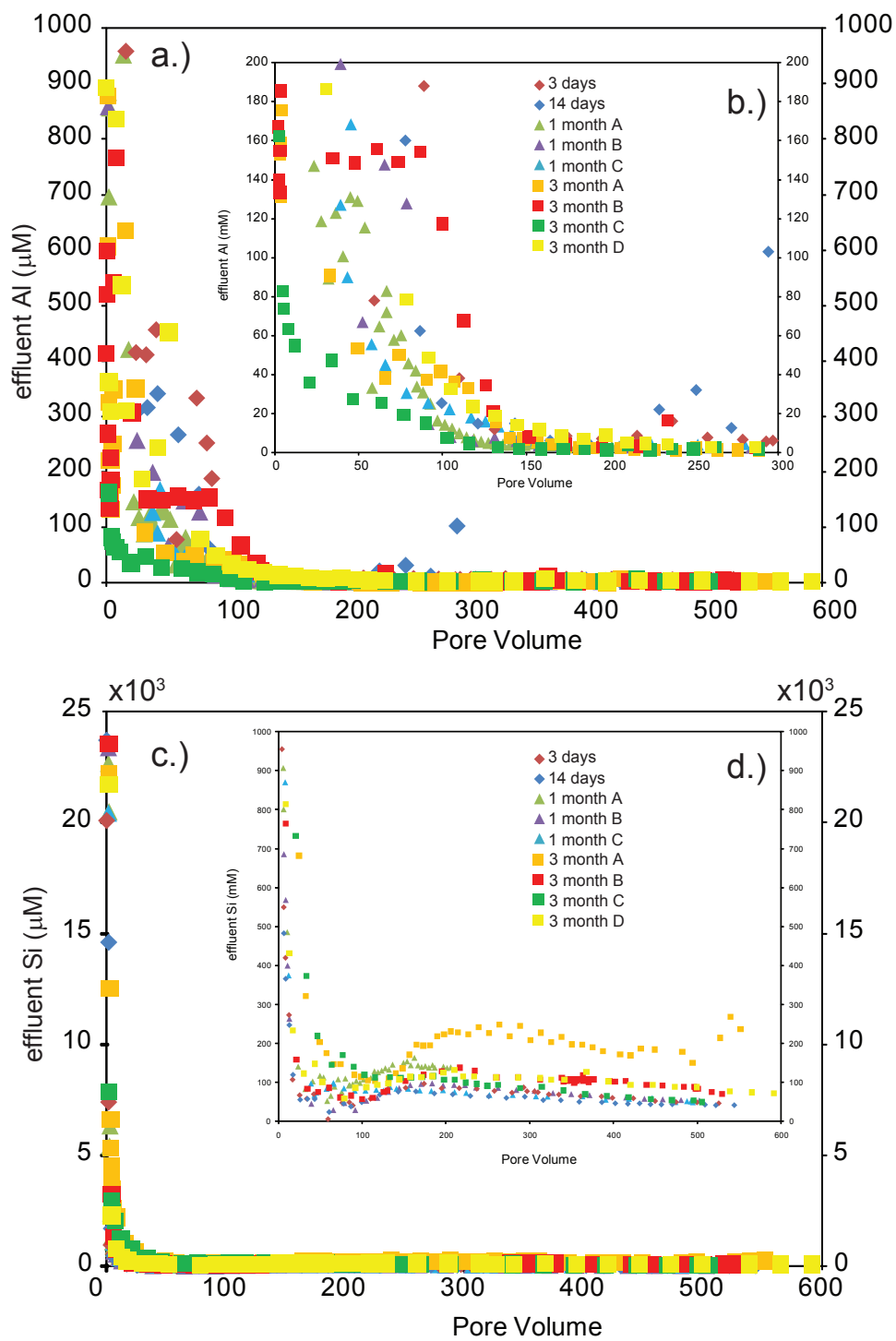
Figure 6.
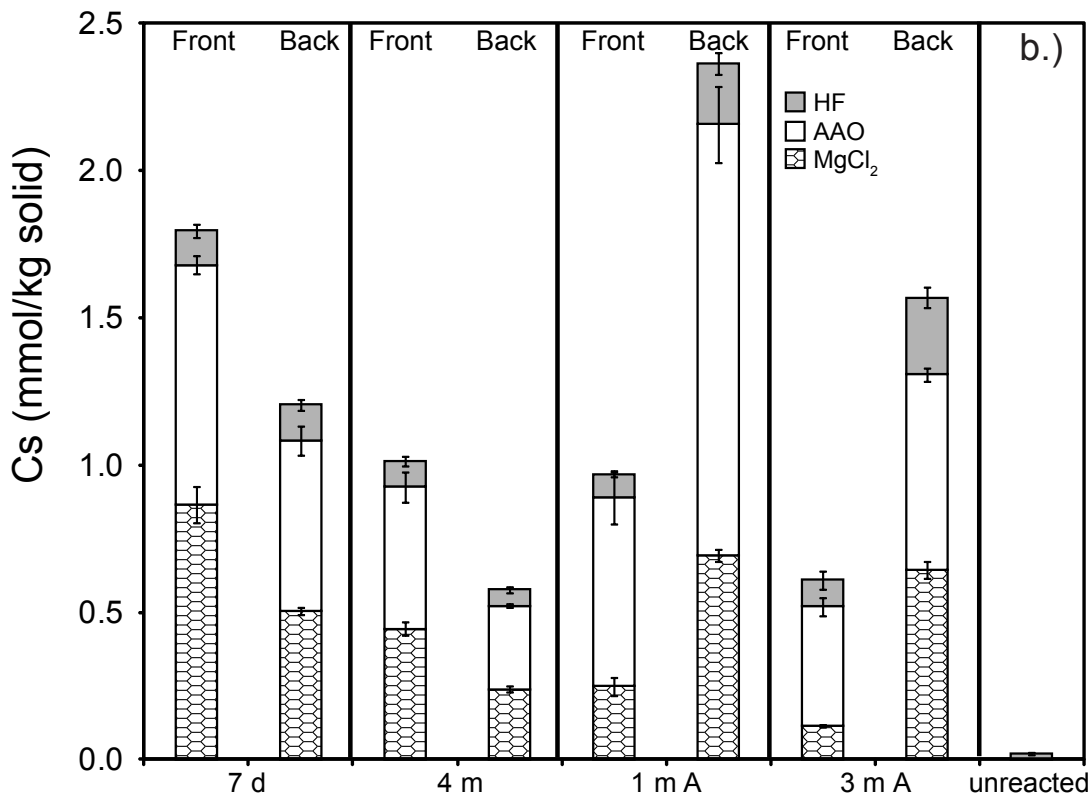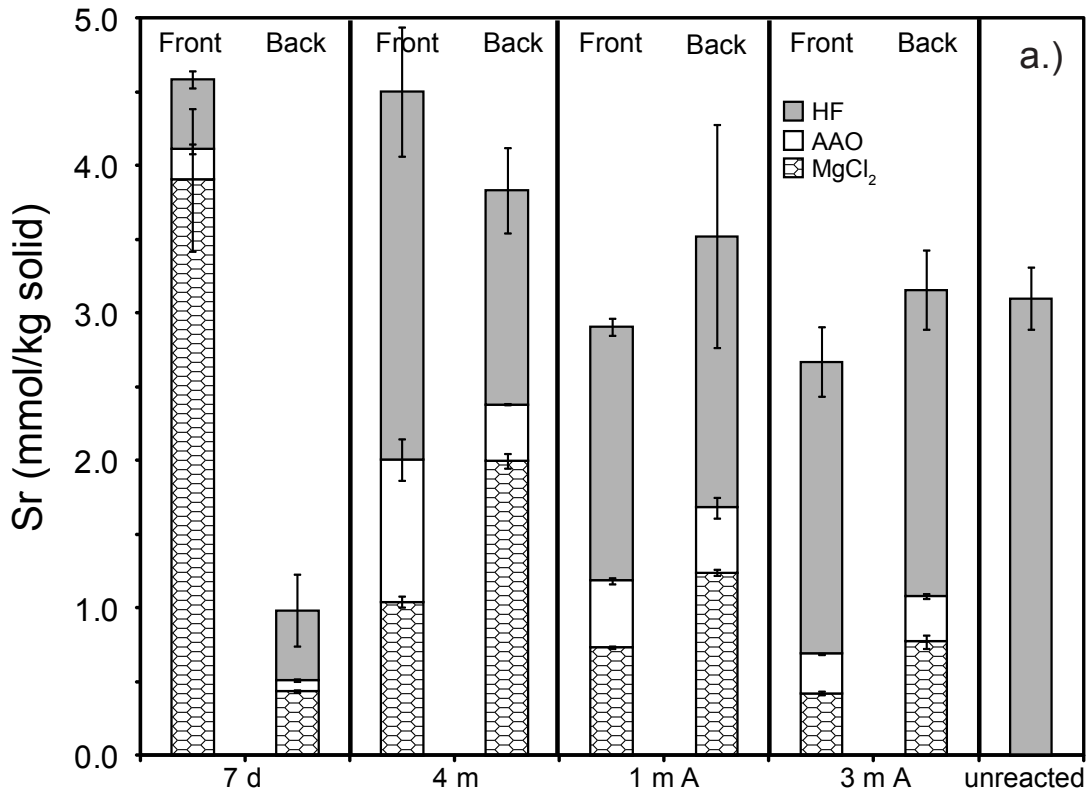
Figure 7.

Figure 8.

Figure 9.

Figure 10.

a) Reference compounds

b) Front 0-13 mm

c) Back 52-76 mm
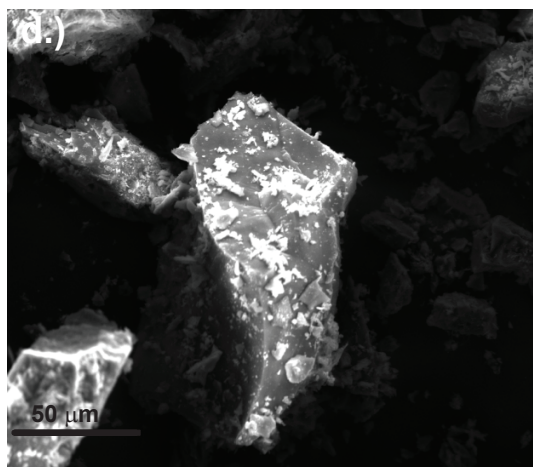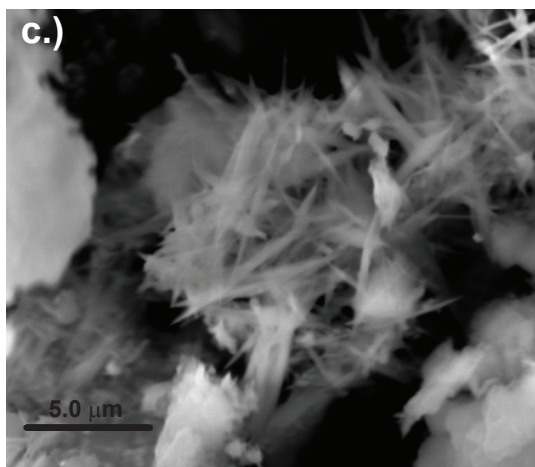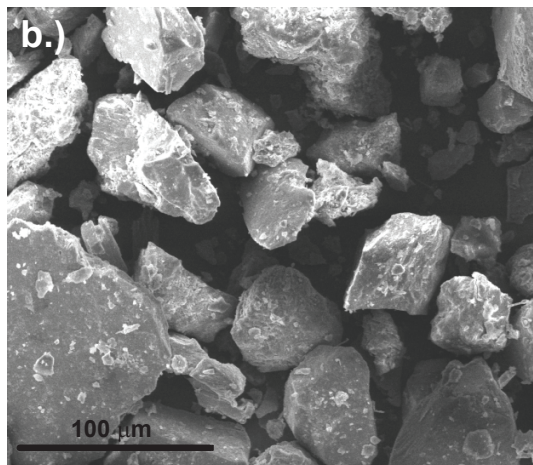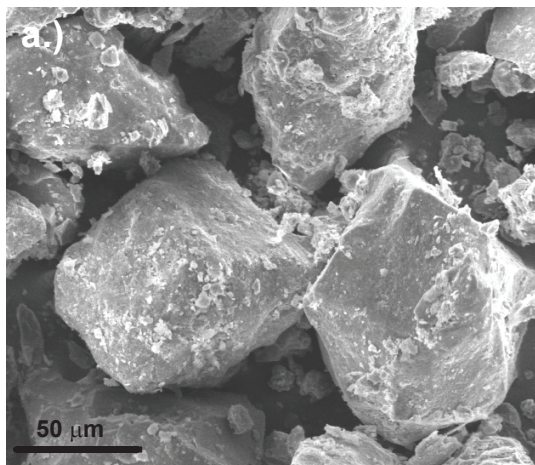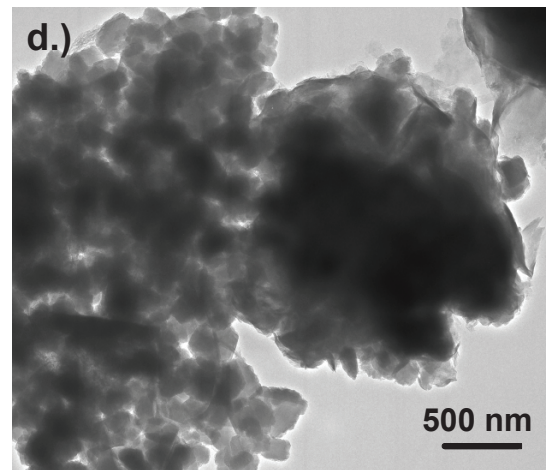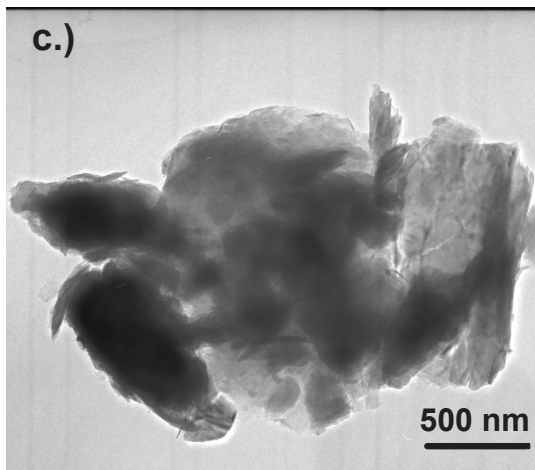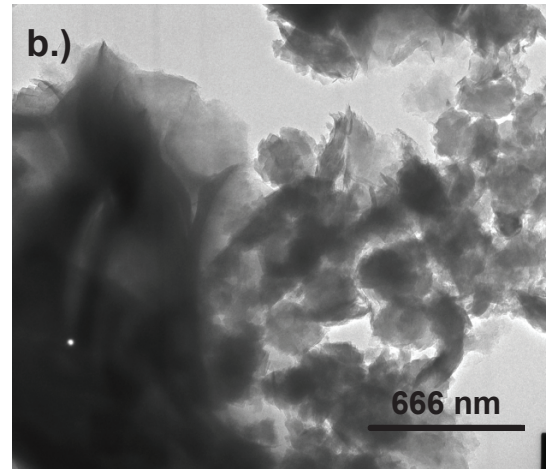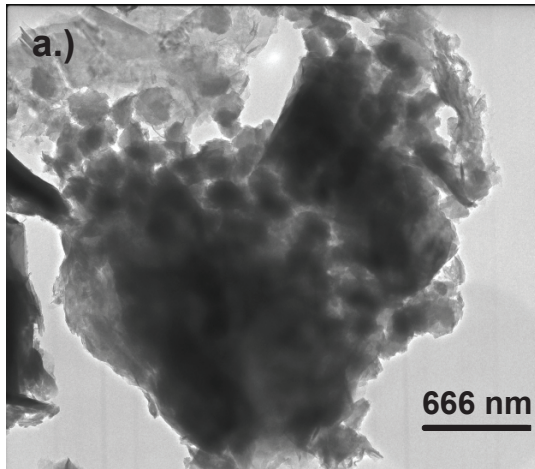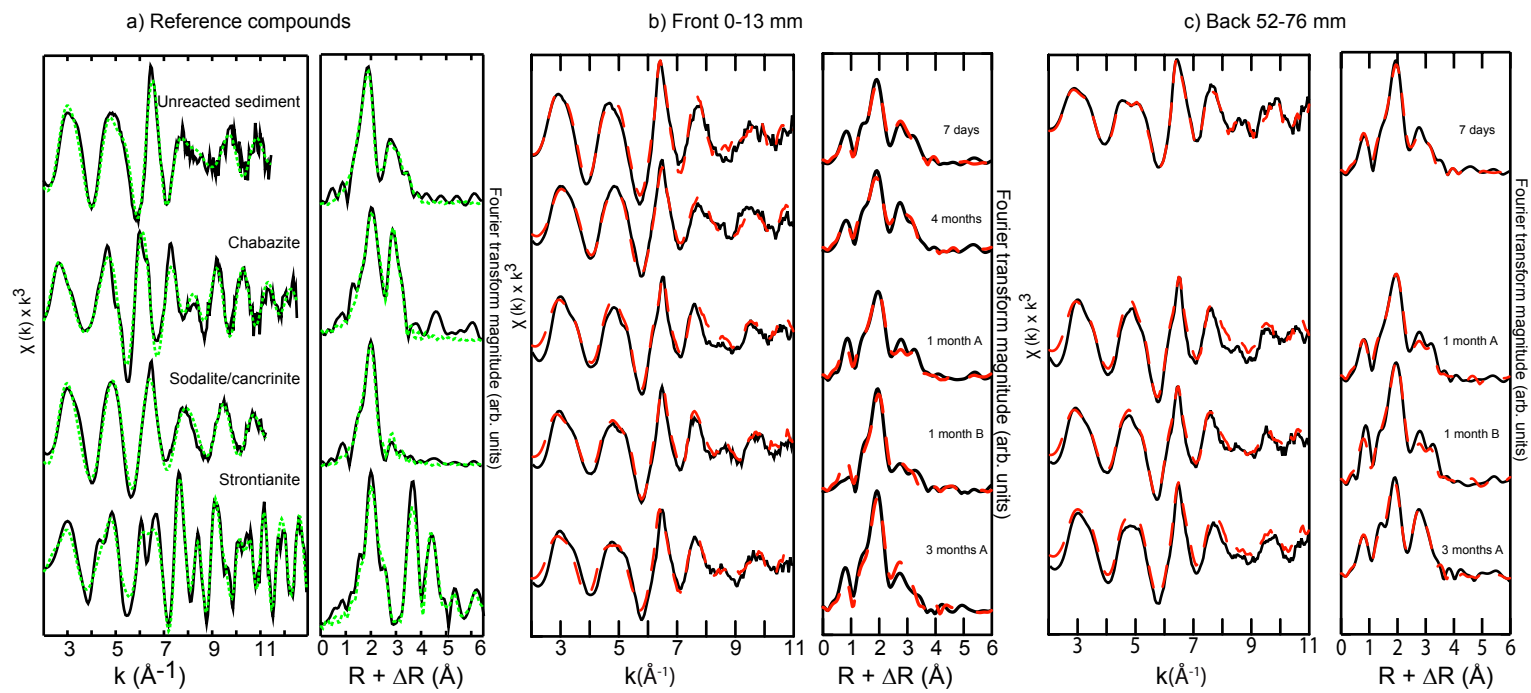
CHAPTER 5: EPILOGUE

5.1 Mineral phases

The studies presented here elucidated several factors controlling the formation of secondary phases of zeolite X and sodalite/cancrinite and the sites Sr and Cs can occupy. First, the presence of carbon dioxide in the initial synthesis solution changed the phases that formed. Zeolite X formed in the absence of carbon dioxide and sodalite and cancrinite formed when carbon dioxide was present at levels in equilibrium with atmospheric carbon dioxide. Another consideration is the elevated temperatures of the waste tanks (60-70 C), which can affect the reaction path of the phases (Deng et al., 2006a; Deng et al., 2006b). At elevated temperatures, zeolite A is the zeolite phase that forms instead of zeolite X and as time progresses, it transforms to sodalite and cancrinite.

Strontium and Cs contribute to the crystallization process of the phases. The absence of Sr or Cs in the synthesis solution for the -CO_2 solution produced less crystalline phases at 30-d as indicated by the decrease in the magnitude of the X-ray diffraction peaks (**see Chapter 2 Figure 2**). For the + CO_2 synthesis, a small percentage of zeolite X formed at 30-d and 548-d when Sr or Cs was present in solution, but zeolite X was not identified in precipitates that did not contain Sr or Cs. An additional factor observed was the inhibition of Sr uptake when Cs was present. For all synthesis experiments, less Sr was incorporated into the structure when Cs was present in solution.

Finally, this study showed the ability of both Sr and Cs to occupy sites considered inaccessible to these cations. For the zeolite X, the D6R sites (I and I') are believed to be occupied only at elevated temperatures (Porcher et al., 1999) due to the need for desolvation of the water surrounding the cation. The zeolite X synthesized in these

studies showed occupation of sites I and I' at room temperature due to co-precipitation of Sr or Cs. Generally, studies are done with the introduction of Sr or Cs through ion exchange with a Na-endmember mineral. Under these conditions, it takes elevated temperatures to occupy the D6R sites. However, when present in the initial synthesis solution, the zeolite X crystal structure, particularly the D6R site, can expand to accommodate larger cations or divalent charge. The location of the contaminants in these sites has implications since these sites are more recalcitrant than the sites located in the supercage (site II). The release of Sr or Cs from these sites would most likely require the dissolution of the zeolite X structure. In sodalite/cancrinite minerals, Sr and Cs occupied large 12-ring channels in cancrinite and six-membered rings of the sodalite structure.

The waste tanks located at Hanford are in contact with atmospheric carbon dioxide due to access ports that allow sampling of the tank (Gephart and Lundgren, 1998). This would suggest the sodalite and cancrinite phases should preferentially form over zeolite crystal structures (zeolite A and X). A study of evaporated tank waste (Buck and McNamara, 2004) showed the formation of both faujasite (zeolite X) and cancrinite. The cancrinite phase was found to be the predominant phase from the tanks solutions. The study did not identify how the contaminants were sequestered in the solids.

5.2 Strontium and Cesium retention on synthesized minerals

The synthesized mineral phases were further studied to test the recalcitrance of Sr and Cs to leaching by a low ionic strength solution mimicking the background pore water concentrations. Both mineral phase and contaminant type played a role in the amount of Sr and Cs release from the solid phase (**see Chapter 3 Figure 3**). When Sr and Cs were sequestered in the zeolite X phase, Cs was released more readily than the Sr, with

recovery of the Cs approaching 30-40% of its initial amount and Sr recovery at 2-8%. The larger release of Cs and the greater retention of Sr in the co-contaminant cases indicates that Cs can influence the sites Sr occupies, particularly to more recalcitrant sites.

The sodalite/cancrinite mineral phases show the opposite retention of the contaminants when compared to the zeolite X. Strontium was released at greater levels than Cs. The Sr-only contaminant phase was the exception with Sr retained at similar levels of the zeolite X system. As with zeolite X, co-contaminant compared to single contaminant phases showed different behavior. The Cs-only system released more Cs than the Sr+Cs columns. These data suggest that Sr in this system was more likely to reside in the large 12-ring channels of cancrinite, making it more accessible than Cs, which may reside in the sodalite or ε-cage of the cancrinite. The Sr-only data was anomalous and due to limited sample could not be run in triplicate. However, Sr and Cs release suggest that Cs may be creating a different nucleation environment than the Sr-only phase which promotes the release of Sr.

The controlling mechanism of Sr and Cs release is likely ion exchange rather than dissolution of the mineral phase. The effleunt Al and Si concentrations, assumed to be from the dissolution of the host phase, measured could not account for the effluent Sr and Cs observed in solution. Also, XRD data did not show secondary phases forming in the columns. Although the solution was undersaturated with respect to zeolite X and sodalite/cancrinite phases, the results of the column experiments show that dissolution of these phases is kinetically slow. Ion exchange constants were parameterized for the each type of phase with a three-site ion exchange model for zeolite X and a two-site exchange

model for sodalite/cancrinite. Since these phases have been identified as contributors in the sequestration of both Sr and Cs, parameterizing the exchange constants would allow for a constraint to be added to existing reactive transport simulations.

5.3 Sediments

The radioactivity of the Hanford site makes characterization of contaminated sediments challenging. However, limited studies have been performed on radioactive sediments to characterize Sr and Cs retention (McKinley et al., 2007; McKinley et al., 2001; Zachara et al., 2007). Cesium-137 was found to bind to edge sites of micas and clays while Sr-90 was shown to be controlled by diffusion into native phyllosilicates. The authors did not identify any secondary mineral phases of zeolites or feldspathoid in field sediments although there was some evidence of possible zeolite precipitation on quartz (Zachara et al., 2004). However, the mineralogy and crystalline nature of these phases has been very difficult to assess in field samples because of high associated radioactivity (Zachara et al., 2007). Numerous laboratory studies have shown that the weathering of Hanford sediments produces secondary phases. However, realistic solutiuon:sediment ratios should be selected when attempting to simulate field-scale waste-sediment interactions in the laboratory (Zachara et al., 2007).

The sediment column experiments performed in this dissertation address this issue by using solution:sediment ratios closer to field settings. Batch experiments in other studies used solution-to-sediment ratios of 50:1 (Choi et al., 2006; Chorover et al., 2008; Chorover et al., 2003; Perdrial et al., 2011) whereas the column experiments performed here had a ratio of 10-15:1. Bulk X-ray diffraction did not show the formation of secondary precipitates. However, techniques such as TEM and XAS revealed secondary

precipitates at low caustic waste solution-to-sediment ratios. Strontium EXAFS data indicated that Sr was bound in a combination of altered native sediment, zeolite, and feldspathoid phases. There was no direct spectroscopic evidence to show Cs sequestration. Chemical extractions performed on the sediment showed the Sr and Cs partition to different fractions of the sediment. Strontium was associated with a crystalline fraction accessed by a HF extraction and Cs was associated with a fraction that is less crystalline and extracted by acidic ammonium oxalate. These results are consistent with field data where Cs is believed to partition to micas and clays. The recalcitrance of the Sr and Cs contaminants as well as the abundance of the secondary precipitates increases with increasing weathering times.

These studies have shown the complexities involved in the sequestration of contaminants at the Hanford Nuclear waste site. Many factors contribute to the fate and mobility of Sr and Cs and make modeling difficult. Future work is needed to better model sediment and field systems. The results of this work will allow for better mechanistic constraints to be applied to simulations of contaminant release.

REFERENCES

Buck, E., and McNamara, B. (2004) Precipitation of nitrate-cancrinite in Hanford tank sludge. Environmental Science and Technology, 38, 4432-4438.

Choi, S., O'Day, P.A., Rivera, N.A., Mueller, K.T., Vairavamurthy, M.A., Seraphin, S., and Chorover, J. (2006) Strontium speciation during reaction of kaolinite with simulated tank-waste leachate: Bulk and microfocused EXAFS analysis. Environmental Science & Technology, 40(8), 2608-2614.

Chorover, J., Choi, S., Rotenberg, P., Serne, R.J., Rivera, N., Strepka, C., Thompson, A., Mueller, K.T., and O'Day, P.A. (2008) Silicon control of strontium and cesium partitioning in hydroxide-weathered sediments. Geochimica Et Cosmochimica Acta, 72(8), 2024-2047.

Chorover, J., Choi, S.K., Amistadi, M.K., Karthikeyan, K.G., Crosson, G., and Mueller, K.T. (2003) Linking cesium and strontium uptake to kaolinite weathering in simulated tank waste leachate. Environmental Science & Technology, 37(10), 2200-2208.

Deng, Y.J., Flury, M., Harsh, J.B., Felmy, A.R., and Qafoku, O. (2006a) Cancrinite and sodalite formation in the presence of cesium, potassium, magnesium, calcium and strontium in Hanford tank waste simulants. Applied Geochemistry, 21(12), 2049-2063.

Deng, Y.J., Harsh, J.B., Flury, M., Young, J.S., and Boyle, J.S. (2006b) Mineral formation during simulated leaks of Hanford waste tanks. Applied Geochemistry, 21(8), 1392-1409.

Gephart, R., and Lundgren, R. (1998) Hanford tank clean up: A guide to understanding technical issues., p. 1-71, Columbus, Ohio.

McKinley, J.P., Zachara, J.M., Smith, S.C., and Liu, C. (2007) Cation exchange reactions controlling desorption of $^{90}Sr^{2+}$ from coarse-grained contaminated sediments at the Hanford site, Washington. Geochimica et Cosmochimica Acta, 71(2), 305-325.

McKinley, J.P., Zeissler, C.J., Zachara, J.M., Serne, R.J., Lindstrom, R.M., Schaef, H.T., and Orr, R.D. (2001) Distribution and Retention of ^{137}Cs in Sediments at the Hanford Site, Washington. Environmental Science & Technology, 35(17), 3433-3441.

Perdrial, N., Rivera, N., Thompson, A., O'Day, P.A., and Chorover, J. (2011) Trace contaminant concentration affects mineral transformation and pollutant fate in hydroxide-weathered Hanford sediments. Journal of Hazardous materials, 197, 119-127.

Porcher, F., Souhassou, M., Dusausoy, Y., and Lecomte, C. (1999) The crystal structure of a low-silica dehydrated NaX zeolite. European Journal Of Mineralogy, 11(2), 333-343.

Zachara, J.M., Ainsworth, C.C., Brown Jr, G.E., Catalano, J.G., McKinley, J.P., Qafoku, O., Smith, S.C., Szecsody, J.E., Traina, S.J., and Warner, J.A. (2004) Chromium speciation and mobility in a high level nuclear waste vadose zone plume. Geochimica et Cosmochimica Acta, 68(1), 13-30.

Zachara, J.M., Serne, J., Freshley, M., Mann, F., Anderson, F., Wood, M., Jones, T., and Myers, D. (2007) Geochemical Processes Controlling Migration of Tank Wastes in Hanford's Vadose Zone. Vadose Zone Journal, 6(4), 985-1003.

Appendix 1:HN Effluent column data

A1-1: 30 d –CO$_2$ Sr/Cs A

Pore volume	Na	SD	K	SD	Mg	SD	Ca	SD	Al	SD	Si	SD	Sr	SD	Cs	SD	S	SD
	mM		mM		mM		mM		µM		µM		µM		µM		mM	
4.91	74.2	0.467			<D.L		<D.L		730	9.4	900	6.84	34.0	0.245	37.9	0.265	1.76	0.0178
9.81	15.8	0.182			<D.L		<D.L		177	1.89	108	0.583	1.56	0.0170	6.36	0.0605	1.71	0.00639
14.7	13.0	0.111			<D.L		<D.L		144	1.022	70.9	1.46	0.800	0.00392	5.44	0.0327	1.70	0.0108
19.6	12.2	0.049			<D.L		<D.L		118	0.42	56.3	0.622	0.507	0.00740	4.99	0.0409	1.70	0.00905
24.5	11.7	0.103			<D.L		<D.L		102	1.60	52.7	0.606	0.405	0.000365	4.56	0.0132	1.69	0.0328
29.4	11.9	0.350			<D.L		0.00429	0.00409	308	7.76	277	2.47	10.8	0.274	4.31	0.0935	1.69	0.0170
34.3	11.5	0.123			<D.L		0.000481	0.000566	40.5	0.23	32.9	1.64	0.370	0.00244	4.14	0.0211	1.69	0.0142
39.3	11.4	0.0625			<D.L		0.00251	0.000543	26.3	0.10	28.9	0.938	0.520	0.000728	4.10	0.01435	1.68	0.0123
44.2	11.3	0.0720			<D.L		0.00106	0.000503	34.5	0.27	34.7	0.710	0.699	0.00426	4.09	0.00368	1.70	0.0146
49.1	11.4	0.126	0.00178	0.000123	<D.L		0.00197	0.00086	22.0	0.3	31.7	0.415	0.832	0.00275	4.20	0.0139	1.73	0.0186
73.6	11.3	0.0867			<D.L		0.123	0.00237	15.8	0.0	36.0	1.86	0.85	0.00560	4.05	0.0417	1.73	0.0184
98.1	11.1	0.209	0.00651	9.18E-05	<D.L		0.387	0.00733	26.4	0.261	45.7	1.16	1.22	0.00244	4.18	0.0205	1.72	0.0128
123	10.9	0.0567	0.0243	0.000374	0.0743	0.000410	0.565	0.0153	14.4	0.09	35.7	1.32	1.50	0.0147	4.20	0.0369	1.72	0.0112
147	10.2	0.0886	0.0787	0.000401	0.202	0.00266	0.838	0.0264	10.7	0.183	33.9	0.379	2.19	0.0199	3.94	0.0158	1.73	0.0155
172	9.66	0.205	0.0821	0.000673	0.349	0.00290	1.27	0.0353	14.2	0.101	36.1	0.771	3.16	0.0206	3.88	0.0310	1.73	0.0217
196	8.80	0.0677	0.114	0.000216	0.481	0.00299	1.31	0.0352	38.0	0.198	61.1	1.38	4.67	0.00420	3.74	0.0213	1.75	0.0153
221	8.04	0.109	0.149	0.00102	0.563	0.00182	1.33	0.0456	10.4	0.203	31.2	1.38	4.53	0.0263	3.51	0.0140	1.72	0.0130
245	8.51	0.139			0.704	0.00374	1.39	0.0424	16.0	0.235	36.4	0.658	6.03	0.0772	3.77	0.0525	1.72	0.0126
270	8.27	0.0910	0.237	0.00161	0.752	0.00935	1.39	0.0565	18.2	0.160	38.1	1.03	6.19	0.0576	3.61	0.0300	1.75	0.0412
294	8.07	0.0783	0.26	0.00283	0.812	0.0117	1.40	0.0414	12.8	0.140	30.9	1.08	6.37	0.0242	3.45	0.0210	1.74	0.00638
319	7.61	0.0358	0.272	0.00123	0.862	0.0258	1.46	0.0336	12.7	0.0966	30.4	0.650	6.60	0.0422	3.26	0.0036	1.75	0.0124
343	7.25	0.108	0.289	0.00424	0.902	0.0429	1.56	0.0503	12.1	0.142	28.7	1.40	6.81	0.0953	3.11	0.0128	1.72	0.0220
393	6.66	0.0260	0.308	0.00169	0.915	0.0171	1.57	0.0264	12.0	0.109	26.2	1.18	6.98	0.0677	2.77	0.0311	1.73	0.0148
442	6.32	0.0544	0.316	0.00379	0.944	0.0167	1.65	0.0401	12.4	0.0670	24.2	0.591	7.09	0.0709	2.53	0.0147	1.72	0.0344
491	5.57	0.0290	0.302	0.00127	0.810	0.0245	1.69	0.0679	14.6	0.076	24.7	0.838	6.15	0.053	2.20	0.0134	1.77	0.0237
540	4.76	0.0567	0.294	0.00038	0.948	0.0215	1.75	0.0429	11.9	0.122	28.7	1.31	6.08	0.0304	2.03	0.0218	1.74	0.0180
589	4.42	0.0530	0.296	0.00219	0.925	0.0382	1.82	0.0426	11.2	0.133	27.7	1.10	6.02	0.0650	1.87	0.0181	1.72	0.0142
677	4.17	0.0392	0.314	0.00232	0.915	0.00427	1.85	0.0484	11.7	0.339	25.2	0.589	6.16	0.0499	1.76	0.0176	1.71	0.0160
716	4.00	0.0424	0.300	0.00482	0.930	0.0101	1.84	0.0318	12.2	0.0705	24.6	1.08	6.21	0.0621	1.65	0.00695	1.71	0.0193

A1-2: 30 d –CO_2 Sr/Cs B

Pore volume	Na mM	SD	K mM	SD	Mg mM	SD	Ca mM	SD	Al μM	SD	Si μM	SD	Sr μM	SD	Cs μM	SD	S mM	SD
5.00	73.1	1.147	0.157	0.001159	<D.L		0.0224	0.000453	1281	12.6	1424	16.6	87.7	0.281	39.3	0.161	1.80	0.0372
10.0	17.3	0.173	0.110	0.000685	<D.L		0.0139	0.00143	813	6.26	844	4.92	53.17	0.4626	7.28	0.0641	1.75	0.01805
15.0	16.8	0.224	0.143	0.00328	<D.L		0.0219	0.000858	3412	58.3	3763	85.6	167	1.11804	8.94	0.0402	1.74	0.0176
20.0	12.4	0.110	0.190	0.001752	<D.L		0.0146	0.000666	281	3.74	232.5	0.677	11.523	0.08181	4.51	0.0401	1.73	0.00883
25.0	11.7	0.102	0.157	0.000736	<D.L		0.00532	0.00123	58	0.192	26.8	0.899	0.512	0.003790	4.20	0.0042	1.73	0.0124
30.0	11.8	0.163	0.125	0.00751	<D.L		0.00655	0.000471	30	0.464	19	0.456	0.5	0.003	4.09	0.0429	1.74	0.00969
35.0	11.8	0.412	0.0840	0.00400	<D.L		0.0118	0.00148	25.9	0.900	19.0	0.881	0.606	0.00321	4.05	0.0190	1.72	0.0328
40.0	11.5	0.0368	0.176	0.00051	<D.L		0.0152	0.00212	24.5	0.0368	20.2	0.570	0.639	0.007546	3.95	0.04192	1.74	0.00953
45.0	11.7	0.2201	0.00201	0.00006	<D.L				69.2	1.11	79.3	1.16	1.991	0.01075	3.96	0.02255	1.73	0.00402
50.0	11.4	0.039	0.0894	0.001403	<D.L		0.0154	0.00152	17.7	0.134	20.2	1.48	0.529	0.00386	3.97	0.0202	1.76	0.0125
75.0	11.8	0.3446	0.00419	0.0002	<D.L		0.0103	0.00157	214	4.0	243	0.792	9.35	0.15239	4.47	0.0532	1.75	0.0083
100	11.6	0.182	0.0148	0.000206	<D.L		0.00598	0.00143	34.4	0.179	55.8	0.589	1.29	0.01435	4.34	0.0643	1.75	0.0163
125	11.0	0.0552	0.0482	0.000650	0.107	0.00158	0.0362	0.000951	12.7	0.10	27.3	1.28	0.80	0.0064	4.40	0.0312	1.77	0.0107
150	10.3	0.0872	0.0786	0.000841	0.363	0.00408	0.143	0.00127	11.0	0.074	28.2	1.24	2.49	0.0356	3.97	0.0107	1.78	0.0307
175	9.69	0.196	0.105	0.00294	0.466	0.00355	0.340	0.0110	11.3	0.265	26.3	0.874	3.79	0.0076	3.98	0.0227	1.78	0.0106
200	9.11	0.0902	0.148	0.00101	0.485	0.00102	0.527	0.0073	11.2	0.083	26.6	1.19	4.40	0.05939	3.77	0.0569	1.75	0.0251
225	8.43	0.158	0.181	0.00141	0.668	0.00531	0.685	0.0227	10.5	0.134	24.5	0.399	5.13	0.0339	3.32	0.0110	1.76	0.0114
250	7.77	0.208	0.470	0.0216	0.739	0.00267	0.992	0.0311	15.2	0.533	27.6	1.02	6.00	0.0150	2.94	0.0268	1.76	0.0124
275	7.19	0.1827	0.232	0.00227	0.788	0.0148	1.19	0.0258	22.1	0.510	35.9	0.629	6.87	0.0536	2.94	0.0021	1.82	0.0272
300	6.84	0.0396	0.244	0.00202	0.793	0.0195	1.29	0.0226	8.0	0.063	25.2	0.530	6.05	0.0139	2.83	0.0164	1.78	0.0215
325	6.50	0.1092	0.254	0.00130	0.807	0.0154	1.39	0.0202	14.4	0.2112	26.5	0.565	6.23	0.0174	2.73	0.0289	1.77	0.0041
350	7.01	0.242	0.292	0.00721	0.852	0.0190	1.56	0.0232	14.2	0.551	28.8	0.561	6.67	0.1201	2.91	0.0189	1.92	0.0151
375	5.86	0.1378	0.274	0.00875	0.824	0.0073	1.62	0.0222	16.0	0.364	26.2	1.29	6.09	0.1103	2.46	0.0111	1.77	0.0176
400	5.82	0.1460	0.279	0.00627	0.819	0.0308	1.62	0.0468	14.9	0.3990	26.6	1.01	6.10	0.0238	2.48	0.0181	1.77	0.0100
425	5.44	0.1382	0.277	0.00967	0.837	0.0292	1.70	0.0507	15.0	0.503	24.4	0.685	5.99	0.183	2.42	0.0776	1.77	0.0235
450	5.22	0.0652	0.303	0.00875	0.841	0.0298	1.83	0.0788	14.2	0.218	24.6	0.614	6.32	0.0809	2.26	0.0348	1.75	0.0218
475	5.13	0.0965	0.312	0.00573	0.864	0.0200	1.85	0.0386	12.9	0.200	23.1	1.17	6.38	0.0344	2.23	0.0266	1.75	0.0172
500	4.98	0.0329	0.568	0.00732	0.894	0.0487	1.92	0.0913	14.3	0.0689	24.8	0.845	6.35	0.0717	2.15	0.0424	1.74	0.0164
525	4.95	0.0975	0.328	0.00450	0.943	0.0352	2.06	0.0656	14.2	0.247	23.5	0.823	6.78	0.0773	2.28	0.02662	1.76	0.0165
550	4.93	0.0390	0.339	0.00115	0.931	0.0115	2.08	0.0202	20.1	0.153	31.9	0.903	7.11	0.065	2.20	0.0130	1.73	0.0270
575	4.79	0.0321	0.340	0.00554	0.960	0.0467	2.16	0.0925	12.6	0.122	25.0	1.05	6.79	0.121	2.05	0.0480	1.76	0.0192
600	4.68	0.0286	0.345	0.000862	0.907	0.0344	2.10	0.0474	12.7	0.0650	24.8	1.03	6.95	0.0598	2.00	0.00779	1.73	0.00603
650	4.60	0.0317	0.348	0.00268	0.962	0.0243	2.12	0.0631	12.6	0.115	25.2	0.398	7.50	0.0382	2.04	0.0177	1.73	0.0167
675	4.55	0.112	0.360	0.00972	0.935	0.0355	2.25	0.0819	11.7	0.280	23.3	0.155	7.86	0.0613	1.97	0.0211	1.72	0.00759
700	4.40	0.0238	0.733	0.00455	0.918	0.0207	2.25	0.0522	12.0	0.0744	25.9	0.864	8.26	0.0107	1.83	0.0166	1.71	0.0241

A1-3: 30 d –CO$_2$ Sr/Cs C

Pore volume	Na mM	SD	K mM	SD	Mg mM	SD	Ca mM	SD	Al muM	SD	Si muM	SD	Sr muM	SD	Cs muM	SD	S mM	SD
5.24	46.1	0.272	0.147	0.001282	<D.L		0.0142	0.000706	504	4.6	635	4.0	42.9	0.112	21.7	0.119	1.77	0.0183
10.5	14.0	0.263	0.135	0.001534	<D.L		0.0115	0.000838	405	4.90	339	1.70	28.06	0.1150	5.32	0.0202	1.75	0.01478
15.7	12.3	0.223	0.156	0.00080	<D.L		0.0055	0.000610	200	2.786	122	1.0	7	0.11419	4.35	0.0322	1.75	0.0123
21.0	11.9	0.077	0.183	0.00256	<D.L		0.0078	0.001055	159	0.92	91.4	0.673	4.261	0.07883	4.12	0.0701	1.76	0.01220
26.2	11.8	0.125	0.223	0.001159	<D.L		0.00894	0.00038	123	1.05	73.2	0.083	2.870	0.055393	3.72	0.0518	1.66	0.0172
31.5	11.7	0.095	0.136	0.00127	<D.L		0.00958	0.000519	87	0.973	43	0.346	1.2	0.010	4.03	0.0363	1.75	0.01167
36.7	10.6	0.044	0.2481	0.00047	<D.L		0.0127	0.00106	104	0.611	65.9	1.979	2.147	0.01975	3.96	0.0170	1.74	0.0298
42.0	10.4	0.1094	0.085	0.00118	<D.L		0.0150	0.00138	88.5	0.983	57.1	0.984	1.578	0.024463	4.07	0.04150	1.77	0.01225
47.2	10.9	0.2023			<D.L		0.0261	0.000619	471	3.25	433.9	1.44	21.972	0.38671	4.69	0.04268	1.73	0.01344
52.4	10.7	0.086	0.1883	0.0016	<D.L		0.0172	0.00124	101	0.7	82.2	0.89	2.942	0.04942	3.96	0.0856	1.74	0.0131
78.7	10.6	0.0560	0.00168	0.0000	<D.L		0.0227	0.00088	46	0.1	45	0.990	0.57	0.00315	4.42	0.0269	1.78	0.0166
105	10.5	0.225	0.0014	2.93E-05	<D.L		0.02903	0.00058	37.5	0.637	43.3	0.474	0.40	0.00344	4.36	0.0048	1.78	0.0081
131	10.5	0.0822	0.0089	0.000038	<D.L		0.0390	0.001267	33.6	0.09	44.1	1.27	0.37	0.0020	4.60	0.0285	1.80	0.0215
157	10.3	0.2535	0.0316	0.001793	0.082	0.00112	0.065	0.00103	30.6	0.655	42.4	0.49	0.74	0.0136	4.82	0.0333	1.75	0.0220
184	9.67	0.088	0.091	0.00022	0.208	0.00207	0.137	0.0032	25.1	0.065	40.6	1.029	1.71	0.0165	4.99	0.0764	1.78	0.0074
210	8.72	0.141	0.165	0.00088	0.529	0.00286	0.296	0.0063	23.7	0.119	36.0	0.83	2.95	0.03039	4.57	0.0261	1.77	0.0035
236	7.44	0.059	0.440	0.00145	0.815	0.01879	0.556	0.0156	15.0	0.205	31.5	0.438	4.16	0.0532	3.73	0.0783	1.77	0.0127
262	6.68	0.037	0.245	0.0022	0.911	0.04336	0.933	0.0295	17.0	0.180	30.3	1.10	6.42	0.0449	3.52	0.0503	1.71	0.0183
288	5.98	0.0221	0.263	0.00195	0.951	0.0240	1.24	0.0321	17.0	0.077	31.2	0.355	5.78	0.0815	2.98	0.0605	1.81	0.0119
315	5.40	0.0130	0.272	0.00237	1.006	0.0262	1.48	0.0485	14.5	0.0376	27.6	0.645	5.66	0.0402	2.51	0.0205	1.79	0.0124
341	4.93	0.0892	0.273	0.00909	1.021	0.0308	1.68	0.0635	14.8	0.165	27.4	0.680	5.93	0.0314	2.36	0.0210	1.77	0.0093
367	4.68	0.029	0.290	0.00165	1.012	0.0347	1.84	0.0630	13.7	0.164	26.1	1.033	5.84	0.1005	2.16	0.0450	1.79	0.0221
393	4.45	0.0076	0.287	0.00195	0.986	0.0367	1.95	0.0572	13.7	0.047	25.1	1.02	5.98	0.0784	2.15	0.0200	1.78	0.0075
420	4.35	0.0309	0.297	0.00178	0.978	0.0303	2.05	0.0428	13.7	0.0931	23.7	1.25	5.91	0.0367	2.06	0.0155	1.75	0.0174
446	4.18	0.0347	0.295	0.00245	0.918	0.0429	2.05	0.0903	13.8	0.231	24.0	1.257	6.04	0.052	2.04	0.0277	1.73	0.0187
472	4.18	0.0230	0.510	0.00484	0.914	0.0272	2.11	0.0706	12.0	0.181	24.5	1.183	5.95	0.0910	1.83	0.0121	1.71	0.0217
498	4.09	0.0519	0.376	0.00229	0.911	0.0281	2.19	0.0512	13.4	0.210	22.3	0.84	6.00	0.1391	1.93	0.0271	1.74	0.0192
509	4.04	0.0347	0.559	0.00626	0.856	0.0138	2.09	0.0412	17.0	0.2103	28.2	0.816	6.49	0.0519	1.89	0.0108	1.70	0.0332

A1-4: 30 d –CO$_2$ Sr A

Pore volume	Na	SD	K	SD	Mg	SD	Ca	SD	Al	SD	Si	SD	Sr	SD	S	SD
	mM		mM		mM		mM		μM		μM		μM		mM	
5.32	95.8	1.73			0.05226	0.000884	0.164	0.00310	2185	36.1	2648	47.0	118	1.11	1.98	0.0152
10.6	18.7	0.740			<D.L		0.0106	0.000447	351	16.0	416	3.99	22.0	0.795	1.76	0.0168
16.0	13.2	0.452			<D.L		0.00853	0.000307	194	7.86	205	1.53	10.3	0.177	1.75	0.00611
21.3	11.3	0.312			<D.L		0.00912	0.00104	138	4.01	135	0.892	5.58	0.107	1.76	0.0101
26.6	10.9	0.460			<D.L		0.00845	0.000829	117	4.46	112	1.215	3.31	0.0974	1.74	0.0155
31.9	11.0	0.385			<D.L		0.0240	0.00126	114	4.78	107	0.724	2.51	0.0695	1.77	0.0168
37.3	10.6	0.190			<D.L		0.00930	0.000924	104	6.11	96.4	1.65	1.07	0.00635	1.76	0.0145
42.6	10.6	0.3504			<D.L		0.00990	0.000617	97.0	2.18	89.3	1.16	0.686	0.0112	1.74	0.0316
47.9	10.9	0.5132			0.01018	0.000641	0.0118	0.000685	104	3.25	94.2	0.163	0.652	0.0280	1.79	0.0086
53.2	10.4	0.334			0.04522	0.00049	0.0129	0.000939	125	3.58	126	1.15	2.17	0.0463	1.77	0.0220
79.9	9.6	0.2124	0.062	0.00098	0.26938	0.00132	0.242	0.00501	51.4	5.96	72.8	1.14	2.90	0.0697	1.79	0.0194
106	8.5	0.045	0.12084	0.00313	0.41434	0.00127	0.522	0.01473	73.6	4.00	92.8	1.30	6.42	0.163	1.80	0.0125
133	7.5	0.0341	0.1644	0.0046	0.5422	0.00362	0.907	0.0212	40.6	4.95	66.6	1.05	8.70	0.190	1.79	0.0140
160	6.5	0.0280	0.2326	0.00389	0.639	0.00594	1.29	0.0294	34.9	1.07	55.4	0.618	10.4	0.223	1.79	0.0172
186	6.14	0.035	0.2371	0.00944	0.659	0.00469	1.43	0.0426	39.1	4.29	58.1	0.283	11.0	0.268	1.77	0.0129
213	6.12	0.0417	0.249	0.00552	0.663	0.00471	1.53	0.0212	29.8	2.78	56.5	0.725	11.4	0.153	1.80	0.0104
240	5.95	0.023			0.664	0.00098	1.53	0.0434	33.9	3.45	58.4	0.306	11.0	0.292	1.79	0.0182
266	5.56	0.026	0.257	0.00938	0.676	0.00609	1.57	0.0597	39.5	4.00	64.8	0.717	10.8	0.420	1.77	0.00807
293	5.54	0.0216	0.258	0.00409	0.669	0.00346	1.56	0.0244	42.3	3.24	64.5	0.405	10.4	0.136	1.76	0.0233
319	5.39	0.0408	0.265	0.0057	0.687	0.0073	1.59	0.0517	35.1	2.19	62.0	0.904	10.5	0.317	1.74	0.0249
346	5.32	0.0329	0.268	0.00509	0.707	0.0036	1.66	0.0554	37.7	2.77	58.5	0.823	10.8	0.318	1.79	0.0188
373	5.13	0.033	0.27	0.00765	0.709	0.0035	1.74	0.0767	34.3	4.31	57.5	0.894	10.9	0.412	1.74	0.0196
399	5.09	0.0359	0.283	0.00575	0.717	0.0034	1.75	0.0255	40.4	3.82	53.9	0.517	10.7	0.124	1.77	0.0147
426	4.97	0.0274	0.292	0.00651	0.726	0.0041	1.81	0.0543	36.3	2.43	56.8	0.273	10.7	0.294	1.76	0.0174
453	4.98	0.0218	0.283	0.00565	0.719	0.0010	1.76	0.0402	33.3	1.97	55.8	0.420	10.2	0.190	1.77	0.0068
479	4.83	0.0385	0.288	0.00647	0.734	0.0050	1.82	0.0351	32.5	5.66	55.8	1.04	10.3	0.205	1.76	0.0126
506	4.92	0.0217	0.289	0.00352	0.748	0.0030	1.80	0.0313	30.6	3.23	54.5	0.814	10.2	0.139	1.78	0.0058
516	4.82	0.0182	0.289	0.00892	0.729	0.00087	1.71	0.0510	26.8	1.39	50.7	1.22	10.0	0.257	1.71	0.0123

A1-5: 30 d –CO$_2$ Sr B

Pore volume	Na (mM)	SD	K (mM)	SD	Mg (mM)	SD	Ca (mM)	SD	Al (µM)	SD	Si (µM)	SD	Sr (µM)	SD	S (mM)	SD
4.93	96.8	3.99			<D.L		0.101	0.00511	2200	105	2512	98.9	112	1.69	2.14	0.0174
9.85	17.1	0.286			<D.L		0.0182	0.000386	367	0.937	398	1.60	17.0	0.592	1.83	0.0281
14.8	13.1	0.567			<D.L		0.0175	0.001371	214	12.1	201	1.16	7.52	0.365	1.82	0.00858
19.7	12.0	0.551			<D.L		0.0181	0.000232	149	7.52	122	1.96	4.12	0.156	1.81	0.0177
24.6	10.8	0.332			<D.L		0.0184	0.000320	120	4.86	93	1.18	2.49	0.0915	1.82	0.0132
29.6	10.9	0.233			<D.L		0.00851	0.000348	106	0.922	108	0.464	1.32	0.0361	1.79	0.0240
34.5	10.2	0.419			0.0393	0.00102	0.0293	0.00213	101	0.936	72.8	0.992	1.74	0.0672	1.82	0.0138
39.4	10.3	0.289			0.0840	0.00133	0.0525	0.00310	98.5	1.23	72.8	1.67	2.27	0.0607	1.81	0.0379
44.3	9.79	0.584	0.0074	0.00346	0.123	0.000647	0.0945	0.00505	92.5	0.237	67.1	0.849	2.76	0.143	1.80	0.0078
49.3	9.74	0.029			0.153	0.00162	0.133	0.00299	113	5.65	96.3	0.845	5.91	0.159	1.83	0.0138
73.9	9.14	0.0570	0.0952	0.00256	0.243	0.00165	0.317	0.0085831	40.2	0.760	48.4	1.42	5.44	0.146	1.82	0.0198
98.5	8.42	0.086	0.105	0.00216	0.356	0.003405	0.517	0.0087486	41.2	0.199	50.2	1.17	7.76	0.156	1.83	0.0230
123	7.72	0.0734	0.125	0.00283	0.450	0.00392	0.736	0.0206	33.2	1.42	47.5	0.575	9.13	0.237	1.84	0.0332
148	7.48	0.0480	0.117	0.00277	0.398	0.00294	0.70	0.0111	28.1	0.484	39.5	1.01	7.76	0.0753	1.46	0.0153
172	7.22	0.046	0.158	0.0046	0.535	0.00180	0.96	0.0310	41.6	0.876	53.0	0.586	10.1	0.319	1.84	0.0197
197	7.01	0.0579	0.172	0.00357	0.585	0.00534	1.03	0.0159	40.6	0.898	52.3	1.10	10.3	0.265	1.83	0.0242
222	6.67	0.078	0.19	0.00396	0.613	0.00630	1.12	0.0281	41.5	0.673	52.9	1.91	10.7	0.354	1.82	0.0200
246	6.08	0.066	0.229	0.00461	0.701	0.00806	1.35	0.0316	35.8	0.464	53.6	1.06	11.2	0.273	1.84	0.0228
271	5.63	0.0634			0.723	0.00641	1.56	0.0260	30.6	0.693	50.0	0.396	12.1	0.209	1.82	0.0101
296	5.60	0.0492	0.266	0.00691	0.766	0.0102	1.66	0.0365	29.6	0.437	48.8	0.710	12.5	0.258	1.87	0.0300
315	5.20	0.0562	0.29	0.00402	0.780	0.0047	1.84	0.0168	28.6	0.496	44.8	0.768	13.0	0.0927	1.85	0.0083
345	4.93	0.033	0.3	0.00949	0.794	0.00923	1.94	0.0485	27.7	0.354	43.1	0.709	12.6	0.293	1.83	0.0300
370	4.75	0.0303	0.297	0.00631	0.802	0.00377	1.98	0.0349	27.3	0.716	40.3	0.819	12.3	0.192	1.84	0.0170
394	4.62	0.0327	0.305	0.0113	0.808	0.00566	2.02	0.0536	26.3	0.369	39.0	1.42	12.1	0.324	1.84	0.0156
419	4.52	0.0104	0.314	0.00743	0.826	0.0396	2.09	0.0277	26.2	0.675	37.5	0.867	12.1	0.119	1.83	0.0106
443	4.49	0.0270	0.3	0.00789	0.812	0.00404	2.11	0.0569	26.2	0.450	36.4	0.95	11.9	0.295	1.84	0.0126
468	4.42	0.0409	0.313	0.0102	0.810	0.0230	2.12	0.0492	27.3	0.847	36.3	0.784	11.6	0.248	1.85	0.0093
493	4.35	0.0185	0.317	0.00894	0.816	0.00227	2.13	0.0490	27.2	0.849	37.5	1.05	11.8	0.243	1.85	0.0147
503	4.39	0.0226	0.3	0.00884	0.818	0.00254	2.11	0.0331003	42.6	0.669	62.4	1.43	16.0	0.222	1.83	0.00526

A1-6: 30 d –CO_2 Sr C

Pore volume	Na	SD	K	SD	Mg	SD	Ca	SD	Al	SD	Si	SD	Sr	SD	S	SD
	mM			mM		mM		mM		μM		μM		μM		mM
4.78	83.7	1.51			<D.L.		<D.L.		1034	27	1404	29.9	35	0.975	1.98	0.0106
9.56	17.5	0.538			<D.L.		<D.L.		228	2.044	278	2.09	6.31	0.08431	1.93	0.0230
14.3	13.8	0.607			<D.L.		<D.L.		159	6.8	157	1.55	5.66	0.248	1.97	0.03973
19.1	12.4	0.364			<D.L.		<D.L.		160	4.54	155	1.77	6.33	0.0960	1.94	0.0146
23.9	11.7	0.308			<D.L.		<D.L.		263	5.97	275	0.98	8.16	0.140	1.99	0.0318
28.7	11.4	0.321			<D.L.		<D.L.		115	7.74	94.1	1.547	0.900	0.0119	2.00	0.0269
38.2	11.0	0.300			<D.L.		<D.L.		103	2.54	90.1	1.02	0.708	0.0288	2.04	0.0218
43.0	10.9	0.181	0.0074		<D.L.		<D.L.		101	7.40	80.3	1.772	0.294	0.008	1.96	0.0157
47.8	10.7	0.291			<D.L.		<D.L.		93.2	8.23	84.4	1.614	0.309	0.008	2.03	0.0182
71.7	9.37	0.122			0.317	0.0207	0.328	0.0096522	63.8	4.90	74.0	1.08	3.70	0.121	2.02	0.0263
95.6	6.71	0.431	0.169	0.00144	0.657	0.006614	1.216	0.0314543	49.3	2.94	55.8	1.00	9.17	0.281	2.06	0.0238
119	6.20	0.181			0.706	0.00782	1.470	0.0311	25.0	8.38	44.4	0.928	10.4	0.196	2.09	0.0284
143	6.10	0.0621	0.196	0.00084	0.711	0.00323	1.63	0.0561	32.7	6.55	46.5	2.52	11.3	0.391	2.06	0.0145
167	4.10	0.145			0.726	0.0138	1.64	0.0630	151	2.18	173	1.540	15.7	0.655	2.07	0.0227
182	5.45	0.120	0.287	0.00155	0.684	0.00502	1.45	0.0363	36.9	4.21	48.0	1.07	10.6	0.235	1.99	0.0407
206	5.51	0.0183			0.704	0.00554	1.66	0.0435	30.5	7.09	47.9	1.17	11.3	0.307	2.01	0.0102
229	4.36	0.147	0.3	0.00311	0.718	0.0217	1.77	0.0528	33.4	3.53	45.5	1.60	11.6	0.421	2.01	0.0343
253	5.30	0.0423			0.759	0.00607	1.89	0.0159	28.8	8.34	43.7	1.575	11.7	0.169	2.11	0.0101
277	5.24	0.1344	0.309	0.00235	0.759	0.0238	1.84	0.0119	22.3	5.22	42.6	1.269	12.0	0.169	2.07	0.0271
301	4.95	0.0317			0.758	0.0139	1.94	0.0167	29.7	4.02	42.7	0.803	11.6	0.116	2.08	0.0381
325	4.73	0.025	0.307	0.00486	0.791	0.00403	2.00	0.0078	26.4	6.20	38.2	1.069	11.4	0.072	2.06	0.0176
349	4.64	0.0350			0.801	0.00474	2.08	0.0577	23.2	3.81	36.8	1.419	11.3	0.310	2.09	0.0251
373	4.53	0.0183	0.329	0.00353	0.830	0.0294	2.18	0.0816	24.4	4.09	35.7	1.25	11.4	0.436	2.10	0.0317
397	4.55	0.0417			0.839	0.0288	2.18	0.0640	24.3	5.39	33.6	1.026	11.4	0.311	2.05	0.0055
421	4.70	0.0351	0.300	0.012	0.827	0.0300	2.12	0.0725	26.0	3.89	38.1	0.90	11.0	0.386	2.17	0.0222
444	4.68	0.0457			0.804	0.0305	2.17	0.0961	31.1	3.33	37.1	1.436	10.9	0.502	2.18	0.0414
468	4.72	0.0301			0.799	0.0237	2.12	0.0545	21.8	4.09	36.5	0.35	10.6	0.251	2.18	0.0163
497	4.70	0.0260	0.300	0.00383	0.791	0.0189	2.16	0.0182838	13.1	2.48	35.3	1.54	10.7	0.107	2.17	0.0391

A1-7: 30 d –CO$_2$ Cs A

Pore volume	Na	SD	K	SD	Mg	SD	Ca	SD	Al	SD	Si	SD	Cs	SD	S	SD
	mM		mM		mM		mM		µM		µM		µM		mM	
5.2	86.2	1.19			<D.L.		<D.L.		1287	21.2	1792	51.3	28.5	0.0826	1.74	0.0114
10.5	18.9	0.168			<D.L.		<D.L.		762	1.30	876	4.59	5.81	0.0843	1.74	0.0329
15.7	15.2	0.0654			<D.L.		<D.L.		2327	26.1	2876	64.5	7.39	0.0333	1.76	0.0372
21.0	11.8	0.00946			<D.L.		<D.L.		218	1.22	159	1.34	3.47	0.0170	1.75	0.0253
26.2	13.5	0.131			<D.L.		<D.L.		2323	22.5	2931	66.9	7.39	0.0451	1.78	0.0157
31.5	13.1	0.0747			<D.L.		0.0312	0.000169	707	4.81	804	6.69	3.85	0.00347	1.83	0.0149
36.7	11.1	0.179			<D.L.		0.0201	0.00143	284	2.78	267	1.67	3.10	0.0205	1.79	0.0113
42.0	11.1	0.0520			<D.L.		0.0188	0.00131	168	1.51	132	1.21	2.94	0.0344	1.78	0.0161
47.2	10.8	0.0824	0.00116	0.0002477	<D.L.		0.0206	0.000548	142	1.08	111	2.56	2.95	0.0080	1.79	0.0200
52.5	10.8	0.0919			<D.L.		0.0226	0.000415	126	2.79	100	0.589	2.69	0.0078	1.78	0.00674
78.7	10.7	0.0779			0.0617	0.00127	0.0440	0.00345	91.8	0.138	103	1.45	2.54	0.0302	1.78	0.0164
131	9.86	0.0769	0.0264	0.0001216	0.244	0.00176	0.207	0.00651	49.6	0.516	74.6	1.04	2.45	0.0132	1.76	0.0225
157	9.01	0.0766	0.0637	0.00733	0.384	0.00334	0.462	0.0104	25.3	0.332	53.0	0.458	2.17	0.0260	1.77	0.0194
184	8.15	0.188	0.0982	0.0007467	0.537	0.00301	0.678	0.0149	36.5	0.686	55.7	1.02	1.87	0.0136	1.78	0.0146
210	7.32	0.0432	0.143	0.00114	0.630	0.00452	1.00	0.0234	23.8	0.217	45.7	0.376	1.59	0.00207	1.80	0.0229
236	6.89	0.0393	0.152	0.0007588	0.660	0.00824	1.06	0.0478	33.8	0.149	45.8	0.944	1.52	0.0134	1.70	0.0244
262	6.32	0.0152	0.172	0.0006714	0.754	0.00389	1.29	0.0441	26.0	0.198	44.6	0.323	1.41	0.0069	1.79	0.0108
289	5.91	0.0484	0.19	0.0005687	0.782	0.0314	1.46	0.0484	24.8	0.064	41.8	0.665	1.36	0.0072	1.78	0.0114
315	5.51	0.0860			0.797	0.0280	1.57	0.0420	23.0	0.358	42.9	0.425	1.26	0.0160	1.76	0.0138
341	5.31	0.0355	0.215	0.00161	0.817	0.0137	1.67	0.0382	22.2	0.305	40.9	0.641	1.26	0.00904	1.76	0.0144
367	4.92	0.0236	0.236	0.0008745	0.832	0.0173	1.82	0.0561	19.5	0.121	36.5	0.953	1.20	0.00862	1.77	0.0161
394	4.65	0.0740	0.252	0.00351	0.829	0.0231	1.92	0.0183	19.2	0.195	36.1	0.214	1.18	0.00918	1.79	0.00157
420	4.42	0.0469	0.266	0.00255	0.847	0.0216	2.06	0.0525	18.4	0.282	34.5	0.726	1.15	0.00402	1.78	0.0102
446	4.54	0.0939	0.282	0.0033	0.810	0.0247	2.08	0.0448	20.5	0.299	32.5	1.22	1.15	0.00392	1.74	0.0221
472	4.36	0.0240	0.29	0.00287	0.837	0.0217	2.20	0.0391	20.3	0.786	32.3	1.16	1.15	0.00588	1.76	0.0248
498	4.17	0.0521	0.29	0.0041	0.799	0.0224	2.18	0.0404	16.0	0.162	30.0	1.42	1.01	0.00474	1.73	0.0195
509	4.03	0.0141	0.29	0.00646	0.776	0.0168	2.16	0.0214	18.0	0.152	32.3	1.78	0.986	0.000789	1.72	0.0222

A1-8: 30 d –CO$_2$ Cs B

Pore volume	Na	SD	K	SD	Mg	SD	Ca	SD	Al	SD	Si	SD	Cs	SD	S	SD
	mM		mM		mM		mM		μM		μM		μM		mM	
5.0	83.0	0.714			<D.L.		0.00180	0.000412	1137	6.37	1572	10.2	28.5	0.2625	1.77	0.0111
9.9	21.1	0.391			<D.L.		0.00218	0.000925	344	5.09	365	0.948	6.47	0.0168	1.80	0.00518
14.9	14.1	0.162			<D.L.		0.00811	0.000662	274	4.03	220	0.836	4.15	0.0216	1.78	0.0247
19.8	12.6	0.240			<D.L.		0.0143	0.000699	269	5.79	205	1.72	3.48	0.0226	1.78	0.0131
24.8	12.1	0.0532			<D.L.		0.00176	0.000427	345	1.62	291	1.20	3.67	0.0279	1.77	0.00796
29.7	11.7	0.0902			<D.L.		0.0147	0.00115	184	0.900	112	1.27	3.26	0.0114	1.76	0.0318
34.7	11.5	0.135			<D.L.		0.0249	0.000894	172	1.89	107	2.43	3.23	0.0216	1.78	0.0132
39.6	11.7	0.092			<D.L.		0.00215	0.000936	313	2.16	268	2.46	3.41	0.0157	1.79	0.0267
44.6	11.4	0.219	0.00116	0.0000189	<D.L.		0.0264	0.00165	101	1.82	77.7	1.14	3.45	0.0614	1.81	0.0173
49.5	11.3	0.163			<D.L.		0.0259	0.000585	86	1.03	67.4	1.03	3.35	0.0873	1.77	0.0142
74.3	11.4	0.142	0.00412	0.000107	<D.L.		0.00554	0.000259	170	2.68	169	2.49	3.15	0.0126	1.70	0.0173
99.0	11.0	0.208	0.0186	0.00113	0.128	0.000841	0.0606	0.000658	60	1.64	81.3	1.41	2.85	0.0174	1.70	0.0218
123.8	10.3	0.206	0.0423	0.000368	0.239	0.00166	0.0858	0.00197	37	0.618	67.6	1.22	2.47	0.00148	1.69	0.0115
148.6	9.44	0.030	0.0931	0.000307	0.540	0.00440	0.299	0.0128	357	2.54	438	2.54	2.69	0.0148	1.69	0.0129
173.3	8.16	0.063			0.626	0.00372	0.696	0.0422	29.2	0.295	54.0	1.03	1.63	0.0129	1.70	0.0172
198.1	7.80	0.083			0.643	0.00353	0.891	0.0105	22.3	0.348	49.7	0.682	1.64	0.00475	1.70	0.0137
222.8	7.89	0.784			0.668	0.00721	1.03	0.0302	30.4	3.03	51.2	0.943	1.57	0.0185	1.71	0.0215
247.6	6.51	0.062	0.189	0.001	0.730	0.00501	1.28	0.0207	28.9	0.260	50.5	0.239	1.49	0.00403	1.69	0.0149
272.4	6.22	0.054	0.202	0.002	0.760	0.00771	1.44	0.0411	25.0	0.218	47.8	0.449	1.44	0.00461	1.72	0.0156
297.1	5.78	0.023	0.211	0.002	0.773	0.00362	1.55	0.0654	23.5	0.021	45.1	0.873	1.38	0.00374	1.71	0.0156
321.9	5.71	0.039	0.227	0.001	0.784	0.00705	1.68	0.0714	22.4	0.177	43.6	0.640	1.35	0.00474	1.71	0.0244
346.6	5.46	0.082	0.236	0.003	0.797	0.00732	1.74	0.0320	21.1	0.217	41.5	1.21	1.33	0.00986	1.70	0.0272
371.4	5.20	0.057	0.246	0.002	0.820	0.00597	1.78	0.0513	20.4	0.204	40.7	0.979	1.27	0.00356	1.71	0.00477
396.2	5.02	0.062	0.256	0.001	0.830	0.00970	1.88	0.0552	19.6	0.258	37.7	1.37	1.22	0.0192	1.71	0.0166
420.9	4.87	0.056	0.267	0.002	0.839	0.0528	1.96	0.0988	18.9	0.112	37.2	0.851	1.17	0.0546	1.71	0.0200
445.7	4.71	0.030	0.281	0.001	0.859	0.0404	2.03	0.0919	18.9	0.166	36.4	0.697	1.17	0.00750	1.71	0.00974
470.4	4.52	0.024	0.293	0.002	0.874	0.0191	2.10	0.0414	16.7	0.0534	33.8	2.38	1.03	0.00606	1.72	0.0135
495.2	4.35	0.047	0.293	0.002	0.901	0.0301	2.20	0.0627	18.0	0.229	32.0	0.163	1.10	0.00496	1.68	0.0181
500.2	4.39	0.035	0.293	0.004	0.882	0.0382	2.19	0.0928	14.7	0.113	31.5	0.783	1.01	0.00528	1.69	0.0200

148

A1-9: 30 d –CO$_2$ Cs C

Pore volume	Na	SD	K	SD	Mg	SD	Ca	SD	Al	SD	Si	SD	Cs	SD	S	SD
	mM		mM		mM		mM		μM		μM		μM		mM	
4.9	78.0	1.37			<D.L.		0.00206	0.000655	948	14.0	1417	13.9	28.4	0.619	1.71	0.0227
9.8	20.7	0.1056			<D.L.		0.00102	0.000172	693	5.47	828	6.88	7.28	0.0109	1.70	0.0194
14.7	14.4	0.0703			<D.L.		0.00086	0.000453	246	0.320	194	1.99	4.41	0.0163	1.70	0.00944
19.6	12.6	0.0881			<D.L.		0.00122	0.000881	226	3.19	164	1.47	3.69	0.0347	1.70	0.0126
24.6	12.1	0.2097			<D.L.		0.00236	0.000405	174	2.92	104	1.64	3.41	0.0304	1.71	0.0185
29.5	11.7	0.1178			<D.L.		0.00429	0.00409	175	2.61	117	2.27	3.22	0.00354	1.72	0.0157
34.4	11.6	0.1874			<D.L.		0.000481	0.000566	329	4.74	315	3.72	3.56	0.0103	1.70	0.0110
39.3	11.2	0.5865			<D.L.		0.00251	0.000543	142	7.43	96	0.428	3.09	0.00525	1.67	0.0207
44.2	11.2	0.1648	0.00116	4.13E-05	0.0113	0.00115	0.00106	0.000503	125	2.81	80	0.643	3.32	0.00962	1.69	0.0112
49.1	11.1	0.0123			0.0565	0.00047	0.00197	0.000859	103	12.9	77.3	0.386	3.05	0.0207	1.69	0.0200
68.8	11.2	0.5504			0.241	0.00257	0.123	0.00237	540	24.0	585	5.13	3.57	0.0182	1.67	0.0123
98.2	9.52	0.0190	0.0737	0.0004935	0.354	0.00147	0.387	0.00733	49.8	0.179	61.8	1.26	2.55	0.00637	1.69	0.0123
122.8	8.94	0.3228	0.1	0.00553	0.456	0.00355	0.565	0.0153	40.3	1.56	57.5	0.222	2.31	0.00968	1.72	0.0313
147.3	8.19	0.0205	0.139	0.00183	0.554	0.00421	0.838	0.0264	35.5	0.107	54.3	0.753	2.05	0.0272	1.73	0.0114
171.9	7.11	0.0477	0.199	0.0003783	0.653	0.00157	1.27	0.0353	31.7	0.273	48.5	0.520	1.51	0.0042	1.73	0.0105
196.5	6.97	0.0662	0.197	0.00157	0.674	0.00525	1.31	0.0352	28.2	0.242	48.3	1.06	1.50	0.0097	1.74	0.0250
221.0	6.82	0.0102	0.2	0.0008186	0.680	0.00163	1.33	0.0456	30.4	0.128	47.8	0.425	1.53	0.0124	1.75	0.0141
245.6	6.57	0.0881	0.201	0.00271	0.676	0.00821	1.39	0.0424	30.4	0.261	47.3	1.04	1.51	0.00500	1.72	0.0329
270.1	6.50	0.0676	0.203	0.0014	0.651	0.00705	1.39	0.0565	31.8	0.464	52.5	0.987	1.62	0.0136	1.71	0.0197
294.7	6.37	0.0956			0.650	0.00330	1.40	0.0414	26.1	0.417	52.4	0.772	1.39	0.0187	1.72	0.0159
319.2	6.24	0.115	0.213	0.00245	0.674	0.00243	1.46	0.0336	26.1	0.374	52.5	0.514	1.53	0.0125	1.73	0.00941
343.8	6.09	0.0499	0.222	0.00182	0.696	0.00675	1.56	0.0503	23.0	0.191	50.3	1.87	1.54	0.00339	1.74	0.0289
368.4	5.98	0.0425	0.231	0.0003464	0.702	0.00554	1.57	0.0264	21.6	0.190	49.4	1.64	1.47	0.00811	1.74	0.00959
392.9	5.78	0.0179	0.234	0.00253	0.706	0.00695	1.65	0.0401	21.8	0.100	47.0	1.36	1.40	0.0149	1.75	0.0314
417.5	5.64	0.0479	0.251	0.00302	0.717	0.00586	1.69	0.0679	18.8	0.113	44.2	0.971	1.40	0.0262	1.75	0.0206
442.0	5.49	0.0253	0.259	0.00122	0.729	0.00096	1.75	0.0429	19.6	0.169	42.7	1.15	1.34	0.00803	1.75	0.0138
466.6	5.34	0.0780	0.265	0.0006615	0.737	0.00334	1.82	0.0426	17.5	0.272	39.2	0.711	1.29	0.00503	1.72	0.0154
491.1	5.17	0.0300	0.265	0.00155	0.759	0.00204	1.85	0.0484	15.0	0.111	37.4	1.81	1.12	0.00831	1.73	0.00752
501.0	5.06	0.0663	0.265	0.00578	0.766	0.00494	1.84	0.0318	14.8	0.187	37.0	1.19	1.11	0.00789	1.71	0.0103

A1-10: 30 d +CO$_2$ Sr/Cs

Pore volume	Na	SD	K	SD	Mg	SD	Ca	SD	Al	SD	Si	SD	Sr	SD	Cs	SD	S	SD
	mM		mM		mM		mM		μM		μM		μM		nM		mM	
5.3	25.3	0.175			<D.L.		<D.L.		8.14	0.133	114	0.548	0.563	0.0032	1280	8.32	1.73	0.0292
10.5	10.2	0.0777	0.08	0.0006	0.58	0.0181	0.285	0.00435	9.71	0.124	90.6	1.11	3.23	0.003	458	3.57	1.83	0.0427
15.8	8.01	0.186			0.82	0.0274	1.12	0.0206	13.4	0.0575	75.5	3.28	6.07	0.039	350	4.41	1.87	0.0391
21.1	6.88	0.116			1	0.0233	1.68	0.0517	9.68	0.0977	65.4	2.1	7.9	0.013	281	1.49	1.97	0.00494
26.4	6.04	0.04	0.179	0.00074	0.941	0.00894	2.01	0.04	9.51	0.0618	57.4	1.01	9.39	0.052	222	1.24	1.95	0.0125
31.6	5.75	0.069	0.207	0.0012	0.901	0.0305	2.31	0.0714	9.63	0.214	56.8	1.4	10.6	0.0478	199	3.82	1.97	0.0148
36.9	5.42	0.0873	0.227	0.001	0.849	0.00475	2.41	0.0568	9.42	0.0433	52.7	0.385	10.8	0.045	179	1.04	1.94	0.0531
42.2	5.23	0.0345			0.824	0.0178	2.46	0.0871	9.58	0.107	49.9	0.375	10.9	0.039	167	2.39	1.92	0.0327
47.4	5.06	0.0537			0.786	0.0132	2.51	0.0189	9.89	0.156	48.8	1.44	10.7	0.051	153	0.858	1.9	0.0651
52.7	5.17	0.0538			0.816	0.00718	2.52	0.0875	10.3	0.218	50.6	1.59	11	0.031	151	1.37	2.01	0.0253
79.1	5.09	0.0305	0.294	0.00147	0.804	0.0233	2.64	0.0623	11	0.0307	35.5	0.0532	11.4	0.0069	116	2.17	1.76	0.015
105.4	4.97	0.0467	0.302	0.00498	0.769	0.00877	2.72	0.041	11.7	0.184	33.6	0.551	11.1	0.064	98.7	0.878	1.74	0.0148
131.8	4.9	0.0436	0.303	0.00258	0.78	0.0292	2.68	0.02	13	0.104	32.6	0.493	10.8	0.065	84.6	0.939	1.73	0.0266
158.1	4.81	0.05	0.302	0.00408	0.783	0.016	2.66	0.0829	11.1	0.118	29	0.528	10.6	0.038	70.8	1.65	1.72	0.0117
184.5	4.92	0.0988	0.313	0.0036	0.776	0.0115	2.75	0.0521	10.8	0.145	26.7	1.04	10.7	0.1	62.7	1	1.75	0.0541
210.8	4.87	0.054			0.783	0.0193	2.68	0.0875	10.2	0.0675	32.2	0.431	10.5	0.049	68.3	1.31	1.75	0.0114
263.6	4.78	0.0201			0.797	0.011	2.72	0.0722	12.4	0.0373	31.4	0.596	9.63	0.017	55.8	0.799	1.74	0.0226
316.3	4.78	0.0947	0.313	0.00385	0.792	0.0229	2.81	0.0692	11.4	0.132	39	0.962	8.97	0.03	49.3	0.355	1.75	0.0338
369.0	4.72	0.0161	0.306	0.00475	0.797	0.02184	2.76	0.0592	10.9	0.0556	33.9	0.251	8.37	0.033	39.7	0.457	1.75	0.0206
421.7	4.74	0.0299	0.307	0.00181	0.786	0.013	2.68	0.0519	11	0.101	28.5	0.995	7.73	0.026	32.2	0.277	1.76	0.0148
474.4	4.65	0.0214	0.307	0.00926	0.784	0.00682	2.74	0.05	10.2	0.0772	29.9	0.27	6.89	0.023	31.8	0.0763	1.74	0.0282
527.1	4.75	0.0403	0.307	0.00127	0.774	0.0161	2.71	0.0727	11.2	0.13	30.3	0.0969	6.33	0.034	29.1	0.0408	1.75	0.0177
542.9	4.73	0.0426	0.307	0.00304	0.772	0.0187	2.72	0.0187	11.7	0.223	35.6	1.62	6.14	0.0061	28.1	0.419	2.01	0.0119

A1-11: 548 d +CO$_2$ Sr/Cs A

Pore volume	Na	SD	K	SD	Mg	SD	Ca	SD	Al	SD	Si	SD	Sr	SD	Cs	SD	S	SD
	mM			mM		mM		mM		μM		μM		μM		nM		mM
4.97	15.9	0.128			0.0265	0.00121	<D.L.		8.1425	0.1327	0.543	1.79	0.35	0.0064	3780	43.85	1.72	0.0333
9.94	9.1	0.169			0.526	0.0198	0.387	0.0346	9.7145	0.124	2.7	4.15	7.13	0.087	1162	15.69	1.9	0.0331
14.91	7.58	0.0318			0.542	0.0203	0.18	0.0271	13.3802	0.058	<D.L.		7.8	0.224	985	19.6	1.88	0.0357
19.88	6.96	0.0801			0.75	0.0037	0.49	0.0174	9.6771	0.098	<D.L.		13.42	0.082	868	2.78	2.12	0.04085
24.84	7.38	0.041	0.08	0.00339	0.926	0.01695	0.29	0.0149	9.5086	0.062	<D.L.		18.4	0.138	852	8.87	2.4	0.0464
29.81	5.86	0.3895	0.148	0.0045	0.632	0.016	0.99	0.0717	9.6263	0.2137	<D.L.		14	0.3799	785	193.42	1.92	0.1214
34.78	6.32	0.0581	0.168	0.01004	0.855	0.01914	1.18	0.1293	9.4225	0.043	<D.L.		19.2	0.033	638	7.53	2.26	0.031
39.75	5.31	0.0525			0.615	0.0054	1	0.0855	9.5798	0.107	2.4	1.165	14.1	0.072	530	0.8	1.88	0.0347
44.72	5.31	0.0027			0.647	0.0098	1.02	0.0574	9.8857	0.156	<D.L.		14.6	0.105	482	4.148	1.94	0.0239
49.69	5.29	0.064			0.67	0.01995	1.13	0.0801	10.3233	0.218	4.1	1.36	14.5	0.296	435	6.05	1.98	0.0299
74.53	5.09	0.0382	0.278	0.00854	0.712	0.0031	1.96	0.092	10.9786	0.0307	15	1.5902	13.1	0.0812	323	12.23	1.66	0.0164
99.38	5.00	0.008	0.276	0.00561	0.71	0.01214	1.95	0.0507	11.7338	0.184	16.5	1.174	10.1	0.065	253.3	0.735	1.69	0.016
124.22	5.03	0.0241	0.269	0.00802	0.746	0.0111	1.88	0.0605	12.989	0.104	17.3	1.117	8.7	0.07	218.1	1.592	1.76	0.0213
149.07	4.73	0.0218	0.235	0.00368	0.663	0.0123	1.45	0.0558	11.056	0.118	12.4	0.684	6.6	0.098	177.8	1.4	1.62	0.0184
173.91	4.8	0.02	0.284	0.01348	0.683	0.0176	1.96	0.1162	10.8069	0.145	15.3	1.09	6	0.06	151.5	1.65	1.66	0.0007
198.75	4.86	0.03112			0.718	0.0178	1.79	0.0447	10.2332	0.068	17.8	1.076	5.3	0.024	159.1	0.33	1.71	0.0024
248.44	4.65	0.005			0.669	0.0083	1.21	0.0747	12.4263	0.037	11.7	1.527	3.96	0.01	148.2	0.845	1.66	0.0043
298.13	4.92	0.04035	0.34	0.01888	0.794	0.0272	2.44	0.1425	11.4494	0.132	27.8	0.942	3.7	0.064	148.5	2.703	1.82	0.0218
347.82	4.69	0.0263	0.291	0.01624	0.713	0.02581	2.01	0.0886	10.9049	0.056	20.1	1.056	2.9	0.03	124.3	1.069	1.7	0.0184
397.51	4.75	0.0152	0.324	0.00367	0.729	0.0179	2.37	0.0442	10.9915	0.101	21.1	1.038	2.64	0.013	104.6	0.795	1.75	0.0052
447.20	4.88	0.0307	0.324	0.02723	0.783	0.01918	2.44	0.0859	10.1523	0.077	28.9	1.691	2.54	0.009	129.7	1.2713	1.82	0.0177
496.89	4.77	0.0482	0.309	0.0158	0.713	0.0177	2.03	0.0775	11.1728	0.13	18.1	1.2569	2.13	0.004	115.2	0.795	1.68	0.0346
511.79	4.78	0.054	0.309	0.0284	0.646	0.0244			11.7361	0.223			1.93	0.0481	110.2	0.639	2.08	0.0399

A1-12: 548 d +CO$_2$ Sr/Cs B

Pore volume	Na	SD	K	SD	Mg	SD	Ca	SD	Al	SD	Si	SD	Sr	SD	Cs	SD	S	SD
	mM				mM		mM		μM		μM		μM		nM		mM	
4.97	15.9	0.128			0.0265	0.00121	<D.L.		8.1425	0.1327	0.543	1.79	0.35	0.0064	3780	43.85	1.72	0.0333
9.94	9.1	0.169			0.526	0.0198	0.387	0.0346	9.7145	0.124	2.7	4.15	7.13	0.087	1162	15.69	1.9	0.0331
14.91	7.58	0.0318			0.542	0.0203	0.18	0.0271	13.3802	0.058	<D.L.		7.8	0.224	985	19.6	1.88	0.0357
19.88	6.96	0.0801			0.75	0.0037	0.49	0.0174	9.6771	0.098	<D.L.		13.42	0.082	868	2.78	2.12	0.04085
24.84	7.38	0.041	0.08	0.00339	0.926	0.01695	0.29	0.0149	9.5086	0.062	<D.L.		18.4	0.138	852	8.87	2.4	0.0464
29.81	5.86	0.3895	0.148	0.0045	0.632	0.016	0.99	0.0717	9.6263	0.2137	<D.L.		14	0.3799	785	193.42	1.92	0.1214
34.78	6.32	0.0581	0.168	0.01004	0.855	0.01914	1.18	0.1293	9.4225	0.043	<D.L.		19.2	0.033	638	7.53	2.26	0.031
39.75	5.31	0.0525			0.615	0.0054	1	0.0855	9.5798	0.107	2.4	1.165	14.1	0.072	530	0.8	1.88	0.0347
44.72	5.31	0.0027			0.647	0.0098	1.02	0.0574	9.8857	0.156	<D.L.		14.6	0.105	482	4.148	1.94	0.0239
49.69	5.29	0.064			0.67	0.01995	1.13	0.0801	10.3233	0.218	4.1	1.36	14.5	0.296	435	6.05	1.98	0.0299
74.53	5.09	0.0382	0.278	0.00854	0.712	0.0031	1.96	0.092	10.9786	0.0307	15	1.5902	13.1	0.0812	323	12.23	1.66	0.0164
99.38	5.00	0.008	0.276	0.00561	0.71	0.01214	1.95	0.0507	11.7338	0.184	16.5	1.174	10.1	0.065	253.3	0.735	1.69	0.016
124.22	5.03	0.0241	0.269	0.00802	0.746	0.0111	1.88	0.0605	12.989	0.104	17.3	1.117	8.7	0.07	218.1	1.592	1.76	0.0213
149.07	4.73	0.0218	0.235	0.00368	0.663	0.0123	1.45	0.0558	11.056	0.118	12.4	0.684	6.6	0.098	177.8	1.4	1.62	0.0184
173.91	4.8	0.02	0.284	0.01348	0.683	0.0176	1.96	0.1162	10.8069	0.145	15.3	1.09	6	0.06	151.5	1.65	1.66	0.0007
198.75	4.86	0.03112			0.718	0.0178	1.79	0.0447	10.2332	0.068	17.8	1.076	5.3	0.024	159.1	0.33	1.71	0.0024
248.44	4.65	0.005			0.669	0.0083	1.21	0.0747	12.4263	0.037	11.7	1.527	3.96	0.01	148.2	0.845	1.66	0.0043
298.13	4.92	0.04035	0.34	0.01888	0.794	0.0272	2.44	0.1425	11.4494	0.132	27.8	0.942	3.7	0.064	148.5	2.703	1.82	0.0218
347.82	4.69	0.0263	0.291	0.01624	0.713	0.02581	2.01	0.0886	10.9049	0.056	20.1	1.056	2.9	0.03	124.3	1.069	1.7	0.0184
397.51	4.75	0.0152	0.324	0.00367	0.729	0.0179	2.37	0.0442	10.9915	0.101	21.1	1.038	2.64	0.013	104.6	0.795	1.75	0.0052
447.20	4.88	0.0307	0.324	0.02723	0.783	0.01918	2.44	0.0859	10.1523	0.077	28.9	1.691	2.54	0.009	129.7	1.2713	1.82	0.0177
496.89	4.77	0.0482	0.309	0.0158	0.713	0.0177	2.03	0.0775	11.1728	0.13	18.1	1.2569	2.13	0.004	115.2	0.795	1.68	0.0346
511.79	4.78	0.054	0.309	0.0284	0.646	0.0244			11.7361	0.223			1.93	0.0481	110.2	0.639	2.08	0.0399

A1-13: 548 d +CO$_2$ Sr

Pore volume	Na (mM)	SD	K (mM)	SD	Mg (mM)	SD	Ca (mM)	SD	Al (μM)	SD	Si (μM)	SD	Sr (μM)	SD	S (mM)	SD
5.05	36.5	0.917			0.0495	0.00198	0.066	0.00027	4981	116	3906	159.337	9.195	0.0919	1.65	0.0395
10.1	12.7	0.096			0.43	0.0127	0.545	0.00176	552	1.38	77.2	0.4	1.8	0.006	1.64	0.0369
15.1	9.15	0.1939			0.685	0.0142	1.32	0.00271	300	5.76	14.3	1.18	2.78	0.006	1.59	0.0424
20.2	7.86	0.0692			0.733	0.02	1.7	0.00411	211	1.5	10.3	0.82	3.07	0.018	1.57	0.06732
25.2	7.21	0.107	0.08	0.00173	0.763	0.00932	1.93	0.00315	164	1.59	9.6	1.27	3.13	0.012	1.59	0.0541
30.3	6.78	0.0597			0.738	0.0185	1.96	0.00504	126	1.28	13.9	0.98	3.1	0.0144	1.57	0.0285
35.3	6.5	0.0533			0.765	0.01697	2.1	0.00402	91.3	0.411	9.2	1.296	3.1	0.016	1.54	0.0303
40.4	6.33	0.0873			0.743	0.0217	2.07	0.00634	98	0.99	16.6	0.941	3.1	0.014	1.57	0.0562
45.4	6.2	0.0806			0.766	0.0174	2.17	0.00553	80.2	0.601	17.3	0.37	3	0.032	1.53	0.049
50.5	6.06	0.0673			0.767	0.01351	2.18	0.00407	56.4	0.993	13.1	1.26	3	0.014	1.53	0.0649
55.5	5.92	0.0539			0.792	0.021	2.29	0.00707	65.9	0.455	18.6	1.53	3	0.0113	1.6	0.0227
60.6	5.84	0.036			0.783	0.03206	2.28	0.0105	49.5	0.149	16.8	0.634	2.9	0.021	1.55	0.0578
65.6	5.78	0.026	0.232	0.00195	0.777	0.0193	2.27	0.0062	49.4	0.292	17.4	0.67	2.9	0.013	1.53	0.0515
70.6	5.87	0.0405	0.243	0.0033	0.795	0.0085	2.33	0.00235	37.1	0.368	17	0.63	2.9	0.016	1.61	0.0344
75.7	5.76	0.037	0.243	0.00192	0.785	0.0176	2.3	0.00666	38	0.156	17.9	0.58	2.8	0.017	1.58	0.0511
101	5.53	0.0558	0.255	0.00304	0.807	0.0193	2.4	0.0073	33.7	0.145	21.6	0.627	2.4	0.016	1.56	0.0318
126	5.4	0.035	0.264	0.00225	0.778	0.0137	2.34	0.00594	31	0.149	24.7	1.52	2.12	0.008	1.63	0.0963
151	5.29	0.03545	0.27	0.00372	0.803	0.012	2.45	0.00466	25.4	0.244	23.7	1.21	1.89	0.007	1.62	0.0648
177	5.27	0.0506	0.277	0.00307	0.801	0.00976	2.45	0.00247	31.4	0.217	30	1.23	1.71	0.005	1.58	0.0364
202	5.2	0.0301	0.279	0.00268	0.813	0.0076	2.5	0.00383	23.9	0.143	26	1.23	1.55	0.007	1.6	0.0648
227	5.17	0.0723	0.281	0.00382	0.796	0.01341	2.46	0.00497	27.4	0.332	27.9	2.05	1.44	0.008	1.54	0.0196
252	5.14	0.037			0.809	0.0172	2.5	0.00625	27.6	0.088	27.9	0.531	1.34	0.013	1.6	0.0642
278	5.11	0.046	0.284	0.00219	0.797	0.0203	2.48	0.00589	24.4	0.241	33	0.929	1.26	0.0065	1.55	0.0558
328	5.07	0.0543	0.285	0.00273	0.796	0.0246	2.49	0.00977	20.5	0.191	33	0.976	1.19	0.007	1.6	0.0843
353	5.11	0.0281	0.288	0.00274	0.795	0.0156	2.49	0.00474	19.7	0.274	33.6	0.732	1.15	0.00515	1.6	0.0589
378	5.05	0.0359	0.287	0.00204	0.813	0.00596	2.56	0.00281	19.6	0.188	32.4	1.61	1.1	0.00527	1.61	0.0731
404	5	0.013	0.287	0.00241	0.805	0.0132	2.54	0.00501	19.7	0.205	31.3	1.84	1.07	0.00663	1.63	0.0573
429	5.03	0.0493	0.289	0.00188	0.786	0.00939	2.47	0.00321	18.3	0.053	30	1.13	1.07	0.00288	1.61	0.0168
454	5.04	0.063	0.294	0.0032	0.802	0.0296	2.54	0.0106	20.8	0.148	31.4	1.44	1.05	0.0069	1.59	0.0222
479	5.06	0.0602	0.298	0.00259	0.791	0.0306	2.48	0.00999	19.4	0.212	29.5	2.17	1.03	0.0154	1.59	0.0653
505	5	0.0305	0.298	0.00252	0.801	0.0242	2.53	0.00949	20.9	0.107	31	0.6	1.01	0.00625	1.58	0.0255

A1-14: 548 d +CO$_2$ Cs

Pore volume	Na	SD	K	SD	Mg	SD	Ca	SD	Al	SD	Si	SD	Cs	SD	S	SD
	mM			mM		mM		mM		μM		μM		nM		mM
4.22	54.8	3.004			0.099	0.00505	0.158	0.00113	25000	1324	1047	28	61000	3871.4	1.62	0.0912
8.6	13.6	0.172			0.511	0.00261	1.02	0.056	1151	10.478	691	31.47	4084	120.1	1.75	0.0527
12.6	8.96	0.0215			0.689	0.00434	1.17	0.151	171	0.444	5.1	0.8	1709	38.44	1.78	0.0488
18.9	8.11	0.0778			0.729	0.00948	1.67	0.112	174	0.94	45.7	2.48	1536	43.2	1.72	0.0239
23.8	7.22	0.059	0.08	0.00233	0.744	0.0063	1.89	0.0769	98	0.854	9.9	0.14	1194	35.57	1.63	0.0397
28.6	6.7	0.069			0.766	0.0077	1.98	0.0346	81	1.1432	10.9	0.05	1054	26.02	1.61	0.0424
33.4	6.41	0.0115			0.78	0.0027	2	0.0618	67	0.419	12	0.258	916	29.85	1.61	0.0944
38.1	6.27	0.0276			0.807	0.0046	2.17	0.0815	58	0.262	13.3	0.077	830	23	1.6	0.0288
42.9	6.07	0.043			0.798	0.0079	2.1	0.0588	60	0.193	15.9	0.38	729	19.11	1.61	0.0394
47.7	5.95	0.0756			0.807	0.00895	2.17	0.0627	57.3	0.361	17.6	2.81	702	14.46	1.57	0.04
52.4	5.91	0.0437			0.817	0.00915	2.23	0.0382	57.1	0.4913	18.2	1.4044	664	18.39	1.57	0.04
57.2	5.96	0.0328	0.249	0.00256	0.837	0.00661	2.26	0.0659	34.6	0.273	15.2	0.297	643	22.11	1.62	0.0406
62.0	5.97	0.0985	0.258	0.00392	0.85	0.01233	2.42	0.0231	32.3	0.368	17.3	2.036	621	15.8	1.63	0.0166
66.7	5.63	0.0799	0.247	0.00205	0.813	0.00797	2.27	0.0542	32.2	0.361	16.5	1.291	573	14.3	1.57	0.0086
71.5	6.52	0.1142	0.294	0.00365	0.949	0.0122	1.82	0.168	36.5	0.299	13.4	1.43	635	17.2	1.83	0.07131
95	5.56	0.074	0.27	0.00337	0.855	0.01077	2.41	0.0691	25.9	0.342	18.9	1.732	461	12.4	1.65	0.031
119	5.46	0.02	0.281	0.00115	0.862	0.0024	2.43	0.0621	28.8	0.181	21.1	2.251	380	11.7	1.6	0.039
143	5.33	0.0826	0.285	0.00374	0.854	0.0127	2.51	0.0942	24.1	0.137	22.9	2.483	342	8.27	1.61	0.0553
167	5.23	0.0293	0.288	0.00133	0.852	0.00392	2.59	0.0984	25.9	0.119	24.2	0.482	299	7.97	1.62	0.0505
191	5.19	0.0659	0.292	0.00286	0.846	0.00803	2.48	0.0315	20.4	0.241	22.4	1.528	259	6.55	1.63	0.0863
215	5.16	0.032			0.841	0.00387	2.48	0.108	26.6	0.104	25.3	2.031	229	6.95	1.61	0.0453
238	5.16	0.0692			0.848	0.0082	2.46	0.0458	20.9	0.242	23.2	2.6562	218	6.21	1.62	0.0541
262	5.2	0.0536	0.304	0.00393	0.848	0.01018	2.46	0.0833	18.5	0.266	26.7	1.96	213	6.99	1.59	0.0688
286	5.19	0.0478	0.307	0.00206	0.856	0.00642	2.53	0.0424	17.1	0.142	31.7	1.86	208	6.5	1.59	0.0354
310	5.24	0.0403	0.314	0.00267	0.855	0.01009	2.57	0.0644	16.9	0.198	32.3	1.82	200	3.36	1.63	0.0338
334	5.14	0.0576	0.308	0.00428	0.853	0.00494	2.56	0.0576	16.7	0.157	27.7	1.1	183	4.86	1.58	0.0261
358	5.17	0.0517	0.311	0.0028	0.858	0.00532	2.54	0.0951	25.8	0.0853	29.6	0.75	175	5.24	1.61	0.0205
381	5.15	0.0665	0.316	0.00645	0.853	0.01135	2.58	0.0687	16.7	0.254	28.1	2.25	165	4.15	1.6	0.0317
405	5.14	0.0781	0.314	0.00332	0.853	0.011	2.53	0.141	17.4	0.237	26.2	3.38	161	4.92	1.57	0.0243
429	5.06	0.0608			0.839	0.00671	2.51	0.0642	18.3	0.135	28.5	2.55	152	3.49	1.53	0.0198
453	5.07	0.0573			0.844	0.012	2.52	0.0209	19.4	0.283	26.5	0.61	145	5.19	1.64	0.0672
477	5.01	0.0621	0.309	0.00247	0.839	0.00982	2.48	0.0889	18.6	0.0855	25.2	0.717	146	0.583	1.59	0.0758
501	5.09	0.0102	0.314	0.00198	0.852	0.00443	2.5	0.0572	19.6	0.159	24.1	0.911	138	3.62	1.61	0.0515
505	5.06	0.0688	0.314	0.00527	0.843	0.0135	2.47	0.0663	20	0.24	27.1	1.65	136	2.16	1.6	0.0438

A1-15: Quartz only

Pore volume	Na	SD	K	SD	Mg	SD	Ca	SD	Al	SD	Si	SD	S	SD
	mM		mM		mM		mM		μM		μM		mM	
5.33	5.31	0.055			0.83	0.007	2.62	0.093	2.37	0.13	19.06	0.59	1.71	0.045
10.7	5.60	0.093			0.89	0.012	2.82	0.037	0.35	0.03	14.17	0.05	1.95	0.009
16.0	5.40	0.031			0.86	0.005	2.75	0.049	0.38	0.02	10.92	0.09	1.92	0.044
21.3	5.47	0.104			0.87	0.018	2.75	0.045	0.34	0.08	9.25	0.05	1.94	0.018
26.6	5.42	0.054			0.86	0.011	2.82	0.018	0.34	0.01	9.11	0.14	1.97	0.047
32.0	5.38	0.175			0.85	0.024	2.76	0.004	0.46	0.04	8.33	0.09	1.96	0.036
37.3	5.63	0.039	0.41	0.002	0.91	0.003	3.02	0.037	0.24	0.05	7.71	0.08	2.09	0.028
42.6	5.36	0.028	0.39	0.002	0.85	0.008	2.72	0.060	0.33	0.04	6.77	0.18	1.91	0.042
48.0	5.47	0.079	0.40	0.009	0.87	0.020	2.79	0.019	0.26	0.03	6.76	0.11	2.02	0.028
53.3	5.50	0.096			0.87	0.018	2.82	0.003	0.23	0.06	6.59	0.05	2.02	0.044
79.9	5.43	0.098	0.39	0.007	0.86	0.011	2.79	0.025	0.29	0.04	4.92	0.02	2.00	0.030
107	5.41	0.016	0.39	0.001	0.87	0.001	2.81	0.009	0.30	0.07	4.46	0.06	2.03	0.013
133	5.53	0.189	0.40	0.008	0.88	0.027	2.81	0.180	0.29	0.03	4.06	0.47	2.05	0.190
160	5.99	0.053	0.43	0.004	0.97	0.012	3.14	0.025	0.30	0.02	4.22	0.05	2.17	0.013
187	5.40	0.005	0.39	0.001	0.86	0.002	2.81	0.026	0.23	0.03	3.41	0.01	2.02	0.015
213	5.26	0.123	0.40	0.005	0.85	0.016	2.83	0.009	0.22	0.04	3.50	0.12	1.98	0.015
266	5.57	0.099	0.34	0.004	0.89	0.014	2.88	0.017	0.16	0.04	2.52	0.03	2.02	0.012
320	5.50	0.246			0.88	0.032	2.78	0.118	0.13	0.02	2.48	0.14	1.98	0.094
373	5.55	0.084	0.34	0.009	0.89	0.018	2.97	0.014	0.27	0.04	2.33	0.09	2.15	0.070
426	5.45	0.115	0.33	0.006	0.87	0.016	2.83	0.025	0.11	0.03	1.97	0.08	2.06	0.030
480	5.65	0.011	0.35	0.003	0.91	0.009	2.98	0.015	0.17	0.02	2.18	0.11	2.16	0.046
533	6.33	0.156			1.02	0.030	3.36	0.038	0.28	0.05	2.65	0.08	2.37	0.039

A1-16: Effluent Nitrate

| 30 d -CO$_2$ | | | | | | 30 d +CO$_2$ | | 548 d +CO$_2$ | | | | | |
| Sr/Cs C | | Sr B | | Cs C | | Sr/Cs | | Sr/Cs A | | Sr | | Cs | |
Pore Volume	Nitrate (μM)	Pore Volume	Nitrate (μM)	Pore Volume	Nitrate (μM)	Pore Volume	Nitrate (μM)	Pore Volume	Nitrate (μM)	Pore Volume	Nitrate (μM)	Pore Volume	Nitrate (μM)
5.2	17.2	4.9	34.5	4.9	27.2	5.3	2.00			5.0	21.4	9.5	3.59
15.7	0.0170	14.8	0.393	14.7	0.468	15.8	0.0174	10.7	0.924	15.1	0.571	23.8	0.234
68.2	0.0190	24.6	0.114	24.6	0.119	26.4	0.0435	21.4	0.254	25.2	0.253	38.1	0.170
136.4	0.113	49.3	0.0319	98.2	0.0195	52.7	0.0142	42.8	0.105	50.5	0.142	47.7	0.126
194.1	0.0169	73.9	0.0180	147.3	0.00676	79.1	0.0168	53.5	0.0111	75.7	0.159	71.5	0.0768
246.5	0.0632	123.2	0.00912	196.5	0.0097905	105	0.0168	107	0.0404	101	0.0659	95.3	0.0503
346.1	0.0225	221.7	0.00619	245.6	0.00753	158	0.0114	161	0.0230	151	0.0356	143	0.0440
493.0	0.0167	295.6	0.0144	294.7	0.00555	211	0.00574	214	0.0180	202	0.0156	191	0.0205
		344.9	0.00969	501.0	0.0130	316	0.00805	268	0.00986	252	0.0315	238	0.0187
		394.1	0.0144			369	0.00963	321	0.0220	328	0.0252	381	0.0371
		443.4	0.00806			422	0.00634	375	0.0354	353	0.0265	477	0.0263
						543	0.00706	428	0.0173	404	0.0240	501	0.0326
								482	0.0157	454	0.0314		

A1-17: pH -CO₂ columns

30 d Sr/Cs -CO₂

A Pore Volume	pH	B Pore Volume	pH	C Pore Volume	pH
4.9	12.5	5.0	10.7	5.2	12.0
9.8	11.3	10.0	10.8	10.5	10.7
14.7	10.9	15.0	10.6	15.7	10.3
19.6	10.7	20.0	10.2	21.0	10.1
24.5	10.4	25.0	10.1	26.2	9.72
29.4	10.3	30.0	9.99	31.5	9.82
34.3	10.2	35.0	9.85	36.7	9.72
39.3	10.1	40.0	9.81	42.0	9.50
44.2	10.1	50.0	9.68	47.2	9.63
206	8.02	60.0	9.59	52.4	9.49
211	8.16	230	8.02	57.7	9.47
226	8.02	235	7.99	231	8.01
245	7.96	240	7.99	236	7.80
255	7.86	245	8.00	241	7.83
265	7.96	250	7.95	246	7.71
280	7.90	255	7.87	252	7.67
466	8.01	485	7.89	472	7.50
471	7.78	490	8.32	488	7.64
476	7.74	495	7.90	509	7.53
481	7.69	500	7.89		
707	7.77	682	7.63		
711	7.90				
716	7.85				

30 d Sr -CO₂

A Pore Volume	pH	B Pore Volume	pH	C Pore Volume	pH
5.3	12.2	4.9	12.4	4.8	12.3
10.6	11.4	9.9	11.5	9.6	11.6
16.0	11.1	14.8	10.9	14.3	11.0
21.3	10.7	19.7	10.6	19.1	10.8
26.6	10.4	24.6	10.3	23.9	10.4
31.9	10.3	29.6	10.1	28.7	10.2
37.3	10.1	34.5	9.96	33.5	10.1
42.6	9.93	39.4	9.82	38.2	9.87
47.9	9.86	44.3	9.58	43.0	9.67
53.2	9.8	49.3	9.58	47.8	9.81
58.6	9.57	54.2	9.48	52.6	9.65
63.9	9.52	59.1	9.4	172	8.85
69.2	9.44	212	8.19	177	8.50
74.5	9.38	217	8.29	186	8.39
240	7.96	227	8.19	210	8.07
245	8.26	232	8.11	220	8.10
256	8.26	251	8.08	225	7.91
261	8.11	266	8.07	229	8.22
282	8.05	271	7.96	234	8.23
298	8.07	281	7.88	249	8.07
304	7.96	291	7.94	397	7.67
314	7.92	443	7.54	406	7.52
490	7.42	453	7.73	416	7.53
495	7.65	463	7.64	425	7.59
501	7.62	473	7.54	435	7.73
511	7.66	483	7.73	444	7.73
516	7.65	503	7.64	454	7.63
				473	7.67
				487	7.67
				502	7.66

30 d Cs -CO₂

A Pore Volume	pH	B Pore Volume	pH	C Pore Volume	pH
5.2	12.8	5.0	12.8	4.9	12.2
10.4	12.2	9.9	12.1	9.8	11.6
15.6	11.2	14.9	11.4	14.7	11.2
20.8	10.6	19.8	10.9	19.6	10.9
31.3	10.1	24.8	10.6	24.6	10.4
36.5	9.93	29.7	10.3	29.5	9.97
41.7	9.90	34.7	10.1	34.4	9.73
46.9	9.81	39.6	9.92	39.3	9.55
52.1	9.72	168	8.19	44.2	9.41
57.3	9.75	173	8.12	49.1	9.53
62.5	9.68	178	7.96	54.0	9.52
67.7	9.53	183	7.97	58.9	9.41
73.0	9.47	188	7.98	63.8	9.21
78.2	9.37	198	7.94	68.8	9.09
83.4	9.37	213	8.02	73.7	9.13
219	8.04	223	8.15	78.6	8.93
224	7.94	243	7.89	83.5	8.93
229	7.84	258	7.70	250	8.1
240	7.85	426	7.55	260	7.98
255	7.81	436	7.48	280	8.14
271	7.82	456	7.58	295	8.05
292	7.66	470	7.68	309	8.06
313	7.78	485	7.62	324	7.99
490	7.60	500	7.60	486	7.66
495	7.55			491	7.55
500	7.55			496	7.53
505	7.55			501	7.48

A1-18: pH +CO$_2$ columns

| 30 d Sr/Cs +CO$_2$ | | 548 d Sr/Cs +CO$_2$ | | | | 548 d Sr +CO$_2$ | | 548 d Cs +CO$_2$ | |
| | | A | | B | | | | | |
Pore Volume	pH	Pore Volume	pH	Pore Volume	pH	Pore Volume	pH	Pore Volume	pH
5.3	7.61	5.4	9.72	5.0	9.17	5.0	9.68	4.2	9.41
10.5	7.46	10.7	9.14	10.0	8.98	10.1	9.05	8.6	8.95
15.8	7.36	16.1	8.9	15.0	8.47	15.1	8.76	12.6	8.78
21.1	7.56	21.4	8.48	20.0	8.42	20.2	8.57	18.9	8.43
42.2	7.35	26.8	8.59	40.0	8.14	25.2	8.4	23.8	8.35
47.4	7.56	32.1	8.43	45.0	8.13	30.3	8.43	28.6	8.48
52.7	7.31	37.5	8.36	50.0	7.94	35.3	8.33	33.4	8.25
211	7.44	42.8	8.3	200	7.57	40.4	8.31	38.1	8.16
242	7.41	48.2	8.28	230	7.57	45.4	8.26	42.9	8.01
264	7.53	53.5	8.29	250	7.74	50.5	8.23	47.7	7.8
300	7.4	58.9	8.12	275	7.6	55.5	8.13	52.4	7.75
474	7.65	64.2	8.07	450	7.64	60.6	7.9	215	7.8
501	7.51	69.6	7.98	475	7.62	242	7.87	229	7.74
527	7.47	268	7.81	515	7.55	252	7.71	238	7.75
543	7.51	278	7.81			262	7.73	248	7.81
		289	7.77			272	7.7	257	7.7
		300	7.73			283	7.64	429	7.6
		503	7.72			469	7.79	439	7.78
		514	7.79			484	7.86	453	7.75
		525	7.69			495	7.75	467	7.75
		535	7.68			505	7.64	486	7.65
								505	7.52

A1-19: Bromide curve and fit:

Data		Fit	
t (min)	Br (mg/l)	t (min)	Br (mg/l)
0.0	0.05	0	0.000
1.0	0.00	1	0.000
2.0	0.00	2	0.000
4.0	0.00	4	0.000
5.0	0.00	5	0.013
6.0	0.08	6	0.118
7.0	0.42	7	0.536
8.0	1.31	8	1.558
9.0	3.17	9	3.367
10.0	5.74	10	5.935
11.0	9.06	11	9.046
12.0	12.68	12	12.399
13.0	16.60	13	15.709
14.0	18.11	14	18.763
15.0	21.13	15	21.433
18.0	28.68	18	26.912
21.0	30.19	21	29.452
23.0	31.70	23	30.227
24.0	31.70	24	30.459
26.0	31.70	26	30.740
27.0	31.70	27	30.821
28.0	31.70	28	30.877
31.0	30.19	31	30.949
33.0	28.68	33	30.446
35.1	25.66	35	27.625
36.1	24.15	36	25.059
37.1	21.13	37	21.951
38.1	19.62	38	18.599
39.0	16.60	39	15.289
40.0	14.19	40	12.236
41.0	11.47	41	9.566
42.0	8.60	42	7.327
43.0	6.64	43	5.515
44.0	4.83	44	4.087
45.0	3.47	45	2.990
46.0	2.42	46	2.162
47.0	1.81	47	1.548
49.0	0.95	49	0.773
50.0	0.72	50	0.541
51.0	0.56	51	0.376
51.9	0.50	52	0.260
52.9	0.41	53	0.179
53.9	0.32	54	0.123
57.9	0.14	58	0.026
59.9	0.08	60	0.012
60.9	0.06	61	0.008
67.9	0.000	68	0.000
69.9	0.000	70	0.000
70.9	0.000	71	0.000
77.4	0.000	78	0.000

Appendix 2: STWL uptake Effluent column data

A2-1: 1 day

Pore Volume	Na	SD	K	SD	Al	SD	Si	SD	Sr	SD	Cs	SD
	mM		mM		mM		mM		μM		μM	
0.351	1.62	0.0579			0.00161	0.000132			1.46	0.459	0.00	0.00
1.23	32.3	0.743			0.00383	0.000148			57.5	0.696	0.00	0.00
1.40	134	19.9			0.000686	0.000172			141	23.0	0.00	0.00
1.75	790	53.5			0.00546	0.000425			492	65.3	0.00666	0.000675
2.11	3360	400			23.6	2.75			5.60	0.433	0.0200	0.00144
2.63	3390	288			44.3	3.77			2.19	0.0547	0.0178	0.000576
2.98	3510	327			49.2	4.53			1.97	0.268	0.0119	0.00171
4.39	3130	191			48.6	2.38			1.20	0.208	1.05	0.162
4.56	3830	560			57.6	8.53			1.38	0.101	2.46	0.210
5.26	3520	456			53.5	7.10			1.37	0.181	16.4	2.05
7.02	3650	74.8			60.3	2.04			1.24	0.0795	133	6.74
8.77	3390	495			57.3	9.55			2.17	0.0923	391	14.3
10.0	3260	399			53.7	6.64			6.82	0.397	530	29.3
10.5	3250	558			55.3	9.39			9.07	0.739	609	48.6
11.6	3460	201			57.6	3.44			20.2	1.16	837	45.4
11.8	3090	385			52.5	7.07			21.5	7.09	799	265

A2-2: 3 days

Pore Volume	Na	SD	K	SD	Al	SD	Si	SD	Sr	SD	Cs	SD
	mM		mM		mM		mM		μM		μM	
3.30	90.2	1.57					0.458	0.0361	187	2.06	4.59	0.111
3.90	1620	29.2					0.242	0.0636	75.7	0.583	1.07	0.0734
4.50	2150	14.2					16.5	0.0557	2.61	0.0550	1.12	0.0255
6.30	2190	21.5			45.7	0.345	12.4	0.101	0.963	0.00809	1.23	0.0263
8.10	2160	22.5			46.8	0.662	10.4	0.0877	0.881	0.0211	1.59	0.0221
9.90	2210	37.4			46.9	0.711	9.10	0.0771	0.862	0.00974	1.56	0.00342
15.9	2200	18.5			47.0	0.349	6.82	0.0772	0.845	0.00237	422	5.19
21.9	2240	10.8			47.5	0.256	5.58	0.107	0.907	0.0117	872	4.97
33.9	2210	34.0			47.3	0.720	4.21	0.0933	9.28	0.0612	1020	2.05
45.9	2250	41.6			47.7	0.782	3.18	0.0811	219	0.459	1060	4.23
51.9	2210	19.5			48.0	0.377	2.84	0.0456	283	0.708	1060	10.7
57.9	2210	12.1			48.7	0.341	2.53	0.137	315	2.61	1060	3.07
63.9	2240	35.9			48.7	0.918	2.35	0.123	326	2.93	1080	7.87
69.9	2210	15.3			48.5	0.411			318	2.45	1100	11.0
71.7	2220	11.8			48.4	0.426			318	3.05	1110	7.56

A2-3: 14 days

Pore Volume	Na	SD	K	SD	Al	SD	Si	SD	Sr	SD	Cs	SD
	mM		mM		mM		mM		μM		μM	
0.581	1.89	0.00363					0.550	0.00945	2.19	0.00221	1.84	0.0427
1.16	1.68	0.00337					0.641	0.00327	2.89	0.00188	1.21	0.0107
1.74	167	0.477					0.226	0.00695	264	0.114	0.816	0.0148
3.49	1830	2.76			22.7	0.457	9.79	0.00541	1.42	0.00212	0.894	0.0110
4.07	1860	1.09			45.5	0.429	20.2	0.0173	0.928	0.000575	0.930	0.00995
8.72	1850	1.34			47.6	0.367	13.8	0.0154	0.761	0.00104	0.954	0.00458
17.4	1870	1.92			44.2	0.386	5.88	0.0122	0.917	0.000871	513	5.95
29.1	1880	2.33			43.9	0.595	3.83	0.00868	18.2	0.0240	1080	9.10
40.7	1900	2.09			44.9	0.491	3.09	0.00807	233	0.474	1160	16.3
52.3	1890	2.75			45.3	0.684	3.17	0.0117	352	0.380	1200	9.39
58.1	2270	2.56			46.2	0.675	2.40	0.00894	325	0.0260	1130	21.2
63.9	1960	1.47			47.2	0.361	9.22	0.0119	52.6	0.0500	1240	9.71
69.7	1920	2.62			45.9	0.636	2.20	0.00826	287	0.0747	1140	16.4
75.6	1900	2.19			46.0	0.648			343	0.264	1210	11.7

A2-4: 1 month A

Pore Volume	Na mM	SD	K mM	SD	Al mM	SD	Si mM	SD	Sr µM	SD	Cs µM	SD
0.417					0.0349	0.000566			0.180	0.00202	0.00316	0.0000812
0.833					0.0662	0.00242			0.241	0.0982	0.00545	0.00174
1.25					0.0307	0.000298			1.39	0.00781	0.00161	0.0000511
1.67					0.0288	0.000262			103	3.59	0.0116	0.000998
2.08					0.133	0.00274			285	2.62	0.0143	0.000292
2.50					13.9	0.103			28.1	3.51	0.0412	0.00524
2.92					29.0	0.203			3.29	0.0582	0.0484	0.000256
5.00					47.2	0.802			0.826	0.0487	0.0552	0.00145
7.08					50.4	9.19			0.667	0.00680	0.0590	0.00191
9.17					78.2	6.80			0.967	0.0115	5.46	0.0655
11.3					56.6	0.763			0.792	0.00499	106	1.23
13.3					55.6	2.40			0.845	0.00819	269	2.37
15.4					99.1	1.10			0.868	0.0117	730	10.7
17.5					59.2	10.8			0.561	0.00634	599	7.49
19.6					56.9	0.529			1.19	0.208	872	94.2
21.7					57.8	4.04			3.48	0.832	791	163
23.8					63.3	7.15			15.2	0.144	1100	19.2
25.8					56.5	1.67			39.3	2.47	1090	62.6
27.9					64.9	2.04			83.6	2.32	1190	33.1
30.0					52.2	2.70			106	6.08	1000	51.3
32.1	1830	8.79			52.0	0.692			18.0	0.408	1080	6.79
34.2	2120	29.7			62.9	1.07			220	3.01	1240	13.4
38.3					77.2	24.3			296	5.30	1240	12.1
39.2	2650	22.8			63.6	0.458			335	11.1	1320	54.4

A2-5: 1 month B

Pore Volume	Na	SD	K	SD	Al	SD	Si	SD	Sr	SD	Cs	SD
	mM		mM		mM		mM		μM		μM	
0.559	0.441	0.0394							0.291	0.0111		
1.12	0.965	0.163							1.23	0.345		
1.68	77.4	6.06							94.2	0.763		
2.24	1020	46.5			0.0482	0.00675			179	14.6		
2.80	2050	141			23.9	1.59			2.34	0.0775	0.189	0.0153
5.59	2000	42.1			42.3	1.01			1.41	0.147	0.271	0.0709
11.2	2010	68.4			44.7	1.78			1.00	0.0791	129	5.16
16.8	2060	105			45.5	2.08			1.86	0.0358	516	3.05
22.4	2100	206			46.0	4.55			12.0	0.249	828	17.1
28.0	2070	72.2			45.8	2.08			49.3	5.63	926	106
33.6	2050	67.8			44.9	1.12			129	3.92	970	52.0
39.2	2070	131			45.5	2.16			204	2.49	939	16.1
44.7	2010	81.6			44.7	0.938			269	20.8	967	60.6
50.3	2040	181			45.3	4.42			352	14.9	1030	41.3
55.9	2180	142			49.3	3.27			435	3.57	1100	1.77
61.5	2050	42.7			47.2	1.09			441	6.62	1010	12.3
67.1	1940	14.3			43.9	0.768			411	24.2	900	46.5
72.7	1970	28.8			44.4	0.506			475	40.7	1030	91.8
75.5	1920	107			42.8	2.35			427	47.5	947	102

A2-6: 1 month C

Pore Volume	Na (mM)	SD	K (mM)	SD	Al (mM)	SD	Si (mM)	SD	Sr (μM)	SD	Cs (μM)	SD
0.573	2.06	0.268			0.0229	0.00866			0.300	0.00651	1.14	0.0622
2.86	1870	18.3			19.0	0.197			5.73	0.00802	0.0904	0.0295
3.44	1990	148			30.0	2.40			3.28	0.116	0.851	0.0455
4.58	1980	20.8			39.4	0.229			2.53	0.00177	34.5	0.0551
5.16	1960	24.1			39.8	0.633			2.96	0.0370	39.3	0.259
5.73	1930	50.6			40.7	0.899			4.60	0.0101	52.8	0.296
6.30	2030	71.9			44.0	1.53			8.57	0.0797	68.4	0.567
6.88	1980	6.34			44.0	0.127			13.5	0.0230	82.7	0.861
7.45	1950	17.5			43.9	0.233			18.7	0.0206	97.0	0.698
8.02	1960	13.5			43.9	0.338			23.4	0.256	111	0.801
8.59	1940	35.4			43.6	0.727			28.3	0.0764	130	1.67
9.17	1950	12.5			43.4	0.239			33.3	0.160	153	1.10
10.3	1950	8.99			43.7	0.284			42.1	0.164	200	0.621
11.5	1960	14.7			43.5	0.0305			54.7	0.284	255	1.07
17.2	1970	31.3			44.3	0.678			103	0.248	504	0.655
22.9	1960	8.04			44.3	0.146			151	0.952	730	5.77
28.6	1950	23.5			44.2	0.398			174	1.63	864	5.01
34.4	1960	30.5			44.9	0.547			187	1.57	936	3.84
40.1	1970	23.2			45.3	0.566			188	0.282	967	5.61
42.0	1960	14.5			45.1	0.464			186	0.501	974	6.04
42.8	1940	65.3			43.9	1.26			180	0.361	968	5.90
43.3	1980	17.7			44.5	0.352			122	0.207	939	3.85

A2-7: 3 months A

Pore Volume	Na	SD	K	SD	Al	SD	Si	SD	Sr	SD	Cs	SD
		mM		mM		mM		mM		µM		µM
0.417					0.00387	0.000503			0.497	0.0648	0.00216	0.0000781
0.833					0.00584	0.000144			0.713	0.00428	0.00279	0.000567
1.25					0.0180	0.00129			0.0148	0.00869	0.000848	0.0000653
1.67									250	12.2	0.0272	0.000936
2.08					5.23	0.0633			39.3	0.0905	0.0567	0.00100
2.50					39.3	5.76			6.95	1.14	0.106	0.0170
2.92					30.3	2.37			1.71	0.133	0.0508	0.00134
5.00					68.1	0.858			1.75	0.0265	0.0743	0.000460
7.08					54.5	4.06			1.24	0.171	0.0441	0.000736
9.17					55.4	0.964			0.684	0.0361	0.0634	0.00899
11.3	1250	5.48			55.1	0.237			0.642	0.0374	138	7.84
13.3					54.7	0.716			0.511	0.0177	455	14.3
15.4					54.7	1.72			0.484	0.0365	732	7.47
17.5					74.4	6.59			0.578	0.162	1140	29.2
19.6	1110	3.68			50.8	7.22			0.360	0.159	838	30.3
21.7					57.1	0.771			0.311	0.0182	1050	2.41
23.8					68.0	5.89			0.364	0.139	1130	74.3
25.8					55.3	7.07			0.197	0.140	1140	14.0
27.9					56.0	4.68			0.213	0.0991	1120	12.6
30.0					61.2	9.56			0.295	0.185	1200	119
32.1					53.6	3.18			1.54	0.116	1100	25.9
34.2					61.9	0.700			13.7	0.352	1350	63.4
36.3	1560	21.9			85.0	9.92			80.9	8.69	1760	27.7
38.3	1100	8.50			58.7	1.28			127	3.78	1270	8.26
39.2	1230	11.1			65.4	1.07			174	0.541	1370	12.9

A2-8: 3 months B

Pore Volume	Na	SD	K	SD	Al	SD	Si	SD	Sr	SD	Cs	SD
	mM		mM		mM		mM		μM		μM	
0.614	1.72	0.0417	0.197	0.0105	0.109	0.00400	1.00	0.0407	0.281	0.0128	0.364	0.0231
1.23	1.98	0.304	0.444	0.0202	0.0340	0.00484			0.627	0.0221		
1.84	170	16.4	2.84	0.264	0.0450	0.00180			247	9.23		
2.46	1800	137	3.09	0.227	9.41	0.750			19.4	1.39		
3.07	1800	74.8	37.6	1.17	28.5	0.928			1.61	0.0806		
3.68	1820	146	129	12.7	35.3	2.89			1.58	0.287		
4.30	1730	112	145	8.03	36.1	2.49			1.89	0.578		
4.91	1650	92.1	145	6.47	35.8	1.27			1.17	0.0697		
5.53	1680	127	147	14.2	36.1	3.25			1.13	0.107	0.938	0.330
6.14	1750	138	153	13.6	38.0	3.31			1.10	0.00701	7.61	1.24
9.82	1710	13.7	162	1.07	41.4	0.451	5.22	0.0642	1.09	0.0111	813	5.37
10.4	1820	27.5	169	0.847	43.7	0.582	6.01	0.321	0.967	0.0133	807	6.13
12.3	1690	112	150	7.86	37.8	2.02			1.05	0.0349	833	38.3
18.4	1770	68.5	156	6.70	40.9	1.59			1.06	0.0949	847	71.6
24.6	1710	36.0	153	2.59	39.7	1.10			1.42	0.0915	915	46.1
30.7	1920	81.3	183	7.66	45.4	2.01			50.5	0.904	1030	18.0
36.8	1860	169	179	12.2	44.5	3.55			203	9.67	1000	55.5
43.0	1660	95.7	158	6.48	39.8	1.81			304	3.28	832	26.1
49.1	1730	65.9	166	8.45	41.6	1.72			412	52.8	948	144
55.3	1820	49.6	173	8.20	43.9	1.83			459	17.9	975	61.1
61.4	1820	73.7	175	7.21	43.9	2.02			520	48.6	1130	113
67.5	1810	7.79	198	2.54	47.3	0.199	3.46	0.157	411	21.8	873	44.1
73.7	1810	91.0	178	6.79	43.4	2.41			465	35.5	1030	80.6
79.8	1710	7.52	188	0.695	44.8	0.300	2.97	0.172	382	11.6	838	34.7
82.9	1710	50.0	163	7.66	41.6	1.52			398	31.8	903	65.8

A2-9: 3 months C

Pore Volume	Na	SD	K	SD	Al	SD	Si	SD	Sr	SD	Cs	SD
	mM			mM		mM		mM		μM		μM
0.420	99.9	1.16	0.240	0.0291	0.0608	0.00147			3.83	0.269	3.20	0.0926
0.839	0.00	0.00	0.212	0.0177	0.0772	0.0134			2.71	0.254	1.88	0.0879
1.26	8.69	0.448	0.492	0.0324	0.0555	0.00987			3.02	34.9	8.12	0.152
1.68	288	10.9	2.56	0.116	0.0144	0.00365			5.26	312	14.0	0.0891
2.10	996	30.7	121	4.45	0.0328	0.0112			0.820	70.0	4.80	0.142
2.52	1180	28.3	475	9.79	20.7	0.478			8.40	5.75	14.7	0.166
2.94	1060	103	529	49.5	28.0	3.03			5.21	2.06	11.9	0.239
3.36	1090	45.3	575	24.3	34.1	1.34			2.60	1.56	1.03	0.429
3.78	982	50.0	533	35.8	34.4	2.61			0.870	1.12	2.62	1.87
4.20	1010	25.1	544	28.4	36.4	1.29			16.9	1.11	19.1	22.6
5.45	961	14.3	644	1.03	42.6	0.878			1.00	0.998	0.490	405
7.55	915	8.15	571	5.54	39.8	0.434			0.260	0.598	0.730	789
8.39	1030	50.4	578	26.6	42.5	1.87			20.6	0.739	17.4	856
12.6	1110	8.56	616	16.6	46.2	0.236			1.14	0.649	1.06	1070
16.8	1100	33.1	599	7.13	46.1	0.673			5.64	0.923	4.61	1070
21.0	1100	89.1	602	44.6	46.3	3.44			6.99	1.68	8.03	1050
27.3	911	31.3	556	16.2	41.4	1.22			0.840	16.9	0.870	886
29.4	1080	47.2	641	40.3	46.2	2.23			7.95	244	5.29	1070
33.6	1040	14.6	627	9.27	43.5	0.523			2.51	347	3.02	1040
35.2	1020	10.8	599	23.9	42.2	0.143			1.29	365	2.50	991
36.1	1010	35.2	592	17.9	40.9	2.23			1.65	330	3.36	1030
39.9	957	41.0	571	32.4	41.9	1.29			12.0	372	12.3	1020

A2-10: 3 months D

Pore Volume	Na	SD	K	SD	Al	SD	Si	SD	Sr	SD	Cs	SD
	mM		mM		mM		mM		µM		µM	
0.598	1.29	0.142	0.157	0.00445					0.533	0.0294	0.157	0.0172
1.20	4.57	0.151	0.224	0.00206					6.25	0.274	0.178	0.00484
1.79	75.0	3.34	0.913	0.0363					69.0	5.14	0.211	0.0261
2.39	1110	62.2	15.8	1.04					160	7.09	1.00	0.0478
2.99	1370	34.3	60.0	1.66	19.0	0.611			1.62	0.108	23.9	1.48
5.98	1780	60.0	165	7.24	40.1	1.83			3.10	0.0506	188	4.60
7.17	1790	75.4	177	8.30	44.6	1.79			6.47	0.0460	331	0.695
10.8	1770	23.2	169	3.62	41.5	0.651			51.6	0.443	612	35.6
15.5	1500	18.4	156	2.60	40.9	0.610			54.5	0.305	865	5.19
17.3	1840	13.2	181	0.542	45.1	0.352			77.0	0.708	989	4.25
17.9	1890	26.5	180	4.58	45.6	0.771			71.0	2.46	959	24.3
23.9	1900	136	180	12.6	45.4	2.29			130	8.73	907	45.1
24.5	1890	10.9	171	1.71	45.8	0.316			148	0.695	960	6.72
29.9	1820	34.6	190	2.67	45.1	0.252			218	9.16	984	55.4
35.9	1910	79.8	200	9.60	48.0	1.74			280	6.37	950	12.7
41.8	1800	47.4	187	5.40	45.3	1.26			338	5.45	993	9.23
47.8	1880	81.0	197	7.78	47.5	1.97			359	13.3	948	34.3
53.8	1830	20.8	188	8.84	46.9	0.455			419	3.06	1020	7.04
59.8	1840	72.3	190	8.53	45.9	1.88			443	8.69	1000	27.6
65.7	1780	25.2	191	5.60	45.7	0.462			460	1.01	983	2.46
71.7	1760	29.2	184	2.46	44.4	0.435			480	12.0	977	33.8
77.7	1790	66.9	185	4.12	45.5	1.30			473	13.5	949	27.8
80.7	1800	73.0	186	7.05	45.6	1.75			483	16.7	971	17.5

A2-11: 4 months

Pore Volume	Na	SD	K	SD	Al	SD	Si	SD	Sr	SD	Cs	SD
	mM			mM		mM		mM		μM		μM
0.573	0.748	0.0666	0.263	0.00766			0.935	0.0622	0.575	0.00310	0.432	0.00704
1.15	0.651	0.0449	0.270	0.00554			0.839	0.0651	0.472	0.00170	0.376	0.0123
1.72	41.7	2.58	1.43	0.00701			0.719	0.118	190	1.14	0.538	0.00688
2.29	763	7.08	4.31	0.0426			0.100	0.0823	203	0.935	0.869	0.0102
2.86	1180	9.35	302	6.22	13.2	0.0579	9.31	0.0873	2.45	0.0218	1.34	0.0255
7.45	986	17.7	565	9.15	38.9	0.638	4.55	0.0655	14.4	0.412	745	4.77
10.3	971	7.71	558	11.6	39.6	0.330	3.82	0.0415	2.97	0.0880	902	7.39
14.3	1000	14.1	564	4.23	40.3	0.361	3.34	0.0851	23.9	0.150	928	4.27
17.2	1020	21.0	572	7.21	40.5	0.634	3.01	0.0814	102	0.797	951	8.08
22.9	1010	17.2	573	9.57	40.1	0.729	2.72	0.0674	308	4.13	951	4.56
28.6	1000	8.56	567	11.5	39.9	0.360	2.50	0.0917	431	5.04	943	3.11

Appendix 3: Flushed sediment Effluent column data

A3-1: 3 days

Pore Volume	Mg	SD	Si	SD	Ca	SD	S	SD	Al	SD	Sr	SD	Cs	SD	Na	SD	K	SD
	µM		µM		µM		µM		µM		µM		µM		mM		mM	
0.423			20100	250	132	4.29	262	103	20100	315	46.5	0.670	806	5.48	1745	61.1		
2.12			7400	15.9	20.4	3.92	1600	33.8	8500	78.3	12.6	0.146	180	0.956	425	3.10		
4.23			956	23.7	50.4	3.10	1680	36.9	5740	51.3	5.98	0.0705	29.2	3.31	63.6	5.78	0.0492	0.00312
6.35			550	12.3	71.0	4.22	1830	87.9	5080	28.8	6.76	0.0911	18.4	0.256	40.7	0.814	0.0447	0.00248
8.47			420	13.3	31.6	3.98	1780	118	4210	75.8	5.26	0.120	14.8	0.227	32.1	0.209	0.045	0.0029
12.7			273	13.2	48.0	2.82	1760	111	2500	10.2	6.24	0.124	12.9	0.225	23.0	0.246	0.0436	0.00184
16.9			107	12.6	179	4.99	1800	59.2	958	25.4	63.6	0.500	23.2	0.186	12.4	0.0260	0.046	0.00282
25.4			67.0	5.10	3380	37.5	1920	104	415	5.86	388	3.62	42.3	0.432	4.50	0.0392	0.0491	0.0021
33.9			58.0	7.76	3980	46.0	1840	18.1	411	7.63	463	5.71	43.4	1.13	4.33	0.192	0.118	0.00126
42.3			69.7	14.7	3730	66.6	1940	43.8	456	5.65	429	2.10	47.8	0.377	4.30	0.0649	0.0883	0.0023
50.8			0.00	0.00	0.00	0.00	0.00	0.00	0.00	0.00	291	2.79	51.6	0.577				
55.0			0.00	0.00	0.00	0.00	0.00	0.00	0.00	0.00	257	0.875	53.3	0.181				
59.3			5.48	0.691	3160	54.3	1820	24.6	78.0	0.793	221	2.35	54.3	0.695	4.19	0.0344	0.264	0.00293
76.2			47.6	0.478	3630	70.7	1820	28.5	333	5.24	139	0.555	51.4	0.308	4.14	0.0902	0.369	0.00507
84.7	4.98	1.07	48.8	1.38	3560	11.3	1820	8.39	252	1.50	125	0.731	49.8	0.588	4.20	0.0315		0.00128
88.9	19.1	0.658	40.6	0.682	3680	37.5	1840	21.8	188	2.68	134	0.939	54.2	1.05	4.16	0.119	0.357	0.00372
110	294	1.94	57.8	2.14	3200	35.7	1830	15.8	38.2	0.593	115	0.765	52.1	0.188	4.18	0.0853		0.00533
131	590	7.52	83.8	2.21	2690	46.4	1830	12.0	12.0	0.493	70.7	0.588	49.6	0.134	4.11	0.0909		0.00919
152	724	5.91	86.0	0.771	2690	39.7	1840	8.54	8.56	0.621	47.6	0.714	35.6	0.221	4.14	0.1015		0.00678
174	872	5.62	96.6	1.69	3110	21.0	1980	27.3	8.60	0.791	41.2	0.372	27.5	0.132	4.48	0.0725	0.396	0.00121
195	819	5.41	84.5	0.725	2880	51.1	1840	13.6	7.24	0.419	32.1	0.507	20.2	0.0787	4.08	0.0453		0.00736
216	809	6.20	85.1	1.88	2800	45.7	1880	16.9	8.74	0.257	25.6	0.445	16.2	0.192	4.21	0.0902		0.0057
237	822	4.69	83.5	1.15	2820	36.6	1860	11.9	16.2	0.493	20.9	0.261	11.5	0.130	4.14	0.244		0.00499
258	858	3.72	78.0	0.721	2890	39.1	1880	15.6	7.80	0.494	18.6	0.233	9.81	0.0304	4.11	0.0599	0.351	0.00258
279	845	4.07	73.4	0.408	2900	14.2	1850	13.7	6.74	0.447	17.1	0.0725	7.81	0.120	4.15	0.0771		0.00329
293	782	5.63	87.1	1.47	2800	32.5	1860	16.2	5.81	0.516	20.4	0.205	8.20	0.0345	4.07	0.0330		0.00394
297	815	5.12	77.1	0.728	2870	45.1	1860	5.85	6.25	0.907	17.7	0.277	8.67	0.0104	4.45	0.210		0.00763
306	814	6.78	76.5	1.68	2860	27.2	1840	13.5	6.38	0.594	16.6	0.158	7.61	0.0685	4.10	0.0959		0.0059
310	829	4.65	74.5	1.29	2930	19.7	1860	24.8	6.53	0.676	16.8	0.115	7.61	0.0776	4.23	0.0406	0.399	0.00216
323	848	5.84	69.2	0.225	2860	49.4	1870	12.3	6.27	0.523	14.9	0.240	6.55	0.0249	4.02	0.0583	0.338	0.00472
335	871	8.97	68.7	1.27	2860	24.1	1850	27.8	7.54	0.853	13.3	0.0988	6.24	0.0568	4.34	0.0365	0.365	0.00218
361	856	2.59	64.2	0.526	2890	53.8	1890	17.5	6.04	0.665	11.7	0.203	5.51	0.0264	4.14	0.120	0.352	0.00538
386	862	7.95	63.8	0.725	2920	11.8	1870	25.2	6.56	0.340	12.7	0.0553	5.28	0.0396	4.26	0.0507	0.348	0.00137
399	862	5.08	60.1	0.944	2930	29.7	1880	25.7	6.71	0.951	14.4	0.146	4.81	0.0236	4.10	0.0357	0.342	0.00322
424	857	8.76	59.0	1.37	2880	24.0	1890	19.5	6.53	0.496	15.5	0.111	4.55	0.0246	4.24	0.0742	0.352	0.00248
450	860	10.1	52.0	1.36	2880	21.9	1900	10.2	6.68	0.921	14.9	0.116	4.10	0.0447	4.10	0.0529	0.333	0.00241
475	870	2.83	49.3	1.89	2900	33.8	1890	2.63	5.48	0.435	14.1	0.169	3.83	0.00920	4.18	0.0259	0.328	0.00263
500	863	3.17	48.6	0.761	2890	22.2	1890	20.7	5.55	0.777	13.1	0.0880	3.71	0.00631	4.19	0.0858		0.00296
526	859	10.0	46.2	1.44	2890	35.3	1890	36.1	6.10	0.196	12.2	0.141	3.57	0.0318	4.18	0.0685	0.34	0.00269

A3-2: 14 days

Pore Volume	Mg (µM)	SD	Si (µM)	SD	Ca (µM)	SD	S (µM)	SD	Al (µM)	SD	Sr (µM)	SD	Cs (µM)	SD	Na (mM)	SD	K (mM)	SD
0.432			23700	222	88.7	3.97	336	98.8	5050	40.6	31.2	0.279	867	13.3	1568	17.9		
2.16			14600	83.3	47.2	4.55	1270	61.3	2330	12.4	24.4	0.303	350	3.85	732	7.25		
4.32			1710	10.8	25.8	4.13	1690	27.3	2480	20.1	1.84	0.0440	25.5	1.18	69.0	6.82	0.0646	0.00207
6.48			483	3.89	50.4	4.84	1660	42.3	4170	55.5	1.15	0.0507	12.9	0.191	39.7	1.04		
8.65			366	4.50	22.4	2.88	1730	125	3750	52.2	0.854	0.0358	10.1	0.148	32.2	0.0676	0.0501	0.00184
13.0			247	17.2	22.2	2.61	1700	89.7	2410	27.2	1.10	0.0337	8.04	0.0804	22.7	0.64	0.049	0.0016
17.3			119	20.6	98.6	3.72	1840	109	1050	5.65	12.1	0.0530	9.10	0.146	13.7	0.0684	0.0505	0.00147
25.9			55.0	9.69	3260	43.4	1820	86.2	309	3.81	150	1.60	17.7	0.0637	4.53	0.0403	0.0556	0.00203
34.6			57.0	5.57	4020	17.5	1750	52.8	316	5.42	174	2.16	18.1	0.144	4.25	0.509		
43.2			56.6	7.12	3940	23.7	1810	61.2	341	4.16	167	2.01	19.9	0.157	4.10	0.0787	0.0729	0.00118
51.9											140	3.30	20.3	0.598	3.85	0.0573		
56.2											124	0.124	20.4	0.225				
60.5			23.3	1.00	3410	16.7	1780	11.7	267	1.87	116	1.00	21.4	0.145			0.184	0.00162
64.8											115	0.851	20.7	0.186				
69.2											110	1.53	21.4	0.186				
77.8	24.1	1.40	45.1	0.862	3550	59.6	1750	21.8	160	2.34	107	1.64	21.5	0.478	3.86	0.145		
86.5	73.1	1.34	37.6	1.65	3260	29.1	1770	16.2	62.4	1.13	101	1.32	22.1	0.224	3.85	0.120		
99.4	265	2.40	48.5	0.295	3080	16.5	1760	22.1	25.4	1.01	93.1	1.28	22.5	0.445	3.88	0.0190	0.32	0.00189
121	549	9.38	67.8	0.740	2850	44.9	1760	26.8	14.9	0.367	74.4	0.600	22.1	0.157	3.77	0.0245	0.328	0.00389
143	706	10.3	75.6	2.08	2790	32.3	1770	27.6	15.0	0.718	61.0	0.268	22.0	0.240	4.30	0.0903	0.331	0.00279
164	788	4.91	76.3	0.913	2760	24.7	1800	26.5	6.21	0.465	49.7	0.439	22.0	0.134	3.98	0.0327	0.324	0.00159
186	802	6.24	71.0	1.59	2790	12.8	1760	29.6	5.57	0.537	42.8	0.682	20.9	0.188	3.93	0.0555	0.325	0.00147
208	806	4.84	68.7	0.796	2770	26.3	1760	13.0	4.77	0.260	37.5	0.0712	20.1	0.141	3.92	0.0408		
229	818	7.39	64.7	2.68	2770	4.76	1760	33.9	22.1	0.411	34.5	0.0786	20.6	0.160	4.60	0.0469	0.329	0.000956
251	813	13.8	63.6	1.81	2750	40.9	1760	25.0	32.1	0.453	31.5	0.429	19.6	0.112	4.81	0.0250		
272	826	6.46	59.6	1.49	2810	31.3	1770	10.6	12.7	0.444	29.8	0.261	18.8	0.111	4.24	0.0543	0.332	0.00342
294	818	4.48	62.7	0.909	2770	15.6	1770	20.8	103	0.875	28.2	0.176	17.9	0.129				
316	825	2.06	53.9	1.28	2830	32.8	1760	28.0	4.68	0.385	27.2	0.281	16.9	0.0406	3.91	0.0336	0.332	0.00244
337	811	10.3	53.6	1.00	2760	22.7	1770	11.3	3.34	0.574	25.8	0.169	15.9	0.132	4.14	0.0927	0.389	0.00377
359	818	3.61	49.5	1.16	2780	64.1	1750	18.1	3.22	0.675	24.9	0.483	17.3	0.348	4.14	0.428	0.327	0.00658
386	868	3.39	48.5	1.85	2830	56.0	1770	19.8	4.42	0.451	24.0	0.151	14.3	0.338	4.33	0.142	0.362	0.00583
402	992	10.4	45.7	0.614	2860	42.5	1850	11.8	5.73	1.05	23.3	0.265	12.9	0.102				
417	869	4.18	44.4	1.67	2810	44.5	1780	22.8	4.23	0.838	22.3	0.204	12.5	0.125	4.14	0.00910	0.361	0.00383
431	834	6.58	45.5	0.696	2810	25.5	1760	22.4	4.42	0.473	22.2	0.201	12.4	0.0298	3.97	0.100	0.336	0.00254
444	830	6.36	43.0	1.62	2830	13.8	1770	19.0	3.62	0.703	21.6	0.108	11.6	0.0844	4.00	0.0964	0.329	0.00114
457	836	3.59	42.5	0.985	2760	34.4	1730	12.1	4.15	0.334	20.3	0.251	11.1	0.0844	3.98	0.0203	0.32	0.00268
470	827	17.1	43.1	0.483	2820	52.4	1780	28.2	4.56	0.629	20.4	0.344	11.3	0.125	4.00	0.0596	0.336	0.00463
509	829	21.5	42.2	0.952	2790	28.5	1740	16.6	4.31	0.308	18.7	0.150	12.0	0.144	4.10	0.0751	0.342	0.00219
522	837	6.31	40.7	0.898	2800	8.65	1770	21.1	3.67	1.06	17.9	0.0779	8.82	0.190	4.12	0.211	0.326	0.00038
544	826	5.22	40.9	1.48	2780	26.3	1740	13.6	2.87	0.410	17.1	0.131	8.38	0.0629	4.09	0.129		

A3-3: 1 month A

Pore Volume	Mg (uM)	SD	Si (uM)	SD	Ca (uM)	SD	S (uM)	SD	Al (uM)	SD	Sr (uM)	SD	Cs (uM)	SD	Na (mM)	SD	K (mM)	SD
0.433					67.3	0.950			4626	318	7.31	0.525	513	35.4	1460	126		
0.867			45271	536	79.1	1.15			2286	180	6.78	0.549	408	36.1	1040	80.3		
1.30			58578	823	79.1	1.15			2428	351	8.35	0.0393	551	2.48	1310	147		
1.73			22661	330	43.4	0.208	1406	176	1556	143	5.12	0.352	270	24.9	749	67.5		
2.17			20484	242	79.6	1.75	3230	385	884	59.6	2.16	0.106	92.9	4.22	261	21.0		
2.60			5420	43.8	46.1	1.28	1820	221	696	27.2	1.27	0.00607	39.8	0.199	98.0	2.89		
3.03			6322	89.5	73.7	1.81	3258	158	856	94.8	1.00	0.00852	26.7	0.109	65.1	6.03		
3.47			2398	34.7	53.3	1.62	1940	118	1195	44.3	1.18	0.0874	19.2	2.09	60.1	4.60		
3.90			2463	36.7	68.8	1.94	2360	163	1372	328	1.07	0.0950	16.6	1.72	48.3	12.4		
4.33			1300	14.9					1711	187	1.21	0.00398	18.2	0.156	45.7	5.52		
4.77			1373	22.0	99.8	1.41	2375	197	2065	107	1.52	0.0942	14.1	1.01	43.2	2.27		
5.20			1099	26.3	99.4	1.08	2529	136	2328	280	1.47	0.0295	13.2	0.341	40.4	4.70		
5.63			908	11.6	102	1.20	2278	78.1	2503	222	1.63	0.117	13.3	1.24	35.6	3.33		
6.07			801	7.12	113	1.46	2210	192	2514	160	1.63	0.116	13.0	2.24	32.6	2.43		
10.4			486	4.38	151	1.41	2240	38.1	1859	259	1.76	0.262	7.54	1.43	21.1	2.62		
14.7			294	32.1	216	12.1			952	45.3	2.06	0.0791	5.97	0.556	15.2	1.10		
19.1			243	14.7	222	7.14			422	22.8	7.02	0.366	6.38	0.843	12.1	0.646		
23.4			141	1.98	858	6.53	2067	18.2	147	15.8	25.3	0.482	6.60	0.102	9.30	1.11		
27.7			92.5	16.0	2660	86.1			119	5.14	69.7	3.39	12.1	0.840	6.66	0.501		
32.1			82.9	0.949	2955	48.6	1847	28.4	89	15.4	85.4	8.86	15.7	1.48	5.00	0.136		
36.4			102	6.41	3900	159			123	5.92	101	3.27	15.1	0.688	4.84	0.853		
40.7			103	1.82	3406	64.8	2114	37.1	101	4.29	120	8.47	13.9	2.68	4.99	0.292		
45.1									131	5.81	134	4.60	13.3	0.765	4.75	0.115		
49.4			117	0.786	3349	27.3	1834	30.0	129	11.1	147	16.4	12.4	0.814	4.70	0.407		
53.7			113	2.03	3641	46.5	2042	22.4	116	16.8	141	7.91	11.4	0.479	4.59	0.640		
58.1			52.3	0.404	3180	58.0	1824	22.3	33.3	2.47	145	9.10	11.6	0.740	4.54	0.248		
62.4	4.70	0.111	65.5	1.11	3196	36.5	1922	25.5	64.8	5.88	146	6.27	10.8	0.588	4.71	0.510		
66.7									83.0	4.74	150	6.16	12.0	0.741	4.66	0.217		
66.7	27.7	0.285	89.2	0.947	3389	21.3	1915	34.2	72.1	3.38	149	11.5	9.51	0.853	4.64	0.280		
71.1	67.3	1.23	108	2.46	4052	60.3	2406	33.3	58.0	7.71	126	7.30	9.83	0.562	4.23	0.559		
75.4	78.1	0.908	75.3	1.19	2757	32.8	1724	27.3	60.3	8.17	128	6.78	9.86	0.632	5.24	0.567		
79.7	164	4.72	110	2.88	3793	103	2206	19.4	45.9	5.40	121	6.51	9.05	0.246	4.68	0.448		
84.1	144	2.44	91.9	1.96	3095	60.3	1934	34.7	42.2	7.02	110	5.45	8.65	0.466	4.34	0.634		
84.8	177	1.16	93.5	1.08	2847	23.3	1908	31.2	34.0	4.02	126	13.8	9.18	1.21	4.54	0.538		
88.4	228	4.31	95.5	2.52	2930	56.5	1869	24.0	31.0	2.90	127	5.97	9.20	0.724	4.47	0.375		
92.7	299	5.45	104	2.09	3162	60.5	2114	27.6	25.2	0.519	119	2.45	9.73	1.12	4.37	0.170		
97.1	358	7.44	98.8	2.58	2912	50.2	1944	29.1	16.6	0.552	119	2.09	9.04	0.613	4.15	0.122		
101	457	2.66	108	0.698	2971	10.5	2067	61.2	14.4	0.509	112	3.63	8.89	0.484	4.09	0.160		
106	522	3.32	109	0.686	2689	15.9	1846	32.0	12.4	0.778	116	1.99	8.96	1.36	4.19	0.104		
110	597	9.33	112	1.99	2592	44.1	1879	67.5	10.0	1.24	109	9.13	7.06	0.919	4.31	0.347		
114	720	8.15	129	2.11	2761	33.8	2100	27.5	8.00	1.28	105	11.8	9.10	1.09	4.14	0.536		
119	706	11.5	126	1.96	2421	36.2	1870	70.6	7.03	0.151	88.2	1.40	7.69	0.132	4.35	0.262		
123	771	11.5	130	2.01	2462	39.0	1921	35.1	5.72	0.526	80.5	3.39	7.24	0.295	3.85	0.231		
127	835	19.5	136	3.42	2537	52.7	1968	29.4	5.09	0.143	93.3	5.32	7.49	0.517	4.13	0.126		
132	817	6.78	133	0.524	2363	21.1	1795	45.2	4.73	0.257	77.4	2.98	7.51	0.228	3.90	0.157		

175

140									4.18	0.631	77.3	3.74	8.26	0.450	3.79	0.445
136	869	12.3	146	3.18	2429	36.5	1851	17.5	4.30	0.645	74.8	8.57	7.70	1.08	4.00	0.513
149	902	14.4	150	2.38	2497	35.5	1933	41.3	4.06	0.506	66.0	2.54	7.23	0.359	3.90	0.418
153	920	12.2	154	2.71	2589	31.5	2077	24.9	4.77	0.259	70.9	3.29	8.01	0.817	3.77	0.193
158	878	7.84	144	1.71	2400	20.9	1918	28.3	3.85	0.329	73.8	5.90	7.51	0.456	4.08	0.247
162	997	19.6	163	4.05	2766	48.2	2250	54.6	3.94	0.409	64.8	4.51	8.18	0.440	3.73	0.294
166	879	16.3	144	3.29	2386	45.2	1887	51.0	3.88	0.922	58.6	1.93	7.26	0.222	4.05	0.670
171	899	13.9	140	3.00	2414	34.7	1880	14.2	3.53	0.326	57.3	1.29	7.23	0.281	3.94	0.451
175	909	22.4	142	3.55	2426	57.3	1867	32.4	3.74	0.633	52.6	1.05	7.08	0.112	4.11	0.546
179	895	4.03	138	1.28	2396	11.3	1863	17.7	3.21	0.195	60.1	5.14	7.52	1.66	3.81	0.418
184	961	10.1	144	2.05	2615	24.5	2043	24.5	3.45	0.301	54.3	1.22	8.11	0.187	3.55	0.392
186	928	9.40	138	1.24	2495	21.0	1917	33.8	3.51	0.360	58.0	2.51	7.13	0.770	3.92	0.375
192									3.51	0.448	56.2	3.62	6.81	0.611	3.77	0.250
197	969	7.44	141	1.18	2650	15.9	2079	42.3	3.19	0.067	47.2	0.94	7.23	0.517	3.40	0.134
201	956	14.9	137	2.83	2616	41.2	2042	24.5	3.27	0.291	42.8	2.08	7.19	0.339	3.89	0.333
205	977	11.9	139	2.09	2665	31.1	2047	14.7	3.29	0.197	41.7	2.74	7.46	0.451	3.72	0.235

A3-4: 1 month B

Pore Volume	Mg	SD	Si	SD	Ca	SD	S	SD	Al	SD	Sr	SD	Cs	SD	Na	SD	K	SD
		uM		uM		uM		uM		uM		uM		uM		mM		mM
0.437			36703	1740					1478	93.4	21.4	0.0470	583	4.67	1480	39.3		
2.19			23395	318					858	104	13.2	0.0965	291	2.82	787	14.2		
4.37			2688	34.9					1343	82.4	1.87	0.00094	22.1	0.210	73.6	0.743	0.0510	0.00124
6.56			686	9.95					2580	259	0.874	0.00306	9.35	0.0589	38.1	0.305	0.0358	0.000573
8.74			568	41.7					3452	328	1.03	0.00636	7.69	0.0384	35.4	1.50	0.0357	0.00110
10.9			400	12.6					2747	371	1.01	0.00614	5.56	0.0501	27.1	0.0704	0.0254	0.000730
13.1			263	3.71	32.5	1.63	1695	97.3	2089	18.2	1.17	0.00947	4.29	0.0206	23.2	0.225	0.0326	0.000416
26.2					2549	50.4	2461	233	257	11.6	86.7	4.32	4.90	0.431	5.45	0.335	0.0595	0.00138
39.3			44.8	1.91	3635	96.6	1837	210	199	2.81	135	0.392	5.61	0.0494	4.01	0.0165	0.0835	0.00272
52.5					3345	78.6	2357	59.2	67.0	11.9	123	12.3	7.05	1.49	4.05	0.598	0.0851	0.00283
65.6			28.5	0.364	3274	59.8	1707	29.7	148	9.53	125	8.09	7.74	0.709	3.87	0.235	0.154	0.00929
78.7	8.19	0.0763	46.8	0.785	3397	51.3	1965	86.9	128	9.20	124	8.77	8.71	1.24	3.90	0.254	0.223	0.0194
91.8	87.7	1.85	28.6	0.558	3317	73.8	1779	18.8	14.6	0.535	118	0.367	9.82	0.0226	3.86	0.0783	0.279	0.0305
105	206	3.96	52.7	0.477	2970	55.8			7.92	1.12	112	11.7	9.47	1.09	3.94	0.403	0.309	0.0373
118	356	2.16	59.9	0.617	2832	16.8	1716	27.7	5.92	0.373	106	3.43	9.25	1.10	3.86	0.204	0.311	0.0379
131	509	5.08	75.4	1.04	2867	25.7	1808	39.7	7.62	0.508	105	3.83	9.42	1.28	3.98	0.118	0.316	0.0390
144	657	18.5	84.9	0.137	2767	81.3	1799	39.7	5.92	0.327	98.6	0.789	9.26	0.0694	3.86	0.0602	0.303	0.0360
157	781	5.98	92.9	0.336	2720	24.6	1944	111	3.63	0.442	89.4	7.20	9.25	1.10	3.85	0.251	0.315	0.0388
170	838	15.3	95.7	2.62	2659	48.8	1754	28.6	3.16	0.280	80.3	3.39	8.34	0.415	3.98	0.182	0.321	0.0402
184	884	5.66	97.2	1.42	2675	20.4	1750	33.3	2.41	0.0647	77.4	0.991	8.93	0.096	3.83	0.0203	0.294	0.0338
197	831	11.9	91.9	1.81	2560	34.5	1686	30.5	4.16	0.212	66.9	2.47	9.20	0.560	3.86	0.155	0.310	0.0376
210	868	10.7	93.2	1.45	2641	31.0	1748	48.0	2.70	0.0629	63.6	2.61	8.67	0.739	3.89	0.126	0.309	0.0373
223	875	28.1	92.8	3.07	2700	83.5	1807	46.4	2.54	0.0117	61.7	0.296	9.16	0.0330	3.89	0.0393	0.296	0.0342
236	846	8.63	86.4	0.903	2672	22.7	1781	56.7	2.45	0.352	56.3	3.33	8.98	0.799	3.95	0.240	0.289	0.0326
249	898	6.50	92.8	2.63	2777	21.0	1846	42.3	2.34	0.0505	53.0	0.260	9.25	0.175	4.01	0.0453		
262	873	14.9	85.7	2.31	2707	48.3	1798	37.0	2.91	0.0783	49.7	0.144	9.56	0.117	3.99	0.106	0.302	0.0356
284	867	8.08	80.3	0.879	2755	30.3	1817	51.4	2.55	0.0441	43.8	0.118	9.41	0.0753	3.99	0.157	0.304	0.0361
306	869	8.53	78.2	0.816	2747	22.1	1858	28.7	2.78	0.0509	40.5	0.296	9.72	0.0729	3.91	0.0613	0.299	0.0349
328	869	17.3	72.3	0.429	2761	49.9	1834	25.7	3.19	0.328	36.6	0.527	9.67	0.0967	3.95	0.152	0.304	0.0362
350	873	8.79	69.7	1.08	2765	33.3	1868	36.8	2.76	0.0959	33.8	0.244	9.66	0.239	4.01	0.0237	0.318	0.0396
372	899	12.0	67.0	0.435	2893	45.2	1912	73.7	2.52	0.0979	30.4	0.380	9.83	0.0540	3.93	0.00787	0.312	0.0381
393	877	11.9	63.2	0.186	2779	39.0	1801	60.5	3.44	0.123	28.1	0.320	10.0	0.241	3.95	0.0533	0.318	0.0395
415	867	5.35	60.9	0.723	2741	18.5	1790	39.6	2.73	0.149	25.2	0.532	9.73	0.188	4.02	0.141		
437	869	9.67	57.6	0.368	2797	35.6	1818	28.5	3.25	0.0737	24.3	0.217	9.75	0.168	3.85	0.00732	0.310	0.0377
459	867	8.22	56.1	0.734	2735	24.7	1826	53.5	4.40	0.241	22.1	0.159	10.0	0.185	3.95	0.0928	0.317	0.0393
481	883	8.07	54.4	0.476	2801	21.9	1884	72.0	3.01	0.190	20.9	0.661	9.54	0.345	3.90	0.0897	0.317	0.0392
503	895	9.34	53.2	0.763	2822	32.4	1842	48.3	2.88	0.0688	19.9	0.197	10.0	0.0713	3.92	0.0333	0.332	0.0431

A3-5: 1 month C

Pore Volume	Mg (uM)	SD	Si (uM)	SD	Ca (uM)	SD	S (uM)	SD	Al (uM)	SD	Sr (uM)	SD	Cs (uM)	SD	Na (mM)	SD	K (mM)	SD
0.411			42883	493					3034	181	7.92	0.0547	650	3.58	1820	29.6		
0.823			40332	944					2382	119	8.34	0.0951	589	5.60	1630	40.2		
2.06			20418	237					1274	51.9	2.80	0.0106	220	1.54	615	9.17		
4.11			2478	50.3					1917	153	0.411	0.00152	19.0	0.190	60.3	0.857	0.0743	0.00151
6.17			1084	8.89					2408	118	0.357	0.00128	12.0	0.0516	38.3	0.123	0.0466	0.00141
8.23			871	42.1					2088	130	0.316	0.00297	9.00	0.198	29.1	0.352	0.0252	0.00126
12.3			375	6.45	23.9	1.66	1847	140	1273	90.4	1.74	0.0332	6.16	0.0616	19.3	1.25	0.0455	0.00550
39.1			97.5	2.50	3087	60.3	1645	165	127	2.15	32.0	0.141	8.97	0.0690	6.31	0.0208	0.114	0.00134
43.2			67.8	0.974	3450	63.7	2546	262	90.2	3.02	36.1	1.89	10.7	1.36	5.20	0.0930	0.168	0.00710
45.2			74.0	0.697	3477	75.7	2600	280	169	11.2	38.8	1.09	10.8	0.453	4.68	0.293	0.168	0.0115
57.6	33.6	0.358	83.8	1.08	3514	38.7	2188	112	55.8	2.88	43.2	1.75	13.3	0.705	4.34	0.250	0.136	0.00900
65.8	68.7	0.751	98.8	1.61	3355	52.4	1904	46.3	45.3	2.06	41.0	1.30	13.6	0.520	4.27	0.256	0.149	0.00583
66.0	68.5	0.837	96.9	1.54	3353	52.1	1815	38.3	44.5	2.01	43.0	1.84	15.4	1.87	4.43	0.226	0.153	0.00716
78.4	198	1.73	85.0	1.46	3338	31.6	1841	48.7	30.8	1.22	41.1	0.357	15.3	0.180	4.10	0.146	0.188	0.00811
91.3	254	2.36	79.0	1.03	3264	29.7	1804	22.0	25.6	1.54	40.5	2.25	14.8	0.660	4.04	0.222	0.210	0.0140
104	318	3.06	79.3	0.868	3250	26.4	1821	33.8	22.4	0.310	39.1	0.207	14.3	0.0573	3.94	0.0189	0.239	0.000884
117	367	2.77	81.3	0.205	3184	22.5	1879	23.6	18.2	1.30	38.1	1.83	14.4	0.585	4.00	0.284	0.266	0.0182
125	401	3.05	79.1	0.930	3124	26.2	1850	32.2	16.2	0.711	38.1	1.27	14.5	1.38	4.10	0.119	0.281	0.00755
133	404	4.40	88.4	1.77	2913	27.3	1816	33.8	13.6	0.775	35.0	0.200	13.1	0.0694	4.41	0.204	0.288	0.0146
141	455	10.2	84.2	1.62	2936	62.8	1857	43.8	10.2	0.927	34.0	1.42	12.0	0.430	4.04	0.280	0.285	0.0183
155	520	4.36	84.1	1.80	2950	24.7	1895	27.6	6.74	0.372	33.1	1.33	10.5	1.02	3.97	0.233	0.289	0.0135
169	535	8.62	79.7	1.02	3027	45.2	1812	42.6	6.45	0.365	36.4	1.51	10.7	0.792	3.97	0.245	0.299	0.0155
183	598	10.4	78.3	0.808	2963	51.4	1910	24.4	5.99	0.187	34.9	1.91	9.69	0.645	3.99	0.131	0.286	0.0142
197	637	14.7	80.3	1.12	3010	69.3	2000	47.2	5.60	0.721	36.4	2.24	9.86	0.784	3.95	0.308	0.293	0.0221
210	692	7.45	75.5	0.438	2858	31.0	1859	34.2	4.81	0.368	35.3	1.92	8.95	0.803	3.97	0.279	0.280	0.0197
224	744	5.62	73.4	0.896	2873	22.7	1824	15.0	4.53	0.039	34.7	0.372	8.49	0.649	3.86	0.0417	0.277	0.00307
252	767	8.70	68.0	0.383	2738	27.8	1759	20.1	4.27	0.256	31.4	1.36	7.31	0.621	3.91	0.198	0.258	0.00822
280	784	9.80	68.1	0.661	2756	34.8	1824	29.6	4.61	0.181	29.4	0.153	7.65	0.0130	3.83	0.0770	0.269	0.00427
308	788	4.55	64.6	0.461	2724	13.4	1872	23.1	4.17	0.843	24.4	2.23	6.71	0.671	3.79	0.214	0.269	0.0165
321	800	8.10	64.0	0.955	2777	25.4	1790	51.0	4.40	0.193	25.5	0.216	6.98	0.105	3.72	0.0729	0.276	0.00348
363	752	5.70	64.7	0.990	2671	19.7			3.89	0.612	21.4	1.12	6.34	0.286	3.81	0.384		
391	790	2.61	56.0	0.567	2761	12.7	1750	35.6	4.17	0.276	21.2	0.151	6.46	0.0297	3.72	0.0190	0.284	0.000653
419	858	9.12	58.1	0.697	2904	33.9	1925	40.2	4.56	0.854	19.3	2.07	6.35	0.721	3.87	0.524	0.291	0.0402
446	777	23.0	59.7	0.560	2729	77.0			4.23	0.506	17.2	0.682	5.83	0.160	3.97	0.372		
474	782	16.0	49.8	0.307	2667	54.4	1763	30.1	4.50	0.503	15.3	0.867	5.57	0.410	3.64	0.298	0.275	0.0197
488	838	20.7	52.2	1.25	2848	66.4	1905	40.6	4.53	0.310	16.4	1.10	6.09	0.702	3.94	0.374	0.344	0.0261
493	832	16.5	51.4	1.06	2815	47.3	1875	62.8	3.81	0.319	16.3	0.474	5.98	0.316	3.86	0.168		
495	828	7.64	49.2	0.803	2854	33.8	1889	63.7	3.88	0.0202	16.7	0.180	6.02	0.0211	3.87	0.0565	0.357	0.00300

A3-6: 3 month A

Pore Volume	Mg (uM)	SD	Si (uM)	SD	Ca (uM)	SD	S (uM)	SD	Al (uM)	SD	Sr (uM)	SD	Cs (uM)	SD	Na (mM)	SD	K (mM)	SD
0.412			114342	2128					1492	76.7	5.94	0.0374	494	4.00	2090	91.6		
0.824			127770	626					1559	37.1	5.42	0.0163	506	1.77	2120	47.4		
1.24			114642	919					1456	51.8	3.71	0.0256	437	1.97	1800	25.3		
1.65			65066	1543					877	4.03	1.76	0.0090	232	0.0232	962	14.6		
2.06			38719	1261					607	5.64	1.09	0.0212	132	0.185	551	4.91		
2.47			22214	203					325	61.1	0.780	0.104	59.7	7.15	333	4.73		
2.88			12539	591					220	11.3	0.838	0.0371	28.8	1.22	157	9.47		
3.30			34305	434					153	45.9			19.7	1.06	101	5.16		
3.71			6630	92.0					131	31.2			13.8	0.913	75.3	8.32		
4.12			5345	32.5					159	5.59	0.353	0.00385	14.2	0.0354	59.6	0.626		
4.53			4537	69.8					175	18.0			11.0	0.584	57.8	3.10		
4.95			3861	42.9					223	35.6			9.77	0.290	53.6	1.68		
5.36			3449	71.5					251	33.6			8.56	0.504	50.2	2.80	0.087	0.0325
5.77			3123	51.4					349	3.31	0.265	0.00755	9.47	0.0350	40.4	0.820	0.0316	0.0032
6.18			2622	18.5					349	9.40	0.277	0.00719	8.86	0.0673	38.0	0.388	0.0195	0.0182
8.24			2188	40.0									6.86	0.954	35.7	0.346		
16.5			1048	31.2					634	12.7	0.350	0.0119	4.78	0.00909	19.2	0.378	0.0206	0.0178
24.7			682	12.3					351	11.2	0.331	0.00357	3.74	0.0258	14.0	0.158		
33.0			322	10.7					91.1	1.62	5.55	0.0172	6.07	0.0279	9.95	0.0737	0.0077	0.002
41.2					1594	12.4					31.7	2.88	8.48	1.28	7.71	0.163		
49.5			203	3.05	2530	28.8	1930	166	53.7	6.19	56.9	1.89	11.0	0.491	4.59	0.309	0.0615	0.0051
57.7			176	3.36	2859	34.5	2099	64.7			68.9	2.03	11.0	0.467	3.96	0.177	0.0616	0.0045
65.9			147	0.353	2777	46.6	2144	243	38.2	3.92	73.6	1.84	11.0	0.370	3.67	0.203	0.0762	0.0069
74.2			147	1.45	2885	45.9	2262	153	50.3	7.69	80.4	3.46	12.1	0.701	3.78	0.354	0.136	0.0138
90.7			119	5.04	3080	70.4	2266	90.6	37.4	2.84	96.0	3.90	14.1	0.474	3.61	0.0733	0.227	0.0147
98.9			115	2.04	3011	30.8	2084	150	41.8	4.37	90.9	3.79	12.9	0.946	3.53	0.177	0.252	0.0191
107			105	2.16	2921	48.1	1874	170	36.3	3.36	87.0	1.20	11.3	0.478	3.28	0.216	0.253	0.019
115	17.7	0.514	103	1.84	2876	47.9	2050	119	33.1	2.57	91.2	4.32	11.6	0.584	3.15	0.294	0.253	0.0148
132	154	1.43	111	1.24	3242	40.8	2417	165	15.4	2.11	108.6	2.94	11.8	0.628	3.61	0.224	0.296	0.0184
140	267	5.99	123	1.55	3241	77.5	2408	324	7.66	1.15	103.2	5.52	10.7	0.864	3.62	0.0948	0.321	0.0231
148	369	2.02	136	1.76	3059	35.7	2314	105	6.94	0.984	101.8	4.94	10.5	0.546	3.91	0.0892	0.325	0.036
157	445	5.99	171	2.58	2869	38.3	2269	61.1	5.46	0.442	89.6	1.52	8.53	0.222	3.93	0.455		
165	517	9.95	197	4.43	2848	55.0	2264	7.40	4.06	0.651	86.4	1.42	8.99	0.330	3.91	0.316	0.327	0.0404
173	526	11.9	195	4.53	2607	62.9	2009	43.2	3.12	0.188	84.0	4.44	8.69	0.434	4.09	0.272	0.323	0.0221
181	571	2.72	195	1.00	2527	13.1	2029	39.1	2.27	0.141	73.6	3.22	7.51	0.282	3.96	0.558	0.298	0.0307
190	646	13.5	218	5.48	2608	52.0	2193	26.4	2.38	0.389	80.3	9.18	7.74	1.09	4.16	0.0242	0.29	0.0028
198	687	8.06	223	2.29	2584	22.3	2179	20.6	1.79	0.270	75.3	4.90	8.26	1.37	4.34	0.118	0.3	0.006
206	719	11.8	231	4.03	2609	39.2	2178	31.7	2.37	0.329	70.9	1.71	8.11	0.351	4.03	0.411	0.347	0.0221
214	759	11.7	228	4.47	2620	33.4	2098	45.9	1.47	0.256	64.8	1.85	7.23	0.252	4.12	0.337	0.322	0.0379
227	783	12.2	223	3.72	2512	46.1	2113	16.9	1.37	0.156	60.6	2.69	7.02	0.385	4.07	0.270	0.326	0.0312
239	867	11.9	241	4.30	2640	35.3	2042	29.4	1.17	0.148	55.9	2.33	7.30	0.711	3.99	0.358	0.322	0.0125
251	777	11.2	227	4.17	2392	35.5	2112	37.2	2.19	0.126	49.4	2.17	6.49	0.281	4.00	0.320	0.322	0.0218
264	860	15.2	249	4.51	2621	43.1	2263	59.6	1.28	0.427	48.4	1.42	6.50	0.203	4.13	0.288	0.313	0.0251
276	775	13.8	219	3.81	2363	40.9	2073	28.4	1.21	0.452	45.9	1.09	6.49	0.234	3.98	0.235	0.354	0.0525
288	903	30.9	245	9.13	2648	81.7	2297	55.8	1.17	0.207	40.9	2.02	5.95	0.241	4.32	0.378	0.315	0.0102

301	831	4.63	209	1.53	2344	10.1	2058	19.4	1.50	0.221	40.0	1.94	5.87	0.400	4.52	0.0899	0.302	0.0032
313	935	16.5	227	3.53	2548	47.1	2231	55.8	1.28	0.386	38.4	2.67	6.07	0.414	4.43	0.0611	0.301	0.003
325	868	7.54	204	2.49	2339	17.4	2126	21.3	1.32	0.333	36.0	0.831	5.76	0.150	4.21	0.193	0.318	0.0227
338	989	13.5	216	3.01	2582	31.5	2217	26.8	1.74	0.457	37.0	4.83	5.84	0.788	4.51	0.114	0.313	0.0041
350	945	20.3	198	5.00	2439	43.8	2112	35.2	1.55	0.277	33.3	2.30	5.51	0.341	4.19	0.310	0.330	0.0267
363	913	16.5	197	4.21	2376	43.8	2071	33.5	1.81	0.151	32.9	1.57	5.14	0.249	4.01	0.513	0.344	0.0178
375	912	10.5	191	2.18	2423	23.3	2081	12.3	1.68	0.461	29.9	2.79	5.16	0.577	4.47	0.0554	0.309	0.0012
387	886	10.9	180	3.00	2390	26.3	2100	64.9	1.89	0.260	29.6	0.623	5.34	0.102	4.17	0.168	0.358	0.0435
408	1080	32.0	172	5.88	2944	83.6	2169	44.8	1.55	0.246	32.2	1.29	5.25	0.316	4.24	0.505	0.352	0.0424
420	1053	17.4	169	3.60	2879	47.5	2162	24.0	1.42	0.303	30.6	1.76	5.27	0.339	4.46	0.536	0.346	0.0415
433	1057	13.0	186	1.55	3013	34.0	2315	67.7	6.57	0.427	29.7	2.22	5.82	0.954	5.00	0.0565	0.335	0.0066
449	962	9.67	184	2.09	3105	35.0	2191	51.9	1.96	0.122	28.1	0.861	5.93	0.406	4.55	0.487		
461	836	78.6			2900	312			1.89	0.253	25.9	2.42	7.21	1.06	4.35	0.252	0.329	0.0291
482	835	27.7	179	21.8	2930	65.0			2.08	0.129	24.7	0.695	5.35	0.195	4.29	0.382	0.326	0.0136
494	824	48.7	150	20.8	2920	142			2.05	0.179	24.5	1.73	5.35	0.453	4.26	0.111	0.312	0.0224
507	839	42.1			3070	258			2.16	0.098	22.2	1.09	4.91	0.343	4.23	0.233	0.32	0.0168
527	977	34.8	214	31.5	3530	36.4			2.46	0.196	19.8	0.490	5.16	0.270	4.77	0.186		
540	997	37.2	268	48.6	3710	247			2.57	0.173	18.8	0.458	4.76	0.171	4.55	0.0982	0.316	0.0039
552	983	15.2	237	34.0	3520	80.5			2.43	0.179	18.1	0.150	4.75	0.0641	4.27	0.0568		

A3-7: 3 month B

Pore Volume	Mg uM	SD	Si uM	SD	Ca uM	SD	S uM	SD	Al uM	SD	Sr uM	SD	Cs uM	SD	Na mM	SD	K mM	SD
0.434			40934	311					414	4.96	6.82	0.0689	404	3.35	1270	9.01	111	1.26
0.868									598	4.18	4.81	0.0212	513	2.10	1700	7.31	147	0.575
1.30									519	6.13	4.87	0.0156	464	6.68	1520	16.2	132	0.727
1.74									269	6.19	2.18	0.0331	226	1.60	720	8.93	68.4	0.684
2.17			23561	426					167	8.35	1.07	0.00703	121	0.399	388	18.4	39.0	1.72
2.60									140	8.94	0.537	0.00623	57.2	0.400	185	11.5	20.4	1.27
3.04									133	0.467	0.371	0.00663	27.7	0.022	87.7	0.377	10.4	0.0574
3.47									155	1.61	0.298	0.00226	21.3	0.051	67.9	0.387	8.27	0.0620
3.90									186	3.62	0.208	0.00251	17.1	0.140	54.4	0.511	6.65	0.0785
4.34			3244	51.9					225	1.66	0.171	0.000206	14.8	0.165	47.9	0.426	5.95	0.0393
6.51			1349	9.17					541	2.71	0.138	0.000386	9.29	0.0789	31.5	0.223	4.24	0.0174
8.68			764	22.2					766	25.6	0.170	0.00133	6.37	0.0102	21.8	0.751	3.37	0.119
21.7			159	3.01	40.1	0.570	2401	474	308	7.20	1.25	0.00828	7.73	0.0340	4.36	0.120	8.73	0.113
34.7			83.9	2.72	2434	43.9	2377	100	151	2.18	20.7	0.0951	6.34	0.0393	3.94	0.0304	3.50	0.0410
47.7			75.3	1.75	3153	47.1	2597	348	149	1.59	29.5	0.0649	5.60	0.0358	3.93	0.0522	2.22	0.0226
60.7			86.0	2.69	2945	30.1	1964	335	156	0.811	29.8	0.2472	4.83	0.00869	3.69	0.00887	1.54	0.00615
73.8			61.3	1.08	3045	45.2	1869	87.1	149	1.07	29.7	0.199	4.24	0.0119	3.64	0.0258	1.07	0.0133
86.8			66.3	0.438	3473	38.4	2047	50.8	154	1.51	35.6	0.0961	4.00	0.0352	3.67	0.0275	0.798	0.00894
99.8	10.7	0.0980	57.0	0.668	3335	36.3	2111	35.3	117	5.50	36.7	0.151	3.85	0.0177	3.93	0.188	0.643	0.0280
113	66.6	0.988	60.5	0.745	3264	40.9	2054	58.5	67.8	0.630	38.9	0.292	3.64	0.0247	3.72	0.0175	0.515	0.00545
126	197	2.99	75.5	0.829	3247	41.6	1903	50.2	34.3	0.295	40.5	0.158	3.59	0.0301	3.79	0.0367	0.739	0.00886
130	251	4.91	78.3	0.358	3210	49.3	1884	63.5	21.3	0.773	41.0	0.172	3.67	0.0235	3.81	0.0328	0.453	0.00381
152	470	8.52	103	1.78	2950	44.9	2000	68.7	8.29	0.141	38.7	0.197	3.48	0.0327	3.71	0.0694	0.381	0.00530
174	604	13.5	119	2.31	2815	62.9	1991	36.1	4.21	0.0590	37.2	0.115	3.45	0.0097	3.73	0.0440	0.426	0.00272
195	687	12.3	128	2.84	2750	44.8	2071	57.5	2.84	0.139	35.6	0.114	3.55	0.0408	3.78	0.0771	0.344	0.00771
217	780	8.98	137	2.16	2903	32.5	1912	43.0	3.23	0.146	34.6	0.145	3.55	0.0124	3.79	0.0144	0.337	0.00226
234	759	19.9	129	5.31	2762	85.1	1901	68.2	16.8	0.445	33.8	0.112	3.56	0.0292	3.73	0.0295	0.330	0.00416
260	706	13.8	112	3.17	2543	49.4	1863	6.0	2.66	0.0766	32.1	0.151	3.61	0.0112	3.78	0.0624	0.329	0.00503
286	769	11.3	114	2.08	2727	41.1	1971	46.7	2.47	0.225	29.8	0.245	3.68	0.0199	3.67	0.0385	0.320	0.00266
312	782	7.45	107	0.780	2778	21.9	2026	33.2	2.53	0.038	28.8	0.320	3.70	0.0144	3.70	0.0540	0.318	0.00239
338	795	20.0	112	3.17	2751	63.3			2.69	0.343	27.0	0.457	3.86	0.0559	3.74	0.192	0.419	0.0203
340	758	15.7	103	2.78	2665	52.9	1825	116	2.28	0.146	27.3	0.0955	3.73	0.0160	3.72	0.0186	0.593	0.00403
343	755	11.4	106	1.41	2673	42.9	1901	74.1	2.86	0.0684	27.3	0.551	3.76	0.0782	3.69	0.107	0.323	0.00845
345	757	15.6	103	2.03	2684	57.8	1934	48.6	2.53	0.0465	27.0	0.221	3.72	0.0391	3.68	0.0817	0.315	0.00580
347	770	4.28	106	0.461	2733	9.7	1939	20.6	2.52	0.173	27.1	0.133	3.72	0.0264	3.69	0.0428	0.314	0.00304
349	772	20.8	108	3.11	2725	71.4	1870	45.6	2.89	0.132	27.2	0.160	3.77	0.0445	3.74	0.0527	0.318	0.00274
351	767	6.40	108	1.15	2720	25.1	1873	56.5	2.57	0.053	26.9	0.153	3.78	0.0397	3.74	0.0225	0.317	0.000825
353	707	7.53	99	1.11	2518	25.7	1827	75.1	2.45	0.138	25.2	0.187	3.54	0.0198	3.48	0.00836	0.299	0.00263
355	741	9.79	103	1.54	2645	36.1	1885	30.9	2.99	0.140	27.2	0.206	3.88	0.0035	3.80	0.0300	0.327	0.00278
357	758	9.13	108	2.47	2726	39.1	2046	79.0	2.67	0.202	27.3	0.0656	3.88	0.0190	3.80	0.0406	0.415	0.00456
358	785	12.2	109	1.60	2783	51.3	1855	22.6	2.91	0.205	26.9	0.156	3.94	0.00157	3.75	0.0184	0.326	0.00277
364	778	26.9	118	1.12	2732	88.9			2.47	0.0947	25.3	0.332	3.74	0.187	3.54	0.0541	0.306	0.00766
364	758	8.82	104	1.96	2698	32.0	2004	35.3	2.64	0.235	27.1	0.149	3.87	0.0286	3.80	0.0141	0.325	0.00234
370	765	11.2	108	1.34	2672	41.4			11.2	0.457	27.1	0.146	3.92	0.0251	3.93	0.0719	0.334	0.00391
370	780	15.2	101	1.10	2741	49.3	1949	67.3	11.0	0.337	27.1	0.323	3.94	0.0193	3.90	0.0273	0.333	0.00422

376	776	12.2	108	0.693	2690	43.7	1780	51.6	3.24	0.127	24.6	0.150	3.93	0.00668	3.47	0.106	0.312	0.00786
395	782	14.1	104	1.70	2726	52.1	1815	31.5	2.68	0.0844	24.0	0.0648	3.92	0.0227	3.54	0.0481	0.312	0.00178
402	787	9.1	102	1.13	2716	24.4	1765	43.7			25.4	0.325	4.11	0.0354				
414	742	16.4	104	0.578	2610	55.6					24.2	0.00966	4.07	0.0310				
421									4.30	0.378	23.2	0.223	4.05	0.0506	3.69	0.264	0.329	0.0253
440	773	10.8	94.1	0.947	2669	42.2	1817	39.3	2.51	0.0929	22.1	0.0176	4.09	0.0360	3.51	0.0615	0.308	0.00447
459	824	11.7	92.2	0.676	2820	33.2	1885	40.8	2.82	0.0350	21.4	0.340	4.01	0.0597	3.50	0.0399	0.304	0.00295
484	823	17.2	88.6	1.41	2748	57.8	1820	29.4	2.68	0.0983	20.3	0.235	4.10	0.0352	3.62	0.0644	0.314	0.00653
496	836	14.5	88.3	1.33	2833	50.2	1831	60.0	2.69	0.140	18.8	0.465	3.86	0.107	3.66	0.209	0.425	0.0228
498	822	9.68	83.7	0.749	2755	33.6	1793	51.2	2.72	0.123	19.8	0.503	4.03	0.0948	3.60	0.111	0.434	0.0135
501	837	6.71	83.7	1.48	2785	26.1	1809	22.1	2.95	0.181	20.5	0.550	4.35	0.112	3.80	0.193	0.331	0.0160
517	822	20.6	75.5	0.346	2760	70.5	1941	39.7	4.75	0.0864	19.4	0.0911	4.32	0.000432	3.63	0.0922	0.315	0.00931
530	814	10.5	70.8	0.682	2726	41.3	1810	45.6	2.81	0.0691	19.0	0.126	4.37	0.0206	3.77	0.0551	0.332	0.00571

A3-8: 3 month C

Pore Volume	Mg	SD	Si	SD	Ca	SD	S	SD	Al	SD	Sr	SD	Cs	SD	Na	SD	K	SD
	uM		uM		uM		uM		uM		uM		uM		mM		mM	
0.432			47391	294					1525	16.5	9.18	0.0330	851	4.85	1480	2.82	111	1.26
2.59			7864	82.6					162	5.03	0.802	0.00409	41	0.284	52.2	1.39	147	0.575
4.75			2973	31.2					83.0	4.04	0.362	0.00409	13	0.00392	16.6	0.266	132	0.727
5.61			2401	107					74.0	2.72	0.372	0.0139	11	0.650	13.9	0.328	68.4	0.684
7.77			2052	18.4					63.3	4.33	0.473	0.0118	9.26	0.925	11.2	0.0618	39.0	1.72
12.1			1265	20.9			3119	304	54.8	0.949	0.802	0.0161	8.72	0.732	6.50	0.0987	20.4	1.27
20.7			732	5.36			2806	460	36.1	0.948	1.43	0.0139	6.89	0.670	5.56	0.0694	10.4	0.0574
33.7	8.30	0.818	374	6.83	337	9.48	1728	226	47.2	1.94	7.57	0.0810	6.44	0.409	4.88	0.130	8.27	0.062
46.6			219	6.03	1932	28.3	3886	763	27.3	0.899	52.4	0.514	5.50	0.530	4.02	0.0539	6.65	0.0785
63.9			145	5.59	2485	77.7	2192	293	25.6	0.920	76.0	0.539	5.44	0.430	4.16	0.0678	5.95	0.0393
76.9			171	1.78	2862	26.3	1995	84.4	19.3	0.193	67.3	0.377	5.39	0.0291	4.02	0.0165	4.24	0.0174
89.8	25.9	0.167	140	3.49	3227	48.3	1987	39.0	15.2	1.20	65.7	0.571	5.41	0.0346	4.37	0.335	3.37	0.119
103	264	1.88	119	1.81	3018	20.9	1844	53.2	7.36	0.382	64.5	1.06	4.94	0.0702	4.16	0.0619		
116	452	5.18	113	1.90	2929	29.8	1863	21.9	4.53	0.173	56.5	0.175	4.73	0.0430	4.10	0.0439	3.50	0.041
133	592	18.3	114	3.44	2840	90.1	1970	38.8	3.06	0.117	49.2	0.359	4.79	0.0589	4.12	0.0395	2.22	0.0226
146	699	14.8	112	3.19	2786	50.2	1834	26.2	2.11	0.132	45.0	0.310	4.56	0.0934	4.08	0.0603	1.54	0.00615
159	722	16.2	113	3.57	2848	63.4	2017	78.7	1.94	0.096	41.1	0.148	4.52	0.0790	4.09	0.0888	1.07	0.0133
172	747	7.70	114	1.12	2856	26.9	1980	54.4	1.81	0.119	37.8	0.363	4.47	0.0942	4.06	0.0475	0.798	0.00894
185	786	8.67	116	5.05	2834	26.5	1840	76.9	1.82	0.0638	35.4	0.088	4.48	0.0609	4.12	0.0260	0.643	0.028
198	774	12.7	107	2.30	2779	47.0	1780	35.8	1.63	0.142	32.4	0.175	4.55	0.0856	4.08	0.0425	0.515	0.00545
211	819	13.1	107	2.63	2792	45.6	1889	80.2	3.68	0.148	30.4	0.158	4.57	0.00914	4.13	0.0343	0.739	0.00886
224	789	9.37	99.4	1.63	2671	30.2	1750	48.4	1.57	0.0641	27.6	0.0772	4.50	0.0910	3.94	0.0335	0.453	0.00381
237	822	13.8	96.2	2.58	2776	49.1	1825	39.7	1.66	0.258	25.9	0.349	4.59	0.0951	4.18	0.161	0.381	0.0053
250	804	11.0	90.9	2.31	2802	37.5	1731	23.4	1.88	0.132	25.3	0.117	4.84	0.0305	4.20	0.109	0.426	0.00272
263	830	14.6	93.4	2.44	2831	48.7	1844	33.5	2.65	0.230	24.3	0.126	4.84	0.0286	4.13	0.0347	0.344	0.00771
288	802	8.63	85.6	0.987	2745	28.2	1845	49.5	1.92	0.0980	22.1	0.168	4.93	0.164	4.07	0.0387	0.337	0.00226
314	811	14.8	88.5	0.23	2871	56.1	1992	55.7	4.55	0.202	20.4	0.198	5.00	0.0655	4.07	0.112	0.33	0.00416
340	842	6.42	79.6	1.58	2861	22.4	1880	50.2	2.01	0.229	20.1	0.085	5.50	0.0330	4.14	0.0414	0.329	0.00503
366	815	15.8	69.2	0.509	2819	43.2	1782	47.1	2.07	0.169	18.3	0.0950	5.33	0.0944	4.02	0.0386	0.32	0.00266
392	853	15.1	64.9	0.0790	2838	52.6	1891	16.9	2.72	0.216	16.9	0.142	5.07	0.0598	4.12	0.0276	0.318	0.00239
418	858	23.3	62.4	0.827	2846	73.2	1831	20.7	2.57	0.00898	15.8	0.119	5.03	0.0256	4.12	0.0679		
445	819	10.7	57.5	0.749	2835	35.5	1939	27.7	6.63	0.402	14.9	0.0895	4.76	0.162	4.07	0.0749		
470	807	12.7	54.6	1.06	2760	41.3	1741	40.0	2.29	0.179	14.4	0.0793	4.74	0.0166	4.06	0.0361	0.323	0.00845
496	815	14.6	54.1	0.568	2833	52.6	1946	22.7	2.38	0.132	13.7	0.0807	4.47	0.0479	4.09	0.0703	0.315	0.0058
506	762	11.7	49.4	0.526	2665	41.1	2131	78.1	2.20	0.0865	13.5	0.110	4.35	0.0196	4.08	0.0566	0.314	0.00304

A3-9: 3 month D

Pore Volume	Mg	SD	Si	SD	Ca	SD	S	SD	Al	SD	Sr	SD	Cs	SD	Na	SD	K	SD
		uM		uM		uM		uM		uM		uM		uM		mM		mM
0.438			42217	317					892	22.9	7.55	0.0483	486	3.01	1340	21.2	117	1.88
2.19			21713	135					363	4.50	0.550	0.00797	146	0.888	391	4.42	38.5	0.374
4.38			2275	20.9					308	1.29	0.0929	0.000585	9.94	0.0497	28.3	0.198	3.72	0.0253
8.76			815	9.7					836	9.7	0.199	0.00143	6.66	0.0386	19.9	0.119	3.29	0.00824
13.1			431	3.10	69.9	1.70	2551	139	537	5.75	0.827	0.0164	6.78	0.671	12.7	0.0940	6.76	0.143
17.5			233	2.52	149	1.90	2486	281	309	10.9	1.98	0.0567	7.41	0.749	7.58	0.0394	6.63	0.0219
30.7			122	1.42	1962	44.3	2520	207	186	1.53	21.0	0.103	7.30	0.107	4.67	0.0290	4.50	0.0468
43.8			148	7.50	4330	24.8	3426	327	243	4.89	53.4	0.497	10.4	0.101	6.77	0.0223	5.19	0.0565
52.6			101	2.25	3470	51.1	4936	104	452	7.78	39.3	0.181	5.96	0.322	8.09	0.153	2.92	0.00731
78.8			58.4	2.62	3176	94.1	2409	169	78.6	1.92	46.0	1.31	5.24	0.294	4.11	0.0736	1.26	0.0215
92.0	58.2	0.342	85.9	0.689	3401	23.2	1752	49.4	48.7	1.65	43.4	0.130	3.92	0.0309	3.82	0.104	0.887	0.0239
105	141	1.55	87.6	0.777	3175	41.9	1790	26.3	32.7	0.981	44.2	0.234	3.73	0.00931	3.78	0.0605	0.678	0.0108
118	238	2.22	93.5	0	3222	30.1	1830	53.8	23.6	0.163	44.3	0.270	3.52	0.0331	3.80	0.0216	0.635	0.00273
131	324	8.10	97.3	3.45	3072	76.4	1802	17.6	19.1	0.336	43.8	0.306	3.50	0.0189	3.87	0.0174	0.607	0.000667
145	428	6.77	108	2.39	3086	47.7	1800	21.8	14.3	0.147	42.9	0.180	3.48	0.0031	3.73	0.0288	0.451	0.00230
158	503	5.63	114	1.68	2979	27.7	1839	49.6	11.9	0.412	40.9	0.197	3.33	0.0467	3.77	0.0864	0.415	0.00881
171	532	3.88	114	1.00	2885	23.9	1785	31.6	8.60	0.351	40.1	0.092	3.48	0.0403	3.67	0.0524	0.391	0.00708
184	583	9.29	116	1.68	2887	47.5	1855	75.4	7.07	0.276	39.3	0.259	3.44	0.0255	3.73	0.0190	0.368	0.00269
197	626	5.85	126	2.28	2897	26.6	1786	33.0	8.94	0.128	37.8	0.359	3.44	0.0333	3.65	0.0307	0.349	0.00265
210	645	10.7	132	3.18	2841	50.9	1812	56.1	5.43	0.243	35.9	0.309	3.50	0.0231	3.83	0.0541		
221	646	7.24	115	1.26	2838	31.2	1729	12.1	4.59	0.360	36.7	0.693	3.59	0.0190	3.79	0.0636	0.353	0.0041
234	693	11.6	116	2.72	2870	47.4	1834	23.5	3.99	0.058	35.0	0.245	3.45	0.0221	3.69	0.0476	0.334	0.00475
260	720	6.57	112	1.47	2792	25.6			3.06	0.121	32.1	0.0803	3.42	0.00890	3.69	0.0306		
286	751	15.4	113	2.39	2891	60.1	1964	79.3	3.12	0.0723	30.4	0.155	3.60	0.0314	3.79	0.0459	0.332	0.00517
313	794	15.2	111	2.70	2875	50.4	1807	57.1	3.09	0.340	28.0	0.0559	3.59	0.0104	3.66	0.0773	0.316	0.00404
326	775	16.8	107	3.23	2769	52.0	1790	23.5	3.07	0.150	26.9	0.183	3.62	0.0217	3.72	0.0275	0.324	0.00211
342	799	6.59	107	0.935	2834	28.2	1839	57.5	2.80	0.0252	26.3	0.129	3.57	0.0328	3.81	0.0434		
368	824	17.1	127	3.53	2911	56.0	1856	15.2	6.69	0.237	24.3	0.212	3.67	0.0228	3.75	0.0232	0.324	0.00194
394	760	13.8	103	0.646	2712	46.5			3.23	0.0646	22.3	0.169	3.66	0.0124	3.69	0.0549	0.315	0.00404
420	806	13.2	93.9	2.19	2778	48.9	1757	33.8	3.12	0.398	19.9	0.242	3.51	0.0320	3.82	0.353		
447	748	11.0	93.8	0.645	2626	38.6			3.52	0.220	19.6	0.0509	3.74	0.0157	3.72	0.0141	0.319	0.00140
473	809	9.7	89.1	0.604	2804	34.6	1807	42.8	3.52	0.101	18.8	0.130	3.79	0.0182	3.68	0.0541	0.320	0.00227
499	811	10.1	87.9	0.515	2795	41.1	1795	42.4	4.33	0.175	17.2	0.140	3.72	0.0115	3.57	0.0790	0.308	0.00759
539	793	20.5	77.4	1.02	2741	66.5	1758	35.9	2.91	0.222	15.4	0.0972	3.81	0.0225	3.58	0.224	0.295	0.0171
565	808	5.36	74.4	0.567	2773	28.4	1768	24.0	3.05	0.0418	14.7	0.0913	3.83	0.0288	3.63	0.0687	0.295	0.00449
591	810	7.36	72.2	0.824	2763	28.3	1769	50.9	2.49	0.185	14.4	0.341	3.75	0.0844	3.46	0.253	0.341	0.0260
617	843	8.59	76.3	1.12	2960	29.6	2028	65.0	4.05	0.0762	13.2	0.0487	3.80	0.0121	3.53	0.0317	0.298	0.00110
631	793	5.48	74.0	0.833	2687	22.7	1753	73.3	11.8	0.393	12.9	0.116	3.61	0.0292	3.44	0.0585		
670	820	7.92	69.4	0.727	2808	26.9	1761	37.7	4.14	0.139	12.3	0.0356	3.76	0.0210	3.51	0.0341	0.298	0.00421
709	813	15.9	65.7	0.802	2727	55.8	1732	43.0	5.03	0.673	11.6	0.0589	3.79	0.0189	3.56	0.408	0.299	0.0332
749	809	9.06	62.0	0.591	2710	29.3	1780	33.2	4.14	0.0402	10.6	0.104	3.69	0.0229	3.46	0.0429	0.296	0.00394
788	811	18.7	58.8	0.269	2695	60.6	1754	21.8	4.27	0.229	10.0	0.0601	3.62	0.0138	3.55	0.0937	0.305	0.00797
801	831	11.9	55.1	0.725	2760	40.4	1792	18.2	4.00	0.162	9.88	0.0563	3.51	0.0112	3.49	0.0352		

A3-10: Effluent pH short term flushed

3 days		14 days	
Pore volume	pH	Pore volume	pH
0.432	13.0	0.423	13.0
0.865	13.0	0.847	13.0
1.30	13.0	1.27	13.0
1.73	13.0	1.69	13.0
2.16	13.0	2.12	13.0
2.59	13.0	2.54	13.0
3.03	13.0	2.96	13.0
4.76	12.4	3.39	12.6
6.48	12.2	5.08	12.3
32.4	11.2	6.77	12.1
34.6	11.3	33.9	11.3
36.7	11.2	36.0	11.2
38.9	11.3	38.1	11.3
41.1	11.2	40.2	11.2
47.1	11.2	46.6	11.2
77.8	10.7	76.2	10.8
82.1	10.5	80.4	10.8
86.5	10.2	82.6	10.7
122	8.33	84.7	10.7
129	8.33	120	8.83
164	8.08	127	8.28
172	8.22	161	8.18
203	8.18	168	8.37
208	8.05	200	8.25
212	7.84	203	8.18
242	8.12	208	8.18
246	7.98	237	7.94
251	7.92	241	8.05
254	8.23	246	8.18
285	8.10	250	8.15
291	7.85	279	8.36
294	7.86	285	8.36
325	8.02	288	8.02
333	7.81	293	7.98
337	8.21	297	8.07
370	8.01	301	8.04
376	8.08	306	8.15
422	8.08	338	8.00
500	8.12	344	7.83
508	8.18	382	7.90
544	8.22	458	7.98
		466	8.00
		500	7.83
		509	7.87
		538	8.22

A3-11: Effluent pH 1 month flushed

1 month A		1 month B		1 month C	
Pore volume	pH	Pore volume	pH	Pore volume	pH
0.426	13.0	0.437	13.0	0.411	13.0
0.853	13.0	0.874	13.0	0.823	13.0
1.28	13.0	1.31	13.0	1.23	13.0
1.71	13.0	1.75	13.0	1.65	13.0
2.13	13.0	2.19	13.0	2.06	13.0
2.56	12.4	3.06	12.8	2.19	13.0
2.98	12.6	3.93	12.3	2.06	13.0
3.41	12.6	5.68	12.2	2.47	12.9
3.84	12.4	6.99	12.1	2.88	12.8
4.26	12.4	34.8	10.9	3.29	12.7
4.69	12.4	39.1	10.9	5.35	12.5
5.12	12.3	43.5	10.8	6.58	12.3
5.54	12.3	74.1	10.8	37.8	11.0
5.97	12.2	82.8	10.3	38.3	11.2
10.2	11.9	87.2	10.2	40.3	11.0
14.5	11.7	121	9.33	42.4	11.0
18.8	10.5	122	8.99	44.4	10.9
23.0	10.1	124	8.98	69.9	10.8
27.3	10.1	126	8.90	73.8	10.7
31.6	10.5	127	9.09	82.8	10.5
35.8	10.8	162	8.27	85.0	10.5
40.1	10.4	164	8.02	112	10.0
44.3	10.7	168	8.06	116	9.98
48.6	10.8	170	8.03	120	9.85
52.9	11.0	172	8.05	123	10.0
57.1	9.30	199	7.92	149	9.82
61.4	9.46	200	7.95	155	9.30
65.7	9.70	213	7.93	159	9.43
69.9	10.02	245	8.30	187	8.97
74.2	10.38	249	8.38	196	8.95
78.5	10.30	257	8.05	199	9.04
82.7	10.40	287	8.28	232	8.78
83.6	10.32	293	8.07	239	8.64
87.0	9.14	297	8.16	245	8.65
91.3	9.81	301	8.02	279	8.60
95.5	8.76	326	8.16	284	8.76
99.8	8.45	331	7.96	290	8.64
104	8.71	338	8.12	319	8.68
108	8.74	339	8.12	328	8.81
113	8.89	375	8.15	368	8.64
117	8.79	378	7.85	376	8.56
121	8.76	379	8.02	409	8.51
125	8.90	415	7.99	410	8.56
130	9.04	419	8.22	417	8.73
134	9.03	454	8.47	418	8.48
138	7.47	456	7.97	452	8.61
142	7.68	460	7.85	463	8.53
147	7.84	466	7.99	465	8.54
151	7.87	502	8.24	469	8.67
155	7.85			493	8.61
159	8.12			498	8.62
164	8.17			500	8.31
168	8.16				
172	7.77				
177	8.11				
181	8.16				
185	8.22				
189	8.23				
194	8.32				
198	8.34				
202	8.42				

A3-12: Effluent pH 3 month flushed

3 months A		3 months B		3 months C		3 months D	
Pore volume	pH	Pore volume	pH	Pore volume	pH	Pore volume	pH
0.411	13.0	0.434	13.0	0.428	13.0	0.438	13.0
0.823	13.0	0.868	13.0	0.855	13.0	0.876	13.0
1.23	13.0	1.30	13.0	1.28	13.0	1.31	13.0
1.65	13.0	1.74	13.0	1.71	13.0	1.75	13.0
2.06	13.0	2.17	13.0	2.14	13.0	2.19	13.0
2.47	13.0	2.60	13.0	2.28	12.9	2.63	13.0
2.88	12.7	3.04	12.8	4.70	12.4	3.07	12.8
3.29	12.5	3.47	12.7	6.84	12.1	3.50	12.7
3.70	12.5	3.90	12.6	10.7	11.9	3.94	12.6
4.11	12.4	4.34	12.5	37.6	10.9	4.38	15.5
4.53	12.3	4.77	12.5	41.5	10.9	4.82	12.4
4.94	12.3	5.21	12.5	46.2	11.0	5.69	12.4
5.35	12.3	5.64	12.4	48.3	11.0	6.13	12.4
5.76	12.1	8.68	12.2	78.7	10.8	9.20	12.1
6.17	12.2	34.7	11.3	81.7	10.7	35.0	11.4
37.0	10.5	39.0	11.3	85.5	10.6	39.4	11.3
41.1	10.7	43.4	11.3	89.0	10.5	43.8	11.3
42.8	10.7	47.7	11.3	122	9.54	48.2	11.2
74.1	10.2	74.2	11.2	124	9.61	52.6	11.2
78.2	10.4	88.5	11.1	128	9.48	75.3	11.0
80.2	10.6	121	10.3	132	9.37	78.8	10.9
115	10.2	126	10.3	163	9.22	83.2	10.9
114	10.4	160	9.32	165	9.16	87.6	10.8
117	10.4	165	9.09	168	8.98	92.0	10.8
119	10.2	169	9.15	171	9.12	123	10.4
121	10.3	174	8.88	201	8.96	127	10.2
124	10.3	208	8.96	205	8.99	131	10.2
156	9.30	213	8.87	209	8.98	136	10.2
157	9.55	245	8.94	215	8.98	163	9.72
160	9.52	254	8.84	242	8.95	178	9.36
163	9.52	291	8.82	246	8.73	209	9.11
193	9.20	295	8.73	250	8.87	215	9.29
199	9.09	333	8.70	253	8.84	241	8.87
202	9.03	338	8.71	284	8.74	247	8.81
204	9.08	340	8.12	291	8.80	260	9.01
229	8.95	355	8.59	297	8.74	260	8.93
239	8.98	357	8.38	325	8.69	295	8.74
244	8.80	375	8.44	332	8.77	300	8.87
274	8.87	378	8.32	335	8.63	331	8.77
280	8.43	397	8.15	366	8.65	342	8.73
282	8.78	399	8.26	373	8.69	379	8.69
315	8.62	399	8.48	379	8.65	383	8.63
321	8.56	418	8.36	410	8.65	420	8.70
325	8.48	437	8.32	414	8.73	426	8.62
354	8.61	442	8.12	420	8.63	460	8.65
367	8.69	457	8.17	447	8.54	466	8.60
391	8.64	462	8.13	455	8.75	504	8.60
397	8.53	476	8.27	491	8.41	510	8.51
400	8.46	496	8.19	500	8.54	548	8.24
404	8.42	498	8.46	501	8.50	552	8.60
432	8.40	537	8.29			553	8.67
442	8.37					593	8.57
481	8.40					631	8.35
551	8.24					642	8.41
						672	8.12
						674	8.23
						683	8.19
						713	8.18
						755	8.37
						797	8.35
						801	8.31